DOCTOR OF PHILOSOPHY

Optimisation of biogas production by advanced process monitoring and the effect of mixing frequency on biogas reactors with and without microbial support media

Ward, Alastair James

Award date:
2009

Awarding institution:
Bangor University

Optimisation of biogas production by advanced process monitoring and the effect of mixing frequency on biogas reactors with and without microbial support media

A thesis presented in partial fulfilment

for the

Degree of

Philosophiae Doctor

in the

School of Chemistry

by

Alastair James Ward

Prifysgol Bangor University

Bangor

Acknowledgements

This thesis was possible as a result of funding from the European Social Fund (ESF) Objective 1 programme, Holsworthy Biogas plc (now AnDigestion Ltd) and Mark Christensen at Bio-Resource Ltd, with special thanks to the Holsworthy plant Operations Director, Jake Prior and former employee Graham Johnson for their assistance in the work behind this thesis.

This thesis would also not have come into being without the support of supervisory staff at the University of Bangor. These being Dr. Peter Holliman in the School of Chemistry and Prof. David Jones in the School of the Environment and Natural Resources. I am particularly thankful for their suggestions into new ways to look at the work, based on their diverse fields of research. Also thanks to Sarah Rugen-Hankey for sharing the driving to the University and helping me with some of the details about how the University works.

Very special thanks must go to Dr. Phil Hobbs of North Wyke Research, Devon, UK (formerly the Institute of Grassland and Environmental Research). Phil has been first contact for the greater part of my Ph.D period, and without his patience, support and suggestions this Ph.D would never have existed. Thanks also go to the support staff past and present at North Wyke Research, including Jon Williams for help in laboratory work and Guillermo Pardo for assistance with LabVIEW programming and the complicated mathematics of the hydrodynamic study. Also thanks are due to Andrew Bristow the Laboratory Manager for his experience and help in demonstrating the use of equipment and to Nadine Loick who went through the experience simultaneously and had to share an office with me for more than two years.

I would also like to thank my family for their support and belief in me throughout the entire Ph.D.

Abstract

The following is a summary of the thesis entitled 'Optimisation of Biogas Production By Advanced Process Monitoring and the Effect of Mixing Frequency on Biogas Reactors With and Without Microbial Support Media' submitted to the School of Chemistry, University of Bangor, Wales, UK in fulfilment of the degree of Doctor of Philosophy.

In the first chapter, current literature was reviewed and specific areas where research was lacking were highlighted. Some of theses research areas were selected and formed the basis for the subsequent chapters. A shortened verson of the review has been accepted for publication in the international journal *Bioresource Technology*.

The second chapter described the construction of pilot scale anaerobic digesters, including a four-stage design, two two-stage designs and four single-stage designs. The four-stage digester was operated continuously for ten months under a variety of loads to gain an insight into the behaviour of digesters during start-up, failure, recovery and stable operation. The hydrodynamics of the system were also examined by a tracer study. This gave valuable information on the mixing and flow patterns within the digester vessels. The single and two-stage digesters were built for investigation into the effect of mixing frequency on digesters with and without microbial support media fitted.

In chapter 3, data collected from the four-stage system was statistically analysed. Curve fitting non-linear regression models were created to estimate the optima of each measured parameter in terms of both methane production and yield. Total alkalinity was found to be a good indicator of process stability and also gas production rate with an R^2 of 64.3 % and standard error of observations of 0.254 $L.L^{-1}$ d^{-1}.

Chapter 4 concentrated on a regression model which could estimate total alkalinity through data obtained by cheap and simple to maintain pH, redox and conductivity probes, *i.e.* a software sensor. The selected prediction model had an R^2 value of 71 % and root mean square error of 1441 $mg.L^{-1}$. The software sensor estimate was used by a rule based supervisory control system which controlled the system stability and gas production by modulating the input feed rate to maintain an optimal alkalinity.

Chapter 5 examined an alternative method of estimating bicarbonate alkalinity using Fourier Transform Near Infrared Spectroscopy (FT-NIRS). A good estimate of total alkalinity was made by optimisation using spectral pre-processing and partial least

squares analysis of the alkalinity titration data, with an R^2 of 87 % and root mean square error of prediction of 1230 $mg.L^{-1}$, suggesting this method could also be developed into an on-line monitoring system.

In chapter 6 the effect of mixing frequency on single and two-stage anaerobic digesters with reticulated polyurethane foam biomass support media was investigated. The work included quantification of extracellular polymeric substances (EPS) which form the structural component of microbial aggregates was performed in addition to measuring the effect on the methane production rate. It was found that mixing frequency had the most effect on methane production with as much as 26 % increase, suggesting that simple optimisation experiments in industrial scale processes could be economically beneficial.

Aims and objectives

The aim of this work was to optimise the organic loading rate and increase the production of methane from anaerobic digesters treating a specific feedstock, a commercially available pig meal, chosen to represent potential feedstocks which could be used in full scale reactors.

The process is difficult to optimise as there is a distinct lack of actuators, so the two basic actuators common to practically all anaerobic digesters were chosen, these being:

1. The input feed rate, in terms of volume flow rate which directly affects the organic loading rate and the hydraulic retention time.
2. The mixing system.

When a digester is built with an optimal input control, this will allow the design of a minimal volume tank, with savings in initial construction, maintenance and heating costs. A primary objective is to produce a method by which the stability of the process can be monitored by using basic hardware that is inexpensive, reliable and suitable for fitting to existing biogas plants.

Mixing of anaerobic digesters uses valuable energy, is expensive to maintain and can add to the loss of active microbial biomass. Investigation into the effect of mixing frequency in conjunction with a method of retaining the biomass that will work with a higher-solids feedstock is expected to result in a more efficient process.

TABLE OF CONTENTS

List of figures

List of tables

List of equations

1 Optimisation of the anaerobic digestion of agricultural resources (Literature review)

1.1 Summary of literature review

It is in the interest of operators of anaerobic digestion plants to maximise methane production whilst concomitantly reducing the chemical oxygen demand of the digested material. Although the production of biogas through anaerobic digestion is not a new idea, commercial anaerobic digestion processes are often operated at well below their optimal performance due to a variety of factors. This chapter reviews current optimisation techniques associated with anaerobic digestion and suggests possible areas where improvements could be made, including the basic design considerations of a single or multi-stage reactor configuration, the type, power and duration of the mixing regime and the retention of active microbial biomass within the reactor. Optimisation of environmental conditions within the digester such as temperature, pH, buffering capacity and fatty acid concentrations are also discussed. The methane-producing potential of various agriculturally sourced feedstocks has been examined, as has the advantages of co-digestion to improve carbon-to-nitrogen ratios and the use of pre-treatments and additives to improve hydrolysis rates or supplement essential nutrients which may be limiting. However, perhaps the greatest shortfall in biogas production is the lack of reliable sensory equipment to monitor key parameters and suitable, parallelised control systems to ensure the process continually operates at optimal performance. Modern techniques such as software sensors and powerful, flexible controllers are capable of solving these problems. A direct comparison can be made here with, for instance, oil refineries where a more mature technology uses continuous *in situ* monitoring and associated feedback procedures to routinely deliver continuous, optimal performance.

1.2 Introduction

Anaerobic digestion is the process of decomposition of organic matter by a microbial consortium in an oxygen-free environment (Pain and Hepherd, 1985). It is a process found in many naturally occurring anoxic environments including watercourses, sediments, waterlogged soils and the mammalian gut. It can also be applied to a wide range of feedstocks including industrial and municipal waste waters, agricultural, municipal, and food industry wastes, and plant residues.

The production of biogas through anaerobic digestion offers significant advantages over other forms of waste treatment, including:

- Less biomass sludge is produced in comparison to aerobic treatment technologies.
- Successful in treating wet wastes of less than 40 % dry matter (Mata-Alvarez, 2002).
- More effective pathogen removal (Bendixen, 1994; Lund *et al.*, 1996; Sahlstrom, 2003). This is especially true for multi-stage digesters (Kunte *et al.*, 2004; Sahlstrom, 2003) or if a pasteurisation step is included in the process.
- Minimal odour emissions as 99 % of volatile compounds are oxidatively decomposed upon combustion, e.g. H_2S forms SO_2 (Smet *et al.*, 1999).
- High degree of compliance with many national waste strategies implemented to reduce the amount of biodegradable waste entering landfill.
- The slurry produced (digestate) is an improved fertiliser in terms of both its availability to plants (Tafdrup, 1995) and its rheology (Pain and Hepherd, 1985).
- A source of carbon neutral energy is produced in the form of biogas.

Treatment of organic wastes is currently of particular importance in the European Union (EU) as the EU Landfill Directive has set the following targets:

- By 2010, to reduce biodegradable municipal waste land-filled to 75 % of the level produced in 1995.
- By 2013, to reduce biodegradable municipal waste land-filled to 50 % of the level produced in 1995.
- By 2020, to reduce biodegradable municipal waste land-filled to 35 % of the level produced in 1995.

Anaerobic digestion provides a viable alternative to landfill for category 3 wastes (these include food industry wastes, domestic wastes and some abattoir wastes).

Once produced, biogas is generally composed of *ca.* 48 – 65 % methane, *ca.* 36 – 41 % carbon dioxide, up to 17 % nitrogen , <1 % oxygen, 32 – 169 ppm hydrogen sulphide and traces of other gases (Rasi *et al.*, 2007). Both carbon dioxide and methane are potent greenhouse gases and possibly 18% of global warming is thought to be caused by anthropogenically derived methane emissions (Ghosh, 1997). Carbon dioxide

released through natural mineralisation is considered neutral in greenhouse gas terms as the carbon has been recently removed from the atmosphere by plant uptake, to be released again as part of the carbon cycle. Controlled anaerobic digestion of organic material is therefore environmentally beneficial in two ways:

- By containing the decomposition processes in a sealed environment, potentially damaging methane is prevented from entering the atmosphere, and subsequent burning of the gas will release carbon-neutral carbon dioxide back to the carbon cycle.
- The energy gained from combustion of methane will displace fossil fuels, reducing the production of carbon dioxide that is not part of the recent carbon cycle.

1.3 Biochemistry of anaerobic digestion

The main reactions involved in anaerobic digestion (Figure 1.1) begin with the hydrolysis of biopolymers into soluble monomers and dimers, then the fermentation of these products to organic acids, acetogenesis of the organic acids and sugars to acetate and hydrogen, and finally to methanogenesis. A delicate balance between the rates of hydrolysis, acidogenesis, acetogenesis and methanogenesis (methane production) must be sustained to ensure enough substrate is produced for the following step without overproduction. This is especially true of the methanogenesis stage, because methanogens are sensitive to the acidic conditions caused by an accumulation of volatile fatty acids. If the rate of hydrolysis is higher than the methanogenic rate, the accumulation of volatile fatty acids may lead to failure of the digester (Pavlostathis and Giraldo-Gomez, 1991).

Methane production in anaerobic digestion is by two pathways as shown below:

$CH_3COOH \rightarrow CH_4 + CO_2$ (Aceticlastic methanogenesis).

$4H_2 + CO_2 \rightarrow CH_4 + 2H_2O$ (Hydrogenotrophic methanogenesis).

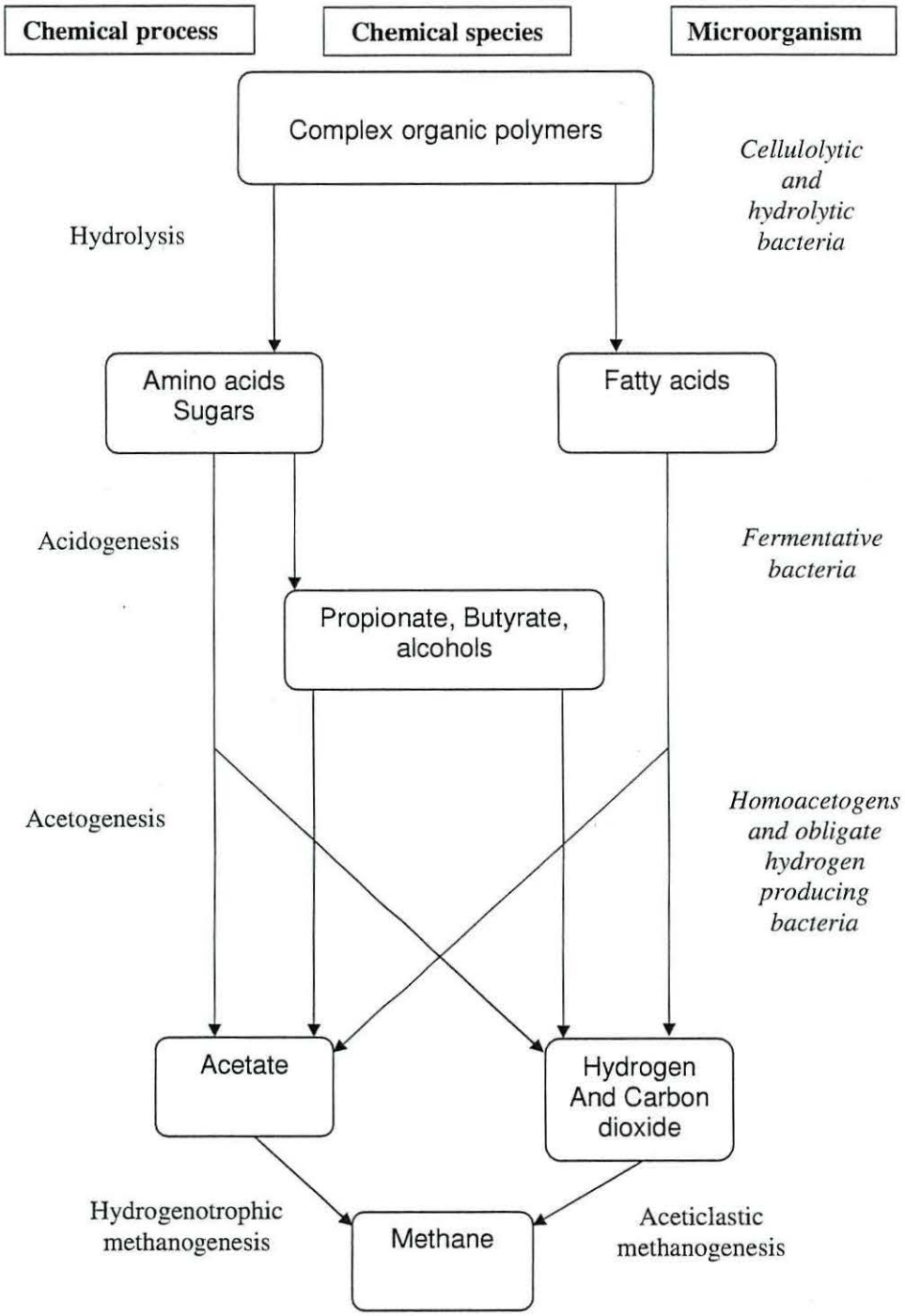

Figure 1.1 Anaerobic digestion (Gujer and Zehnder, 1983).

A large proportion (73%) of methane produced in anaerobic digestion is from aceticlastic methanogenesis (Smith and Mah, 1966). This is because the hydrogen required for hydrogenotrophic methanogenesis is in short supply as it is used in many other reactions during anaerobic digestion: for instance, the hydrogenation of long-chain fatty acids, the reduction of sulphate and nitrate, and also in cell maintenance. The requirement for hydrogen in many different reactions reduces hydrogen partial pressure, which is an important factor in anaerobic digestion (see below).

A more detailed description of the processes is given below (adapted from Pohland, 1992):

Hydrolysis, or depolymerisation, is performed by exocelluar hydrolytic enzymes which are inhibited by an excess of sugars and amino acids. It is therefore important that these products are utilised efficiently in downstream processes to prevent inhibition at this first stage: The hydrolysis stage can be the limiting step in anaerobic digestion if the feed material is high in cellulosic content, which is more difficult to break down by extracellular enzymes. Bacteria responsible for the hydrolysis stage are principally the strict anaerobes such as *Bacterioides*, *Clostridia* (Rivard *et al.*, 1991) and facultative bacteria such as *Streptococci* (Hobson and Shaw, 1974).

Acidogenesis by fermentative bacteria degrades solubilised sugars and amino acids to mostly form volatile fatty acids, hydrogen, carbon dioxide, alcohols and some other minor compounds. Some of these equations are shown in Table 1.1. Acidogenesis is inhibited by an excess of volatile fatty acids (Kalyuzhnyi, 1997). *Thermoanaerobacterium thermosaccharolytium* and *Desulfotomaculum geothermicum* are examples of thermophilic (optimum temperature of 55°C) acidogenic bacteria, while *Thermotogales* and certain *Bacillus* species are mesophilic (optimum temperature of 35°C) acidogens that have been found in digesters by Shin *et al.*, (2004).

Reduced compounds are oxidised to hydrogen, carbon dioxide and acetate by obligate hydrogen-producing acetogens, for example *Syntrophomonas wolfei*, an organism which oxidises butyrate and straight-chain, monocarboxylic, saturated C5 – C8 fatty acids. This process requires syntrophy with hydrogen-consuming organisms such as *Methanospirillum hungatei* (McInerney *et al.*, 1981), as $\Delta G^{0'}$ suggests the thermodynamics of the reactions are not favourable under STP conditions (Table 1.1). Loss of hydrogen pushes the equation to the right hand side and more products are formed. Hydrogenotrophic methanogenic archaea and sulphate-reducing bacteria keep hydrogen partial pressure low ($<10^{-4}$ atm or 10 Pa), which favours the production of

methane and carbon dioxide, whereas high hydrogen partial pressure appears to favour the accumulation of propionate and butyrate (Harper and Pohland, 1986). However, Inanc *et al.*, (1996) found that artificially elevated hydrogen partial pressure had no discernible effect. Instead, the accumulation of propionate was found to be a result of a shift in the dominant species of acidogenic populations. Acetate is also produced as an end product by Group I sulphate-reducing bacteria (for example *Desulfovibrio*) from malate, formate and some primary alcohols, whereas Group II sulphate reducing bacteria such as *Desulfobacter* oxidise acetate and other fatty acids to carbon dioxide (Mata-Alvarez, 2002). Homoacetogenic bacteria, for example *Clostridium formicoaceticum* (Zellner *et al.*, 1997) produce acetate as a sole product of anaerobic digestion.

Aceticlastic methanogenic bacteria such as *Methanosaeta concilii* (van Bodegom *et al.*, 2004) convert acetic acid to methane. These archaea have a long doubling time of approximately 2.6 days (Mosey and Fernandes, 1989), due to the small amount of energy available from the limited substrates they use. The long doubling time of these microbes, which provide a significant proportion of the methane production, can mean this stage of anaerobic digestion is often a limiting step. This is more likely when an easily-degradable feedstock is used, increasing the rate of hydrolysis.

Hydrogenotrophic methanogenic bacteria such as *Methanospirillum hungatei* (van Bodegom *et al.*, 2004) convert carbon dioxide and hydrogen to methane. These bacteria also have a relatively long doubling time, but at six hours it is considerably shorter than that of the aceticlastic methanogens (Mosey and Fernandes, 1989). Their contribution to the overall production of methane is small. They do, however, have an important role in maintaining low hydrogen partial pressure. Some methanogens (for example *Methanosarcina barkeri*) can utilise acetate and hydrogen / carbon dioxide (van Bodegom *et al.*, 2004).

Table 1.1 shows the free energy of some fermentative reactions involved in anaerobic digestion. Many of the reactions producing hydrogen will not proceed unless hydrogen is at a very low partial pressure. This emphasises the importance of hydrogenofil methanogenic bacteria utilising hydrogen in methane production. Sulphate reducing bacteria and nitrate reducing bacteria also lower the hydrogen partial pressure by oxidation of hydrogen and formate. Hydrogen can also be removed by inorganic oxidants such as Fe^{3+} salts. Studies of *Methanobacterium thermoautotrophicum* (a common methanogen in anaerobic digesters) have shown hydrogen-concentration-

dependant control of isoenzymes. In the presence of hydrogen at high partial pressure, cell biomass production is at its greatest, but genetic switching at very low hydrogen concentrations allows methane production in this species without growth of the bacterial population (Reeve *et al.*, 1997). This situation is ideal for maximum methane production in an anaerobic digester without directing substrate towards cell growth.

Table 1.1 Oxidation reactions involved in anaerobic digestion (Mata-Alvarez, 2002).

Reaction		$\Delta G^{0'}$ (KJ mol^{-1})
Propionate → Acetate	$CH_3CH_2COO^- + 3H_2O \rightarrow CH_3COO^- + H^+ + HCO_3^- + 3H_2$	+76.1
Butyrate → Acetate	$CH_3CH_2CH_2COO^- + 2H_2O \rightarrow 2CH_3COO^- + H^+ + 2H_2$	+48.1
Ethanol → Acetate	$CH_3CH_2OH + H_2O \rightarrow CH_3COO^- + H^+ + 2H_2$	+9.6
Lactate → Acetate	$CHCHOHCOO^- + 2H_2O \rightarrow CH_3COO^- + HCO_3^- + H^+ + 2H_2$	-4.2
Lactate → Propionate	$3CHCHOHCOO^- \rightarrow 2CH_3CH_2COO^- + CH_3COO^- + H^+ + HCO_3^-$	-165
Lactate → Butyrate	$2CHCHOHCOO^- + 2H_2O \rightarrow CH_3CH_2CH_2COO^- + 2HCO_3^- + 2H_2$	-56
Acetate → Methane	$CH_3COO^- + H_2O \rightarrow HCO_3^- + CH_4$	-31.0
Glucose → Acetate	$C_6H_{12}O_6 + 4H_2O \rightarrow 2CH_3COO^- + 2HCO_3^- + 4H^+ + 4H_2$	-206
Glucose → Ethanol	$C_6H_{12}O_6 + 2H_2O \rightarrow 2CH_3CH_2OH + 2HCO_3^- + 2H^+$	-226
Glucose → Lactate	$C_6H_{12}O_6 \rightarrow 2CHCHOHCOO^- + 2H^+$	-198
Glucose → Propionate	$C_6H_{12}O_6 + 2H_2 \rightarrow 2CH_3CH_2COO^- + 2H_2O + 2H^+$	-358

1.4 Reactor design

The basic requirements of an anaerobic digester design are: to allow for a continuously high and sustainable organic load rate, a short hydraulic retention time (to minimise reactor volume) and to produce the maximum volume of methane.

Reactor shape must take into consideration the construction practicalities of both mixing and heat loss. Although underground reactors constructed from concrete blocks may be simpler to build in a square or rectangular shape, mixing will be suboptimal as flow will be limited in corners, leading to a build up of refractory material that will reduce the effective digester volume over time and also increase maintenance and down-time.

There are several types of reactor in use today, and the design is related to the material to be digested. There are three main groups; batch reactors are the most simple. These are simply filled with the feedstock and left for a period that can be considered to be the hydraulic retention time, after which they are emptied. The second type are one-stage continuously fed systems, where all the biochemical reactions take place in one reactor, and, finally, two-stage (or even multi-stage) continuously fed systems where the hydrolysis/acidification and acetogenesis / methanogenesis processes are separated.

Solid waste digesters are also divided into "wet" or "dry" types. Wet reactors are those with a total solids value of 16 % or less, whilst dry reactors have between 22 and 40 % total solids, and those that fall between wet and dry are considered semi-dry (Mata-Alvarez, 2002). The dry reactor technology is mainly used with municipal solid waste or vegetable wastes rather than with manures. One-stage reactors for municipal solid waste in Europe are equally split between wet and dry types (De Baere, 2000). The "wet" total solids value of 16 % or less is typical of many types of manure, which should require little further treatment other than the use of chopper pumps to reduce particle size to reduce the risk of blocked pipes. Their high water content also means a larger overall volume to treat a similar mass of feedstock when compared to "dry" or "semi-dry" technologies. If using a wet reactor for treatment of dry feedstocks, pre-treatments of pulping and slurrying are required before digestion (Mata-Alvarez, 2002). Using either fresh or recycled process water to obtain less than 15 % total solids has the advantage that any inhibitors of methanogenesis which may be present in the fresh material, such as excessive short chain fatty acids or ammonium are diluted, but there is also the possibility that these inhibitors will spread quickly through the reactor if dilution is insufficient.

The completely stirred tank reactor (CSTR) is a common design in anaerobic digestion processes. This type of reactor consists of a tank that is mixed regularly if not continuously, and is usually also fed intermittently but, at least, once a day (Figure 1.2). CSTRs attempt to create an ideal flow pattern known as mixed flow, where the vessel contents are uniform throughout. This is not practical in real digesters, at least because mixed flow requires a constant input / output stream and perfect mixing. The typical gas production rate from a CSTR is quite low because of the coupled solid and hydraulic retention times, *i.e.* both solids and liquids have, on average, an equal residence time, which allows little opportunity for the retention of a large population of microbial biomass (Rozzi and Passino, 1985).

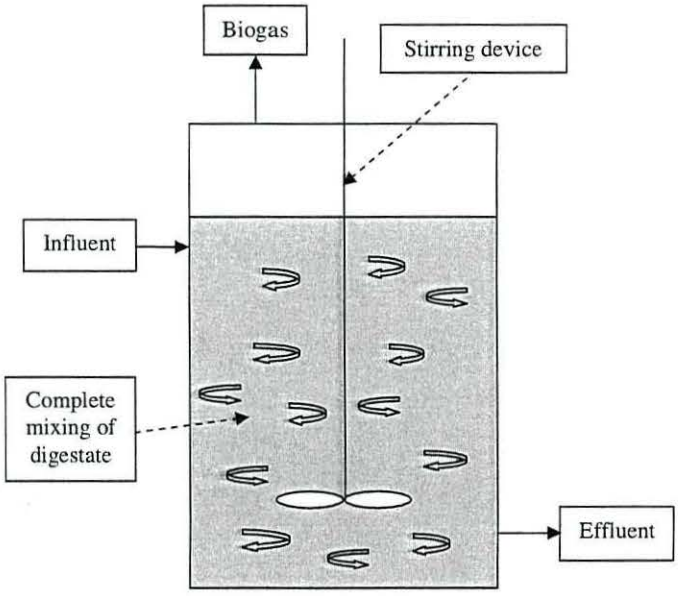

Figure 1.2. Single-stage CSTR anaerobic digester.

Plug flow reactors (Figure 1.3) are often used for the treatment of municipal solid wastes in Europe (Mata-Alvarez, 2002). Plug flow reactors simply involve adding fresh material to the reactor either at one end of a horizontal vessel or the bottom of a vertical vessel and then collecting the digested solids at the opposite end to ensure adequate retention time. Plug flow should also have an ideal flow pattern, where there is no axial mixing (*i.e.* in the direction of flow) but complete radial mixing (*i.e.* the plane perpendicular to the flow). Rather like the CSTR, plug flow reactors are unlikely to exhibit ideal flow conditions due to the complex and unpredictable nature of flow

patterns within vessels, and also because many plug flow reactors use some form of mixing to help move the digestate through the vessel. There is an advantage if there are no moving parts inside the reactor and short circuiting is less likely. However, the problem of inoculating the fresh material has to be overcome by recycling the output material, thus increasing the necessary volume of the reactor.

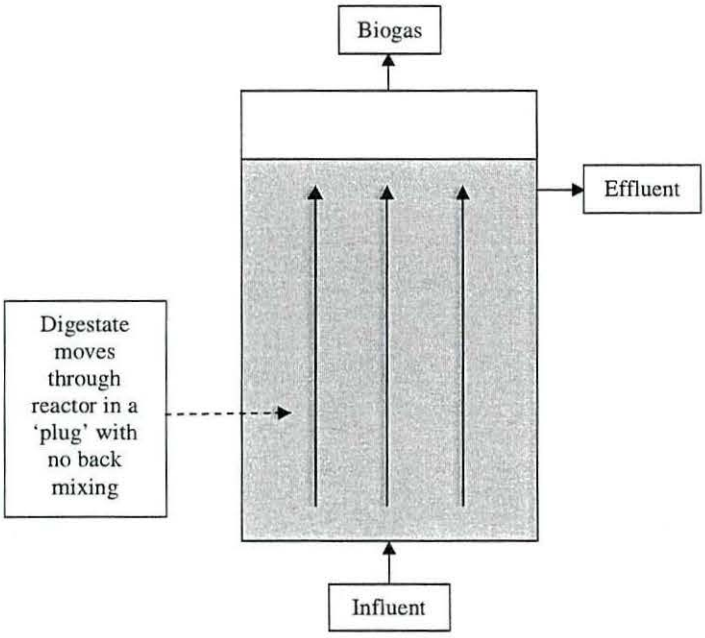

Figure 1.3. Plug flow anaerobic digester.

Waste waters are commonly treated anaerobically (Lettinga, 1995). Waste waters can be either domestic (Elmitwalli *et al.*, 2002) or industrial (Macarie, 2000), and may also be combined with rainwater. Waste waters have total solids content of approximately 0.5 % w/v which is, considerably less than raw biomass, manures, municipal solid wastes or vegetable wastes. This allows the use of reactors which can either settle active biomass or use a biomass support medium to ensure the retention of a large population of microbial biomass. Reduction of the hydraulic retention time to between four and forty hours, with either an inoculum of granular sludge or digested sludge, is also possible (De Man *et al.*, 1986; Lettinga *et al.*, 1983). The upflow anaerobic sludge blanket (UASB) reactor was developed in the 1970s (Lettinga *et al.*, 1980) and is probably the most widely-used method of anaerobic waste water treatment today because of it's simplicity in design and rapid digestion rate (Figure 1.4). The

UASB reactor relies on a sludge bed at the base formed by incoming solids and bacterial growth. The sludge bed may contain flocs or granules (Pol *et al.*, 1983) which settle well by gravity. Turbulent flow and the release of biogas ensure good contact between the influent and the flocs or granules (Heertjes and Vandermeer, 1978) without causing much damage to these microbial aggregates. The waste water is pumped from below through the sludge bed, forming a sludge blanket of suspended solids, flocs and granules. The top of the reactor is designed to allow the settling of the solids, upon which they fall back into the sludge bed.

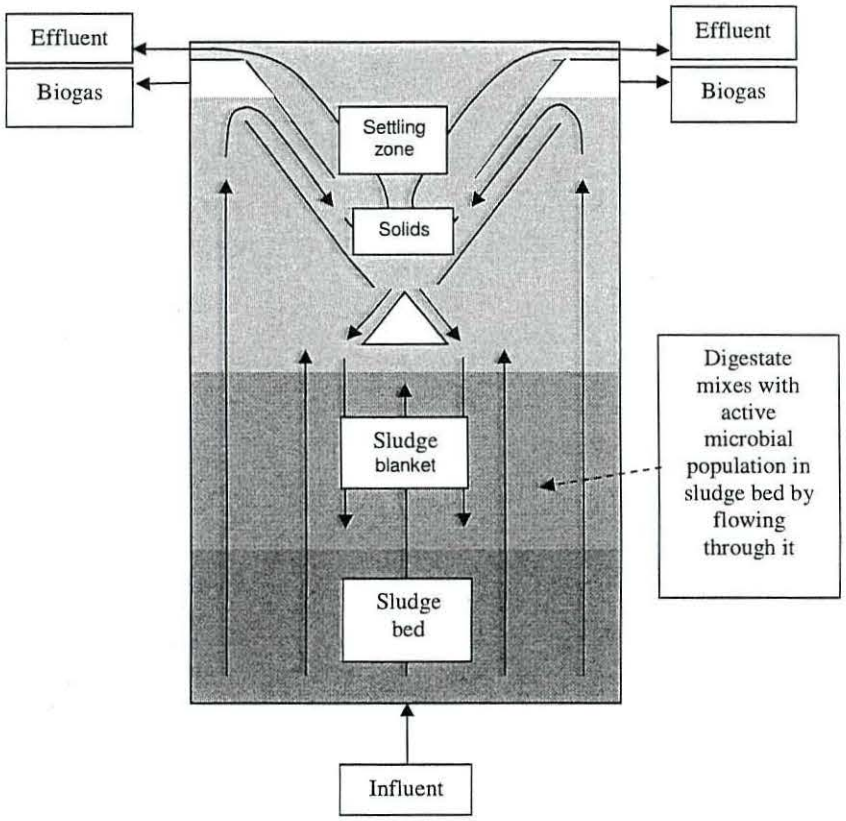

Figure 1.4. Upflow anaerobic sludge blanket anaerobic digester.

Packed bed reactors are usually upflow and contain synthetic media such as biolite (Beteau *et al.*, 2005) or natural media, for example sintered coal dust (Rozzi and Passino, 1985) packed within a column. The pores on the surface of the media provide a good anchor for biofilm formation, protecting the cells from shear forces and reducing the proportion washed out with the digested material.

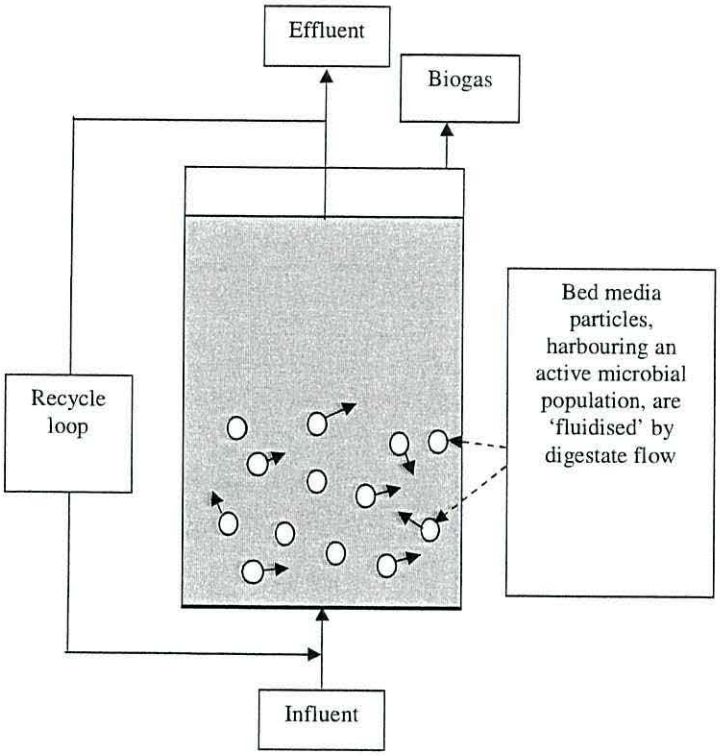

Figure 1.5. Fluidised bed anaerobic digester with recycle loop.

Fluidised bed reactors (Figure 1.5) use support media such as polyurethane foam (Yang *et al.*, 2004) or sintered glass (Perez-Garcia *et al.*, 2005) to maintain micro-organisms but require a high liquid flow rate, often by recycling the effluent at ratios of recycle to influent of up to 100:1 (Aye and Loh, 2003; Rozzi and Passino, 1985), to maintain fluidity of the bed materials. It has been shown that fluidised bed reactors are less affected by adverse operating conditions than packed bed reactors (Farhan *et al.*, 1997).

Batch-fed reactors are simple in terms of design and technology and are suitable for the highest levels of dry matter of all digesters (Rozzi and Passino, 1985) as continuous pumping is not necessary. The feedstock is loaded into the reactor, often with an inoculum of approximately 10 %. In some batch reactors liquid leachate from the base is collected and recirculated back to the top, or in the case of sequential batch reactors, leachate from an "old" reactor is applied to a "new" reactor, and *vice versa* (Mata-Alvarez, 2002). Because the batch-fed design produces biogas at an increasing

rate up to about fourteen days, then falls to a steady, lower rate, batch feeding is often best done with several reactors working out of phase for a more continuous input of feedstock and output of gas (Mata-Alvarez, 2002).

Batch reactors generally produce less biogas than a continuously-fed reactor handling the same volume of feedstock in a given time (De Baere and Boelens, 1999). It is possible that this poor performance is due to channelling of the leachate, rather than it spreading and flowing evenly through the feedstock. There is also the possibility of clogging of the floor channels required for collection of the leachate.

Multi-stage anaerobic digesters (Figure 1.6) use two or more digester vessels in series in an attempt to separate the hydrolysis and acidogenesis reactions from the acetogenesis and methanogenesis reactions. They are more complicated and expensive to build than a single stage system. Multi-stage anaerobic systems have been described since the 1970's (Pohland and Ghosh 1971; Ghosh *et al.* 1975) and attempt to separate the hydrolysis/acidification processes from the acetogenesis/methanogenesis processes, as these do not share the same optimum environmental conditions (Ghosh *et al.* 1982; Liu *et al.*, 2006; Zoetemeyer *et al.*, 1982). Multi-stage reactors are usually only two stages. A multi-stage system can improve the stability of the process compared to one stage systems, particularly when digesting easily hydrolysable or high strength feedstocks (Bouallagui *et al.*, 2005; Ghosh *et al.* 1982; Mata-Alvarez, 2002). Instability can be caused by fluctuations in organic loading rate, heterogeneity of wastes or excessive inhibitors. Multi-stage systems provide some protection against a variable organic loading rate as the more sensitive methanogens are buffered by the first stage. Thus, the material passing from the first stage to the second stage has become homogenised and therefore more stable (Mata-Alvarez, 2002). However, multi-stage digesters are more expensive to build and maintain, but are generally found to have a higher performance than single stage digesters. For instance, Ghosh and Henry (1981) found that during conventional single stage digestion of soft drink waste in a 5 litre digester, gas production almost completely ceased at a hydraulic retention time of 7.1 days and a feed chemical oxygen demand of 38,000 $mg.L^{-1}$. In a later publication, Ghosh *et al.* (1985) fed similar soft drink waste to a two stage process consisting of a completely mixed first stage of 2.5 litres and an upflow filter second stage of 5.5 litres. The two stage process showed stable methane production from the second stage at a retention time of 7.4 days and a feed chemical oxygen demand of 45,000 $mg.L^{-1}$. In a comparison of one and two stage thermophilic reactors treating cattle manure (Nielsen

et al., 2004), it was found that the two-stage digester had a 6 % to 8 % higher specific methane yield and a 9 % more effective volatile solids removal than the conventional single-stage reactor. Liu *et al.* (2006) found a 21 % increase in methane yield in a two-stage reactor when compared to a single stage reactor, both operating on municipal solid waste. It is more likely for complete mix, one-stage reactors to suffer from short-circuiting than multi-stage systems. Short circuiting is where the feedstock passes through at a shorter retention time than is required, reducing biogas yield and preventing complete sanitization of the material. The use of a pre-chamber in the reactor can reduce the effect of short circuiting, which is effectively a similar approach to a multi-stage digester.

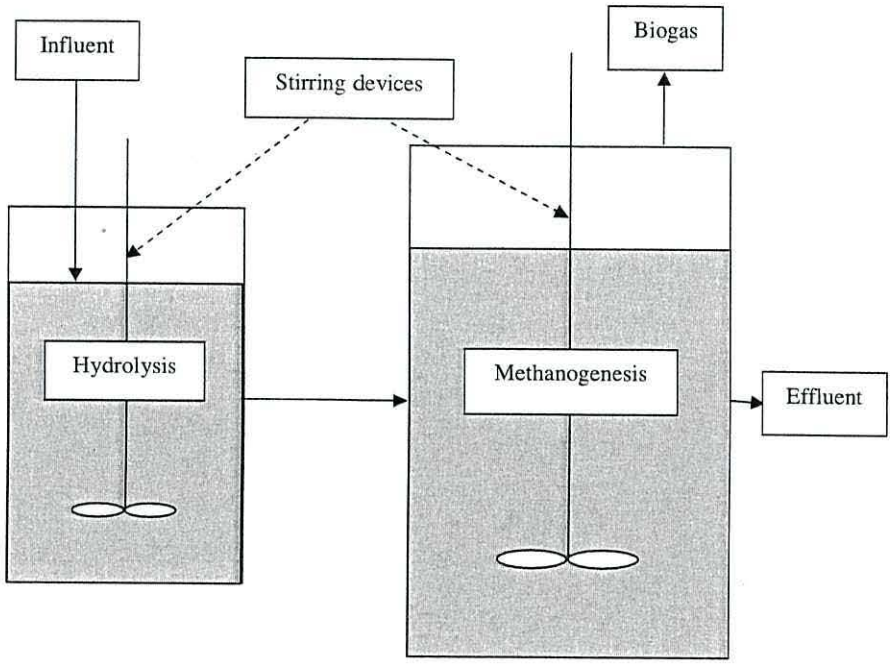

Stages can be of CSTR or plug flow design.In this case, both are CSTR with mixing characteristics similar to Figure 1.3 in each vessel.

Figure 1.6. Two-stage anaerobic digester.

1.5 Mixing

In addition to basic reactor design, the contents of most anaerobic digesters are mixed to ensure efficient transfer of organic material for the active microbial biomass,

to release gas bubbles trapped in the medium and to prevent sedimentation of denser particulate material. Mixing does not always take place continuously; it is often intermittent and may be active several times a day or several times an hour, with energy inputs from 10 to 100 Wh m^{-3}, which is determined by the type of reactor, the type of agitator used and the total solids value of the feedstock (Burton and Turner, 2003). The method of mixing employed can vary greatly (Karim *et al.*, 2005). To mix the material within the reactor, propellers can be used if the feedstock is of a suitably low viscosity. Some pilot scale reactors have used a screw in a central tube to give downwards movement, and some European manure digesters use a similar principle to give upwards movement from a propeller located at the bottom of the digester, through a central draught tube. To prevent the need for moving parts within the reactor, the recirculation of biogas through the bottom of the reactor or hydraulic mixing by recirculation of the digestate with a pump can be used to achieve adequate mixing.

Mixing systems not only affect the digestion process but are often expensive to install, maintain and run. Therefore an efficient mixing system will be beneficial in terms of productivity and cost. A certain degree of mixing is necessary for presenting substrate to the bacteria, but excessive mixing can reduce biogas production. It has been shown that low speed mixing conditions allowed a digester to better absorb the disturbance of shock loading than did high speed mixing conditions (Gomez *et al.*, 2006) and reducing the mixing level improved performance and could also stabilise a continuously-mixed unstable digester (Stroot *et al.*, 2001).

The reason for excessive mixing having a negative effect is unclear but the formation of anaerobic granules has been shown to be of great consequence in anaerobic digestion. It has been postulated that propionate oxidising bacteria and methanogenic archaea live in close proximity in granules (de Bok *et al.*, 2004) with H_2 and formate as electron carriers. For the reaction to be energetically thermodynamically feasible, concentrations of the electron carriers need to be low and therefore the high rate of propionate conversion observed can only be explained by the short diffusion distance possible in obligate syntrophic consortia. Excessive agitation can disrupt the granule structure, reducing the rate of oxidation of fatty acids which can lead to digester instability (McMahon *et al.*, 2001). Extracellular polymeric substances (EPS) are a combination of proteins and carbohydrates which are responsible for the formation of granules (Liu *et al.*, 2004). Measurement of EPS can be indicative of the state of granule formation in a digester, as has been shown with the anaerobic digestion of cattle

manure where an increase in mixing decreased the amount of extracellular polymeric substances found. This would suggest that minimal mixing produced larger anaerobic granules as greater quantities of EPS are required to maintain their structure (Ong *et al.*, 2002). Combining research on mixing with biomass support media could be an important area of for digester optimization as the support media could provide a safe anchorage for the granular microbial communities, allowing a high-shear type of mixing that would increase soluble COD (Pinho *et al.*, 2004) without disruption of the colonies.

The efficiency of a reactor and its mixing can be measured by hydrodynamic studies, which is important to determine if a reactor vessel is operating to its full capability (Levenspiel, 1999). Hydrodynamic studies use easily detectable tracers, typically Li^+ in anaerobic digestion (Olivet *et al.*, 2005) as this is non-toxic to the process in low concentrations and not likely to be present in any significant concentrations in most feedstocks (Anderson *et al.*, 1991). Li^+ is added to the feed as $LiCl_{(aq)}$ and output samples are periodically measured for Li^+. Analysis of the residence time distribution (RTD) curve which can be calculated from the Li^+ concentration profiles will reveal any dead-zones or areas within a reactor that are not mixing well and therefore not receiving fresh substrate, and also any short-circuiting or channelling where feedstock is not being distributed throughout the digester but taking a more direct route between the input and output.

Examples of systems with optimal flow include the continuously stirred tank reactor (CSTR) where incoming material is dispersed evenly throughout the vessel by perfect mixing and the plug flow reactor (PFR) where material moves through the vessel as a coherent plug with no mixing with the existing vessel contents in the axial direction. Non-ideal flow models include the axial dispersion system, which is essentially a plug flow reactor with axial diffusion and the tanks in series which describes the behaviour of a series of continuously stirred tank reactors (Levenspiel, 1999).

1.6 Immobilisation of microbial biomass

Immobilisation of microbial biomass can involve the use of an inert or degradable medium to which the microbial populations attach, for example anaerobic filter reactors (AF). Another method of immobilising biomass is to take advantage of the natural tendency of cells to form dense granules which settle in the digester, for example the upflow anaerobic sludge blanket reactors (UASB). Both of these methods

reduce the amount of micro-organisms washed out of the digester. This practice has long been in use in the treatment of waste water, particularly waste water from industry where the large throughput volumes would otherwise require a very large reactor. Clogging of the support medium can be a problem with feedstocks of high total solids value, and fixed film reactors are considered unsuitable for feedstocks greater than 2 or 3 % total solids, a problem which has been overcome by using an anaerobic hybrid reactor (AHR) which combines the suspended granule principle of sludge blanket type reactors in the bottom part with an anaerobic filter in the upper part (Demirer and Chen, 2005).

Microbial support materials can be either inert or degradable, in the latter case they act as part of the feedstock. The use of straw as a biofilm carrier in a packed bed was found to have a greater methane production than a glass packed bed or suspended plastic carriers (Andersson and Bjornsson, 2002). This research was carried out on a synthetic substrate resembling leachate from the primary stage of hydrolysis of crop residues. It has been reported that gas production rates of up to 3 m^3 m^{-3} d^{-1} were attained when using synthetic liquid feedstock and green plants as a support medium (Chanakya *et al.*, 1998). A comparison of the performance of digesters using carbon filter, rock wool, loofah sponge and polyurethane foam as support media found the loofah sponge produced the highest methane yield (Yang *et al.*, 2004). Polyurethane foam was a popular support material in the 1980s (Bossier *et al.*, 1986; Fynn and Whitmore, 1982; Fynn and Whitmore, 1984; Poels *et al.*, 1984), and appears to be of interest again in current research (Damasceno *et al.*, 2007; Fazolo *et al.*, 2007; Pinho *et al.*, 2006; Yang *et al.*, 2007). Pored glass material (75 % porosity) and PVC (porosity 90 %) used for support were found to have a chemical oxygen demand removal of up to 77 % compared to 57 % with smooth PVC (porosity 75 %) in laboratory scale reactors using artificial substrate (Show and Tay, 1999). Clay mineral support has been shown to be more efficient in anaerobic digestion than the support free control (Maqueda *et al.*, 1998), and the best COD removal was experienced with sepiolite and stevensite. It was also suggested that these clays stimulated anaerobic digestion by release of Fe^{3+}, Co^{2+} and Ni^{2+}. Other porous materials successfully used as a microbial support in recent research include activated carbon and porous stone (Mijaylova-Nacheva *et al.*, 2006) and sintered glass (Breitenbucher *et al.*, 1990; Perez *et al.*, 2006). The growth of micro-organisms on open-pore sintered glass material was found to start in the crevices of the material at first, where they were protected from shear forces (Perez *et al.*, 1997). Pore

size distribution in the support media is a key issue: a comparative study of pore size in polyurethane foam media in 300 ml fixed and fluidised bed reactors found that foam with 20 cells per 25 mm had a higher methane production than foam with 13 cells per 25 mm, and also that the fixed bed reactors outperformed the fluidised bed reactors in terms of methane production (Yang *et al.*, 2004).

It should be noted that many non-porous materials have also been used in earlier laboratory scale investigations, including glass beads (Salkinoja-Salonen *et al.*, 1983), clay, sand and a number of different plastics (Nebot *et al.*, 1995).

1.7 Temperature

Anaerobic digestion can take place at psychrophilic temperatures below 20°C (Bouallagui *et al.*, 2003) but most reactors operate at either mesophilic temperatures or thermophilic temperatures, with optima at 35°C and 55°C respectively. The structures of the active microbial communities at the two temperature optima are quite different. A change from mesophilic to thermophilic temperatures (or *vice versa*) can result in a sharp decrease in biogas production until the necessary populations have increased in number. Even small changes in temperature, from 35° C to 30° C and from 30° C to 32° C have been shown to reduce biogas production rate (Chae *et al.*, 2008). Studies of both mesophilic and thermophilic digesters have conflicting results: Gannoun *et al.* (2007) examined the anaerobic digestion of combined olive mill and abattoir waste water at 37° C and 55° C and found that the thermophilic reactor produced a higher COD removal and biogas yield than the mesophilic reactor, and could sustain this at a high organic loading rate. During batch digestion of vegetable waste and wood chips, more rapid degradation of fatty acids was found at 55 ° C than at 38 ° C, and also 95 % of the methane yield was realised after 11 days under thermophilic conditions compared to 27 days under mesophilic conditions (Hegde and Pullammanappallil, 2007). It has also been shown that the net energy output from 18 litre thermophilic digesters was 427 kj per day higher than that produced by mesophilic digesters (Fezzani and Ben Cheikh, 2007). However, Parawira *et al.* (2007) compared two-stage digesters of mesophilic – mesophilic, mesophilic – thermophilic and thermophilic – thermophilic configurations treating potato waste and found that the methane yield was higher in the mesophilic second stage than the thermophilic second stage, but the thermophilic second stage reactors could manage a shorter retention time.

Table 1.2. Optimal growth temperatures for some methanogenic bacteria (Gerardi, 2003).

Temperature range	Genus	Optimal temperature (°C)
Mesophilic	*Methanobacterium*	37-45
	Methanobrevibacter	37-40
	Methanosphaera	35-40
	Methanolobus	35-40
	Methanococcus	35-40
	Methanosarcina	30-40
	Methanocorpusculum	30-40
	Methanoculleus	35-40
	Methanogenium	20-40
	Methanoplanus	30-40
	Methanospirillum	35-40
	Methanococcoides	30-35
	Methanohalophilus	35-45
Thermophilic	*Methanohalobium*	50-55
	Methanosarcina	50-55

There is also evidence that mesophilic temperature digesters have improved degradation rates when compared with thermophilic digesters. For instance, experiments with proteinaceous wastewater using 2.8 l UASB laboratory scale reactors under mesophilic (37° C) and thermophilic (55° C) conditions showed that the mesophilic reactor removed *ca.* 84 % of COD whereas the thermophilic reactor removed only 69 – 83 % (Fang and Chung, 1999). COD is a good indicator of the degree of completeness of the degradation process, as any undigested material will require oxygen (in an aerobic environment) to complete degradation.

It must also be remembered that an increase in methane yield or production rate from a thermophilic process has to be balanced against the increased energy requirement for maintaining the reactor at the higher temperature. This is not often an important consideration when the biogas produced is used for the generation of electricity, as heating the reactor is accomplished by routing the waste heat from the gas engines to heat exchangers within the reactor, and the engines generally produce more

heat than the reactor requires. Surplus heat could theoretically be sold to local homes or businesses but the expense and practical difficulties involved make this practice rare. The surplus heat is therefore usually wasted. Table 1.2 illustrates the optimal growth temperature of some methanogenic bacteria. It is clear that the optimum temperature for methanogenesis may not necessarily be the optimum for other processes in anaerobic digestion, such as hydrolysis or acidification. Thus, multi-stage digesters could possibly be used for temperature optimisation of the separate processes taking place in the respective tanks.

1.8 pH and buffering capacity

The ideal pH range for anaerobic digestion is very narrow: pH 6.8 – 7.2. The growth rate of methanogens is greatly reduced below pH 6.6 (Mosey and Fernandes, 1989), whereas an excessively alkaline pH can lead to disintegration of microbial granules and subsequent failure of the process (Sandberg and Ahring, 1992). Although the optimal pH of methanogenesis is around pH 7.0, the optimum pH of hydrolysis and acidogenesis has been reported as being between pH 5.5 and 6.5 (Kim *et al.*, 2003; Yu and Fang, 2002). This is an important reason why some designers prefer the separation of the hydrolysis / acidification and acetogenesis / methanogenesis processes in two-stage processes.

Buffer capacity is often referred to as alkalinity in anaerobic digestion, which is the equilibrium of carbon dioxide and bicarbonate ions that provides resistance to significant and rapid changes in pH, and the buffering capacity is therefore proportional to the concentration of bicarbonate. Buffer capacity is a more reliable method of measuring digester imbalance than direct measurements of pH, as an accumulation of short chain fatty acids will reduce the buffering capacity significantly before the pH decreases. Increasing a low buffer capacity is best accomplished by reducing the organic loading rate, although a more rapid approach is the addition of strong bases or carbonate salts to remove carbon dioxide from the gas space and convert it to bicarbonate, or alternatively bicarbonate can be added directly (Guwy *et al.*, 1997). Direct bicarbonate addition is more accurate as converting carbon dioxide to bicarbonate will require a time lag for gas equilibrium to occur which could result in over-dosing. It has also been demonstrated that the inoculum-to-feed ratio can be modified to maintain a constant pH (Gunaseelan, 1995).

1.9 Short chain fatty acids

Short chain fatty acids are a key intermediate in the process of anaerobic digestion and are also capable of inhibiting methanogenesis in high concentrations. Anaerobic processes will alter the pH, particularly the production of fatty acids, and it has been shown that fermentation of glucose is inhibited at total VFA concentrations above 4 g. l^{-1} (Siegert and Banks, 2005). Acetic acid is usually present in higher concentrations than other fatty acids during anaerobic digestion (Wang *et al.*, 1999), but propionic and butyric acids are more inhibitory to the methanogens. Propionic acid concentrations over 3000 $mg.L^{-1}$ have previously been shown to cause digester failure (Boone and Xun, 1987) but in a more recent study, Pullammanappallil et. al. (2001) found that propionic acid was an effect rather than a cause of inhibition of anaerobic processes. Monitoring of fatty acids, particularly butyrate and isobutyrate has been demonstrated to indicate process stability (Ahring *et al.*, 1995) as an increase in fatty acids can be indicative of an overload of the organic loading rate. Essentially, the reason here is that the methanogens will not be able to metabolise the acetate produced by the acetogenic organisms until the number of methanogenic organisms has increased sufficiently. This is especially true of feedstocks which are rapidly hydrolysed. With poorly-degradable feedstocks, the hydrolysis stage is more likely to be the limiting step. Inhibitors of methanogenesis such as excessive fatty acids, hydrogen sulphide and ammonia are toxic only in their non-ionised forms. The relative proportion of the ionised and non-ionised forms (and therefore toxicity) is pH dependant. Ammonia is toxic above pH 7; volatile fatty acids and hydrogen sulphide are toxic below pH 7 (Mata-Alvarez, 2002).

1.10 Feedstocks

The direct comparison of biogas production from different feedstocks is difficult as performance data for specific types is often produced under a wide variety of experimental conditions (e.g. mixing regime, temperature, total solids, volatile solids, hydraulic retention time). For this reason, it is better to compare feedstocks by their ultimate methane yield (B_0), determined by the biochemical methane potential (BMP) assay (Owen *et al.*, 1979). The BMP assay provides information on the potential extent and rate of methane production available from a specific feedstock.

1.10.1 Municipal solid wastes

Municipal solid wastes (MSW; Table 1.3) are perhaps the most variable feedstock as the methane yield value depends not only on the sorting method, but also the location from which the material was sourced and the time of year of collection. Summer waste collections will often have a larger proportion of garden wastes, which have a lower ultimate methane yield. Different locations also have lifestyle and cultural differences, in terms of both recycling practices and the type of food waste produced. The data in Table 1.2 show that meat scores highest in the BMP assay amongst the Korean MSW for the figures presented (Cho *et al.*, 1995), but will not represent a significant proportion of the waste if a society is largely vegetarian. If MSW is not separated at source, a considerable amount of pre-processing is required to remove plastics, metals, glass and any other objects not suitable for anaerobic digestion. This can be done by hand or mechanically, the mechanised method consisting of screening, pressing and pulping. Another form of municipal or industrial waste is sewage sludge from the treatment of waste water. This is an easily-degraded material, so more of the organic matter is available for anaerobic decomposition. It therefore has a higher ultimate methane yield.

1.10.2 Biomass

Biomass (Table 1.4) is a promising feedstock for anaerobic digestion. Grasses, including straws from wheat, rice and sorghum are a plentiful supply of biomass, much of which is a waste product of food production. B_0 values are typically high from these feedstocks, although the high proportion of recalcitrant materials often requires pre-treatments to fully realise the potential yield (Lissens *et al.*, 2004; Mishima *et al.*, 2006; Petersson *et al.*, 2007). Harvesting time can also significantly affect the biogas yield of plants, as demonstrated by Amon *et al.* (2007) where maize crops were harvested after 97 days of vegetation at milk ripeness, 122 days of vegetation at wax ripeness and 151 days of vegetation at full ripeness. The maize varieties produced between 9 and 37 % greater methane yields at 97 days of vegetation when compared to 151 days of vegetation.

1.10.3 Fruit and vegetable wastes

Fruit and vegetable wastes tend to have low total solids and high volatile solids, and are easily degraded in an anaerobic digester (Table 1.5). The rapid hydrolysis of

these feedstocks may lead to acidification of a digester and the consequent inhibition of methanogenesis. It was discovered in the late seventies and early eighties that many carbohydrate-rich feedstocks were found to require either co-digestion with other feedstocks or addition of alkaline buffer to ensure stable performance (Hills and Roberts, 1982; Knol *et al.*, 1978). Two stage reactors effectively use the first stage as a buffer against the high organic loading rate which offers some protection to the methanogens. Separation of the acidification process from methanogenesis by the use of sequencing batch reactors has been shown to give higher stability, a significant increase in biogas production and an improvement in the effluent quality when used with fruit and vegetable waste (Bouallagui *et al.*, 2004).

Table 1.3. Methane yields of municipal solid wastes and sewage.

Feedstock		Methane yield m^3 per kg volatile solids (SD in parentheses)	Reference
Municipal solid waste	Cooked meat	0.482	Cho *et al.* 1995
	Cellulose	0.356	
	Boiled rice	0.294	
	Cabbage	0.277	
	Mixed food waste	0.472	
	Mechanically sorted (fresh)	0.222 (0.014)	Owens and Chynoweth, 1993
	Mechanically sorted (dried)	0.215 (0.013)	
	Hand sorted	0.205 (0.011)	
	Yard waste (grass)	0.209 (0.005)	
	Yard waste (leaves)	0.123 (0.005)	
	Yard waste (branches)	0.134 (0.006)	
	Yard waste (blend)	0.143 (0.004)	
	Paper (office)	0.369 (0.014)	
	Paper (corrugated)	0.278 (0.012)	
	Paper (newspaper)	0.100 (0.003)	
	MSW and corn silage	0.110	Forster-Carneiro *et al.* 2007
	MSW and cattle manure	0.030	
	MSW and digested sludge	0.290	
Sewage	Primary sludge	0.590	Chynoweth *et al.* 1993

Table 1.4. Methane yields of biomass varieties.

Feedstock	Methane yield m^3 per kg volatile solids (SD in parentheses)	Reference
Winter rye	0.360	Petersson *et al.* 2007
Oilseed rape	0.420	
Faba bean straw	0.441	
Maize (whole crop silage)	0.390	Amon *et al.* 2007
Winter wheat straw	0.189	
Summer barley straw	0.189	
Sugar beet leaves	0.210	
Sunflower (whole crop silage)	0.300	
Maize (Tonale, early harvest)	0.334 (0.0057)	Amon *et al.* 2007
Maize (Tonale, mid harvest)	0.283 (0.0049)	
Maize (Tonale, late harvest)	0.280 (0.0114	
Maize,	0.313 (0.0214)	
Maize,	0.326 (0.0161)	
Maize,	0.287 (0.0078)	
Maize (PR34G13, early harvest)	0.366 (0.0262)	
Maize (PR34G13, mid harvest)	0.302 (0.0070)	
Maize (PR34G13, late harvest)	0.268 (0.0042)	

1.10.4 Manures

Manures are a plentiful source of organic material for use as feedstock in anaerobic digesters, in England and Wales alone approximately 67 million tonnes are collected annually (Chambers *et al.*, 2000). Using manures for biogas production also reduces the volume of greenhouse gasses normally released during storage (Husted, 1994; Moller *et al.*, 2004). Some BMP assay results for manures are shown in Table 1.5 which illustrate that the methane potential varies widely between livestock types. Factors which contribute to the methane potential of manures are the species, breed and growth stage of the animals, feed, amount and type of bedding and also any degradation processes which may take place during storage (Moller *et al.*, 2004). Farm manures contain concentrations of ammonia which are greater than that necessary for microbial growth and may be inhibitory to anaerobic digestion (Hansen *et al.*, 1998; Sung and Liu, 2003). A high concentration of ammonia can be advantageous when used with other feedstocks which have low nitrogen concentrations. Manures often contain recalcitrant organic fibre which is difficult to degrade anaerobically (Angelidaki and

Ahring, 2000), including variable quantities of straw bedding material, although the volumetric methane yield of bedding straw has been found to be higher than that of the manure solid fraction (Moller *et al.*, 2004). Pre-treatment of the manure to reduce the fibrous particle sizes can improve methane production by up to 20% (Angelidaki and Ahring, 2000).

Table 1.5. Ultimate methane yields of fruit and vegetable wastes and manures.

Feedstock		Methane yield m^3 per kg volatile solids (SD in parentheses)	Reference
Fruit and vegetable wastes	Banana peel (*Robusta* variety)	0.277 (0.007)	Nallathambi Gunaseelan, 2004
	Mango (*Neelum* variety)	0.373 (0.012)	
	Lemon pressings	0.473 (0.011)	
	Rotten tomato (mean of varieties)	0.298 (0.012)	
	Onion outer peel	0.400 (0.014)	
	Cauliflower leaves	0.190 (0.009)	
	Cauliflower stem	0.331 (0.013)	
	Potato peel	0.267 (0.017)	
	Turnip leaves	0.314 (0.010)	
	Radish shoots (pale pink variety)	0.304 (0.012)	
	Garden pea pods (seeds removed)	0.390 (0.013)	
	Carrot (leaves)	0.241 (0.008)	
	Carrot (petiole)	0.309 (0.010)	
	Garden beet (leaves)	0.231 (0.008)	
Manures	Pig	0.356	Moller *et al.* 2004
	Sow	0.275	
	Dairy cattle	0.148	
	Beef cattle	0.328	Hashimoto *et al.* 1981

1.11 Co-digestion

Co-digestion of sewage sludges with agricultural wastes or MSW can improve the methane production of anaerobic digestion processes (Angelidaki and Ellegaard, 2003; Bolzonella *et al.*, 2006; Gomez *et al.*, 2006; Romano and Zhang, 2008) and has been recently reviewed (Alatriste-Mondragon *et al.*, 2006). The co-digestion of cattle manure with MSW (Callaghan *et al.*, 1999; Hartmann and Ahring, 2005) has also been shown to enhance methane production.

A particularly strong reason for co-digestion of feedstocks is for the adjustment of the carbon-to-nitrogen (C:N) ratio. Micro-organisms generally utilise carbon and nitrogen in the ratio of 25-30:1, but C:N ratios can often be considerably lower than this ideal, for example sewage sludge has a C:N ratio of approximately 9:1 (Kizilkaya and Bayrakli, 2005). Feedstocks can vary widely in their C:N ratios, and some reactors are affected more than others by non-ideal ratios. Indeed, the two-stage reactor with biomass retention has been reported to be considered the only type capable of reliable activity with C:N ratios less than 20 (Mata-Alvarez, 2002). Co-digestion of a low C:N ratio feedstock with a high C:N ratio feedstock such as biomass can adjust the ratio closer to ideality.

1.12 Pre-treatments and additives

Pre-treatment of feedstocks can increase biogas production and volatile solids reduction (Tiehm *et al.*, 2001) and increased solubilisation (Tanaka *et al.*, 1997). The use of pre-treatments is particularly useful in the digestion of biomass feedstocks, as these tend to be high in cellulose or lignin. Pre-treatment can break down these recalcitrant polymers physically, thermally or chemically. Additives can enhance the production rate of a reactor or increase the speed of start up, but their additional cost must always be balanced against resultant improvements in efficiency. Pre-treatments are discussed as follows.

1.12.1 Alkali pre-treatment

Alkali treatment can be particularly advantageous when using plant material in anaerobic digestion. Gunaseelan (1994) compared the anaerobic digestion of *Parthenium*, an invasive weed with high lignin content, with and without alkali pre-treatment and found methane production and cellulose reduction were significantly enhanced in the presence of alkali. The degradation rate of paper waste was also found to increase by adding NaOH at 10 % (Clarkson and Xiao, 2000).

Alkali treatments, however, are not without problems. In continuous reactors fed with alkaline-treated samples (whose initial concentration of sodium or potassium was 0.21 mol l^{-1}), acetate and glucose degradation rates were found to fall to 5 and 50 % respectively, due to toxic compounds generated during the saponification reaction (Mouneimne *et al.*, 2003).

1.12.2 Thermal / thermochemical pre-treatment

Thermal pre-treatments are effective at increasing methane production; this is ascribed to thermal hydrolysis. Thus, heating the solid fraction of mixed cattle and swine manure to 100-140° C prior to anaerobic digestion improved methane production and volatile solids reduction in thermophilic continuously stirred tank reactors (Mladenovska *et al.*, 2006). An earlier study of thermal hydrolysis of pig slurry thermally treated using waste heat from biogas utilisation also found significantly more soluble substances after treatment at 80° C than at 60° C (Bonmati *et al.*, 2001). Thermochemical pre-treatments use a combination of heat and chemicals to reduce particle size and enhance solubilisation. On comparing thermal, chemical, ultrasonic and thermochemical pre-treatments of waste activated sludge from a sewage treatment plant in Korea, the thermochemical pre-treatment gave the best results in that the production of methane increased by more than 34 % and soluble COD demand removal increased by more than 67 % (Kim *et al.*, 2003). Thermochemical pre-treatment of chicken manure with NaOH or H_2SO_4 at 100° C was found to increase both the biodegradability and the methane yield (Ardic and Taner, 2005).

1.12.3 Ultrasonic pre-treatment

This technique is commonly used to break down complex polymers in the treatment of sewage sludges. Methane production was found to increase by 34 % with ultrasonic-treated sludge compared to untreated sludge (Kim *et al.*, 2003). Mechanical shear forces caused by ultrasonic cavitation could be a key factor for sludge disintegration, and collapse of cavitation bubbles could significantly alter the sludge characteristics in waste water treatment (Mao *et al.*, 2004).

1.12.4 Particle size

Particle size can affect the rate of anaerobic digestion as it affects the availability of a substrate (*i.e.* the surface area) to hydrolysing enzymes, and this is particularly true with plant fibres: fibre degradation and methane yield improve with decreasing particle size from 100 mm to 2 mm (Mshandete *et al.*, 2006). Maceration of manure to reduce the size of recalcitrant fibres was found to increase biogas potential by 16 % with a fibre size of 2 mm, and a 20 % increase in biogas potential was observed with a fibre size of 0.35 mm, no significant difference was found with fibre sizes of 5-20 mm (Angelidaki and Ahring, 2000).

European Union Animal By-Products Regulation requires particle sizing of less than 12 mm for sanitization by heating at 70° C for 1 h, which has proved successful in reducing pathogens such as *Salmonella* to undetectable levels (Paavola *et al.*, 2006).

1.12.5 Cell lysate

Cell lysate can be used to speed up the hydrolysis of feed material. The activity of intracellular enzymes and stimulating compounds released from the cells can increase methane production by about 60 % in raw sewage sludge (Dohanyos *et al.*, 1997). In this instance, the cell lysate was prepared by a partial mechanical destruction of the sludge by a thickening centrifuge.

1.12.6 Metals

Addition of certain metals to the feed material has been found to increase biogas production. It has been demonstrated that efficient removal of propionate at high levels of volatile fatty acids requires supplementation of Ca, Fe, Ni, and Co in a thermophilic non-mixed reactor (Kim *et al.*, 2002). Anaerobic co-digestion of cattle manure with potato waste was improved in terms of biogas production by the addition of heavy metals at 2.5 $mg.L^{-1}$ rather than 5 $mg.L^{-1}$, with the greatest increase from Cd^{2+} followed by Ni^{2+} then Zn^{2+} (Kumar *et al.*, 2006). Methanogenic cell concentrations in excess of 1.32, 1.13, 0.12, 4.8 and 30 g l^{-1} have been found to be limited by Fe at a concentration of 5 $mg.L^{-1}$, Zn at 1 $mg.L^{-1}$, Cu at 0.1 $mg.L^{-1}$, Ni at 1.2 $mg.L^{-1}$ and Co at 4.8 $mg.L^{-1}$ respectively (Zhang *et al.*, 2003). These metals are used by the organisms as part of their enzyme structure. A novel phosphodiesterase enzyme in *Methanococcus jannaschii* has been characterised, which has an absolute requirement for divalent metal ions, with Ni^{2+} and Mn^{2+} being the most effective (Chen *et al.*, 2004). Nickel sites in the acetyl-CoA decarboxylase / synthase enzyme complex have been identified. This enzyme appears to have an important role in the conversion of acetate to methane (Funk *et al.*, 2004).

1.12.7 Seeding

Digested material from an established reactor or similar materials such as ruminant manure is often used to seed a new reactor, reducing the start-up time. Many reactors use methods of inoculating the fresh material with either digested material or the liquid fraction from the reactor, thus reducing washout of micro-organisms. The

microbial populations available in rumen fluid have been used as a seeding material in anaerobic digestion, often to increase the production of fatty acids from lignocellulosic feedstocks (Hu and Yu, 2005; Hu and Yu, 2006; Kivaisi *et al.*, 1992; Kivaisi and Mtila, 1998). The rumen bacterium *Fibrobacter succinogenes* has shown promise in a fibre liquefaction reactor as part of a larger process in which 70 % food waste, 20 % faecal matter and 10 % green algae were digested, giving biogas yields of up to 90 % conversion of the original organic material (Lissens *et al.*, 2004). A higher reduction in biological oxygen demand (BOD) was observed when swine waste was anaerobically digested with both a commercial seeding material and one derived from chicken manure at 5 ml l^{-1} (Rodrigues *et al.*, 2004). Treatment of manure with the hemicellulose degrading bacterium B4 gave an increase in methane potential of *ca.* 30 % (Angelidaki and Ahring, 2000). Optimisation of seeding is expected to give a constant biogas output during the process stabilisation period (Martin *et al.*, 2003). Some current ideas on seeding optimisation are based on the reaction front hypothesis (Martin *et al.*, 2003) where it is proposed that reactions occur in a defined mobile interface between raw and depleted wastes (Martin, 2001) as a boundary of independent micro-sites within the reactor.

1.13 Monitoring

Monitoring of anaerobic digestion is difficult and a complex, multi-variate process with few reliable on-line (*i.e.* those that monitor the process constantly) sensors for the measurement of important parameters. Even some of the basic measurement parameters can be difficult to obtain reliably over extended time periods as the sensory devices can become blocked or obscured. Advanced devices, such as biosensors can be even more susceptible to fouling.

Many anaerobic digesters have variable feedstock sources, which can cause fluctuations in the chemical composition of the reactor. As a result of poor monitoring systems, most anaerobic digesters are currently run at a less than optimum loading rate to prevent instability occurring in the digester. This instability is often a result of inhibition of methanogens by excess fatty acids (Pullammanappallil *et al.*, 1998). It is therefore important to maintain a balance between fatty acids and the buffering capacity of the system.

Measurement of parameters can take place in either of the two phases:

- Liquid phase: includes volatile fatty acids, pH, alkalinity (buffering capacity), COD, dissolved hydrogen.
- Gas phase: includes total gas production rate, gas composition and also the individual production rates of methane, carbon dioxide, hydrogen sulphide and hydrogen.

1.13.1 Basic sensory devices

Many parameter measurements can be made by simple electrodes or other sensors (e.g. spectroscopic), which need to be cleaned regularly to maintain functionality. Cleaning can be with water, brushing or ultrasonically, and can be automated (Mata-Alvarez, 2002). These types of sensors have been used in many industries; their long-term operation tends to be well understood and they are available at relatively low cost.

Temperature is most often measured with a thermistor, and logic systems use this data in a feedback loop to control the digester heating system. The measurement of temperature is probably the most basic of all, but is of vital importance to anaerobic digestion because methanogenic organisms in particular are sensitive to temperature.

Measurement of pH, conductivity or oxidation / reduction potential is by simple electrodes which functions well if cleaned and calibrated regularly. Gomez-lahoz *et al.* used pH for monitoring anaerobic digestion (2007) and controlled pH by addition of $NaHCO_3$, and Gomec (2006) found enhanced biodegradation rates and reduced digestion times when using pH control for digestion of primary sludge. However, a fall in pH is indicative of a depletion of the bicarbonate buffering capacity and is often considered to be a sign of a failed rather than a failing system. A better use of a pH electrode is the measurement of alkalinity or fatty acids by titration, preferably automated on-line methods (Di Pinto *et al.*, 1990; Feitkenhauer and Meyer, 2003; Feitkenhauer *et al.*, 2002). The various titration methods for anaerobic digestion monitoring have been reviewed by Lahav and Morgan (2004).

1.13.2 Gas phase measurements

Measurement of gas composition can include hydrogen monitoring by electrochemical cells (Mathiot *et al.*, 1992), whilst methane and carbon dioxide can be determined by infrared spectroscopy (Holubar *et al.*, 2002; Liu *et al.*, 2004). Laboratory scale experiments may analyse gas composition by gas chromatograph (Alzate-Gaviria

et al., 2007; Yang *et al.*, 2007; Yu *et al.*, 2002) although this device is too expensive and complicated for industrial use. A continuous method of dissolved hydrogen measurement has been suggested where hydrogen diffuses across silicone tubing and is measured by a trace gas analyzer. In this example, increased hydrogen partial pressure of 6.5-7 Pa indicated the early stages of digester overload, and this correlated with organic loading rate overload (CordRuwisch *et al.*, 1997).

Alkalinity can be measured in the gaseous phase, for example the carbon dioxide flow rate evolving from a stream of sampled solution has been measured (Hawkes *et al.*, 1993). This method eliminates the need for a pH probe, which can be subject to fouling. Gas samples from the digester headspace have been used to measure fatty acids by gas chromatography and flame ionisation detector (Boe *et al.*, 2005).

1.13.3 Infrared spectroscopy

Infrared spectroscopy (IRS) in the mid range has been used to monitor volatile fatty acids, COD, total organic carbon (TOC), and partial and total alkalinity on-line in the liquid phase (Steyer *et al.*, 2002). The results closely followed those obtained with a TOC analyser and a titrimetric analyser, but the authors stated that the instrument required careful calibration using a wide range of sample values. Mid-infrared spectroscopy has also been used to measure sulphate, ammonium and total Kjeldahl nitrogen (Spanjers *et al.*, 2006).

Near infrared spectroscopy (NIRS) operates in the 780-2526 nm wavelength region of the electromagnetic spectrum, which corresponds to overtones that occur at multiples of the fundamental vibrational frequency and also combination bands from vibrational interactions (Reich, 2005). NIRS shows promise as an on-line measurement technique in anaerobic digestion processes because the high water content in digestate samples does not interfere with the spectra. Several parameters can be measured together using a single instrument with no sample preparation once a calibration has been performed with conventional off-line analyses. Changes in propionate concentrations, C:N ratio, failure of stirring and increased foaming have been measured in real time (Hansson *et al.*, 2003), and NIRS in conjunction with electronic gas sensors to quantify microbial biomass by measurement of total phospholipid fatty acids (PLFA) and acetate concentration (Nordberg *et al.*, 2000). Both these previous studies used the organic fraction of MSW as a feedstock. NIRS has also been used to estimate the density of the methanogenic microbes within a digester by measuring the absorption

spectrum peaks of alpha proteins and lipids in the cytoplasm and cell membrane, although this experiment used a pure synthetic substrate (Zhang *et al.*, 2002). NIRS will be discussed in more detail in Chapter 5.

1.13.4 Other sensory devices

These include using existing sensors with modifications and the quantification or activity of methanogenic organisms. Fatty acids have been estimated through the use of a modified nitrate sensor to measure nitrate reduction by denitrifying organisms mixed with partially digested feedstock in an excess of nitrates. The reduced fraction of nitrate is proportional to the biodegradable organic carbon and can be measured by titration (Rozzi *et al.*, 1997).

Biological oxygen demand (BOD_5) is a five day assay for measuring organic matter. Sensors for short term biological oxygen demand (BOD_{st}) have been developed which use either respirometric methods or immobilised aerobic bacteria with an oxygen probe. A dissolved oxygen sensor with an easily-replaceable aerobic bacteria in the form of a paste gave detection linearity over a range of 5–700 mg BOD_5 l^{-1}, ± 7.5% repeatability and ± 7.3% reproducibility (Liu *et al.*, 2004).

COD is a laboratory analysis that, although considerably quicker than BOD, is still too long for on-line measurement purposes. As was the case with BOD, shorter methods have been proposed for on-line measurement of COD, such as reducing the digestion time (Korenaga *et al.*, 1990) or to change the digestion process with the use of different oxidising agents (Meredith, 1990).

There have been several proposed methods to measure methanogenic activity. The MAIA (Methanogenic Activity and Inhibition Analyser) measures the titrant flow rate of acid to a pH statim. The acid is used to neutralise the alkalinity produced by aceticlastic methanogens (Rozzi *et al.*, 2001). A pH statim can be used to predict the response to any reaction involving the production or consumption of H^+, hydroxyl ions, or inorganic carbon chemical species (Ficara *et al.*, 2003).

Hydrogenotrophic methanogenic activity is usually assayed by analysing the gas collected in the headspace of sealed vials by gas chromatography (Mata-Alvarez, 2002). An alternative method has been proposed (Coates *et al.*, 1996) where a pressure transducer monitors the decrease in headspace gas pressure as the hydrogen/carbon dioxide substrate is converted to methane.

Spectrophotometric methods have been used to measure alkalinity in anaerobic digesters (Bjornsson *et al.*, 2001; Jantsch and Mattiasson, 2004), using pH indicators rather than probes. Samples for this technique require some processing and reagents, including centrifugation and the addition of supernatant to a dilute mixture of HCl and pH indicator.

1.13.5 Software sensors

Software sensors are a combination of hardware sensors and an inferential software estimator, which predicts parameters that require expensive equipment or are impossible to measure directly. Software sensors were first conceived in the 1960's, with the estimator providing on-line estimation *via* a mathematical model or algorithm from the measurements supplied by the sensor (Luenberger 1966). Such sensors may be cheaper to buy when compared with more sophisticated devices or perhaps even already installed, and can also be more familiar to operatives in both their operation and maintenance.

Software sensors have been used to monitor anaerobic digestion processes. Some examples include the measurement of inorganic carbon and fatty acids (Bernard *et al.*, 2001) and also in the same system a separate software sensor for estimation of bacterial biomass. The basis of the software sensors is a mass balance based model considering two microbial populations: acidogenic and methanogenic bacteria, and predictions were found to be very close to off-line measurements. A mass balance based model of anaerobic digestion has also been used to design software sensors for measurement of the intermediate alkalinity to total alkalinity ratio, inorganic carbon and fatty acid concentrations in conjunction with adaptive linearising and fuzzy controllers (Bernard *et al.*, 2000).

1.14 Control systems

The main aim of on-line monitoring is to create a closed loop automated control system, where the sensor measurements are read by a decision making element and achieves control *via* operation of actuators. Commercial anaerobic digestion processes are not only lacking in control systems, but the process itself has few potential actuators. Control of the organic loading rate is perhaps the most significant, and control of the mixing frequency is also possible. Controllers can be simple or advanced. Simple controllers are often nothing more than on-off switches, which switch on or off when a

measured parameter deviates from a set point. With advanced controllers, a non-linear process like anaerobic digestion requires a non-linear control strategy. The decision as to which advanced control is most suitable can be summarised as follows (Olsson *et al.*, 2005):

- If a reliable model is available it should be used, for even a linear model is valid around an equilibrium point, but not at a larger range of operating conditions.
- A situation whereby a large amount of data is available but no reliable model and little knowledge of how the process works could be solved by artificial neural networks.
- If there is no data or model but we know how the process works, fuzzy logic may represent a possible solution.

1.14.1 Switching devices

A simple on-off switching device is the most basic of all control systems. The principle behind the design is that actuators are switched when a measured parameter deviates from a set point. This type of control is subject to 'overshoot', where the value of the measured parameter increases or decreases above or below the set point when compared to more advanced methods such as artificial neural networks (Guwy *et al.*, 1997). A control that suffers from overshoot will take longer to reach the set point value, and is also poor at maintaining a steady output as the value may increase and decrease around the set point in an oscillatory pattern.

1.14.2 Proportional integral derivative devices

The proportional integral derivative (PID) controller is a common method of process control in many industries (Astrom *et al.*, 2001). The proportional part subtracts the measured value from the set point to obtain an error. The error is then multiplied by a constant to give a controller output. PID controllers can suffer from a steady state error in which the actual value remains steady but not at the set point. To avoid steady state error, the integral of the error is taken and multiplied by a constant. A steady state error will increase the integral component every time the integral is measured, so a large error will soon add a significant value when multiplied by the integral constant. Finally, the derivative of the error is measured to use the rate of change of the error multiplied by another constant. Tuning the controller for the correct constants can be difficult; using the wrong values can cause overshoot or oscillation of the measured value.

The use of a PID controller in anaerobic digestion for stability control by bicarbonate dosing has been considered a viable option through model simulation (MarsiliLibelli and Beni, 1996) and a PID-controlled heat exchanger has been used to examine temperature oscillations (Femat *et al.*, 2004). It is not always necessary for all three components of a PID controller to be used, and successful control of anaerobic digestion by PI-only controllers (having no derivative calculation) has been achieved using on-line fatty acid titration and methane production rate as input variables and feed rate as a control variable (von Sachs *et al.*, 2003) and also when using effluent COD as the input variable and influent dilution rate as the control variable (Alvarez-Ramirez *et al.*, 2002).

1.14.3 Fuzzy logic

Fuzzy logic is a problem solving control system that can arrive at a definite conclusion from imprecise or vague information, allowing intermediate values rather than simple yes / no evaluations. They are empirically based, using an operators experience rather than an understanding the process. The limits as to what is considered a significant error and a significant rate of change of error are input based on this experience, with gentle transitions between the various error sets. The ability to process vague information makes fuzzy logic ideal for anaerobic digestion, and has featured in several publications (Bernard *et al.*, 2001; Genovesi *et al.*, 1999; Polit *et al.*, 2001).

1.14.4 Artificial neural networks

Artificial neural networks are constructed from a network of interconnected processing elements, the weighting of which can be adjusted as part of the adaptation process. The first layer of processing elements or nodes receives an input from sensory devices, and passes an output to the next layer. This may continue through a cascade of layers until outputs are obtained (Holubar *et al.*, 2002). The adjustment of the weightings is known as the training period (Andrasik *et al.*, 2004), and the magnitude of the various weights can be considered to be the memory of the network. The training period should cover a wide variety of operating conditions to cover all eventualities of normal operation. The method of training that is best suited to anaerobic digestion processes is the feed forward back propagation (FFBP) net which corrects the weights starting in the last layer then working backwards to the input layer (Holubar *et al.*, 2000). A neural network that has been sufficiently trained can be used within a decision

support system to optimise a process. Decision support systems are designed to suit the type of information supplied to them and to efficiently automate a process (Holubar *et al.*, 2002).

Neural networks have been used in anaerobic digestion systems to describe trace gases (Strik *et al.*, 2005), controlling the addition of $NaHCO_3$ buffer (Guwy *et al.*, 1997), digester start up and recovery (Holubar et al., 2003) and advanced control (Holubar *et al.*, 2002).

1.15 Conclusions

1. Separating the hydrolysis and acidification stages from the acetogenesis and methanogenesis stages is important in optimising the anaerobic digestion process.
2. Many anaerobic digesters are simple in design and run well below their potential organic loading rate to prevent overloading which can cause digester failure. In addition, many current full scale monitoring systems give a poor indication of process stability. On-line monitoring of parameters such as buffering capacity can provide the necessary early warning of a potential overload situation or ensure optimal efficiency to maximise yield.
3. . Evidence suggests that minimal mixing in the digester is preferable unless there is some form of microbial support material used which prevents the lost of active microbial biomass.

1.16 Future research

In the context of a rapidly maturing biogas industry in mainland Europe, economic returns are increasingly important. For the future, reactor design needs to increase methane yield from an increasing range of feedstocks and reduce short circuiting, both of which can be accomplished using a multi-stage system or by improving mixing characteristics. Such benefits also include reduction of pathogen content. Design has an effect on mixing and mixing is an important parameter that provides a means of access of substrate to the fermentation organisms and organisms to the substrate (i.e. those that are mobile). The arguments and opportunities of developing a microbial community structure and kinetic perspective based improvement of biogas production are promising. Primarily because evidence suggests that consortia of organisms work together to improve yield and reduce HRT, so mixing has to be good but not too rigorous to disrupt syntrophic activity. Also an obvious way to increase yield

and reduce HRT is to increase the microbial density by immobilisation. However mixing can become more critical as nutrient flows are reduced. Immobilising the microbial biomass has the potential advantages of improved reactor efficiency and reducing fermentation failure. Mixing and microbial immobilisation are studied further in Chapter 6.

Co-digestion studies have recognised ways of improving biogas yield and reducing HRT, often the feedstock should contain some form of ruminant manure which contains high levels of organisms able to hydrolyse lingo-cellulose material. This is the most topical area of research at present because of the increasing use of biomass crops for biogas production in Europe. Such crops offer better biogas yields, but are difficult to hydrolyse completely. Plant material or energy crops produce more methane that manure sources but this is at the expense of higher retention times of often over 100 days. New studies have shown that improved hydrolysis rates are observed with pre-treatments involving chemical e.g. alkali addition, physical in the form of heat and also enzymatic or microbial additions. The latter offers the more economic option because specific organisms can produce the necessary enzymes, but such organisms often need demanding environments to encourage their growth.

Important developments for the future must include monitoring both the hydrolysis and fermentation processes. There are few sensors that are sufficiently robust to monitor on-line, but the use of electrochemical probes and spectroscopic scanning has proved successful. Spectroscopic sensors can be calibrated to observe multiple parameters as proved by the use of NIRS in several studies. The use of NIRS to monitor process stability in terms of alkalinity is investigated in Chapter 5. Gas sensors have been considered more recently as they are not in contact with the fermentation liquid products, but sulphides are know to poison sensor surfaces although there has been some success with heated sensor devices. A software sensor approach, as described in Chapter 4, can be effective and can predict important parameters such as alkalinity or fatty acids; other parameters may also be measured once calibration has been performed.

Control systems that incorporate optimised biogas production are an immediate goal for the near future. Real time measurements that can ensure feedback times of a few minutes at most are able to adjust the feedstock input or physical fermentation parameters. An organic loading rate control system is described in Chapter 4. The lag time of feedstock input to biogas production becomes important and needs to be

considered for new process control designs. Although there are process control systems available they have not been successfully applied at the commercial scale and may reflect the complexity of the multitude of biogas plant designs. The use of a range of process control options needs to be considered and a generic process model, possibly based on theoretical approaches such as the ADM1 model or the dynamic model may be the ultimate objective.

2 Construction of anaerobic digesters

2.1. Introduction

Anaerobic digesters are usually built to a design to suit a particular purpose. The primary concern in this thesis was to build a novel digester that would produce as much useful data as possible, and also be reasonably reliable in operation. The criteria that were considered of primary importance were; digester type (based on the total solids value of the feedstock) and digester size.

The process of anaerobic digestion requires large reactor volumes to be viable on a commercial scale. This can be illustrated by a simple calculation using typical data values of dairy cattle manure feedstock as follows:

A single dairy cow of body weight *ca.* 500 kg will produce 41 litres of excreta per day (West, 1985), and, assuming a hydraulic retention time of 20-25 days (Nielsen, 1985), a working digester volume (excluding gas headspace) of 820-1025 litres will be required per head of cattle. This takes into account only the volume of the excreta as it exits the animal, whereas in many anaerobic digesters, there may be considerable dilution from washing water which further increases the input volume.

This is a major problem for laboratory experiments, where the vast differences in scale can produce results that may not compare well to those found in full scale operations (Melidis *et al.*, 2003). Scale-up of processes changes the physical and chemical parameters that affect the behaviour of microorganisms (Buckland, 1984). This is particularly important with mixing characteristics (Smith *et al.*, 1996) as this is responsible for gas-liquid absorption, fluid shear rates, blending and heat transfer (Oldshue, 1966).

However, the literature has many examples of laboratory scale experiments with volumes of less than one litre (Andersson and Bjornsson, 2002; OKeefe *et al.*, 1996) or a few litres (Nielsen *et al.*, 2004; Rivard *et al.*, 1990; Show and Tay, 1999) and pilot scale experiments at hundreds of litres (Anozie *et al.*, 2005; de la Rubia *et al.*, 2006; Knezevic *et al.*, 1995) or thousands of litres (Mendez *et al.*, 1992; Puhakka *et al.*, 1992; Tilche *et al.*, 1994) in volume. The lack of direct comparison between many of these digesters and full scale operations make the choice of the correct size a difficult one, but it was considered important to build as large a digester as possible in the experiments described in this thesis.

2.2. Materials and methods

2.2.1. Four-stage digester

2.2.1.1. Overview

It was decided to construct a multi-stage anaerobic digester with four separate stages in series, each representing a completely stirred tank reactor (CSTR). The reasoning behind this design was twofold. Firstly, such a design would enable close monitoring of changes and progressions in the anaerobic digestion process as the feedstock moves through consecutive tanks. Secondly, combining CSTRs in series would enable adequate mixing of the individual tanks whilst minimising short-circuiting.

The digester was modified considerably on several occasions to improve reliability. These modifications will be mentioned in each section of the text as necessary. Schematic diagrams of the digesters at 1st June 2005 and 6th June 2006 can be seen in Figure 2.1 and Figure 2.2 respectively.

2.2.1.2. General construction

Four, 90 litre polyvinyl chloride (PVC) containers were used to form the outer water-bath vessels and these were covered with 'bubble wrap' packaging material to provide some heat insulation. Reaction vessels were sixty litre high density polyethylene (HDPE) containers with polyethylene (PE) lids, and were situated inside the ninety litre containers. Vessels were labelled 1-4, *i.e.* the order in which feedstock was passed through.

The ninety litre containers were mounted on an base constructed from a sheet of 18 mm plywood, and a frame of 1 m^3 external dimension built of 50 mm L-section angle iron. The whole apparatus was mounted on four 125 mm diameter rubber-tyred castors. An overhead photograph (Figure 2.3) shows the vessels 1-4 anti-clockwise from top left to top right (pre 26th August 2005).

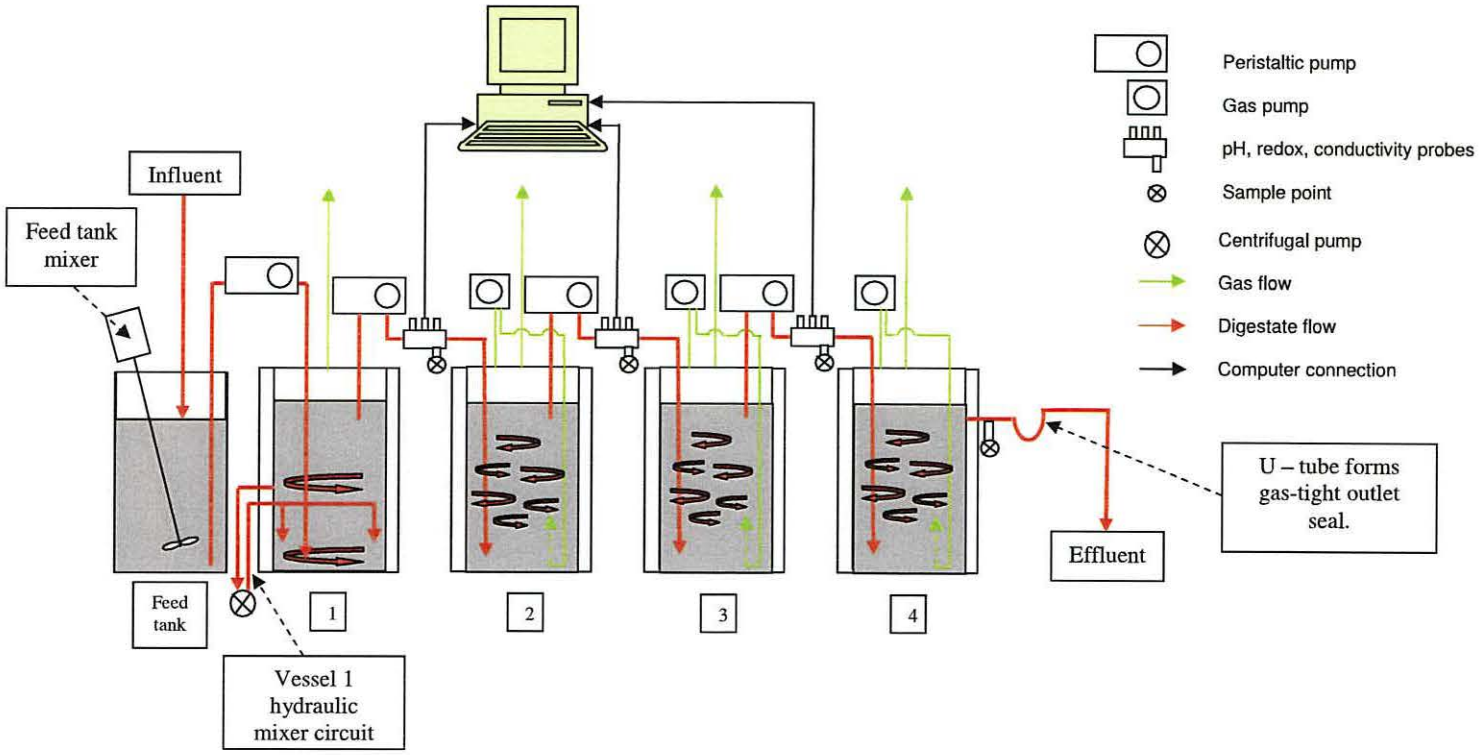

Figure 2.1 Schematic diagram of four stage digester, 1st June 2005.

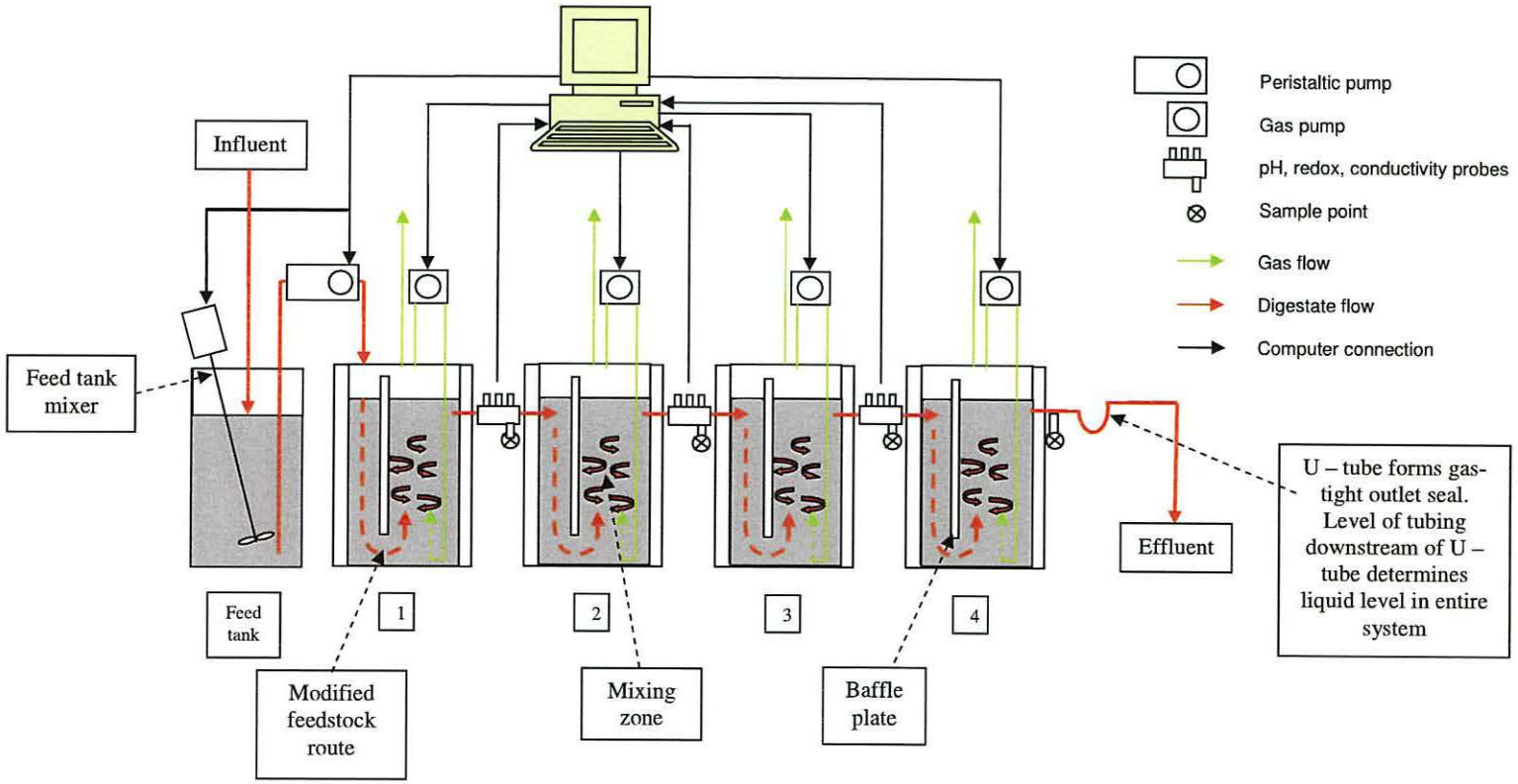

Figure 2.2 Schematic diagram of four stage digester, 6th June 2006.

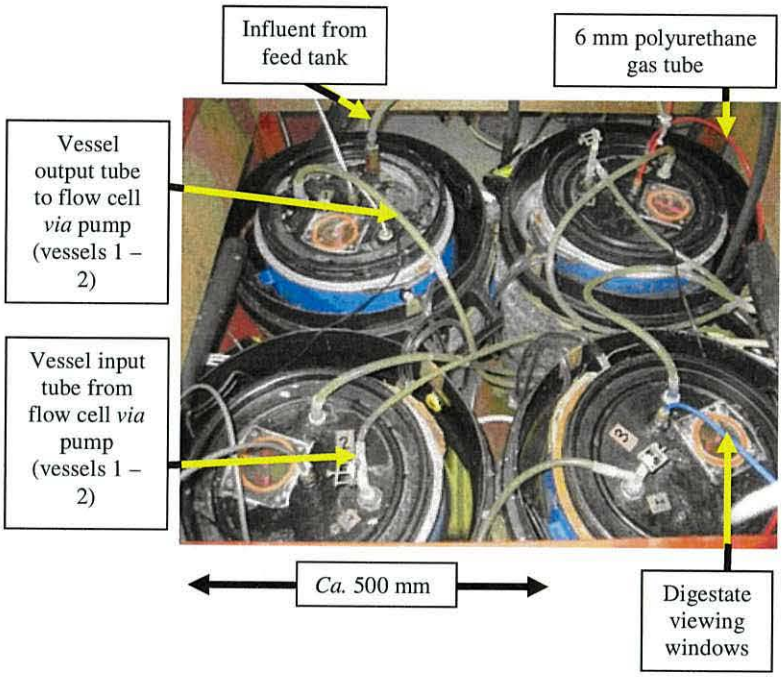

Figure 2.3 Overhead photograph of four-stage anaerobic digester.

2.2.1.3. Mixing systems

Mixing of vessel 1 was initially chosen to be by the hydraulic method as this was thought to be the vessel most likely to suffer a build up of solid material. Inlets were designed to stir-up solids deposited at the bottom of the vessel, using a centrifugal pump (Jabasco Utility 20, Figure 2.4) to remove feedstock from the upper level of the vessel and to then pump it back into the vessel at the bottom through 22 mm tubing (Figure 2.5). The mixing of vessels 2-4 was by recirculation of biogas. Pumping of the biogas (Figure 2.4) was by three Charles Austen A85.S/E pumps (Charles Austen Pumps Ltd, Royston Road, Byfleet, Surrey KT14 7NY) with outputs passed through regulator / flow gauges (0–10 litres per minute, RS No.198-2931). Both hydraulic and gas mixing cycles were controlled by a four-channel Midirex D64 (RS No. 328-077) seven day programmable timer (Figure 2.6). Frequency of mixing was chosen to be one minute of mixing in every hour.

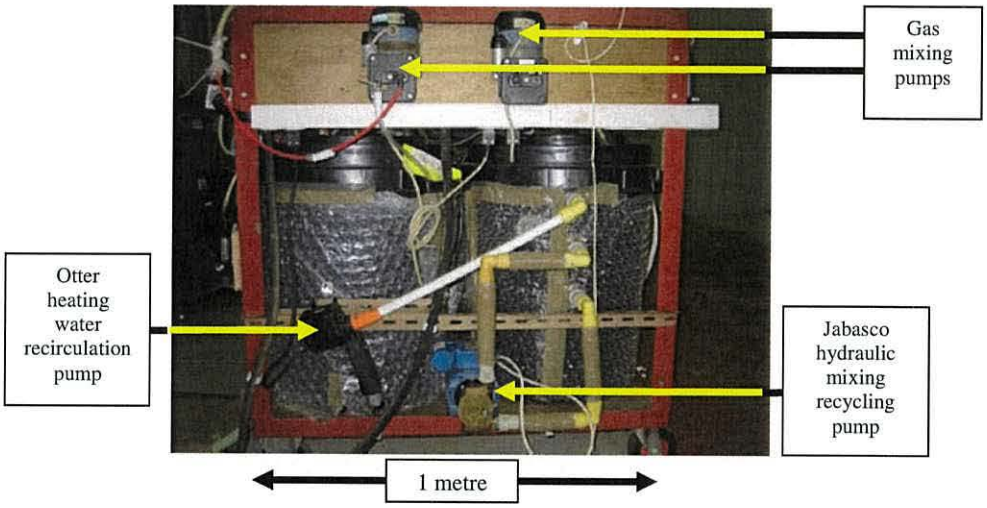

Figure 2.4 Hydraulic mixing, water recirculation and gas mixing pumps.

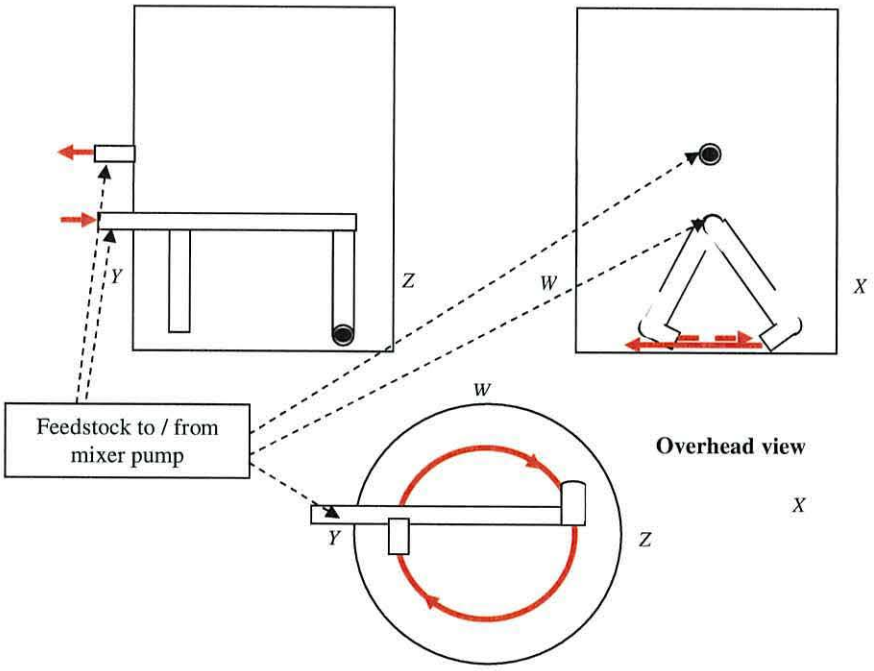

Partially hydrolysed feedstock is drawn from the upper of the two tubes located in the side of vessel 1 by a centrifugal pump, then pumped back *via* the lower tube. This tube splits inside the vessel into two separate pathways, each directing feedstock towards the base of the vessel and then, *via* a 90° bend, feedstock exits at a shallow angle to the vessel base to stir settled solids.

Figure 2.5 Vessel 1 hydraulic mixing details.

Figure 2.6 Midirex four-channel time switch.

The construction of the gas mixing apparatus is shown in Figure 2.7. Two hose-mounting clips were attached on the inside at the bases of sixty litre vessels 2, 3 and 4 to fix the mixing bubblers. The bubblers were 15 mm I.D. plastic tubes, 200 mm long and drilled with 15 holes of 1.5 mm diameter on each side. The tubes were fixed so that the perforations were on the tube sides rather than the top and bottom in an attempt to reduce the amount of particulate matter falling into the holes. Three tube clips running down the inside of the vessel from top to bottom secure the connecting gas hose (PVC, 8 mm ID).

After 28th September 2005, the hydraulic mixing method was abandoned due to continuous problems with blocking of the tubing. This was discovered when very little solid material was seen passing through the transparent tubing that connected vessel 1 to vessel 2 *via* the peristaltic pump, suggesting the mixing of vessel 1 was not effective. A gas mixing pump, as used with vessels 2, 3 and 4 was added to vessel 1 at this time, after which particulate matter was again seen to pass between vessels 1 and 2.

Gas pumping rates were fixed at 5 litres per minute; this was equivalent to recycling the headspace volume every minute of mixer operation and appeared to give adequate agitation (of water) by visual examination. Higher gas flow rates appeared too violent, causing splashing at the surface which was thought could lead to feedstock blocking the gas outlets in the lids. The pump flow rate used was estimated by simple visual observations as data on mixing rates are highly variable in anaerobic digestion. This is discussed further in Chapter 6.

2.2.1.4. Gas and feedstock fittings

Gas fittings are of the Swagelok ™ 6 mm type (Swagelok Bristol, Fourth Way, Avonmouth Way, Avonmouth, Bristol BS11 8DL) and are fitted to the vessel lids. Gas outlets are fitted to the centre of the lids (except vessel 3 lid which already had a hole cut off-centre so this was utilised). Mixing gas inlets were situated towards the edges of the lids, approximately 45° from the internal hose clips to allow for extra length in the hose for lid fitting / removal. Twisting the lid 45° upon removal / refitting prevented the over-long hose becoming kinked (Figure 2.7).

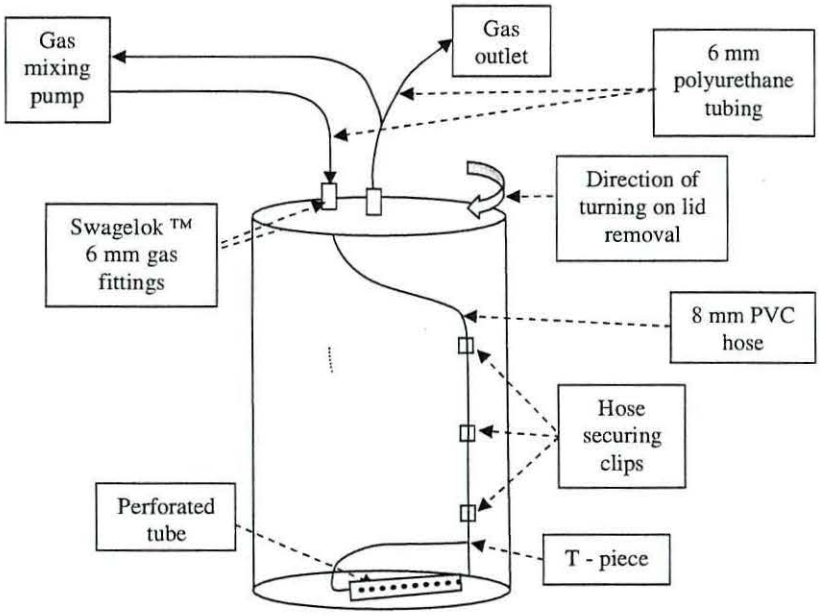

Vessel gas fittings. Twisting the lid 45° upon opening as illustrated allowed the extra length of the mixer tubing to be used to lift the lid sufficiently for access to the lid underside fittings.

Figure 2.7 Vessel gas fittings.

Feedstock fittings were as follows:

Before 31st October 2005, all vessels used 15 mm tank adaptors as inputs, with 15 mm rigid plastic tubes extending to a depth of 500 mm inside the vessels.

Vessel outlets were 8 mm ID tubing, connected to the vessel lids by compression-type tank adaptors, and extended to a depth of 200 mm below the lid on the inside.

The digester was modified considerably on 31st October 2005, by adding baffle plates to reduce the risk of short circuiting and a new method of transferring digestate between vessels. This was a simple overflow method, using 22 mm tank adaptors set in opposite vessel sides, below the liquid level at 160 mm below the lid level. The 22 mm tubing was connected to the flow cells by 10 mm I.D. rubber tubing. The output of vessel 4 dictated the entire system level, and was set at a higher level (135 mm below lid level). Vessel 4 output tubing was made into a 'U' shape to provide a natural gas-tight liquid lock at the output, and the connection of the outlet pipe to the waste tank was set at 80 mm below lid height to maintain the liquid level above the transfer tubing connections (Figure 2.2). The baffles were 310 mm width x 400 mm depth plastic plates mounted 280 mm from the output side (*i.e.* nearer to the input side) and secured by tubing clips and cable ties. A gap of 120 mm was left at the bottom to allow digestate to flow beneath, and a gap of 40 mm below lid level at the top.

2.2.1.5. Heating of the vessels

Heating of the system was by 20 m of 10 mm copper tubing coiled in the bases of the four outer (90 litre) vessels, in the order 1 – 4. Therefore there was approximately 5 m of coiled tubing in the base of each outer vessel. This tubing was connected to a gas central heating boiler *via* a thermostatically controlled valve, equipped with a thumb-wheel temperature setting control and a thermocouple probe to control the flow of heating water. It was initially decided to increase the amount of tubing in contact with the outer vessel water jacket at each consecutive vessel (1 - 4) to allow for the temperature decrease along the pipe length. This would have been difficult to control accurately so equal lengths were used in each vessel and the temperatures were monitored. In the interest of safety, temperature experiments were conducted using water rather than feedstock. It was assumed that digestate would have similar thermal properties.

Temperatures were measured at the top, middle and bottom of the vessels after twenty four, twenty four and a half and twenty five hours of heating to allow time to reach temperature. (The thermostat in all experiments was set to 38° C, thermostat control probe placed in vessel 1).

Temperature variations between vessels were expected as the heating tubing would inevitably be hotter at the inflow end than at the outflow end, so a system was developed to draw water (through 15 mm PVC tubing) from the top of number 1 water-

bath container and pump it to the bottom of number 4 container using an 'Otter Baby' garden pond pump (Figure 2.4). Water levels in the vessels were designed to equalise by gravity through connecting pipes: from the top of vessel 4 to the bottom of 3, from the top of 3 to the bottom of 2, from the top of 2 to the bottom of 1, *i.e.* against the flow direction within the copper heating pipe.

The heating system was tested as follows:

The pump was switched on at 15:45 and switched off at 9:45 the following day (after 18 hours). Temperatures were again measured after this time period.

The recirculating pump was very hot after 18 hours continuous operation and this was a cause for concern. Therefore an on – off regime was tested to allow cooling of the pump motor. Control of this pump was by the Midirex D64 programmable timer switch (Figure 2.6). The pump was switched off after the previous experiment at 9:45 and the temperatures were measured at one and two hours afterwards.

Temperatures were also measured during an experiment with a pumping regime of 1 hour on, 1 hour off.

During normal running, the 'Otter Baby' pump was found to temporarily fail on several occasions. Therefore after 28th September 2005, the 'Jabasco' pump, formerly used for hydraulic mixing, was used instead. This pump has a much higher flow rate and so was tested for use for only one minute of pumping per hour.

2.2.1.6. Calibration of input flow rates

A retention time of 23 days was chosen as a starting point for setting the flow rate of the feed pump. This worked well with the pumping rate data and is a common retention time for anaerobic digesters (Nielsen, 1985).

The pump chosen for feedstock pumping was a Watson-Marlow 323 D/u peristaltic pump (Watson-Marlow Bredel pumps, Falmouth, Cornwall TR11 4RU UK) equipped with three 313x extension pumping heads in addition to the single pump-head supplied with the pump, *i.e.* four heads in total. The pump heads were driven by a common drive shaft and therefore operate at the same rotation speed (Figure 2.8).

Pump flow rates were measured in triplicate using the chosen feedstock, Sow SM16 (Crediton Milling Co. Ltd, Fordton Mills, Crediton, Devon, EX17 3DH) pig meal feedstock at 5 % dry matter with 8 mm I.D. 'Marprene' tubing and 10 mm I.D. silicone tubing. The feedstock was hand stirred during pump testing.

The pump is fully controllable through industry-standard 4 – 20 mA current input for pump rate, and digital inputs for pump on / off and forward / reverse switching. All control inputs are through a 25 pin D-socket, and can be controlled by LabVIEW software (National Instruments Corporation [U.K.] Ltd. Measurement House, Newbury Business Park, London Road, Newbury, Berkshire RG14 2PS) *via* a suitable interface.

During the early stages of the experiment, the remote control capabilities of the pump were not used due to inexperience with the LabVIEW software. Instead, the pump was operated at a constant speed but with the feeding duration controlled by the D64 programmable timer switch. In later experiments, LabVIEW was programmed to include a calculation of pumping duration from an organic loading rate input *via* the user interface. To achieve this, the pump power supply was disconnected from the D64 time switch and instead was connected to one of a set of eight relays (Audon electronics PPO–RL8, rated 3 amps at 230 volts, Audon Electronics, 123 High Road, Chilwell, Nottingham NG9 4AT UK), controlled *via* the computer parallel port.

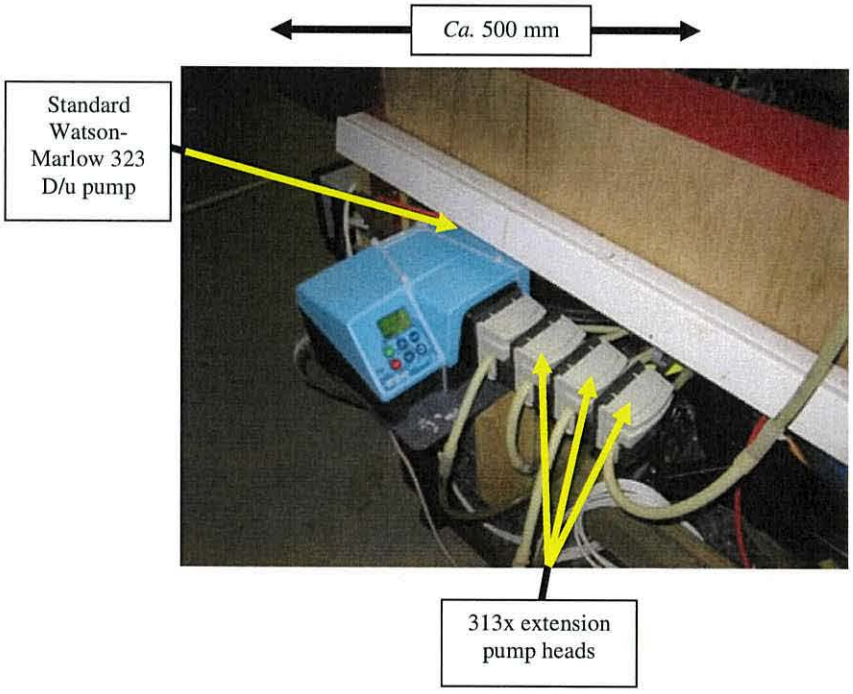

Figure 2.8 Watson-Marlow 323 D/u peristaltic pump.

2.2.1.7. Visualisation of the process

To visually check the liquid level of each vessel, a 70 mm circular window was fitted into each lid. Figure 2.9 shows the clear window and opaque strengthening plate in plan view. Wiper-blades constructed from 8 mm outer diameter rubber tubing over steel wire were used to clear condensation from the windows. (Figure 2.10).

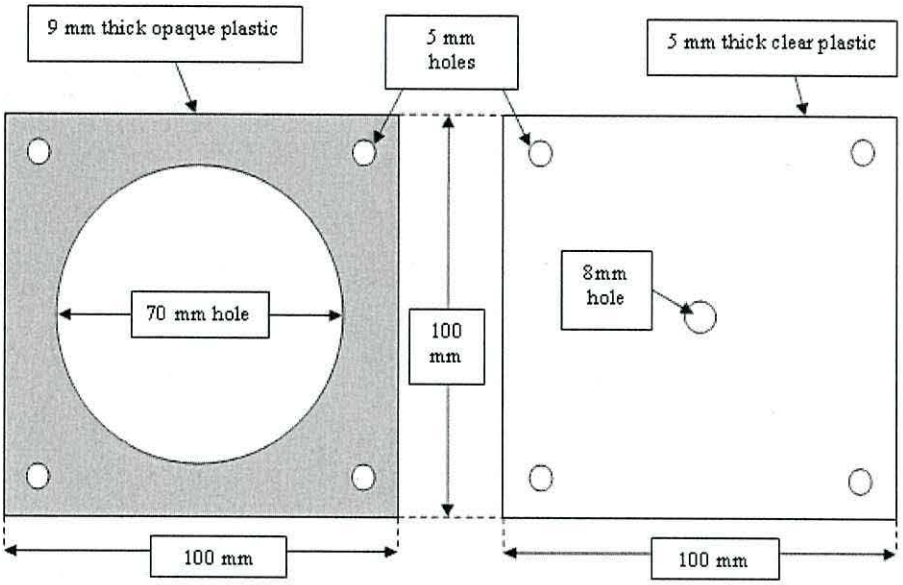

Figure 2.9. Plan view of vessel lid viewing window components.

The wipers were sealed to the window by insertion of the handle-part of the wire into an 8 mm rubber tube, which was bonded to the window with silicone sealant, easily allowing 90 degrees of turning movement of the wiper blade in either direction by twisting of the rubber tube. This arrangement gave a gas-tight fitting without the complexity of rotary seals. To make the digestate visible, submersible 10 watt halogen lights (GET Luneta low voltage IP68) were then attached to the underside of each lid to illuminate the inside of the vessels. The fitted windows and wiper assemblies can be clearly seen in Figure 2.8.

It was found in practice that digestate quickly covered the interior lights due to a small amount of surface splashing during mixing. The window wiping mechanisms were unreliable and prone to leaking. For these reasons, the visualisation option was abandoned after 26th August 2005 and new lids were fitted that did not contain windows.

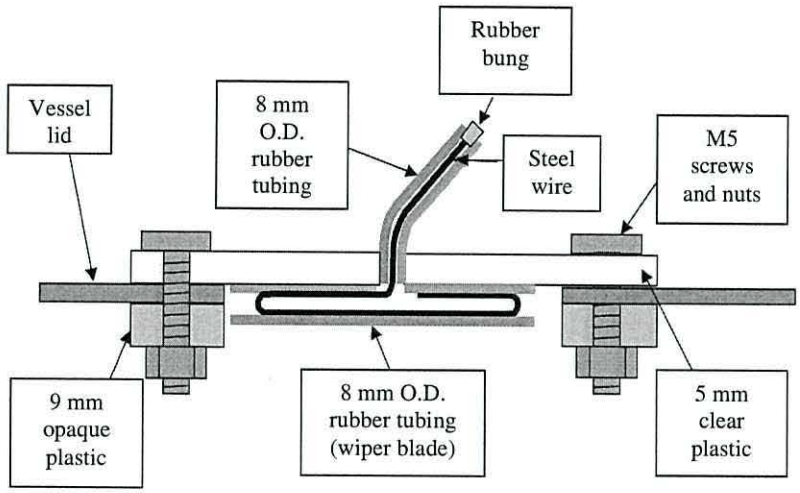

Figure 2.10 Side view of window wiper assembly.

2.2.1.8. On-line measurement of pH, redox potential and conductivity

Measurement of pH, oxidation-reduction potential, conductivity and temperature was by Partech Waterwatch 2610 flow cells, each with a ball-valve outlet for sample collection. One of these is shown in Figure 2.11. Three of these flow cells and their corresponding control / display boxes were used, placed between vessels 1 - 2, 2 - 3 and 3 - 4. Initially, only one flow cell was purchased for evaluation and was placed in the middle of the process (*i.e.* between vessels 2 and 3). These units produce industry standard 4 - 20 mA signals for all four parameters, in addition to a built-in visual display. The outputs were connected to National Instruments SCB68 data acquisition interface voltage inputs (100 kΩ shunt resistors were added to covert the 4 – 20 mA signal to 0 – 5 V), which in turn supplies digital control signals to a National Instruments PCI-6229 M Series Multifunction DAQ Device, installed in a PC computer.

LabVIEW software with NIDAQ Measurement Services Software (for data acquisition), also from National Instruments, were used initially only to monitor *via* on-screen graphs and to store the data at a reduced sample rate of one set of measurements every 100 seconds (graph data updated every second) to make data files a more manageable size.

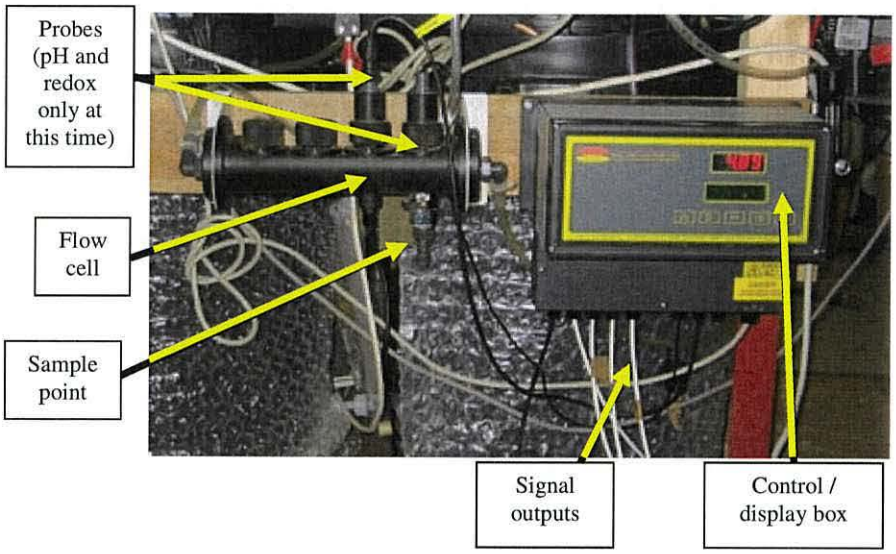

Figure 2.11 Partech Waterwatch 2610 flow cell and control box.

2.2.2. Construction of anaerobic digesters with and without biomass support media

2.2.2.1. Overview

This section describes the construction of single-stage and two-stage digesters for the comparison of the effectiveness of the inclusion of microbial biomass support media when subjected to a variety of mixing frequencies. The experimental work regarding the digesters constructed in this section is discussed in Chapter 6.

2.2.2.2. Biomass support media

The chosen support medium was reticulated polyurethane foam with a polyether polyol additive (Foam Techniques Ltd, 39 Booth Drive, Park Farm South, Wellingborough, Northamptonshire, NN8 6GR) and a pore size of 10 pores per linear inch (*ca.* 2.5 mm diameter). A photograph of a small section of the foam is shown in Figure 2.12. The reticulation process involves heat and pressure to form skeletal foam structures devoid of cell membranes. The open structure has a stated surface area of *ca.* 400 m^2 m^{-3}. The finished material has uses as diverse as an explosion suppressant in fuel tanks and as a filtration medium.

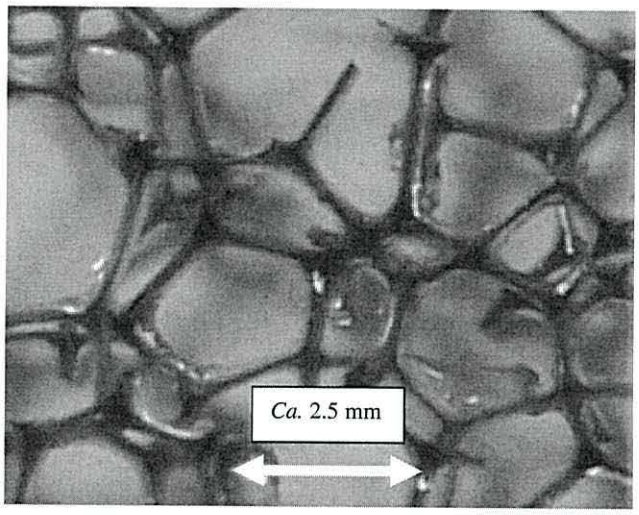

Figure 2.12 Small sample of reticulated polyurethane foam.

The polyurethane foam for the two-stage pilot scale digester had a net volume of 7262 cm^3 and a mass of 179.08 g. Foam for the single-stage experiments had a net volume of *ca.* 497 cm^3 each and masses of 11.99 g for vessel A and 12.18 g for vessel B. The porosity of the foam was calculated by displacement of water (Equation 2.1).

Equation 2.1

303 cm^3 foam – 11 cm^3 water = 292 cm^3 void volume / 303 x 100 = 96.4 % porosity

The foam was also measured for density, using the average density of the single–stage and two-stage digesters as follows (Equation 2.2 density of foam in two-stage pilot scale digester, Equation 2.3 density of foam in single-stage laboratory scale digesters.

Equation 2.2

$$179.08 \text{ g} / 7262 \text{ cm}^3 = 0.0247 \text{ g cm}^{-3} = 24.66 \text{ kg m}^{-3}$$

Equation 2.3

$$\text{Vessel A} = 11.99 / 496.8 = 0.0241 \text{ g ml}^{-1} \text{ x } 1000 = 24.13 \text{ kg m}^{-3}$$
$$\text{Vessel B} = 12.18 / 496.8 = 0.02451 \text{ g ml}^{-1} \text{ x } 1000 = 24.52 \text{ kg m}^{-3}$$

Average foam density = 24.45 kg m^{-3}

2.2.2.2. General construction of single-stage digesters

The single-stage reactors were constructed from four five litre vessels (Figure 2.13). Quickfit glass fittings were used for gas outlet, gas outlet to mixer pump, mixer pump inlet and feedstock in / out. The gas fittings were all adaptors from the vessel-lid neck size of 22 mm to 6 mm to accept polyurethane tubing of the same diameter. The feedstock tube was 8 mm I.D. and extended to a depth of 20 mm above the base of the vessel.

Figure 2.13 Single stage digesters with (left) and without (right) polyurethane foam biomass support media.

Mixing was by gas pumps (Charles Austen D5 DE), modified with short–throw cranks to reduce the pump flow rate from 5 l min^{-1} to 2 l min^{-1} at atmospheric pressure and fitted with PTFE membranes for chemical resistance to hydrogen sulphide and methane. The mixing gas was pumped through sintered glass bubblers situated in the centre of the vessels.

The biomass support media was formed into a cylinder and secured with stainless steel wire. More stainless steel wire was used to support the media by attaching

it to the bubbler. The media was fitted to two of the four vessels, the other two having no support media fitted.

2.2.2.3. General construction of two-stage digesters

The four-stage digester described in section 2.2.1 was simply split into a pair of two-stage digesters; the methanogenesis (second) vessel of each pair was fitted with the support medium. This was designed to fit against the inner wall and baffle plate of the digester vessel, on the outlet side of the baffle as it was found to be too difficult to maintain a tubular foam structure as used with the single-stage digsters (Section 2.2.2.3).

No other physical changes were made to the digesters, but a fourth set of probes was added so that data could be collected at the output of each vessel. The individual probes were identical (Partech Waterwatch 2610) to the others but differed in that they were fitted into a single 'sonde' instead of a flow cell. The sonde is a cylindrical housing for a complete set of probes, designed to be immersed in liquid wastes. This required the construction of a vessel from a plastic bottle to hold the sonde. The top of the bottle was removed and the sonde sealed into place with a silicone sealant. This was placed in-line with the output of the 'with support' methanogenesis vessel. The digested material entered through a 25 mm diameter tank adaptor at the lowest possible position of the bottle side, and exited through a similar fitting at a point that was level with the required vessel output, thereby dictating the overall digester liquid level.

2.2.3. Hydrodynamic study of four-stage anaerobic digester

2.2.3.1. Overview

To fully characterise the physical performance of the four-stage digester a hydrodynamic study was conducted. This would aid in the understanding of the system and reveal any channelling, dead space or short-circuiting, all of which can cause deviations from the ideal flow patterns of plug flow and mixed flow. The residence time distribution (RTD) is also known as the exit age distribution, E, because it is a measurement of the distribution of the times taken for elements of the feedstock to pass through the digester.

The E curve can be compared with theoretical curves for various combinations of compartments and through-flow, and a best fitting model can be found. In the compartment models, the total volume of the vessel can be divided into V_p (plug flow

region), V_m (mixed flow region) and V_d dead region, and the throughflow can be divided into v_a (active flow), v_b (bypass flow) and v_r (recycle flow) (Levenspiel, 1999). Some of the compartment models are illustrated in Figure 2.14, and represent the phenomena of dead space as a separate vessel and bypass flow as a literal bypass route.

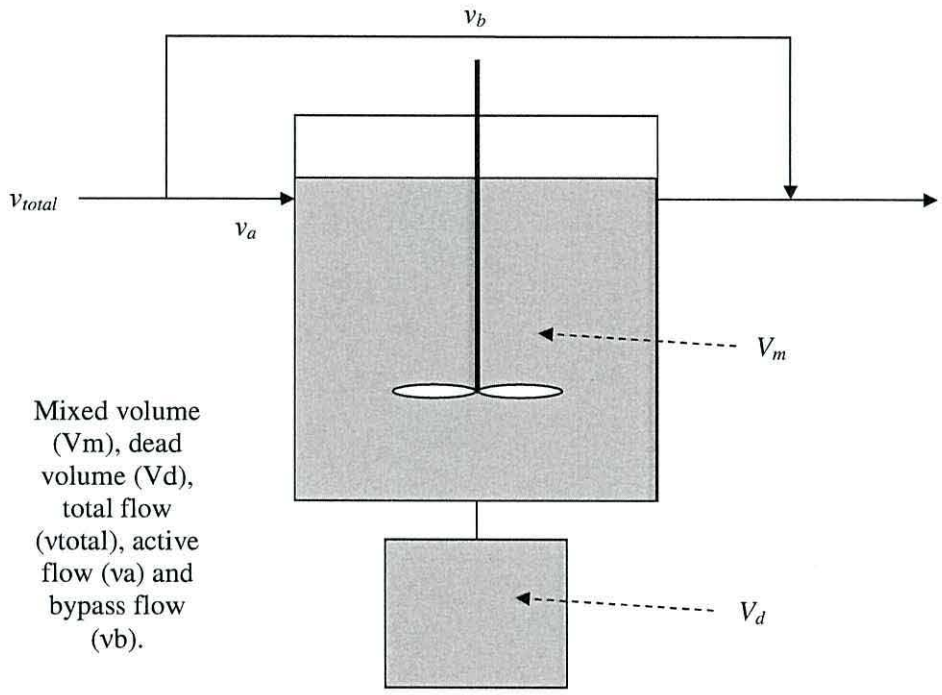

Figure 2.14. Compartment model of a reactor vessel.

An ideal tracer for use in anaerobic digesters is Li^+ as LiCl (Leighton and Forster, 1996; Olivet *et al*, 2005) in a pulse experiment, as lithium is unlikely to be found naturally in the digestate and has a negligible inhibitory effect on anaerobic digestion in very low concentrations. A prolonged lithium concentration of 0.25 g l^{-1} has been found to have a minor inhibitory effect on specific methane activity and no inhibition was found with temporary exposure up to 1 g l^{-1} (Anderson *et al.*, 1991).

2.2.3.2. Loss of lithium

It was believed possible that some of the Li^+ could become adsorbed onto the solid material and therefore not measured after this material was filtered out. Seguret and Racault (1998) have found that lithium was not adsorbed onto microorganisms whereas Olivet *et al* (2005) found a maximum of approximately 10 % lithium adsorbed

onto sludge. It was decided to examine the lithium concentration of samples from a batch experiment over a period of forty days using the available digestate from the four-stage digester. If any loss of lithium was detected after filtering the samples, this would be taken into account in the results.

One litre of digestate from vessel 4 was collected. A sample of 25 ml was collected for measurement as a blank, and 56.53 mg LiCl (AnalaR) was then added to the 1 litre digestate to give a total concentration of 9.2 mg Li l^{-1}. At the same time, a calibration standard was made up at 5 mg.L^{-1} Li^+ in reagent grade H_2O.

The digestate was then incubated at 38° C to mimic the digester conditions. Samples were taken at intervals over a period of 48 days, with the first sample taken immediately after addition of the LiCl. The digestate was shaken vigorously before each sample was taken to ensure a representative sample was obtained.

2.2.3.3. Hydrodynamic study

6 g of LiCl was made up in 250 ml reagent grade H_2O, and was pumped in through the feedstock loading tube by the feed pump. The pump was set to 458 ml per cycle, so as the solution was nearly all added, the container was rinsed with more reagent grade H_2O to ensure practically all LiCl had entered the digester and that no air had entered the system.

In accordance with the inhibitory lithium concentrations of 0.25 g l^{-1} published by Anderson *et al.* (1991), addition of Li^+ to a concentration of < 0.02 g l^{-1} when completely mixed was expected to be of no detrimental effect to the microorganisms and therefore performance of the digester. The initial input concentration of lithium introduced was 3.67 g l^{-1} (6 g LiCl or 0.976 g Li^+ in 250 ml water), but this was diluted the moment it made contact with the digestate, and the input cycle was followed immediately by a mixing cycle to rapidly disperse the solution.

A digestate sample was taken before work commenced as a control and immediately after addition of the LiCl solution, then every thirty minutes afterwards for the first day to ensure that any rapid changes in concentration were measured. Gradually the sampling became less frequent until the system had samples with Li^+ concentrations that were as low as the background measurement taken before introducing LiCl solution. Samples were taken from vessel 1 and vessel 4 outputs. This would give a residence time distribution (RTD) curve for individual vessels and for the four-stage process as a whole.

Samples were centrifuged at 1500 g for twenty minutes and the supernatants filtered through Whatman 542 filter paper (2.7 μm pore size) to prepare the samples for Li^+ measurement by flame photometry.

Samples were diluted 1:4 to increase the volume (a necessary step as the flame photometer required several minutes to obtain a steady reading, during which time several millilitres of sample were used). A standard of LiCl solution was made up at 5 mg Li l^{-1} and a 0 mg Li l^{-1} blank of reagent grade H_2O were used to calibrate the machine. The flame photometer response had already been established as linear for lithium at concentrations from 0 to 15 mg Li l^{-1} in a previous study.

2.3. Results and discussion

2.3.1. Heating of the system

Variation of the temperature distribution in the vessels was measured to the nearest whole 1° C, and an acceptable result was considered to be +/- 1° C of the thermostat value. Temperatures in the 60 litre vessels after 24-25 hours of continuous heating are shown in Table 2.1.

The variations between the three measurements at different depths were all within 1° C (therefore the differences within each vessel were deemed acceptable), even without mixing of the vessel contents. However, the temperature difference between vessels was not acceptable. Temperatures in vessel 1 remained at the thermostat set point (this vessel contained the probe) but temperatures fell through the system, reaching a low of *ca.* 33° C in vessel 4.

As mentioned in the materials and methods section above, this was expected as the heating tubing would be cooler at distances further from the heating boiler. The results of testing the system with a recirculated water jacket for 18 hours are shown in Table 2.2, and demonstrate that this addition would keep the entire system at an even temperature.

The concern over pump over-heating led to an experiment where the temperatures were measured at hourly intervals after the recirculating pump was stopped (Table 2.3). Temperature variations were found to be within +/- 1° C of the set temperature 1 hour after the pump was switched off. This variation was considered acceptable. After 2 hours, however, temperature variations were outside this range and even more so after 3 hours. A 1 hour on, one hour off pumping cycle was therefore selected (Table 2.4) and satisfactory results were obtained.

Table 2.1. Temperatures measured at top, middle and bottom of vessels after 24 to 25 hours of heating, to the nearest 1° C.

Measurement point	24 hours	24.5 hours	25 hours
Vessel 1 top	38° C	38° C	38° C
Vessel 1 middle	38° C	38° C	38° C
Vessel 1 bottom	38° C	39° C	38° C
Vessel 2 top	37° C	36° C	37° C
Vessel 2 middle	37° C	37° C	37° C
Vessel 2 bottom	36° C	38° C	37° C
Vessel 3 top	35° C	36° C	35° C
Vessel 3 middle	35° C	36° C	34° C
Vessel 3 bottom	36° C	36° C	36° C
Vessel 4 top	33° C	33° C	34° C
Vessel 4 middle	33° C	34° C	34° C
Vessel 4 bottom	33° C	33° C	33° C

Table 2.2. Temperatures measured after 18 hours of pumped water jacket recirculation.

Vessel	Initial temperature	Temperature after 18 hours
1	38° C	38° C
2	37° C	37° C
3	35° C	37° C
4	33° C	38° C

Table 2.3. Temperatures measured at times after recirculation pump was stopped.

Vessel	9:45 (Pump off)	10:45	11:45
1	38° C	38° C	38° C
2	37° C	37° C	37° C
3	37° C	37° C	36° C
4	38° C	37° C	36° C

Table 2.4. Temperatures measured during a '1 hour on, one hour off' pumping cycle.

Vessel	13:00 (Pump on)	14:00 (Pump off)	15:00 (Pump on)
1	38° C	39° C	39° C
2	39° C	39° C	38° C
3	38° C	38° C	38° C
4	39° C	38° C	39° C

Reliability problems with the 'Otter baby' recirculation pump led to substitution with a 'Jabasco' pump, which had a much higher flow rate, from October 2005. Temperature variations during a 1 minute per hour pumping cycle were acceptable when measured at 30 minute intervals (Table 2.5) so the 'Jabasco' pump and shorter

pumping time were used without any concern for pump overheating. This method was used in subsequent experiments.

Table 2.5. Temperatures measured during 'one minute per hour on' pumping cycle using the high flow rate Jabasco pump. Pumping starts on each hour.

Vessel	10:00	10:30	11:00
1	38° C	38° C	38° C
2	38° C	39° C	38° C
3	38° C	39° C	38° C
4	38° C	38° C	38° C

2.2.2. Feedstock pumping

The pump was calibrated at speeds up to 120 rpm, which was the highest pump speed that was expected to be required. The maximum recommended pump rate was 50 rpm with 4 heads fitted, although this referred to smaller-bore tubing than the 8 mm used. For longer term usage, a safe maximum of 30 rpm (136.7 ml min^{-1}) would reduce the possibility of damage due to strain on the pump drive. The pump showed good linearity over the range, with an R^2 value of 0.9998 (Figure 2.15).

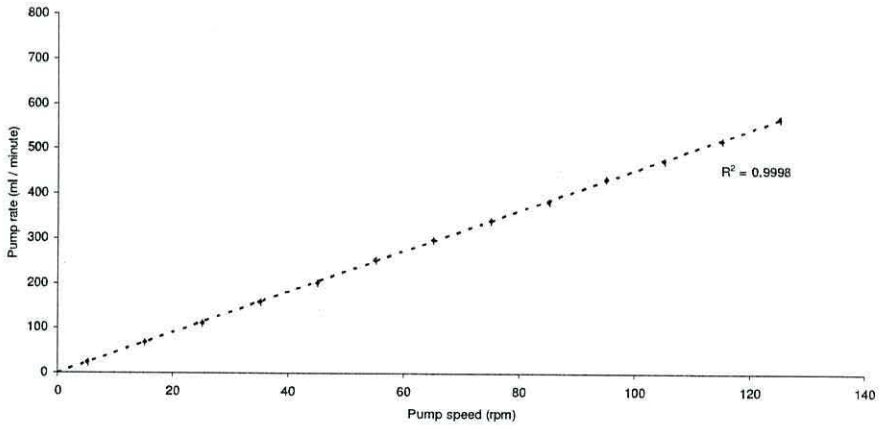

Figure 2.15 Watson-Marlow 323 D/u pumping rate data, 8 mm I.D. Marprene tubing.

Total (liquid) volume of digester is 220 litres; estimated hydraulic retention time for calculation purposes is 23 days. Thus, calculation of flow rate is as Equation 2.4.

Equation 2.4

Estimated flow rate = 220000 ml / 23 days = 9565.217 ml day^{-1} = 6.643 ml min^{-1}.

A flow rate of 399 ml $hour^{-1}$ (6.643 ml min^{-1}) was required, but the minimum flow rate from the pump was 13.4 ml min^{-1}: the minimum pump flow rate was approximately double that required for continuous pumping. However, continuous pumping is not necessary in anaerobic digestion, operation of a feed pump for a short, regular period is sufficient.

Due to many problems with pump lines becoming blocked, it was found that a higher pumping speed reduced the occurrence of blockages. It was also found that at low pump speeds, the particulate feedstock drawn up from the feed tank often settled back down the tube and into the feed tank during pump operation. The result being that the feed entering the digester was estimated at being somewhat less than 5 % total solids, although this was not possible to measure without removing the vessel feed tube and taking a sample, thereby risking the possibility of air entering the system. The transparent tubing used to transfer feed and digestate around the system clearly showed that little particulate matter was present.

From 19th October 2005, the pump rate was set to 30 rpm. It was then decided that the narrow bore (8 mm I.D.) tubing and the lengthy route that the feedstock took between vessels was not suitable for a reliable system. From 31st October 2005, the pump system was removed from between the vessels, leaving just the feed to vessel 1 as a pumped system. The remaining transfer of the partially digested feedstock between vessel 1 and the output was by gravity as described above in section 2.2.1.4, and proved to reduce the frequency of blockages between vessels considerably from almost daily to less than weekly.

However, the narrow peristaltic pump tubing was still a source of blockages. The blockages occurred most frequently where tubes were connected. The feedstock, at 5 % dry material, was not the source of the problem as blockages appeared to result from a 'plug' of particulate matter accumulating at the tube connections after settling between pump operations. As a result of this problem, the Marprene tubing was replaced by 10 mm I.D. silicone tubing, as used for the digestate transfer tubing between vessels. The calibration curve is shown in Figure 2.16. A steeper gradient can be observed when compared with the 8 mm I.D. Marprene tubing in Figure 2.15 as the wider bore tubing increases the flow rate of the pump at a given rotational speed. Similar to the Marprene tubing, the silicone tubing also has a high degree of linearity,

with an R2 value of 0.9999. This remained the method of feeding the digester throughout the experiment from 19th December 2005 onwards.

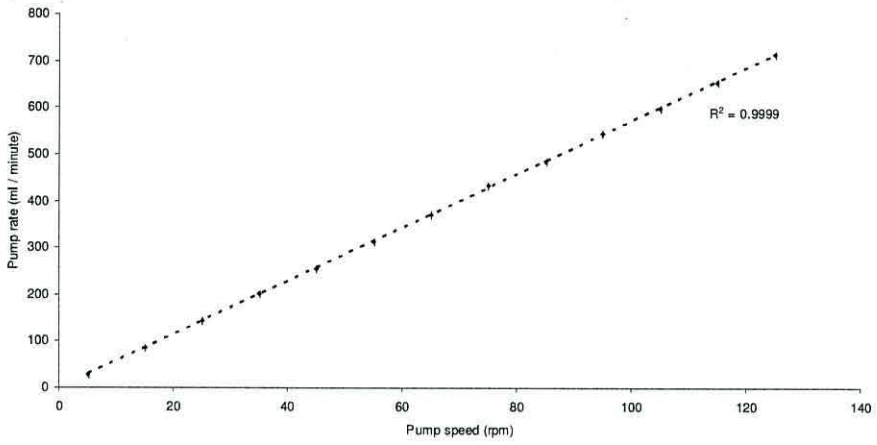

Figure 2.16 Watson-Marlow 323 D/u pumping rate data, 10 mm I.D. silicone tubing.

2.2.3. Loss of lithium over time

The mean Li^+ concentration over the forty eight day period was compared to the initial Li^+ concentration of 9.2 $mg.L^{-1}$ and found to have a mean of 9.12 $mg.L^{-1}$ with a standard deviation of 0.12. The results are displayed in Figure 2.17. The difference between the input lithium concentration and that obtained over the forty eight day period of anaerobic digestion was insignificant so lithium lost in the filtered samples was also considered to be insignificant in this experiment and no modification of the results was required.

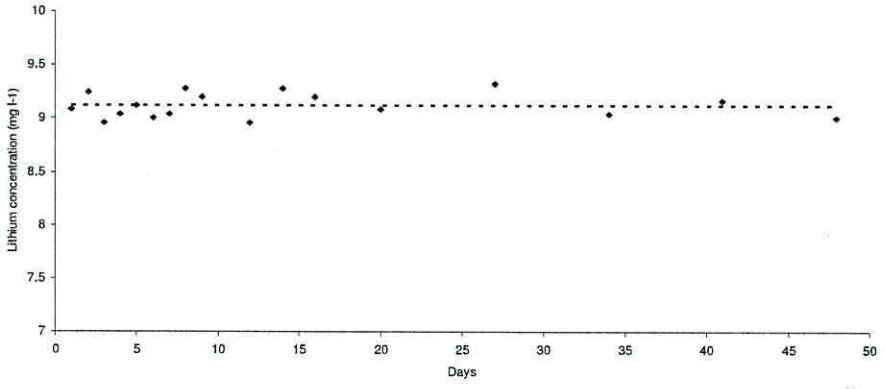

Figure 2.17 Lithium adsorption onto microorganisms, batch experiment.

2.2.4. Vessel 1 hydrodynamic study

The vessel 1 results explained below are shown in Table 2.6. For a vessel of volume V litres, through which flows v litres per second of material, M units of tracer were introduced instantaneously and the concentration of tracer leaving the vessel was recorded periodically.

This produced a C_{pulse} curve (Figure 2.18), and from the material balance the area under the curve was calculated (Equation 2.5)

Equation 2.5

$$Area = \int_0^\infty C.dt = 2383 \cong \sum_i C_i \Delta t_i = \frac{M}{v} = \frac{976}{0.354} = 2788$$

The E curve is calculated by changing the concentration scale to unity. This is achieved by dividing the C(t) values by the total area, M / v (Figure 2.19). The RTD value is used in later calculations for the compartment models.

The known system parameters of vessel 1 volume (V) divided by the flow rate (v) can be used to calculate the theoretical hydraulic retention time (Equation 2.6)

Equation 2.6

$$\frac{V}{v} = \frac{55}{0.354} = 155.29 \text{ hours}$$

The mean residence time of molecules in the reactor, $\bar{t}$ can also be calculated as in Equation 2.7 using data obtained in the pulse experiment.

Equation 2.7

$$\bar{t} = \frac{\int_0^\infty t.C.dt}{\int_0^\infty C.dt} \cong \frac{\sum_i t_i C_i \Delta t_i}{\sum_i C_i \Delta t_i} = \frac{V}{v}$$

$\bar{t}$ = 138.75 hours

Table 2.6. Pulse experiment data.

Area (t)	t (hours)	C(t)	M (mg Li)	% M
0.000	0.000	0.000	0.00	0.0%
0.088	0.016	10.980	0.03	0.0%
5.428	0.516	10.380	2.15	0.2%
12.204	1.001	17.580	4.83	0.5%
23.134	1.501	26.140	9.16	0.9%
36.494	2.001	27.300	14.45	1.5%
47.024	2.501	14.820	18.61	1.9%
55.994	3.001	21.060	22.16	2.3%
66.274	3.501	20.060	26.23	2.7%
78.264	4.001	27.900	30.98	3.2%
101.764	5.001	19.100	40.28	4.1%
118.104	6.001	13.580	46.75	4.8%
134.764	7.001	19.740	53.34	5.5%
379.864	22.001	12.940	150.36	15.4%
392.714	23.001	12.760	155.45	15.9%
405.294	24.001	12.400	160.43	16.4%
417.354	25.001	11.720	165.20	16.9%
429.134	26.001	11.840	169.87	17.4%
441.014	27.001	11.920	174.57	17.9%
452.874	28.001	11.800	179.26	18.4%
476.394	30.001	11.720	188.57	19.3%
487.274	31.001	10.040	192.88	19.7%
641.999	46.001	10.590	254.12	26.0%
663.259	48.001	10.670	262.54	26.9%
683.999	50.001	10.070	270.75	27.7%
704.299	52.001	10.230	278.78	28.5%
724.639	54.001	10.110	286.84	29.4%
876.159	70.001	8.830	346.81	35.5%
920.409	75.001	8.870	364.33	37.3%
938.189	77.001	8.910	371.37	38.0%
1080.479	94.001	7.830	427.69	43.8%
1096.099	96.001	7.790	433.87	44.4%
1111.799	98.001	7.910	440.09	45.1%
1127.499	100.001	7.790	446.30	45.7%
1680.999	190.001	4.510	665.40	68.1%
1712.569	197.001	4.510	677.89	69.4%
1785.499	214.001	4.070	706.76	72.4%
1815.249	221.001	4.430	718.54	73.6%
1883.419	238.001	3.590	745.52	76.3%
1907.989	245.001	3.430	755.25	77.3%
1963.579	262.001	3.110	777.25	79.6%
1986.889	269.001	3.550	786.48	80.5%
2170.839	334.001	2.110	859.29	88.0%
2185.749	341.001	2.150	865.19	88.6%
2217.879	358.001	1.630	877.91	89.9%
2229.989	365.001	1.830	882.70	90.4%
2259.739	382.001	1.67	894.48	91.6%
2272.619	390.001	1.55	899.58	92.1%
2294.859	406.001	1.23	908.38	93.0%
2320.539	430.001	0.91	918.55	94.1%
2383.179	502.001	0.83	943.34	96.6%

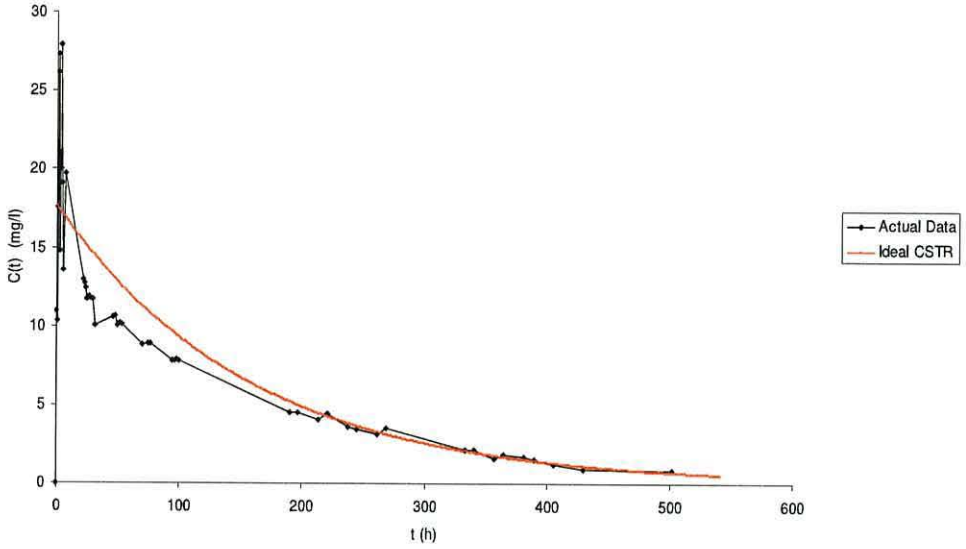

Figure 2.18 C_{pulse} curve for vessel 1 of four-stage digester.

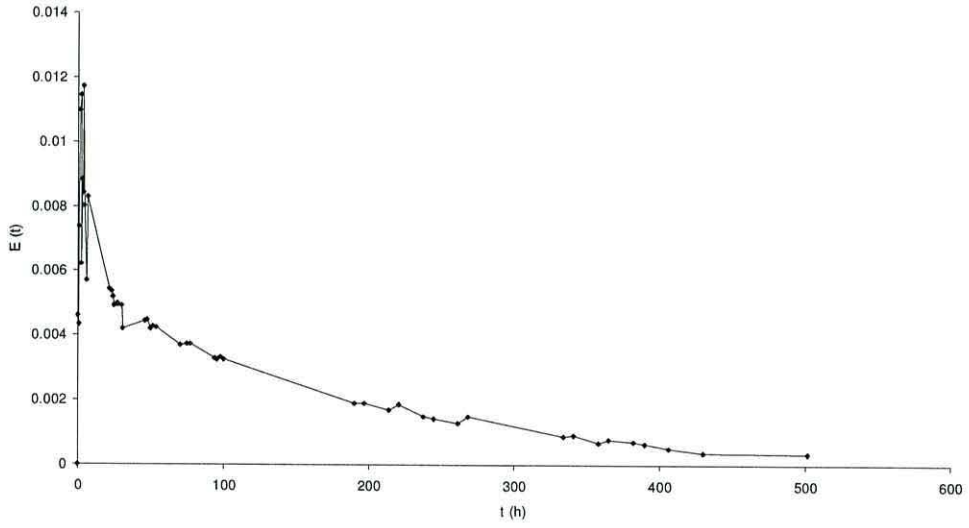

Figure 2.19 E(t) curve for vessel 1 of four-stage digester.

The actual hydraulic retention time is somewhat less than the theoretical hydraulic retention time. This suggests non-ideal flow in vessel 1, which could be due to dead volume within the vessel. In addition, the C_{pulse} curve (Figure 2.18) is indicative of some bypass flow as there is a peak greater than the ideal CSTR curve at t = 0 to 7 hours.

The area below the first peak of the (normalised) E(t) curve (Figure 2.19) can be used to find the percentage of lithium exiting the vessel by a bypass route. Bypass occurred either during the first seven or twenty two hours, as there is no data between these points it is impossible to be sure which is correct so both have been used to calculate the bypass flow. Equation 2.8 shows bypass flow assuming bypass occurred during first seven hours and Equation 2.9 shows bypass flow assuming bypass occurred during first twenty two hours.

Equation 2.8

$$\nu_b = \text{Area} \times \nu_{total} = 0.06 \times 8.5 = 0.51 \text{ l hour}^{-1}$$

Equation 2.9

$$\nu_b = \text{Area} \times \nu_{total} = 0.16 \times 8.5 = 1.36 \text{ l hour}^{-1}$$

Active flow can then be calculated as in Equation 2.10 (Active flow ν_a assuming bypass occurred during first seven hours) and Equation 2.11 (Active flow ν_a assuming bypass occurred during first twenty two hours).

Equation 2.10

$$\nu_a = \nu_{total} - \nu_b = 8.5 - 0.51 = 7.99 \text{ l hour}^{-1}$$

Equation 2.11

$$\nu_a = \nu_{total} - \nu_b = 8.5 - 1.36 = 7.14 \text{ l hour}^{-1}$$

Therefore ν_b is between 6 % and 16 % of ν_{total}

To find the dead volume in the digester vessel, *i.e.* regions which are not mixed, the observed and theoretical hydraulic retention times must be compared as follows:
If $\bar{t}_{observed} < \bar{t}_{theoretical}$ then the vessel has dead spaces, but if $\bar{t}_{observed} = \bar{t}_{theoretical}$ then the vessel has no dead spaces.

$\bar{t}_{observed} = 138.75$ hours

$\bar{t}_{theoretical} = 155.29$ hours

As the observed hydraulic retention time is less than the theoretical hydraulic retention time, vessel one must contain some dead space (V_{dead}), as calculated below.

Equation 2.12

$$\bar{t}_{\text{observed}} = \frac{V_{active}}{\nu}$$

Equation 2.13

$$\bar{t}_{\text{theoretical}} = \frac{V_{total}}{\nu}$$

Therefore

Equation 2.14

$$V_{\text{active}} = \nu . \bar{t}_{\text{observed}} = 48.91 \text{ litres}$$

Equation 2.15

$$V_{\text{dead}} = V_{\text{total}} - V_{\text{active}} = 55 - 48.91 = 6.09 = 11.07 \text{ \% dead space}$$

The effect of the bypass flow and dead volume will be discussed in the following section where the hydrodynamics of the entire system will be calculated.

2.2.5. Complete system hydrodynamic study

The four tanks in series arrangement of the complete system was expected to be comparable to the dispersion model or the tanks in series model. The dispersion model deviates slightly from the plug flow model, and assumes a dispersion-like process superimposed onto the plug flow model. The spreading process is represented by the dispersion coefficient (m^2 s^{-1}). D / uL is the dimensionless group characterising the spread in the whole vessel.

The tanks in series model can compare observed data with a model of N CSTRs arranged in series. Calculating the dispersion model first to find how like or unlike a plug flow reactor the four-stage digester was provided a value for the variance, σ which will be useful in determining how many ideal serial CSTRs the system best fits.

The four vessels in series arrangement was not expected to suffer with significant bypass overall. Therefore it was assumed that the difference between actual and theoretical retention times was due to dead space.

The average observed retention time, $\bar{t}_{observed}$ is calculated in Equation 2.16, as for vessel 1.

Equation 2.16

$$\bar{t}_{observed} = \frac{\int_0^\infty t.C.dt}{\int_0^\infty C.dt} \cong \frac{\sum_i t_i C_i \Delta t_i}{\sum_i C_i \Delta t_i} = \frac{956248.54}{1848.61} = 517.28 \text{ hours}$$

Theoretical retention time is calculated in Equation 2.17

Equation 2.17

$$\bar{t}_{theoretical} = \frac{V}{\nu} = \frac{220}{0.354} = 621.18 \text{ hours}$$

The mixed volume can be calculated from the theoretical ($\bar{t}_{theoretical}$) and observed ($\bar{t}_{observed}$) retention times (Equation 2.18)

Equation 2.18

$$\frac{\bar{t}_{observed}}{\bar{t}_{theoretical}} \times 100 = 83\ \%$$

Therefore mixed volume V_m = 83 % of 220 litres = 183.200 litres, and it follows that the remaining 17 % is dead volume V_d = 36.800 litres (17 %)

This averages per vessel as

V_m = 45.800 litres

V_d = 9.200 litres

To find D / uL, the variance (σ^2) must be calculated. This is the square of the spread of the distribution as it passes the vessel outlet.

Equation 2.19

$$\sigma^2 = \frac{\int_0^\infty (t-\bar{t})^2 C.dt}{\int_0^\infty C.dt} = \frac{\int_0^\infty t^2 C.dt}{\int_0^\infty C.dt} = \bar{t}^2 = \frac{585534827.1}{1848.606277} - 517.28^2 = 49164.50603$$

The variance calculation assumes a closed vessel, *i.e.* no back-mixing from the vessel through the inlet or outlet tubes. This cannot be guaranteed in this experiment but the degree of back-mixing is assumed to be too small to be of much consequence.

Equation 2.20

$$\frac{\sigma^2}{\bar{t}^2} = 2\left(\frac{D}{ul}\right) - 2\left(\frac{D}{ul}\right)^2 .\left[1 - e^{-ul/D}\right] = \frac{49164.5063}{267579.4} = 0.1837$$

By estimating values of D and uL until the above equation was satisfied:

$D / ul = 0.102$

The relevance of D / uL values can be summarised as follows:

D / uL = ∞ → Mixed flow (CSTR)
D / uL > 0.01 → Large deviation from plug flow
D / uL < 0.01 → Small deviation from plug flow
D / uL = 0 → Plug flow

Therefore there is a large deviation from plug flow. This can be described as a single plug flow reactor with large regions of mixed flow within. The system hydrodynamics can also now be compared to the tanks in series model. This is the theoretical model of of perfect CSTRs in series. The number of perfect CSTRs in series (N) the system compares to is calculated as follows:

Equation 2.21

$$\frac{\sigma^2}{\bar{t}^2} = \sigma_\theta^2 = \frac{1}{N} = 0.1837$$

Therefore N = 5.44 tanks in series.

The proportion of bypass flow and dead volume in vessel 1 were not considered to be high enough to cause problems with the data collected from the digester operation. The design of the vessels (*i.e.* the baffles) could have been partly responsible for the dead space measured. The internal baffles were designed to reduce the bypass flow. Some amount of bypass flow was believed likely as the vessels were fitted with inputs and outputs at approximately the same level as described in section 2.2.1.4. The baffles were placed near to the inlet sides of the vessels and this region was not expected to be mixed by the biogas recycle mixing system as the perforated sparger was situated on the 'outflow' side of the baffle. It may have been better to turn the sparge tubes 90 degrees, thus allowing bubbles of biogas to mix the vessel contents on both sides of the baffle plates.

2.5. Conclusions

The four-stage digester described above was a successful design for examining the anaerobic digestion process. The hydrodynamic study has shown that the first vessel (and presumably the other three as all are identical in design) demonstrated CSTR behaviour, thus providing sufficient mixing of feedstock with active microbial biomass. The four vessels together were effective in reducing by-pass flow to such an extent that sampling points between the vessels gave a reasonably accurate example of digestate of a certain age, *e.g.* the sample point between vessels two and three provided a digestate sample that was approximately half the residence time of the entire system. The design therefore allowed on-line monitoring of pH, redox and conductivity and off-line analysis of collected samples at three temporal points within the overall hydraulic retention time. The on-line data was recorded to computer and analysed with the off-line data as described in Chapter 3.

The digester supplied a large number of samples for development of a software sensor for key process parameter prediction based on the on-line probe data and consequent development of dynamic control of the organic loading rate for complete automated system as described in Chapter 4. The samples collected also allowed construction of a calibration dataset for FT-NIRS prediction of a key process parameter in Chapter 5.

The four-stage system was also easily modified to produce two-stage digesters for comparison of mixing frequencies in digesters with and without microbial biomass support media in Chapter 6. The smaller single-stage digesters provided replication of the biomass support and mixing frequency experiments.

3 Monitoring of anaerobic digestion and identification of key process parameters

3.1. Introduction

Experimental work in anaerobic digestion research can be complicated by the lengthy time periods required for start-up and stabilisation of a reactor, and for the time period required, for changes made to operating conditions to have a significant effect. Typical hydraulic retention times for solid substrates can be in the region of nine to twenty five days (Cecchi *et al.*, 1986), and to make a change in the operation of a digester requires a period of at least three times the operational retention time to appreciate the full implications of the change. This is mainly because the retention time is the period taken for the digester to theoretically change its entire volume. As shown in Chapter 2, Figure 2.18, there should be very little of the original material left in a digester after a period of three retention times.

The four-stage anaerobic digester (described in Chapter 2) was operated for a period of ten months which included start-up, failure, recovery and stable operation at the maximum loading rate, established as parts of the experiment. The carbon to nitrogen ratio and the methane production curve of the feedstock were also determined, the latter by batch experiment. The individual parameters monitored in these experiments are not new, but there follows a comprehensive account of the long term monitoring of all these parameters under a variety of operating conditions and establishing optima of interest which do represent novel data. pH is perhaps the most common parameter to be monitored in anaerobic digestion. It has been used to indicate the process state of digesters, in conjunction with biogas flow rate (Liu *et al.*, 2004) or as part of more comprehensive monitoring systems including COD and fatty acids (Morel *et al.*, 2006; Steyer *et al.*, 2002). Monitoring redox potential is not common in anaerobic digestion, but it has previously been demonstrated that methane can be produced at redox potentials up to -9 mV (Stephenson *et al.*, 1999). Di Berardino *et al.* (2000) found that an average redox potential of -268 mV was favourable in an anaerobic filter treating food industry waste water. Electrical conductivity provides information on the total dissolved ionisable solids in solution, but does not discriminate between different species. Conductivity has been monitored in anaerobic digestion (O'Keefe *et al.*, 1996), where waste dilution was found to affect conductivity but not process performance when treating crab-picking wastes. The monitoring of alkalinity in

anaerobic digestion has been found to be useful in assessing process stability (Hawkes *et al.*, 1993; Jantsch and Mattiasson, 2003; Jenkins *et al.*, 1991). Alkalinity measurement gives information on the buffering capacity of a system and an early warning of failure. The degree of destruction of volatile solids in digestates has been used in comparing digester efficiency (Zahller *et al.*, 2007) as this should give an indication of the conversion of carbon to methane. Gas phase measurements such as biogas flow rate or biogas methane content are important parameters on an industrial scale as they are directly related to energy output. However, it has been suggested that gas phase measurements are not sensitive to the state of the process (Frigon and Guiot, 1995). However, biogas flow rate has been mentioned above in conjunction with pH as a process monitoring parameter, and the inclusion of the proportion of methane in the biogas to calculate methane yield has been used to evaluate start-up of a fixed film reactor. Gas phase measurement of methane in conjunction with near infrared spectroscopy (NIRS) has also been shown to be an effective monitoring combination (Nordberg *et al.*, 2000). Dissolved hydrogen concentration can give information on process stability (Bjornsson *et al.*, 2001; Pauss and Guiot, 1993; Strong and Cord-Ruwisch, 1995) as it is a product of fatty acids metabolism (Schmidt and Ahring, 1993), which are important intermediates in anaerobic digestion. It has been suggested that the gas phase hydrogen cannot be used to accurately predict dissolved hydrogen (Pauss and Guiot, 1993), but gaseous hydrogen was included in this study as it was an auxiliary sensor fitted to the infrared methane monitoring device.

3.2. Materials and methods

3.2.1. Characterisation of feedstock

The feedstock chosen was a commercially available pig meal as this provided an easily available and consistent feedstock composition. The feed used was from the same batch throughout the experiment and individual 20 kg bags were mixed after purchase when the material was put into a plastic storage bin. The feedstock was primarily composed of cereals with the overall manufacturer-stated composition as follows:

Oil 4.5 %

Protein 16 %

Fibre 7.5 %

Copper 8 mg kg^{-1}

Lysine 0.54 %

The carbon-to-nitrogen ratio of the feed was determined using a Carlo Erba NA2000 Elemental Analyser (Carlo Erba Reagenti SpA, Export Division, Strada Rivoltana km 6/7 I-20090 Rodano, Milan). This involved combustion of the sample (15 – 25 mg) and measurement of the evolved gas. Samples were homogenised by grinding to achieve a more representative sample and dried thoroughly at 105° C until no further change in mass was detected. The dried sample was carefully weighed (in duplicate) in 8 mm x 5 mm tin capsules.

The feedstock was also analysed for cellulose, hemi-cellulose and lignin content, by neutral detergent fibre (NDF) analysis, acid detergent fibre (ADF) and acid detergent lignin (ADL) respectively, using an Ankom 2000 fibre analyser and methods based on Van Soest et al (1991).

The NDF procedure extracted lipids, sugars, organic acids and soluble proteins, leaving an insoluble residue primarily composed of cellulose, hemicellulose and lignin, and also some proteins and minerals. The ADF procedure dissolved hemicellulose and cell wall proteins from the NDF residue. The ADF residue contained cellulose, lignin, lignified nitrogen, cutin, silica and some pectins. The ADL procedure dissolved cellulose from the ADF residue, the remaining ADL residue was predominantly lignin with some ash and traces of proteins. The relative proportions of hemicellulose and cellulose were calculated by subtraction: Hemicellulose = NDF minus ADF, and cellulose = ADF minus ADL. Incineration of the post-ADL residue provided an ash value, which was subtracted from the ADL mass to produce the percentage lignin.

Samples were analysed in triplicate. 0.45 – 0.55 g of dry feedstock (particle size < 1 mm) was placed into Ankom F57 filter bags, which retained particles of > 25 μm, and heat sealed. The samples were then placed in the analyser where the bags were agitated in NDF solution (30 g sodium lauryl sulphate USP; 18.61 g ethylenediamine – tetracetic disodium salt dihydrate; 6.81 g sodium tetraborate decahydrate; 4.5 g sodium phosphate dibasic, anhydrous; 10 ml triethylene glycol in 1 l distilled water: pH 6.9 – 7.1, 20 g Na_2SO_3 as a stock solution, then 4 ml α-amylase was added at the start of the analysis) then rinsed with water at 70° C with α-amylase added automatically by the instrument, four times during the 1.25 hour process. Bags were then removed and soaked in 250 ml acetone for 3 – 5 minutes, air dried to remove the acetone then oven dried at 102° C for 2 – 4 hours. The dried filter bags were weighed to achieve the ADF value.

Hemicellulose was determined by NDF minus ADF. The sample preparation was as described above for NDF, but the analyser required ADF solution (20 g cetyl trimethylammonium bromide (CTAB) dissolved in 1 litre of 1N H_2SO_4). The analyser process was similar to NDF, and finished sample bags were then soaked in acetone, air dried then oven dried as for NDF analysis, and weighed.

Lignin determination by ADL consisted of making up a solution of 72 % H_2SO_4 (1200 g H_2SO_4 in 440 ml water, in a cooled 1 litre volumetric flask). The filter bags from ADF analysis were then added to the acid in a 3 litre beaker, and a 2 litre beaker used to gently press the bags thirty times at thirty minute intervals for three hours. The acid was then poured off and rinsed with water repeatedly until the pH was neutral. The bags were again soaked in acetone, air dried then oven dried as for NDF analysis. The weighed bags were then incinerated at 550° C until no further change in mass was found upon further incineration to find the ash mass.

The feedstock was sieved through a 2 mm screen before use, the retained particles were ground to ≤ 2 mm before being added to the sieved feedstock and mixed-in. To make-up liquid feedstock, the dried feed was weighed as required and mixed vigorously with approximately half the required volume of water at *ca.* 38° C. This was added to the feed tank and the remaining water was used to wash the remnants of feedstock in the container into the mixing tank.

3.2.2. Feedstock methane production batch experiments

It was of interest to find the shape of the methane production curve over time. This was found by adding 4.5 litres of digestate from the four-stage digester (construction described in Chapter 2, section 2.2) to four single-stage digesters (construction described in Chapter 2, section 2.3) without biomass support media. The digesters were incubated at 38° C and mixed for one minute every hour for eight weeks without feeding to acclimatise the microbial populations. The digesters were then fed for two months at an average (working rules prevented daily feeding) organic loading rate of 3.13 g VS l^{-1} d^{-1} (grams of volatile solids per litre per day) (15 g dry feed per day). This was considered long enough for acclimation of the digesters. Feeding then ceased for one week, after which two of the digesters were fed once at the same daily loading rate as earlier (15g of feed added). The other two digesters were not fed and acted as a control. Biogas volume and composition were measured as described in sections 3.2.7 and 3.2.8 respectively, and the mean control (unfed) digester methane

volumes were subtracted from the mean 'fed' digester methane volumes to calculate the methane produced as a result of the single feeding event.

3.2.3. System operation

The system was initially started in mid September 2005, using 10 % v/v inoculum (*ca.* 5 % total solids) of digestate from the AnDigestion biogas plant storage tank (AnDigestion Ltd, Chilsworthy, Holsworthy, Devon, UK, EX22 7HH). The inoculum material was analysed for total alkalinity and found to be approximately 27000 $mg.L^{-1}$. The remaining 90 % of the start-up material was pig feed solution at 3 % w/v solids. This proportion of inoculum had proved sufficient for anaerobic digestion of plant material (Gunaseelan, 1995) but was found to be unsuccessful in this instance. The system was therefore re-started on 28th September 2005 with 100% inoculum, to which 2 % total solids pig meal was added by hand at a low organic loading rate of 0.53 g VS l^{-1} d^{-1} from 7th October 2005. The feed was initially supplemented with 3.44 g l^{-1} $NaHCO_3$ until 30th October 2005. This increased the total HCO_3^- (*i.e.* without Na^+) concentration by 2500 $mg.L^{-1}$, which was estimated to be sufficient to maintain stability.

The system was then operated on 5 % total solids pig meal from 20th October 2005 (with due consideration for the effect on the organic loading rate) controlled by the input pump. This was the feedstock used for all subsequent experimental conditions except recovery of the failed system, where material similar to that used as inoculum was used to speed recovery.

3.2.4. Collection of samples

Samples were taken Monday to Friday each week at 9 am. Each sample was collected in plastic universal containers *via* the flow cell ball valves for vessels 1 to 3 and through a ball valve fitted to a 'T' piece of tubing at the outlet of vessel 4. Samples were stored at + 4° C for analyses or preparations that were not carried out immediately.

3.2.5. On-line monitoring – pH, redox, conductivity

The system was constantly monitored for pH, redox and conductivity at the outputs of vessels 1, 2 and 3 using appropriate probes. Temperature was also measured but the values were not recorded as the temperatures in the flow cells varied depending on whether digestate was flowing through them or not at any particular time.

Temperature in the flow cells was not considered important to the process as the main digester vessels maintained a constant temperature. However, the control box for the probes used the temperature reading to correct the initial value for pH and conductivity (adjustment). The probes were initially tested for suitability with digestate sourced from the AnDigestion Ltd plant. Materials from all areas of the plant; mixing tank, post-pasteurisation, methanogenic digesters and storage tank were analysed and found to be in the region of pH 4.5 to pH 8.2, redox from -100 to -400 mV and conductivity from 3 to 6.5 mS cm^{-1}. Data recording commenced on 22nd November 2005 at the mid point of the system, between vessels two and three, followed by the points between vessels one and two, and three and four from 24th November 2005. The probes were scaled 0 to 14 for pH (0.01 unit increments), -700 to +700 mV for redox (1 mV increments), and 0 to 10 mS cm^{-1} for conductivity (1 µS cm^{-1} increments).

Probes were calibrated every two months (manufacturer recommendation) by two point calibrations: pH probes were calibrated using calibration buffer solutions (BDH) at pH 4.00 and pH 10.00 and were at no time found to have an error of more than 0.2 pH units.Calibration of the redox probes was carried out using calibration solutions (Jenway) of 200 mV and 465 mV. The redox probes were found to be more likely to suffer with fouling than the pH probes, as highlighted in section 3.3.4, although normally they were within 50 mV of the calibration standards. The conductivity probes were calibrated by a 0.005 M KCl solution (HMSO, 1978); 3.728 g KCl (dried at 110° C for 2 hours) in 200 ml H_2O, made up to 1 litre. This solution was diluted to 1.492 g l^{-1} (2767 µS cm^{-1}) and used neat at 3.728 g l^{-1} (6668 µS cm^{-1}). The accuracy of the conductivity probes was never found to be more than 500 µS cm^{-1} from the standards during calibration. This demonstrates that the probes used were relatively stable in the material used in this work.

3.2.6. Determination of total alkalinity (HCO_3^- concentration)

Samples for total alkalinity determination were taken from the bulk 30 ml sample within one hour of collection. The bulk samples were shaken well to give a more representative sample before removing 2 ml, which was added to a centrifuge tube and centrifuged at 1500 x g for 20 minutes. The supernatant was drawn off and added to a 2 ml tube for storage at -20° C until analysis.

The analysis was conducted twice weekly by titration using an auto-titrator (Metrohm 716 DMS Titrino, Metrohm House, Unit 2, Top Angel, Buckingham

Industrial Park, Buckingham MK18 1TH). Stored samples were thawed at room temperature before analysis. 100 µl of sample was added to approximately 70 ml of laboratory grade H_2O, all samples being analysed in duplicate. The volume of sample added for titration was determined by preliminary investigations using digestate collected from the AnDigestion biogas plant. It has been shown that the stable operation of anaerobic sludge digesters requires a supernatant total alkalinity of between 2000 $mg.L^{-1}$ and 4000 $mg.L^{-1}$, expressed as $CaCO_3$ (Pohland and Bloodgood, 1963). More recently, Borja *et al.* (2004) found that during the mesophilic anaerobic digestion of wastewater from chickpea flour manufacture, total alkalinity in the range 1090 $mg.L^{-1}$ to 2130 $mg.L^{-1}$ (as $CaCO_3$) prevented pH falling below pH 7.2. The procedure is that of the Standard Methods for the Examination of Water and Wastewater, 2320 Alkalinity, potentiometric titration to end point pH (APHA, 1976). During the titration (using 0.02 M H_2SO_4), carbon dioxide is liberated from carbonate and bicarbonate. The rate at which the carbon dioxide remaining in solution comes into equilibrium with carbonic acid is measurably slow and affects the stability of the end-point of a single titration to pH 4.5. Once the equivalence point of the titration at pH 4.5 has been exceeded, a plot of hydrogen ion concentration against volume of acid added becomes linear, so that extrapolation of this linear section of the titration curve to zero hydrogen ion concentration determines the equivalence point due to the total alkalinity of the sample. In practice titrations to pH 4.5 and 4.2 are sufficient to define the linear section of the titration curve. The total alkalinity calculation is shown below. Equation 3.1 shows that, at the equivalence point:

Equation 3.1

$$Titre_{acid} \; x \; Normality_{acid} = Volume_{sample} \; x \; Normality_{sample}$$

Therefore,

Equation 3.2

$$Normality_{sample} = \frac{Titre_{acid} \; x \; Normality_{acid}}{Volume_{sample}} \; equivalents / litre$$

Substituting the equivalent weight of calcium carbonate, 50.045, half the molecular weight, as shown in Equation 3.3:

Equation 3.3

$$Alkalinity = \frac{[(2xT_{4.5})-T_{4.2}]xNx50.045x1000}{vol} \quad mg\ CaCO_3\ /litre$$

Where:

$T_{4.5}$ = titre to pH 4.5 (ml)

$T_{4.2}$ = titre to pH 4.2 (ml)

N = normality of acid

vol = volume of sample titrated (ml)

To convert from mg $CaCO_3$ / litre to mg HCO_3 / litre, the $CaCO_3$ result was multiplied by 1.22.

Prior to analysis, the auto-titrator was calibrated using pH 4.00 and pH 7.00 calibration buffers (BDH). Standards were also run as part of the laboratory quality control schedule, these were water samples spiked with $CaCO_3$ at 155 $mg.L^{-1}$ and 450 $mg.L^{-1}$.

3.2.7. Determination of total and volatile solids in digestate samples

Total and volatile solids of feedstock and vessel 4 (output) samples were measured using the method specified by the APHA (1976). Volatile solids is a crude method of determining organic material in a sample, but the alternatives of COD or BOD give a chemical or aerobic biological oxidation of the sample respectively, and are therefore also only approximate comparisons to an anaerobic system.

Samples stored at +4° C were analysed for total and volatile solids monthly. Samples were shaken vigorously and approximately 2 ml was removed by pipette and placed into a pre-weighed porcelain crucible. The crucible had previously been placed in a muffle furnace at 550° C for one hour to incinerate any organic residues, and then cooled in a dessicator to room temperature. Samples were always kept in a dessicator except when in the oven or during weighing due to their hygroscopic nature, particularly after drying or incineration. The imprecise volume of sample was due to difficulties with pipette blockages, but was of little consequence as the crucible was

weighed again with sample present to determine the exact sample mass to an accuracy of 0.1 mg.

Weighed sample crucibles were placed in aluminium foil trays and these in turn were placed in an oven at 105° C. Samples were heated for three hours before weighing, then heated for another hour and weighed again. If no change in mass was detected between three and four hours drying the samples were considered dry. If a change in mass was detected, the samples were returned to the oven for another hour and the process repeated.

The total solids percentage was calculated as shown by Equation 3.1.

Equation 3.4

Total solids = (dry weight / wet weight) x 100

The dried samples from above were used to determine volatile solids as a percentage of the dry mass. The weighed sample crucibles were placed in a muffle furnace at 550° C and removed after three hours and weighed as described in the total solids method until no further change in mass was found.

The volatile solids percentage was calculated as shown by Equation 3.2.

Equation 3.5

Volatile solids = 1- (ash weight / dry weight) x 100

3.2.8. Gas volume measurement

Initially, the gas volume for the entire four-stage system was measured through a single Zeal DM3A (G. H. Zeal Ltd. 8 Deer Park Road. Merton, London, SW19 3UU) wet-type positive displacement gas meter. This performed well at the volumes produced by the system as a whole, but was not sensitive enough to measure the low gas outputs from individual vessels. It was realised that this was not going to produce sufficient data for statistical analysis and that the meter had also developed a leak (probably due to the corrosive H_2S present in the biogas). Therefore from 27th April 2006, a gas volume measuring system for each vessel was constructed using the water displacement principle. One of these sets of apparatus is shown in Figure 3.1.

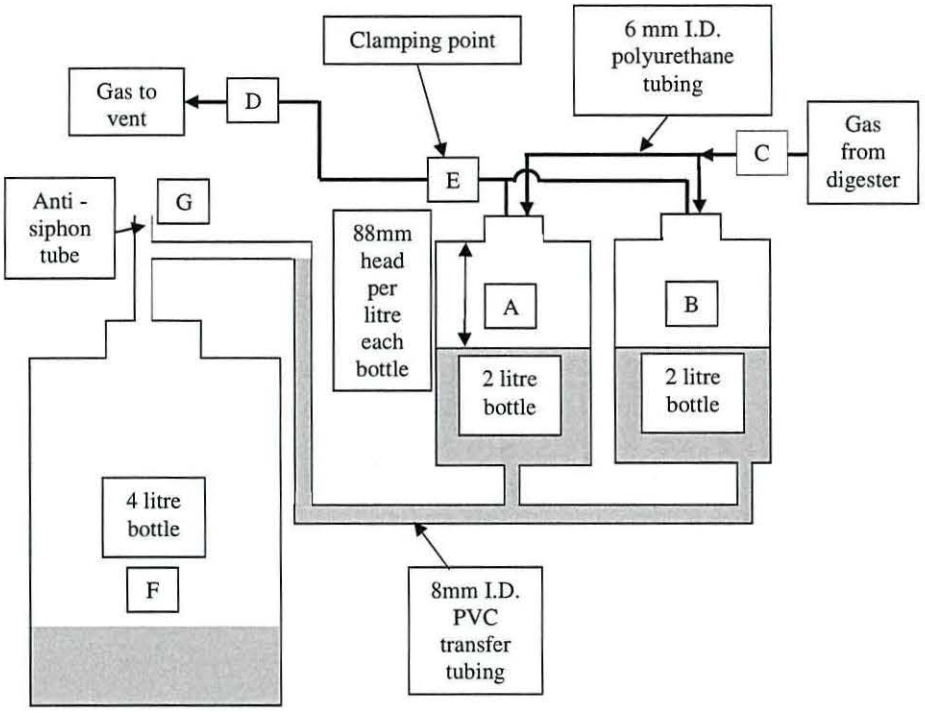

Figure 3.1 Gas volume measurement apparatus.

Two 2 litre bottles (A and B) were filled nearly to the top with water. The small remaining headspace was used in-line with the biogas outlet tubing (C). Under normal circumstances the gas was vented *via* a tube to the outside of the building (D), but when measurement takes place the gas outlet tubing was clamped with tube clamps at point E (as shown in Figure 3.1), thus preventing the escape of gas. The gas pressure forced the water from the 2 litre bottles into the 4 litre bottle (F). The bottles were arranged with the 'full' water level in the 2 litre bottles at the same height as the inlet tube to the 4 litre bottle to reduce the head of water and therefore the pressure needed to start the transfer of water to the 4 litre bottle. The inlet for each set of apparatus was also fitted with a 'T' piece (G) to prevent the small amount of siphoning that would otherwise have been possible during the measurement process.

Upon completion of measurement, the clamp was removed and the water poured from F into a measuring cylinder, the volume recorded and the measuring cylinder emptied equally into the 2 litre bottles.

3.2.9. Biogas composition

The composition of the biogas was measured using a Crowcon Triple + plus IR gas monitor (Crowcon Detection Instruments Ltd, 2 Blacklands Way, Abingdon Business Park, Abingdon, Oxfordshire OX14 1DY, UK). This used an infrared sensor to measure methane on a 5 - 100 % volume scale and also 0 - 100 % lower explosive limit (LEL) which was useful for monitoring the safety of the experimental area. The LEL is set by the manufacturer as 5 % volume methane in air, which is considered 100 % LEL. Therefore 1 % LEL is equivalent to 0.05 % volume, and once 100 % LEL is exceeded the instrument displays percentage volume. The instrument also monitored hydrogen (0 to 2000 ppm) with an electrochemical sensor.

3.2.10. Pressure and dry gas adjustments

The biogas produced was saturated with water and a small amount of pressure was needed to displace the water, so the effects of pressure and saturated gas on the volumes were calculated to provide a normalised gas volume at standard temperature and pressure (STP):

Water has a saturated vapour pressure of 238 mm water at 20° C, which was the ambient temperature of the experimental room.

Each of the 2 litre gas collection bottles have an 88 mm head of water per litre displaced. 2 bottles are used in parallel in the multi-stage experiments, so this equals 44 mm head per litre of water displaced from the paired bottles:

Standard atmospheric pressure =101.325 kPa = 10,300 mm H_2O
The combined gas law (Equation 3.3) states:

Equation 3.6

$$\frac{P_1 \times V_1}{T_1} = \frac{P_2 \times V_2}{T_2}$$

10300 mm H_2O + 238 mm H_2O (vapour pressure) at 293K + 44 mm head
= 10582 mm H_2O

$$\frac{10582 \times 1}{293} = \frac{10300 \times V_2}{273}$$

$V_2 = 0.957$ litres, $1 / 0.957 = 1.045$ litres

All volumes were therefore multiplied by a 1.045 correction factor.

3.2.11. Statistical analyses

The entire dataset was subjected to principal component analysis (PCA) using The Unscrambler software (CAMO, Software A/S, Nedre Vollgate 8, N-0158 Oslo, Norway) to indicate key factors in the anaerobic digestion process. The data was also analysed using GenStat v.9.2 software (Lawes Agricultural Trust, Rothamsted Experimental Station, 2007) to produce regression models.

The regression models were constructed to predict methane production and yield across the measured range of each parameter, and the models were then used to find the values of each parameter at which maximum methane production or yield were attained. Linear and non-linear regression models were tried for best fit with each parameter, with the non-linear quadratic curve models found to be most suitable in all instances. The best-fitting curves were chosen by the highest percentage variance accounted for and lowest standard error of observations, and also by visibly comparing the curve with the observed data. The models were constructed from the individual vessel data, the combined individual vessels data and also global parameters such as organic loading rate and volatile solids reduction to find the best prediction of methane production and yield from each individual vessel. The individual vessel and global data were also used to estimate the total methane production or yield of the entire system. The optimal values of each parameter in terms of methane production and yield were found by simply reading the peak value from the graph curves drawn from the regression models. This method was considered more suitable than complicated mathematical methods such as the bisection method or Newton-Raphson method (Dauhoo and Soobhug, 2003) for finding the optima of the large number of imperfect curve-fitting models.

3.3. Results and discussion

3.3.1. Carbon to nitrogen ratio of feedstock

The carbon and nitrogen analysis gave % N values of 2.3 % and 2.33 % (average 2.32 %, standard deviation 0.02) and % C values of 40.5 % and 40.81 % (average 40.66 %, standard deviation 0.22). This gave a C:N ratio of 17.55, which is lower than the optimum of 25-35 (Parr and Hornick, 1993), but the multi-stage process was expected to handle this input (Mata-Alvarez, 2002) and therefore this was not considered to be a problem.

Crude protein was calculated by multiplying the percentage of N by a constant, 6.25 (Gizachew and Smit, 2005) as shown in Equation 3.7.

Equation 3.7

$$2.32 \times 6.25 = 14.5\ \%\ \text{crude protein}$$

The crude protein estimate is similar to the manufacturers stated composition of 16 % protein.

3.3.2. Neutral detergent fibre, acid detergent fibre and acid detergent lignin analysis of feedstock

The NDF and ADF measurements are each calculated in the same way, as shown in Equation 3.8. The various weights recorded for NDF and ADF analyses are shown in Tables 3.1 and 3.2 respectively.

Table 3.1. Weights of feedstock during NDF analysis.

Sample	W_1 (Bag tare)	W_2 (Sample weight)	W_3 (Bag + fibre after extraction)	% NDF
AW1	0.5092 g	0.4216 g	0.5052 g	59.94
AW2	0.5113 g	0.4102 g	0.4978 g	59.54
AW3	0.5023 g	0.4026 g	0.5014 g	62.67

Equation 3.8

$$\text{NDF or ADF} = \frac{(W_3 - (W_1 \times C_1)) \times 100}{W_2}$$

Where C_1 = blank bag correction = 0.4959 g.

Table 3.2. Weights of feedstock during ADF analysis.

Sample	W_1	W_2	W_3	% ADF
AW1	0.5161 g	0.4116 g	0.3924 g	33.16
AW2	0.5078 g	0.4213 g	0.3897 g	32.73
AW3	0.5035 g	0.4035 g	0.3768 g	31.50

The equation for calculating ADL differs slightly from the NDF and ADF equation, as shown in Equation 3.9. Combustion of the post-ADL residue provided an ash percentage value, which was subtracted from ADL to produce the lignin percentage.

Equation 3.9

$$\text{ADL} = \frac{(W_4 - (W_1 \times C_2)) \times 100}{W_2}$$

Where:

W_4 = Organic matter (loss of weight on ignition of bag and ADF residue).

Table 3.3. Weights of feedstock during ADL analysis.

Sample	W_1	W_2	W_4	% ADL	Ash %
AW1	0.5161 g	0.4116 g	0.2967 g	9.90	2.89
AW2	0.5078 g	0.4213 g	0.3014 g	11.77	3.01
AW3	0.5035 g	0.4035 g	0.2974 g	11.83	3.14

The mean values are as follows:

NDF = 60.72 %

ADF = 32.46 %

ADL = 11.17 %

The overall proportions of hemicellulose, cellulose and lignin can be calculated as shown in Equations 3.10, 3.11 and 3.12.

Equation 3.10

% hemicellulose = NDF – ADF = 28.25 %

Equation 3.11

% cellulose = ADF – ADL = 21.30 %

Equation 3.12

% lignin = ADL – Ash = 8.15 %

The resulting nitrogen, crude protein, NDF, ADF and ADL values can be compared to values obtained in literature for organic materials that could conceivably be used for full scale processes. Rodriguez *et al.* (2005) recorded mean analysis values for grass silage, a potential energy crop from set-aside land, of 13.5 % crude protein, 53.2 % NDF, 36 % ADF and ADL 6.2 %. De Visser *et al.* (1993) found mean values of 3.1 % nitrogen, 44.43 % NDF, 25.66 % ADF and 2.1 % ADL for various grass silages on their own and mixed with molasses or formic acid. The authors also found 61.4 % NDF and 4.4 % nitrogen for ensiled spent brewers grains, a potential animal feed or anaerobic digestion substrate. The brewers grains compare well in terms of NDF to the pig meal used in these experiments as this too was largely composed of grain material.

The relatively low percentage of lignin (8.15 %) compares well with the manufacturer's claim of 7.5 % fibre. Lignin has been shown to be a very slowly-degraded material in anaerobic systems, although cellulose is relatively easily degraded (Kivaisi and Eliapenda, 1994). Therefore the relatively high proportion of cellulose and hemicellulose would account for the rapid methane production seen from this feedstock.

3.3.3. Feedstock methane production batch experiments

The batch experiments produced an interesting curve of methane production after a single feeding event (Figure 3.2). The data are also presented in cumulative form (Figure 3.3). The cumulative figures have been normalised to show production from 1 kg of dry feed, although the actual experiment used only 15 g. The production rate of methane increased rapidly during the first two days and then decreased throughout the remaining experimental period. The graphs demonstrate that the methane production rate fell to almost insignificant levels after twenty days. This suggested that the feedstock contained a high proportion of material that was easily hydrolysed (or already in solution), fermented and converted to biogas in a very short time. Methane

production after twenty days digestion was so low that it may be uneconomical to design a full-scale digester that handles feedstocks with these characteristics to have a retention time in excess of this. The methane percentage in the biogas decreased from 49.5 % to 40.5 % content v/v during the first twenty four hours after feeding (Figure 3.4), but after the first day the methane percentage increased steadily to *ca.* 60 % v/v by the end of the twenty five day experiment. It was assumed that this was a result of fatty acid inhibition during the rapid hydrolysis and fermentation of the feedstock during the first few days, although the nature of the batch experiment prevented any sample being removed for analysis.

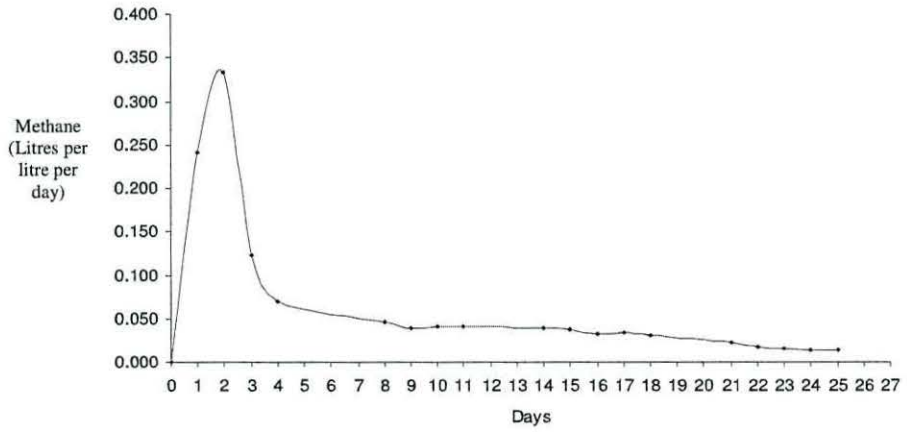

Figure 3.2 Methane production rate in litres per litre digester volume per day during a batch experiment after a single feeding event.

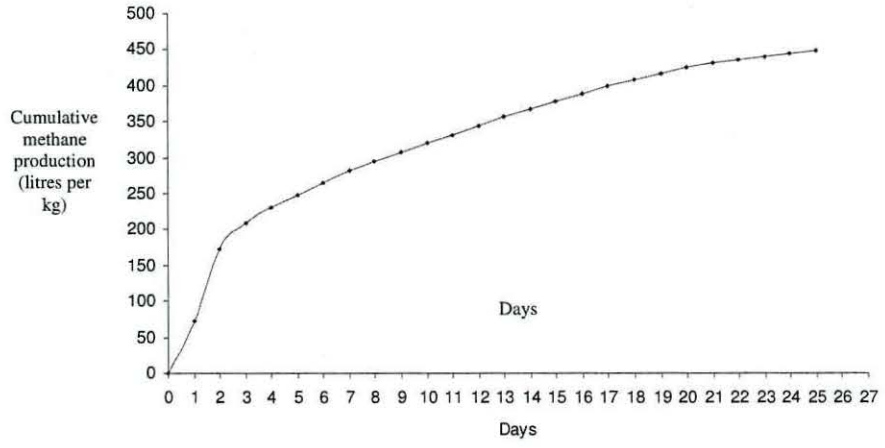

Figure 3.3 Cumulative methane production per kg of dry feed during a batch experiment after a single feeding event.

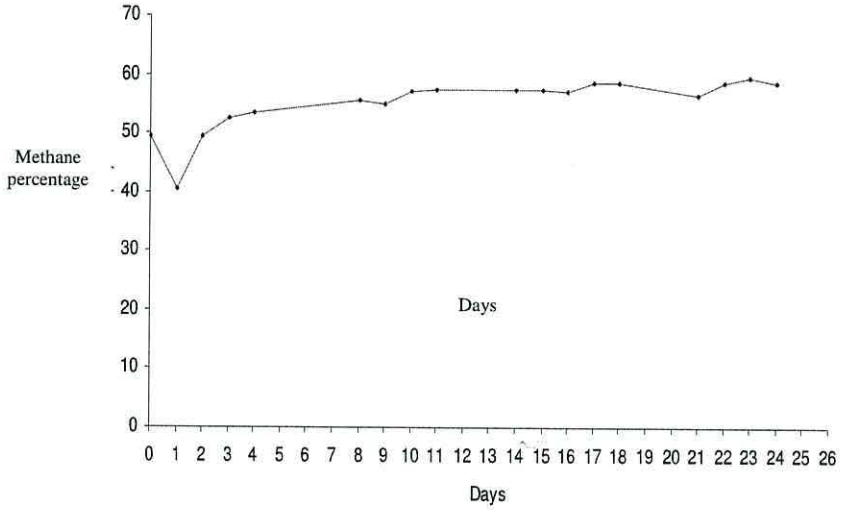

Figure 3.4 Methane percentage in biogas during batch experiment after a single feeding event.

3.3.2. System start-up

During the first attempt at start up, the whole system rapidly became acidic and gas production was lower than the sensitivity of the gas volume measurement method. The total alkalinity of the inoculum material, sourced from the AnDigestion plant storage tank, was very high: ranging from between 7000 and 12000 $mg.L^{-1}$ in the early stages (Mixing tank and post pasteurisation) to between 24000 and 42000 $mg.L^{-1}$ in the digesters and storage tank.

This was considered to be an advantage as such a high concentration of HCO_3^- provided a buffer to protect the digester from acidification. The re-started system, with a 100 % inoculum, maintained a pH of between 7.5 and 8 (inoculum pH was relatively high at *ca.* pH 8.1) for the first few weeks, although the LabVIEW software was not set up to record the probe data from the single set of probes fitted at that time. The start of feeding was at an organic loading rate of 0.53 g VS l^{-1} d^{-1} and a flow of 6.18 l d^{-1} (Figure 3.5), doubled to 1.07 g VS l^{-1} d^{-1} (12.36 l d^{-1}) on the day 20 and then increased to 1.58 g VS l^{-1} d^{-1} on day 24, at which point the total solids value of the input was changed to 5 %. Therefore the organic loading rate to flow rate ratio changed from this point.

The start-up period ran for a total of 158 days. A dramatic decrease in pH in vessel 1 to *ca.* pH 5 due to the acidification of the feedstock was observed form day 70

(Figure 3.6) which was to be expected in a multi-stage design. The loading rate was increased to 1.93 g VS l^{-1} d^{-1} on day 84 but this caused a sudden drop in pH in vessel 2. This was a cause for concern and suggested a lower organic loading rate was necessary. The organic loading rate was therefore decreased to 0.61 g VS l^{-1} d^{-1} from day 89 to day 127. The organic loading rate was then increased over a thirty day period from day 128 to day 158 reaching a maximum of 2.11 g VS l^{-1} d^{-1}.

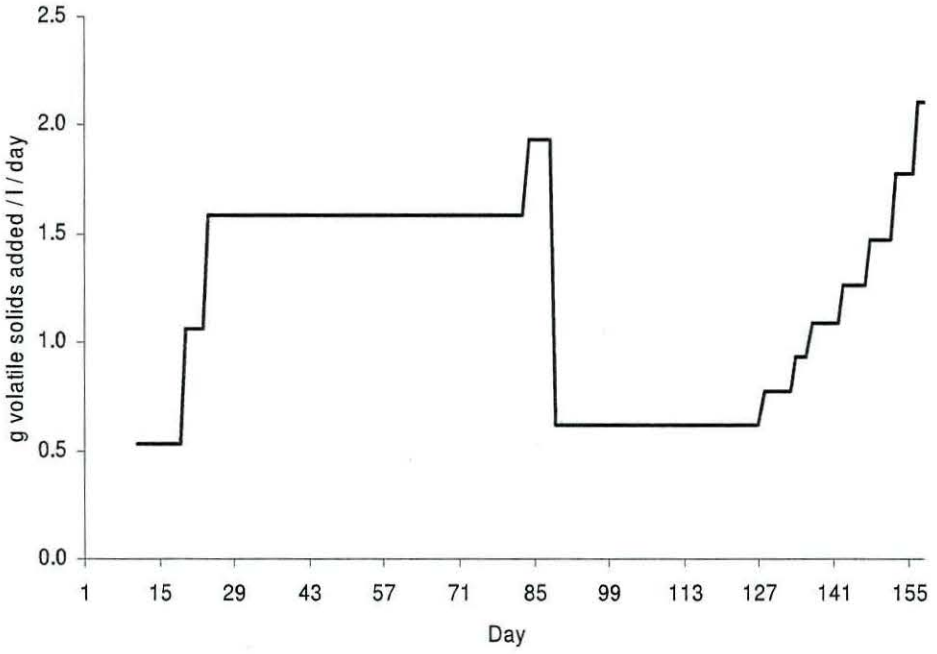

Figure 3.5 Organic loading rate: system start-up.

The low organic loading rate during days 128 to 158 caused an increase in pH at all measurement points: pH in vessel 1 increased to *ca.* pH 7 and both vessels 3 and 4 averaged around pH 7.5, but fell to *ca.* pH 7 as the loading rate increased. The increased load also caused a decrease in the pH of vessel 1, but the fall was more gradual than previously seen and settled at *ca.* pH 6.5 around day 140. The greater stability of pH in all vessels when subjected to changes in loading rate suggested the system had stabilised.

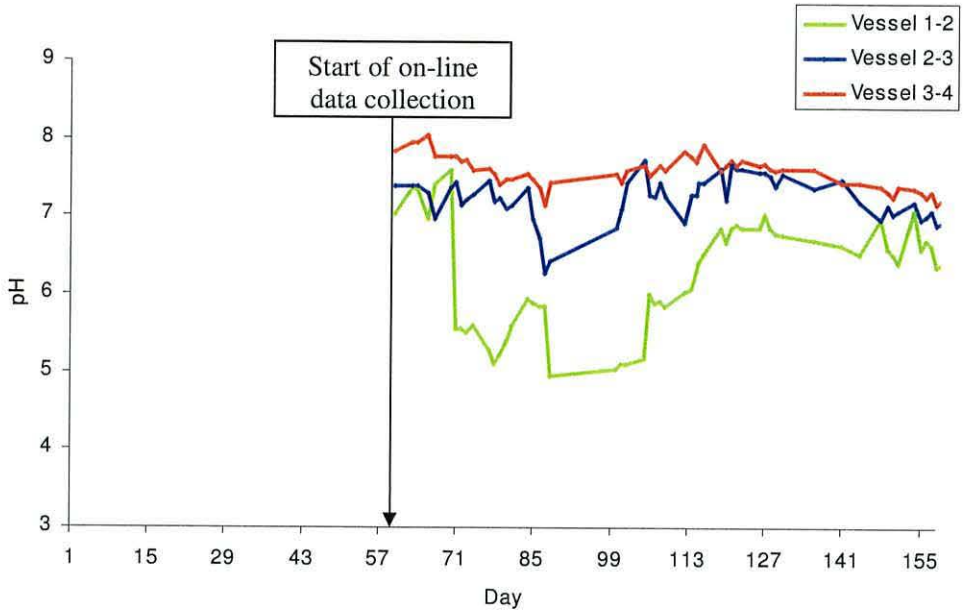

Figure 3.6 pH: system start-up.

Redox values (Figure 3.7) remained constant for vessel 1 during start up, at *ca.* -490 mV, but did increase briefly to *ca.* -300 mV around day 85 when the loading rate was increased only to fall again around day 100 following the decrease in the loading rate. Redox increased steadily during start-up in vessels 2 and 3, starting at *ca.* -500 mV and -550 mV respectively, and ending the start-up period at *ca.* -370 mV and -310 mV respectively. This corresponded with the fall in pH, as was expected. The increase in redox potential would suggest a decrease in the concentration of reduced molecules, and it would seem that higher redox potentials are associated with larger organic loading rates and therefore greater stress on the system. There is evidence that methanogenesis can occur at redox potentials as high as -9 mV (Stephenson *et al.*, 1999), so the values obtained were not a cause for concern in terms of the biochemical environment but they did reflect reduced efficiency of reduction in line with dropping pH.

A problem with the on-line measurements was noticed soon after beginning the experiment: the conductivity probe positioned between vessel 3 and 4 was reading 9.999 mS (the maximum value) throughout the early start-up period (Figure 3.8). The probe was cleaned and calibrated and was found to be working correctly, but it would seem the conductivity value at this point in the process was beyond the range of the instrument, despite the preliminary measurements suggesting otherwise. The manufacturers were contacted but there was no way to increase the full scale deflection.

Conductivity values for vessels 1 and 2 fluctuated at high values during start-up: vessel 1 at greater than 8 mS cm^{-1} and vessel 2 at greater than 7.5 mS cm^{-1} during early start-up, but all conductivity values began to fall from around day 130 onwards as the loading rate was increased. This seemed to follow the increase in redox potential and the decrease in pH as the organisms became established to the pig feed.

Total biogas production (Figure 3.9) fluctuated between 0.2 – 0.7 l $l^{-1}d^{-1}$ during the early start-up process, and fell as the organic loading rate was lowered between days 128 and 158. Methane production fell from *ca.* 0.3 l $l^{-1}d^{-1}$ to *ca.* 0.15 l $l^{-1}d^{-1}$ upon the sudden decrease in pH in vessel 1. This would suggest that vessel 1 was contributing significantly to the production of methane, but there was not a noticeable decrease in methane production associated with the decrease in the pH of vessel 2. This can be explained by the feedstock characteristics of rapid methane production during the first few days, followed by a much slower production rate.

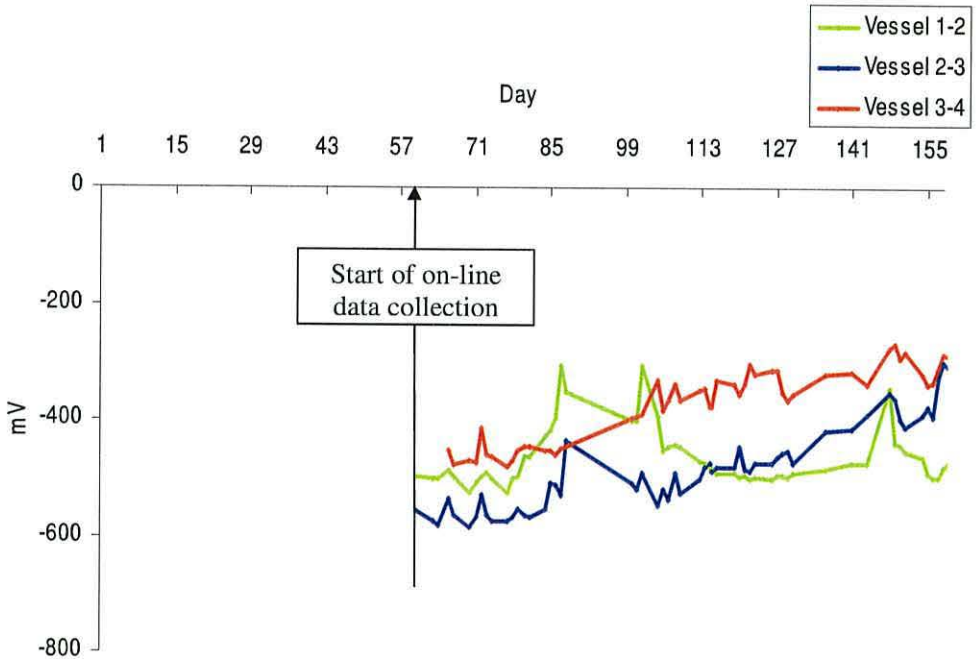

Figure 3.7 Redox potential: system start-up.

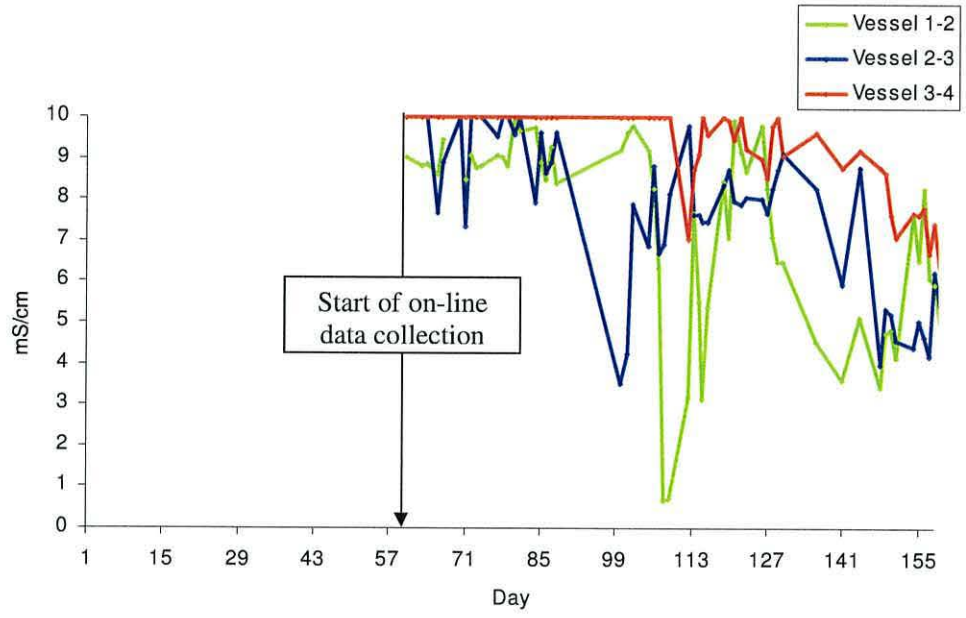

Figure 3.8 Conductivity: system start-up.

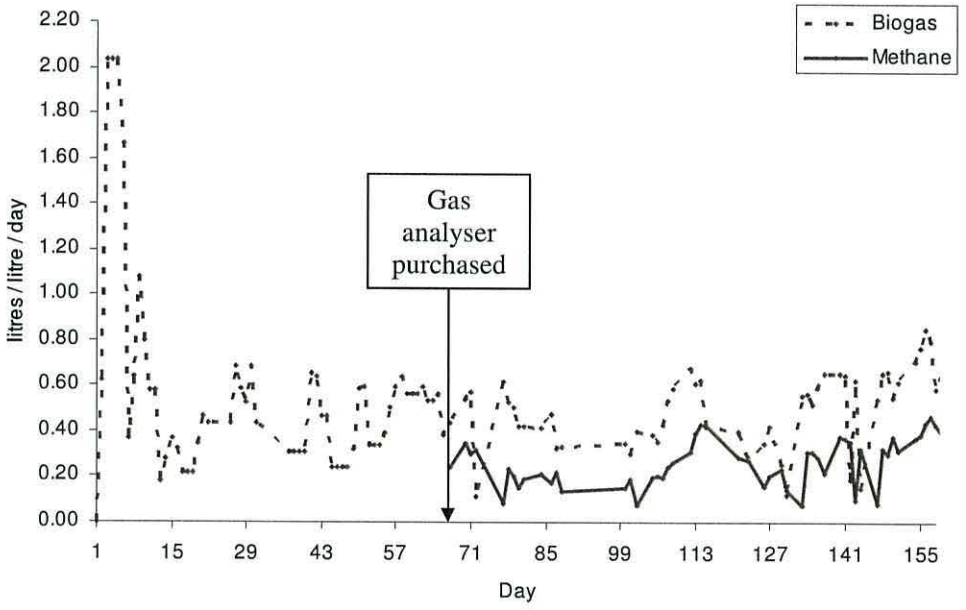

Figure 3.9 Gas production: system start-up.

Methane yield (Figure 3.10) followed production quite closely at first as there was little change in the organic loading rate, but later the yield increased dramatically until day 114, after which the yield fell rapidly. The loading rate was constant (and low at 0.61 g VS l^{-1} d^{-1}) throughout this period, but the peak-yield period corresponded with

the increasing pH and sudden (and brief) fall in conductivity in vessel 1, and a slight peak in the pH of vessel 3 of *ca.* pH 7.9. After this point, pH and conductivity values in all vessels began to fall. pH values tended to be higher at longer retention times, probably as a result of the lower organic loading rate associated with longer retention times leading to a production rate of fatty acids that was less than or equal to the consumption rate. Based on these observations, it is reasonable to say that a higher pH as a result of a longer retention time tended to produce a higher methane yield.

Methane percentages (Figure 3.11) were erratic for the first few months of start-up. Concentrations between 0 and 80 % v/v methane were recorded, although vessels 3 and 4 generally remained above 45 % v/v methane. From approximately day 125 onwards the system had stabilised enough for methane concentrations in all vessels to be within the range of 45 to 65 % v/v, although at this time there was no real pattern of methane concentrations changing through the four stages.

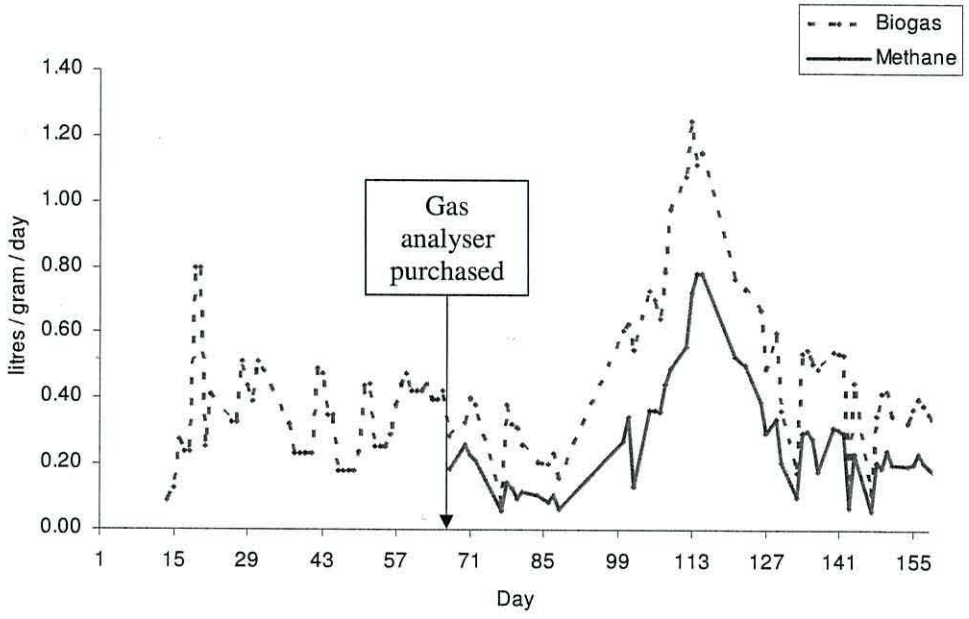

Figure 3.10 Gas yield: system start-up.

Alkalinity decreased throughout start-up as acid production depleted the extremely high buffering capacity (*ca.* 27000 $mg.L^{-1}$) of the inoculum (Figure 3.12) despite the fact that the feed was supplemented with $NaHCO_3$ to increase alkalinity by 2500 $mg.L^{-1}$. The sudden drop in pH noticed around day 70 for vessel 1 and day 85 for vessel 2 was accompanied by a total alkalinity of less than 5000 $mg.L^{-1}$, suggesting this

may be a threshold HCO_3^- concentration for maintaining a neutral pH. However, increasing the organic loading rate during after day 127 saw total alkalinity in all vessels fall below 5000 $mg.L^{-1}$, and yet pH remained above neutral in vessels 2 and 3 and total methane production increased to *ca.* 0.45 l l^{-1} d^{-1} by the end of the start up period. This would suggest that the previously estimated threshold alkalinity level of 5000 $mg.L^{-1}$ was unlikely to be correct.

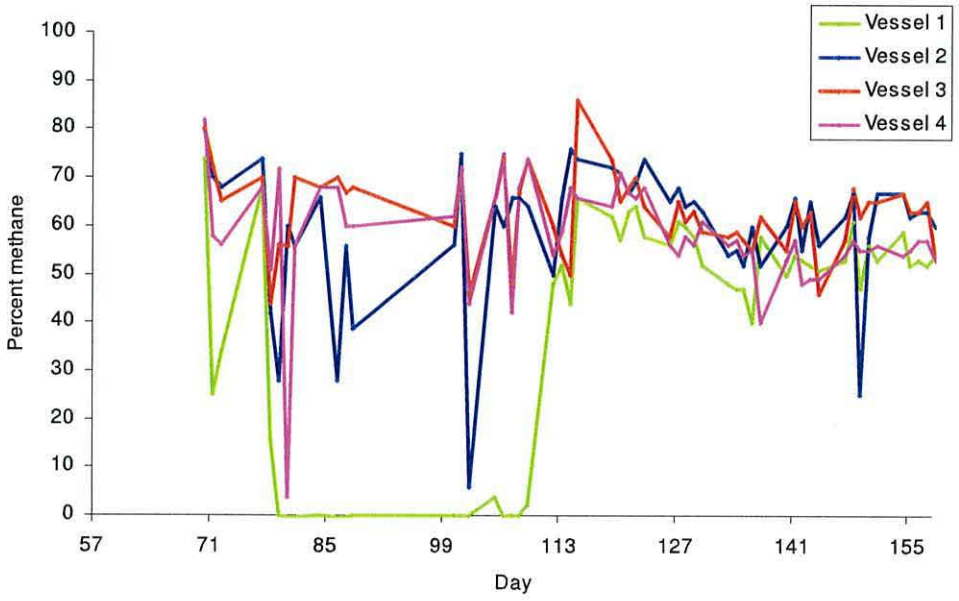

Figure 3.11 Methane percentage: system start-up.

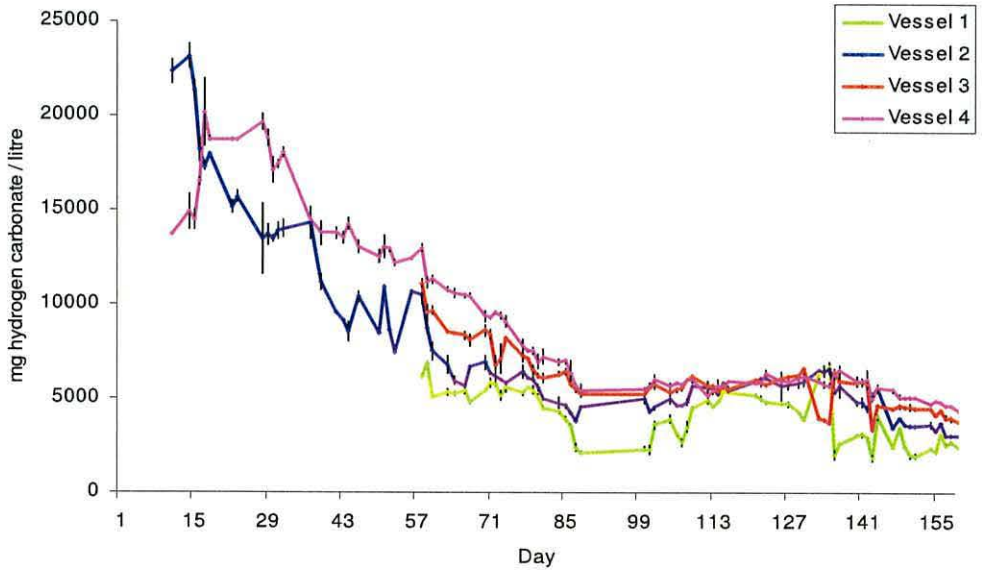

Figure 3.12 Total alkalinity: system start-up.

Gas phase hydrogen concentration (Figure 3.13) was not measured during early start-up as the gas monitor was not fitted with a suitable detector until day 135. H_2 concentrations were very erratic during start-up, and no real observations could be made except for a possible increase in H_2 from approximately day 143 after the organic loading rate was increased. It was also noticed that on several occasions, H_2 concentrations were above the limit of the sensor, which was 2000 ppm (the scale continued up to 3141 ppm but it was uncertain if the measurement remained accurate above the stated maximum). The electrochemical sensor was easily saturated by these over-range values, and required a great deal of purging with air to bring the value down again. A different type of H_2 measurement instrument, with a greater range, would be of value in future experiments.

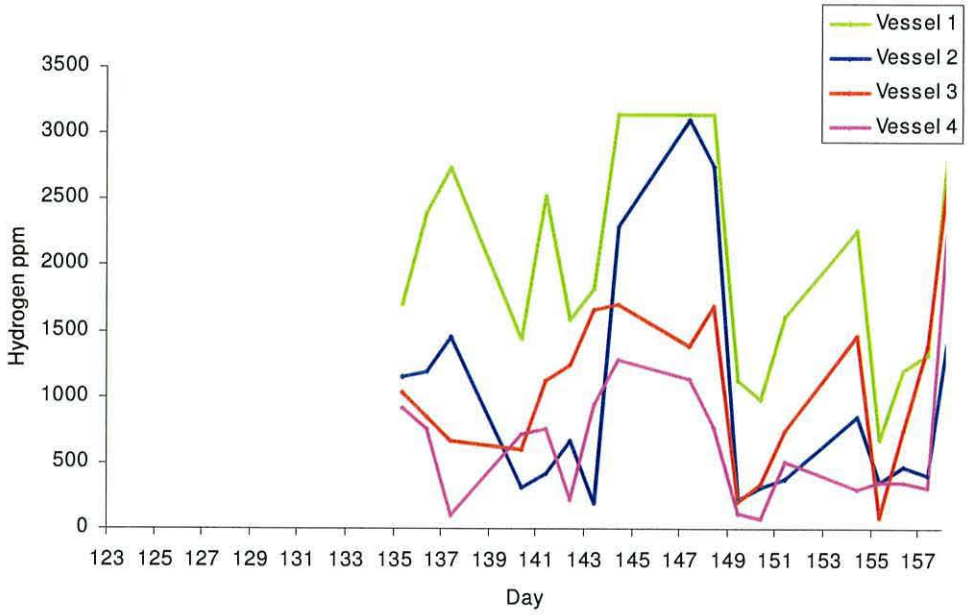

Figure 3.13 Hydrogen concentration: system start-up.

The reduction in organic material (the output volatile solids as a percentage of the input volatile solids) decreased from *ca.* 40 – 50 % to *ca.* 30 – 35 % between days 58 and 77 (Figure 3.14), but increased again to *ca.* 35 – 40 % around day 81, which corresponded with the lower pH found in vessel 1. However, the reduction in organic material fell again to *ca.* 27 % at the same time that vessel 2 experienced a fall in pH.

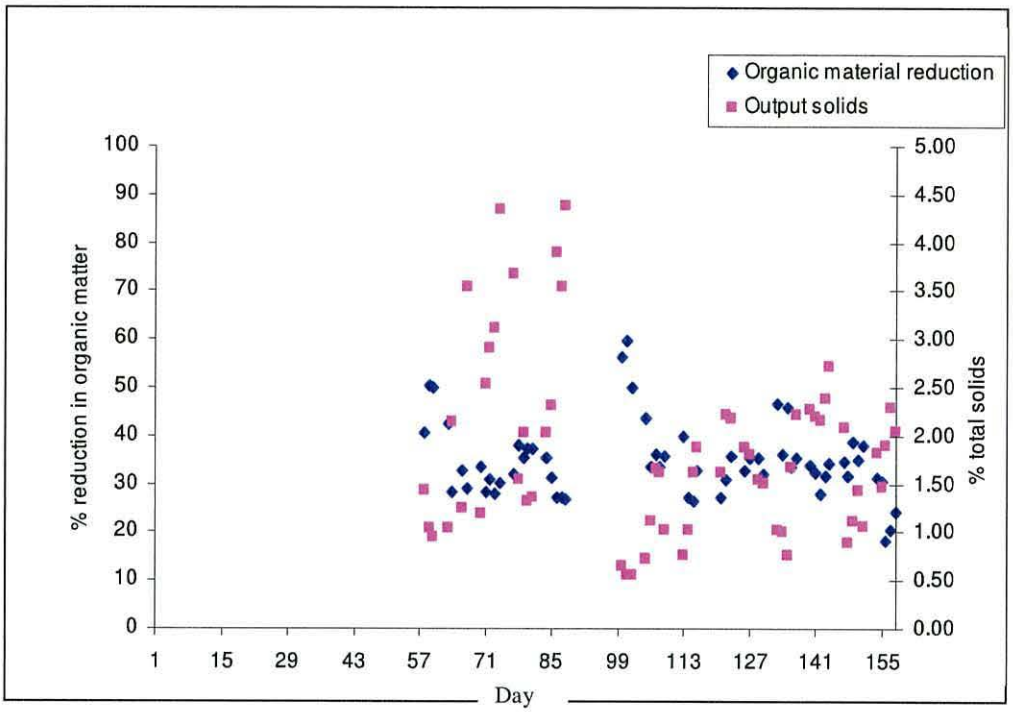

Figure 3.14 Total and volatile solids reduction and total solids: system start-up.

The former of these two comparative observations could suggest an improved hydrolysis of the feedstock at a lower pH, and a decrease in a different process, possibly acetogenesis or methanogenesis, may result from a lower pH in the mid-point of the system (vessel 2). These possibilities could explain the variation in organic reduction. After day 105 the organic reduction appeared to stabilise at *ca.* 34 %. The values for organic reduction appear rather low, but the volatile solids are measured as a percentage of the output total solids in relation to the input total solids. It must be noted that output total solids at *ca.* 1.75 %, as shown in Figure 3.14, was considerably lower than the input values of 3 – 5 % so there was a considerable reduction in the volume of organic material per litre of output digestate. This was seen in the relationship between total solids and volatile solids reduction around day 100, after a period of low organic loading rate. However, it is possible that there were settled solids remaining within the digester due to poor mixing.

3.3.3. System failure

The start-up period was the time taken for the system to stabilise. The system demonstrated reasonable methane production after *ca.* four months of operation, but

was eventually overloaded and failure occurred during the period 3rd March 2006 until the 7th of April 2006.

Overloading was accomplished deliberately by constantly increasing the organic loading rate (Figure 3.15), from 2.11 g VS l^{-1} d^{-1} on day 176 to 3.51 g VS l^{-1} d^{-1} on day 189.

The failure of the system occurred sequentially from vessel 1 to 4 according to the data obtained. The overload began by a decrease in the pH (Figure 3.16), a less negative redox potential (Figure 3.17) and a decrease in conductivity (Figure 3.18) of vessel 1. These data were accompanied by low total alkalinity (Figure 3.19) in this vessel (*ca.* 2400 $mg.L^{-1}$).

The pH in vessel 1 dropped to a low of pH 3.8, conductivity to *ca.* 2.3 mS cm^{-1}, redox increased into positive values and total alkalinity eventually reduced to below the detection limit during the failure period.

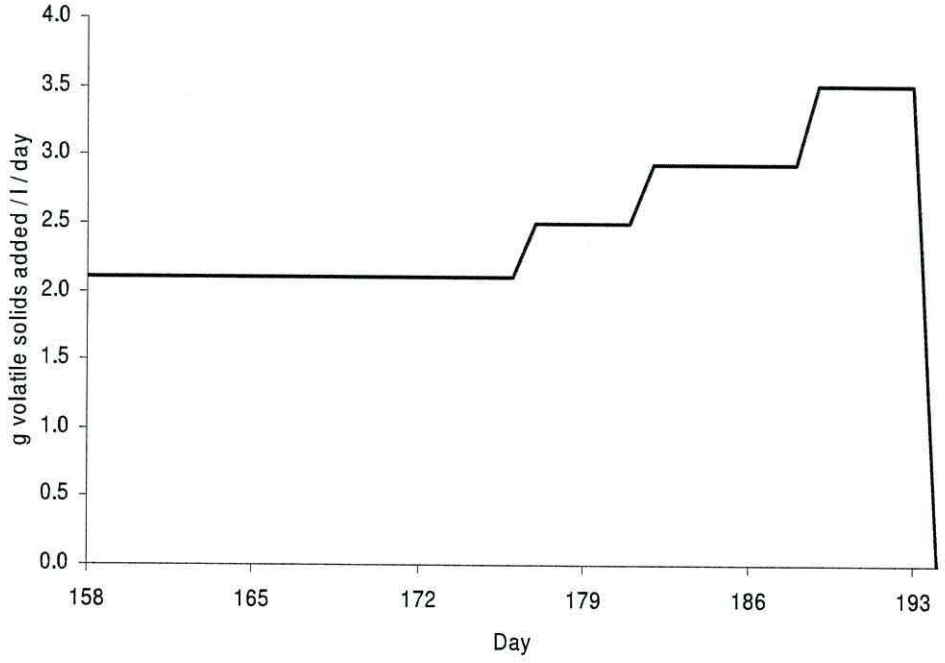

Figure 3.15 Organic loading rate: system failure.

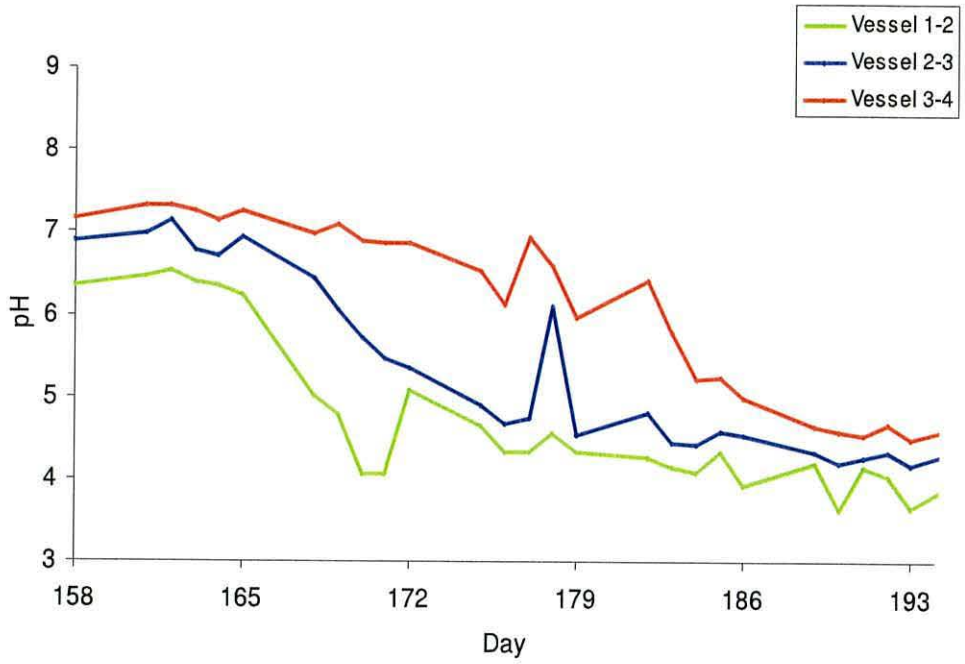

Figure 3.16 pH: system failure.

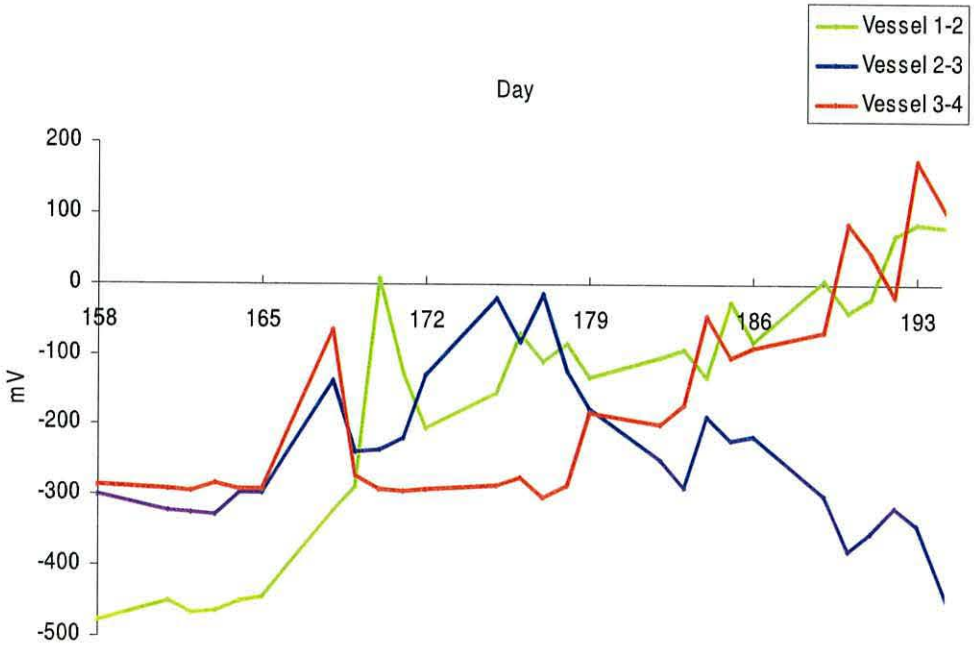

Figure 3.17 Redox potential: system failure.

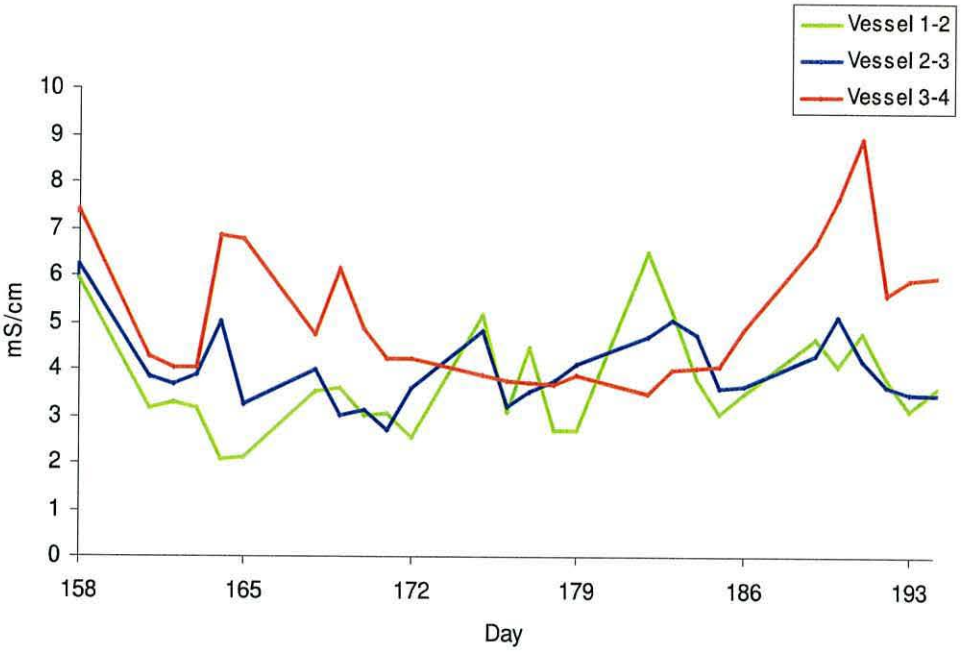

Figure 3.18 Conductivity: system failure.

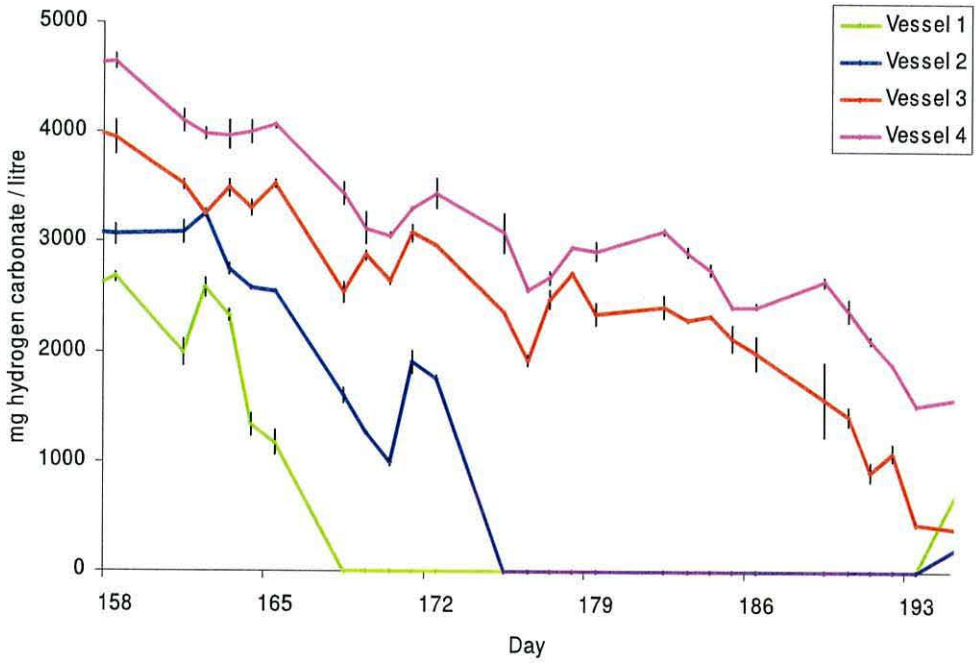

Figure 3.19 Total alkalinity: system failure.

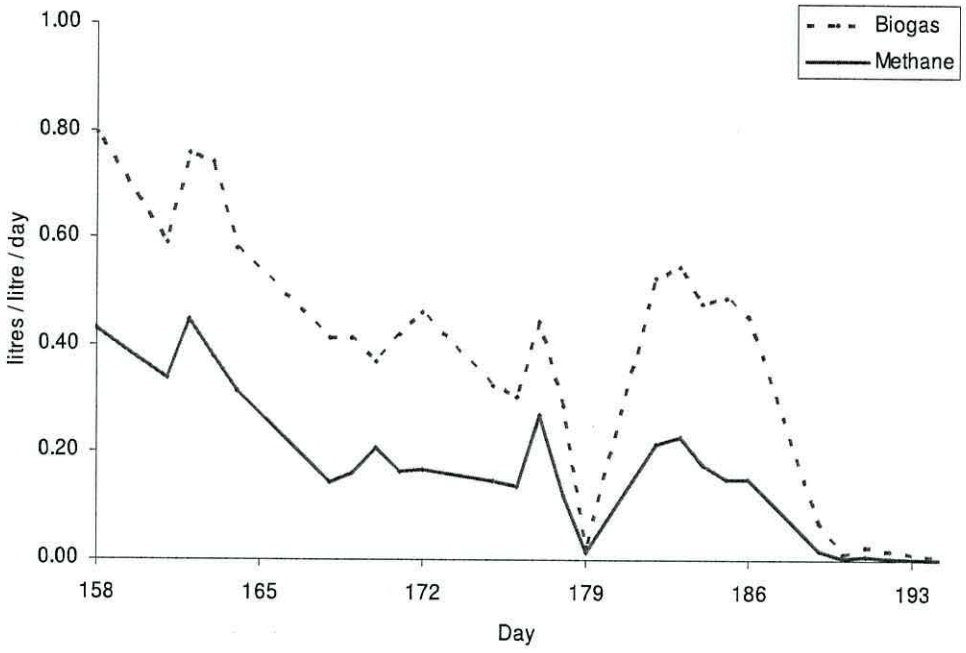

Figure 3.20 Gas production: system failure.

Figure 3.21 Gas yield: system failure.

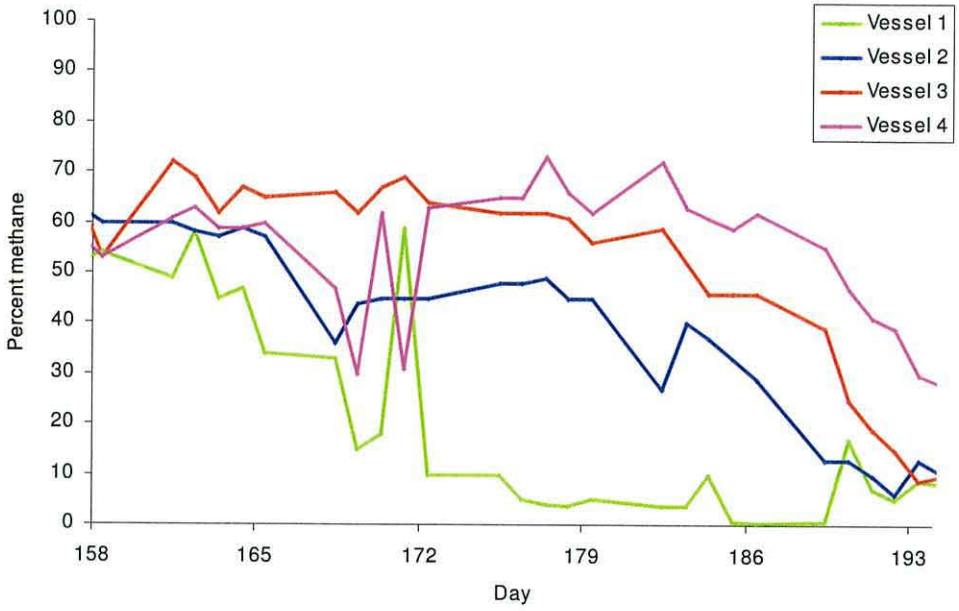

Figure 3.22 Methane percentages: system failure.

Failure was marked by a significant decrease in methane production (Figure 3.20) and yield (Figure 3.21) as methanogenesis apparently became inhibited. Low pH was probably responsible for this inhibition (Mosey and Fernandes, 1989). The effects of methanogenic inhibition could also be seen in the methane concentration of the biogas (Figure 3.22), which decreased in all vessels.

The above changes occurred in all vessels, but with a noticeable delay between the sequential stages. For instance, a particular vessel started to fail *ca.* six days after the preceding vessel.

Hydrogen concentration of the biogas (Figure 3.23) was seen to decrease suddenly in all vessels during the early stages of failure, only to increase again to levels beyond the scale of the measurement instrument. Gas phase H_2 concentration has previously been measured in anaerobic digesters to determine the effectiveness of this parameter for process state determination (Guwy *et al.* 1997: Mathiot *et al.* 1992). It has been shown that the partial pressure of H_2 is an important disturbance indicator, in that changes in both the quantity and composition of the substrate produces rapid peaks in H_2 partial pressure (Guwy *et al.* 1997) but this did not necessarily mean process failure. In addition, the absolute concentration of biogas hydrogen was not constant following similar process overload situations (Guwy *et al.* 1997). H_2 in anaerobic digestion is

mainly the product of fatty acid catabolism. A high concentration of H_2 would logically suggest an overall increase in total fatty acids and an increase in shorter chain fatty acids, particularly propionic and acetic acids as longer chain fatty acids are broken down. A high fatty acid concentration is often a symptom of an overloaded digester (Boone and Xun, 1987) but no correlation between hydrogen gas concentration and propionic acid concentration was found in a study by Guwy *et al.* (1997). The fall followed by a rapid increase in H_2 concentration found in this study can be attributed to a short term inhibition of the organisms responsible for fatty acid catabolism.

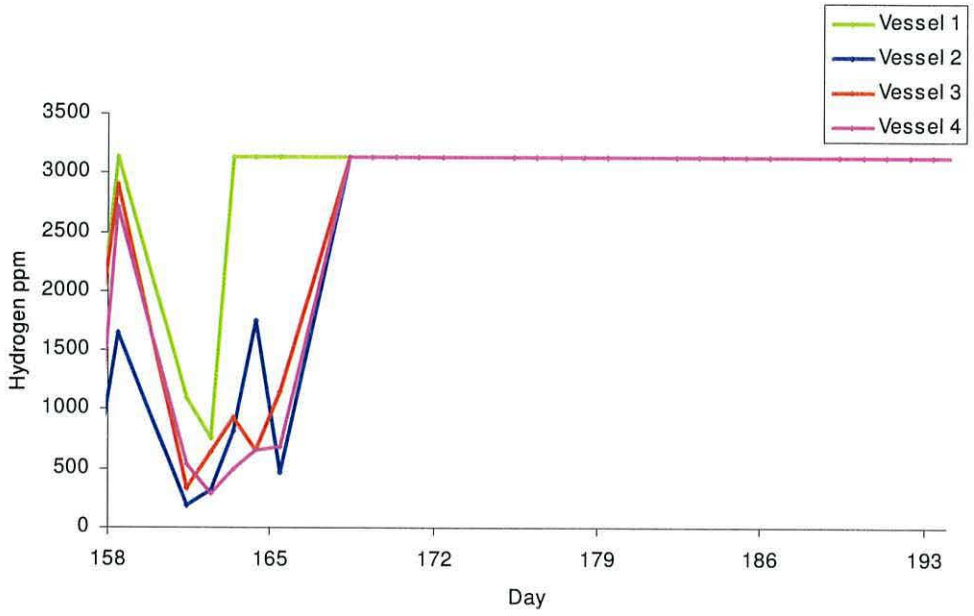

Figure 3.23 Hydrogen: system failure.

The reduction in volatile solids (Figure 3.24) also decreased during failure, from *ca.* 35 % during start-up to *ca.* 20 % during failure. The lowest values were noticed to coincide with the sudden decrease in vessel 1 alkalinity, pH and methane percentage, suggesting vessel 1 could be of key importance. The total solids of the output increased as the volatile solids reduction decreased. This further added to the overall organic content of the output, and would suggest that the overload situation may have inhibited the hydrolysis process, leading to more solid material remaining after digestion. It has been reported that hydrolysis can suffer from product inhibition (Mata-Alvarez, 2002), which could in turn result from the inhibition of acidogenesis by excessive fatty acids (Kalyuzhnyi, 1997). It would therefore seem that the entire anaerobic digestion process

is inhibited under extreme overload conditions such as those encountered in this experiment.

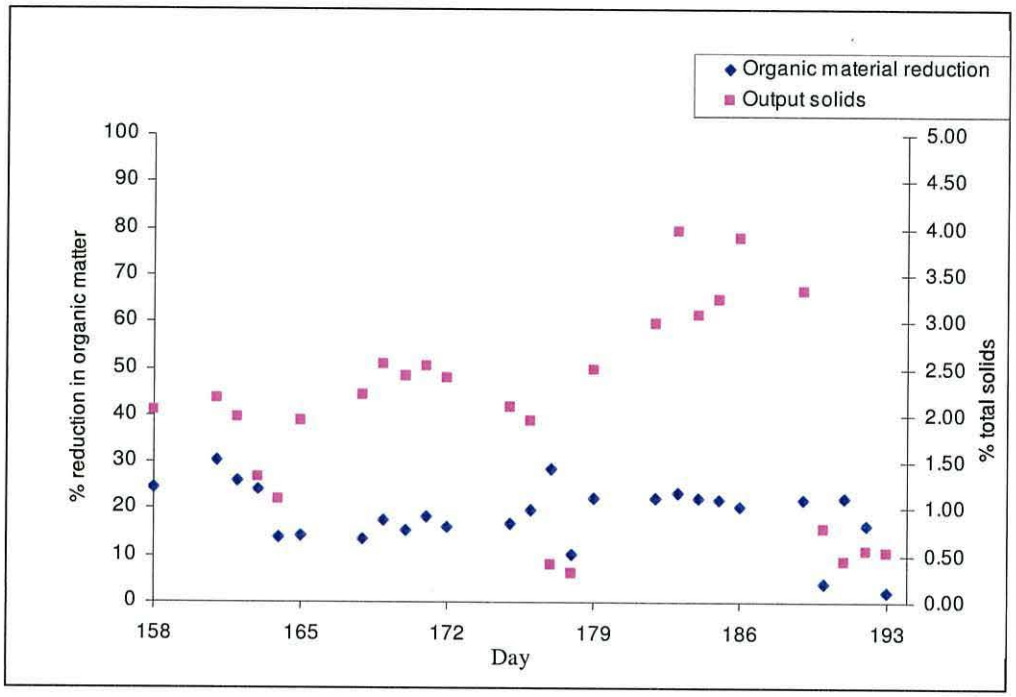

Figure 3.24 Volatile solids reduction and total solids: system failure.

3.3.4. System recovery

Recovery of the failed system consisted of bringing the organic loading rate to zero for ten days (Figure 3.25), followed by feeding with the remains of the same inoculum material used in the start-up process (stored at room temperature) at a low organic loading rate of 0.25 g VS l^{-1} d^{-1} for twelve days. The feedstock was supplemented with 3.44 g l^{-1} $NaHCO_3$ (2.5 g l^{-1} HCO_3^-) to increase the total alkalinity.

An increase in pH in all vessels (Figure 3.26) and conductivity (Figure 3.27) and a decrease in redox potential (Figure 3.28) occurred slowly during the quiescent period where no feeding occurred, and rapid changes were observed after the addition of $NaHCO_3$. The changes occurred sequentially through the system from vessel 1 to 4 as the $NaHCO_3$ spread through the system, but it was four weeks before any measurable methane was produced (Figure 3.29) suggesting that the organism population needed time to recover even though the pH was not at an inhibitory level. Once methane was

detected, feeding with normal feedstock (*i.e.* not supplemented with $NaHCO_3$) began at a low organic loading rate of 1.16 g VS l^{-1} d^{-1}.

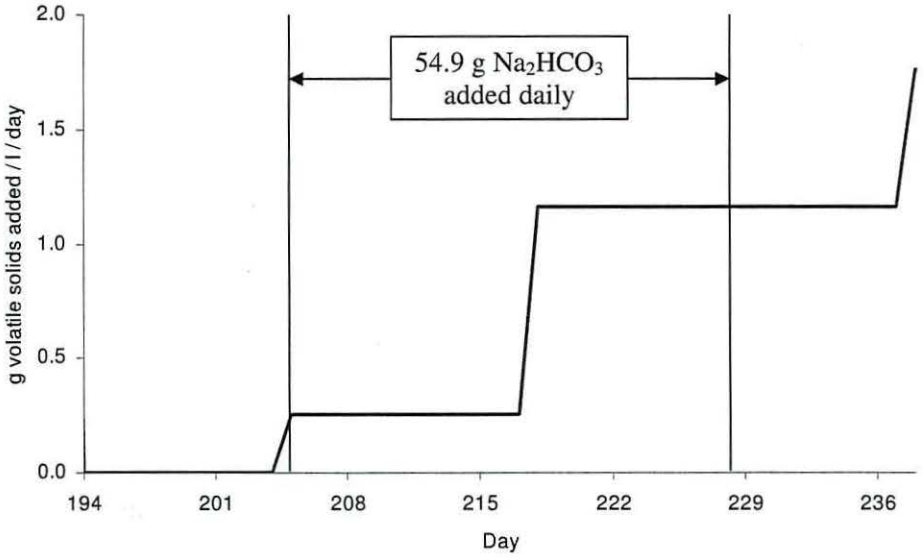

Figure 3.25 Organic loading rate: system recovery.

The sudden decrease in redox potential to -700 mV in vessel 2, well below the readings from the other vessels, and the sudden increase to over +200 mV was a cause for concern. The probe was removed and cleaned, after which redox suddenly reached *ca.* -70 mV, which was similar to the other vessels. This change was ascribed to fouling of the probe and highlights the need for occasional maintenance operations. It is not known how long fouling of the probe had affected results, the previous calibration having taken place on day 184.

The system generally demonstrated a roughly inverted pattern of data during the recovery period when compared with normal operation. For example, vessel 1 displayed greatest pH and alkalinity and vessel 3 the lowest. This was because of the remedial action taken to improve recovery: *i.e.* high buffering capacity digestate pumped through the vessels in sequential order. The effect of the 'remedial digestate' can be clearly seen in the total alkalinity data (Figure 3.30).

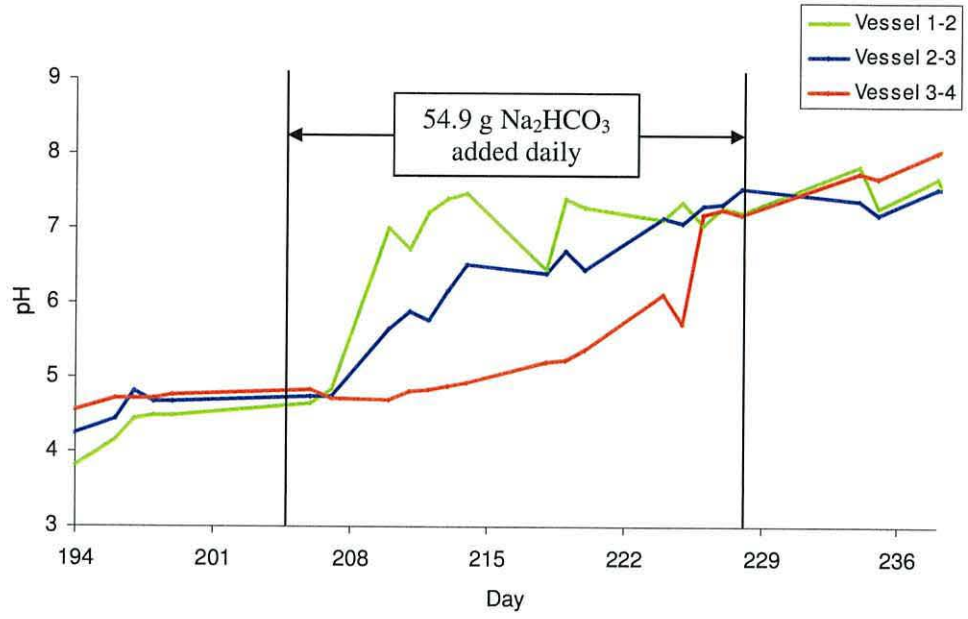

Figure 3.26 pH: system recovery.

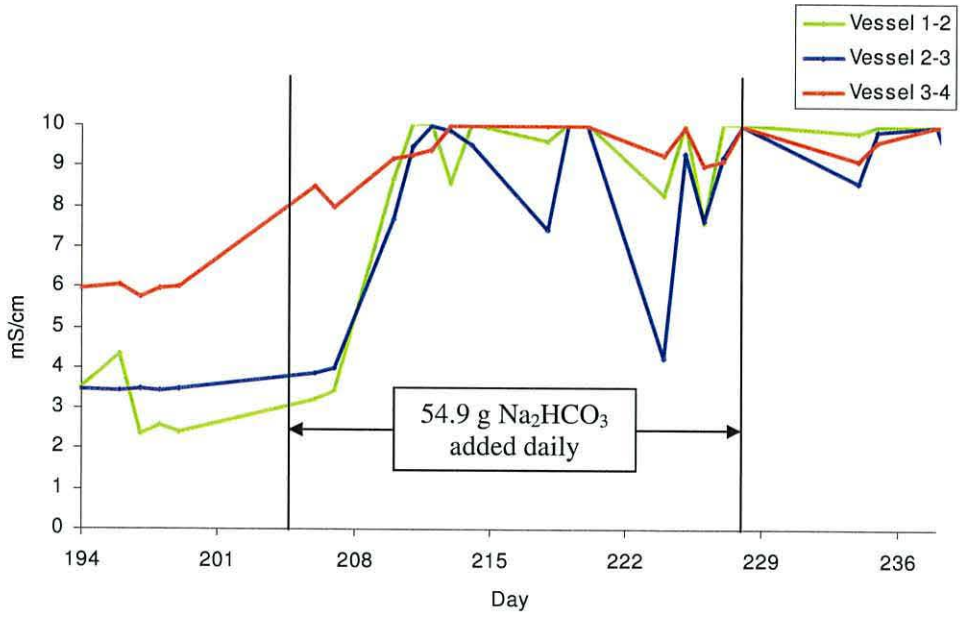

Figure 3.27 Conductivity: system recovery.

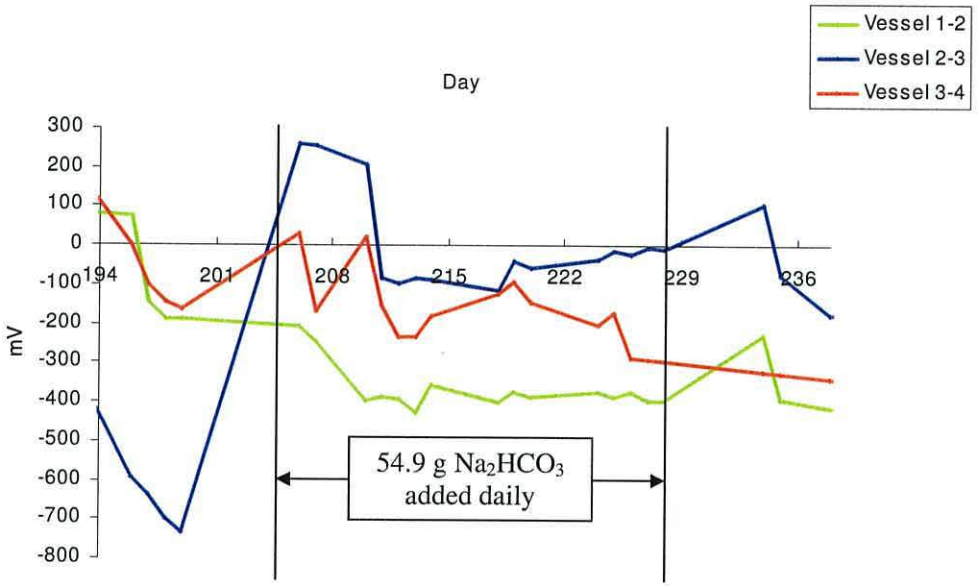

Figure 3.28 Redox potential: system recovery.

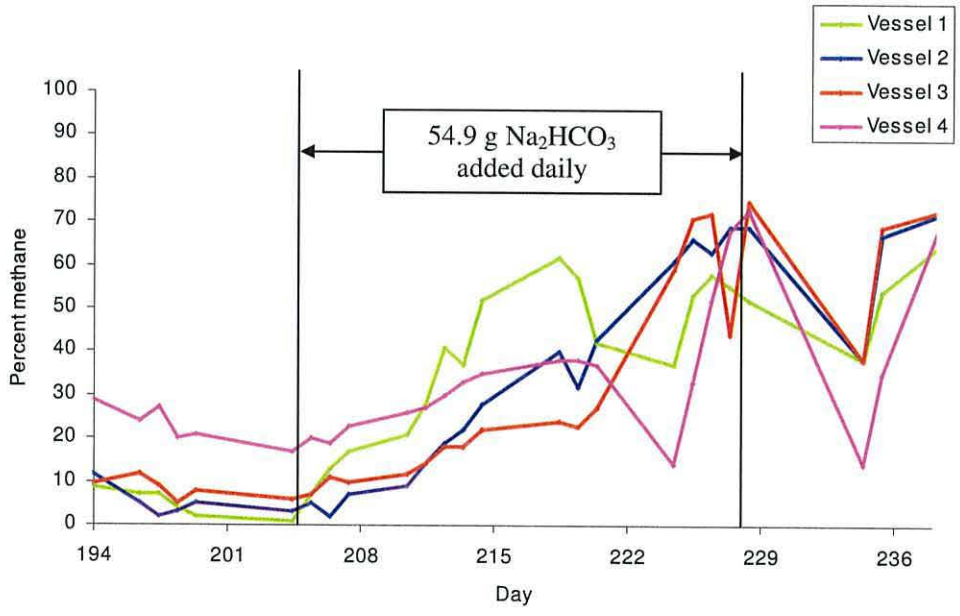

Figure 3.29 Methane percentage: system recovery.

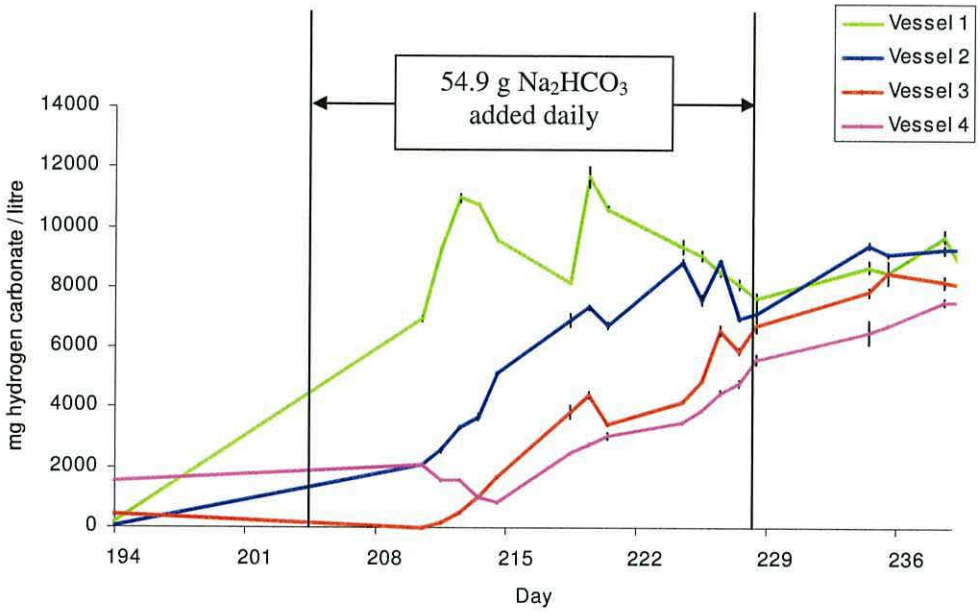

Figure 3.30 Total alkalinity: system recovery.

After the remedial digestate was added, individual vessel biogas volume measurements increased. The daily gas production and yield values (Figures 3.31, 3.32 respectively) were very erratic during the recovery period, with very little pattern emerging except an unexplained maximum in methane production of 0.6 to 0.9 l l^{-1} d^{-1} from all vessels from day 194 to 197, followed by a decrease to between 0.05 to 0.25 l l^{-1} d^{-1}.

The percent methane within the biogas volume (Figure 3.29) was also highly variable during recovery, but showed a generally increasing trend from <1 % to 30 % v/v methane (vessels 1 to 4 respectively) when the system began to recover to *ca.* 70 % v/v methane in vessels 2 to 4 at the end of the recovery period.

Vessel 1 methane percentage dropped suddenly from 65 % to 39 % v/v methane when the organic loading rate was increased from 1.16 g VS l^{-1} d^{-1} to 1.76 g VS l^{-1} d^{-1}. This was reflected in the sudden fall in vessel 1 alkalinity during this time. By comparison, vessel 4 methane did not drop below 17 % during either failure or recovery. This experiment demonstrated the sequential changes to the system, as the final vessel was least affected by the overload, and also that a failed system can be very delicate during a rapid recovery period, as implemented in this section of the experiment.

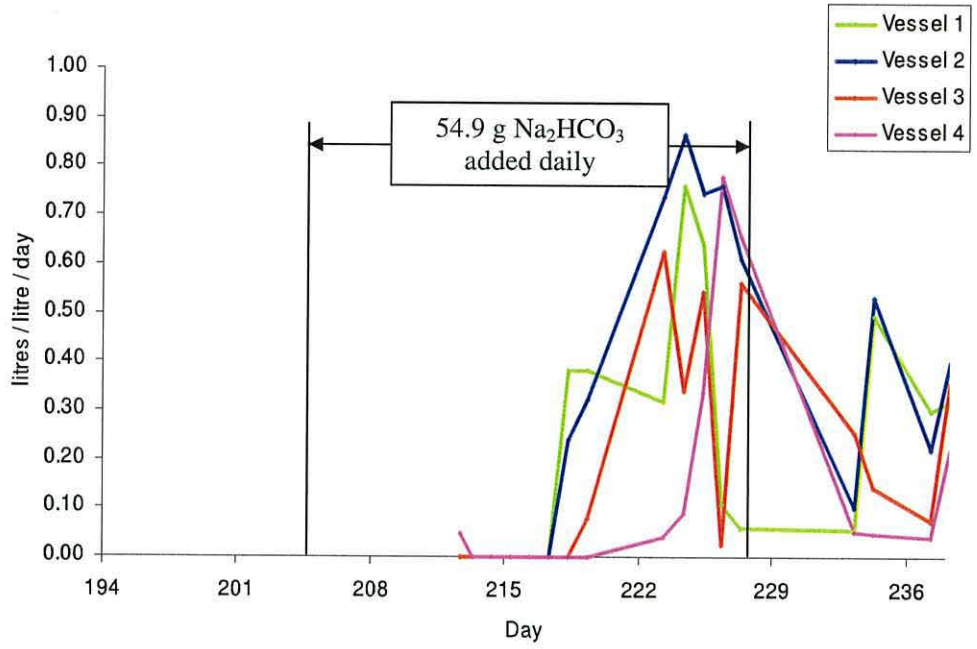

Figure 3.31 Methane production: system recovery.

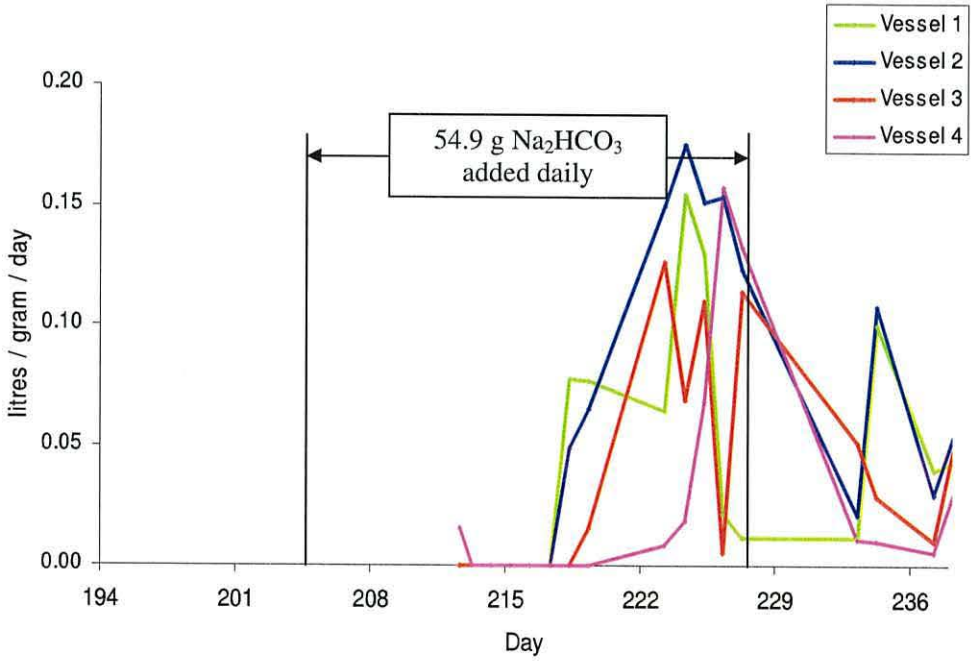

Figure 3.32 Methane yield: system recovery.

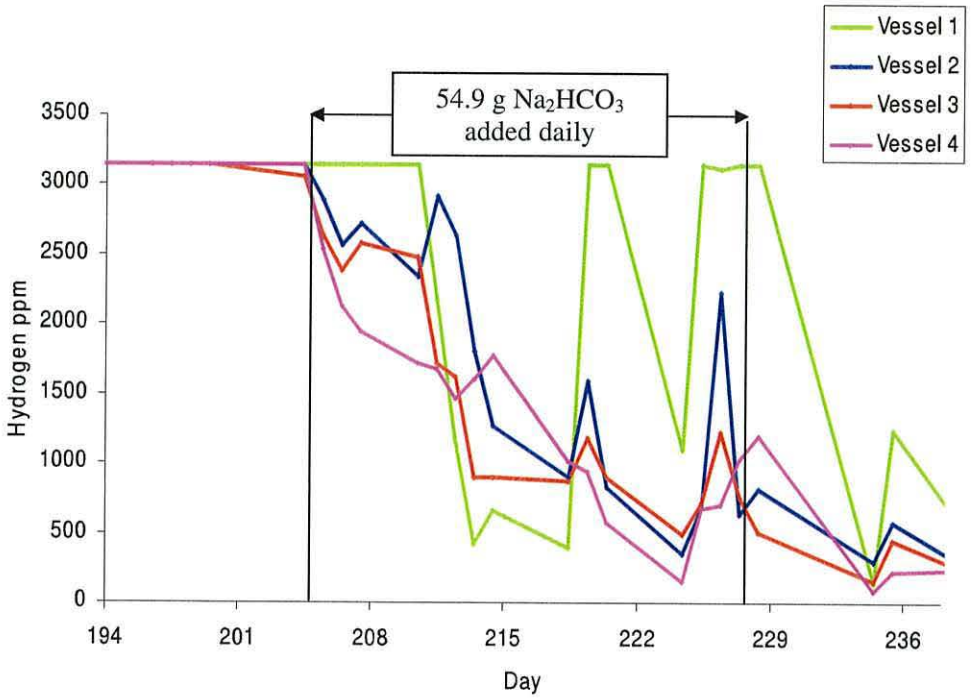

Figure 3.33 Hydrogen: system recovery.

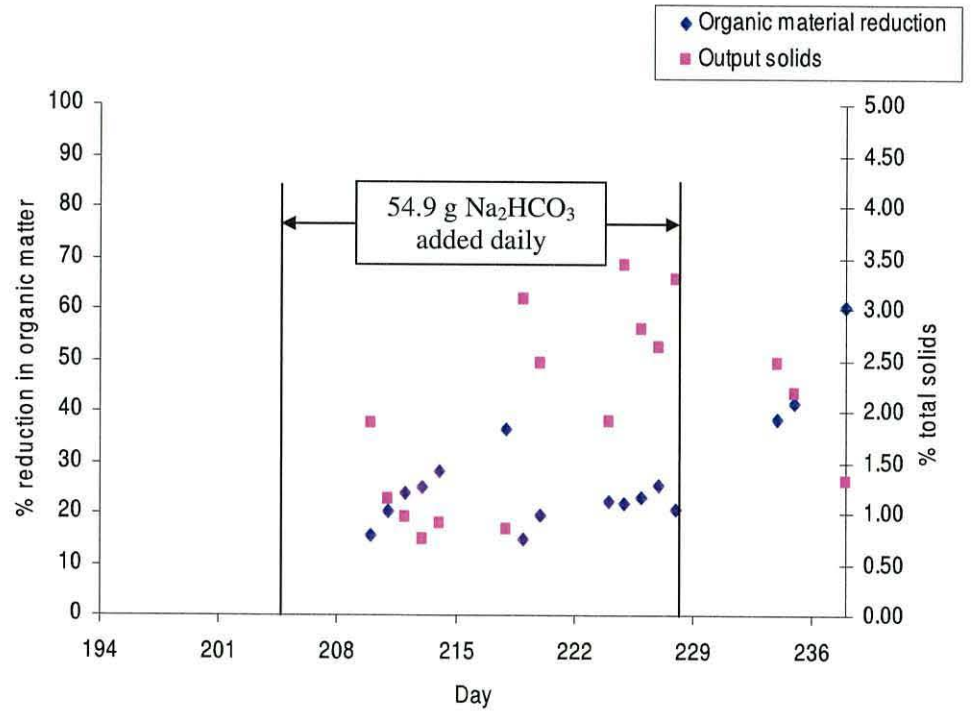

Figure 3.34 Volatile solids reduction and total solids: system recovery.

Further evidence that the system was recovering could be found in the hydrogen concentrations (Figure 3.33), which decreased to within the instruments range in vessels 2, 3 and 4 as they were before the failure period, but the data also remained very erratic. This would suggest a decrease in fatty acid production as the excess formed during failure were slowly metabolised. Also, the percentage of volatile solids reduction (Figure 3.34) also increased during this period to *ca* 50 %, as more and more organic carbon was lost to the gas phase as methane and carbon dioxide.

Once the relationship between vessels had returned to normal, particularly the pH and alkalinity increasing through the system from vessel 1 to 4, the recovery period was considered to be over.

3.3.5. Stabilisation at the maximum sustainable loading rate

During the stabilisation period, the organic loading rate was increased from 1.76 g VS l^{-1} d^{-1} to 2.34 g VS l^{-1} d^{-1} to investigate maximum sustainable loading rate (Figure 3.35). The result of this was stability of the on-line probe measurements: pH in vessel 2 was *ca.* pH 7 (Figure 3.36), and in vessel 3 was *ca.* pH 7.5. However, the pH in vessel 1 fell from pH 7 to *ca.* pH 6.2 during the stability period, but there was no sudden change that was considered a cause for concern.

The redox potential (Figure 3.37) remained between -350 mV and -400 mV throughout the stable period in all vessels, and conductivity (Figure 3.38) remained at *ca.* 7.8 mS cm^{-1} in vessel 1, *ca.* 8.3 mS cm^{-1} in vessel 2 and *ca.* 9.7 mS cm^{-1} in vessel 3. The problem with conductivity values being greater than full scale deflection was again noticed in vessel 3, suggesting a higher degree of mineralisation through the system.

The final increase in loading rate to 2.64 g VS l^{-1} d^{-1} produced a decrease in pH and an increase in the redox potential. This effect was seen sooner and was more pronounced at the front end of the system, as was expected from the sequential pattern seen during the failure part of the experiment. This would suggest the system was again becoming unstable.

All *in situ* measured parameters also remained reasonably steady during the stabilisation period. Total alkalinity (Figure 3.39) was *ca.* 3200 and 4200 $mg.L^{-1}$ for vessels 1 and 2 respectively, and *ca.* 5600 $mg.L^{-1}$ for vessels 3 and 4. This period was considered 'stable' in terms of the methane production rate (Figure 3.40), which averaged at 0.55 l l^{-1} d^{-1} overall. The production of methane was, however, distributed unevenly amongst the vessels. Thus, methane production from vessels 1 and 2 was *ca.*

1.1 $l\ l^{-1}\ d^{-1}$, whereas vessel 3 methane production was 0.25 $l\ l^{-1}\ d^{-1}$ and vessel 4 only 0.1 $l\ l^{-1}\ d^{-1}$. This was attributed to the rapid methane production characteristic of this feedstock (Section 3.3.2).

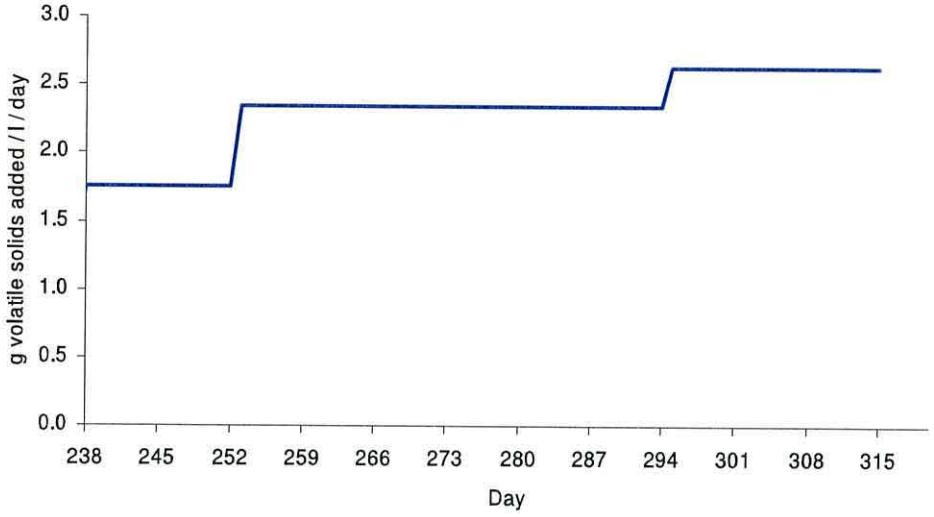

Figure 3.35 Organic loading rate: system stabilised.

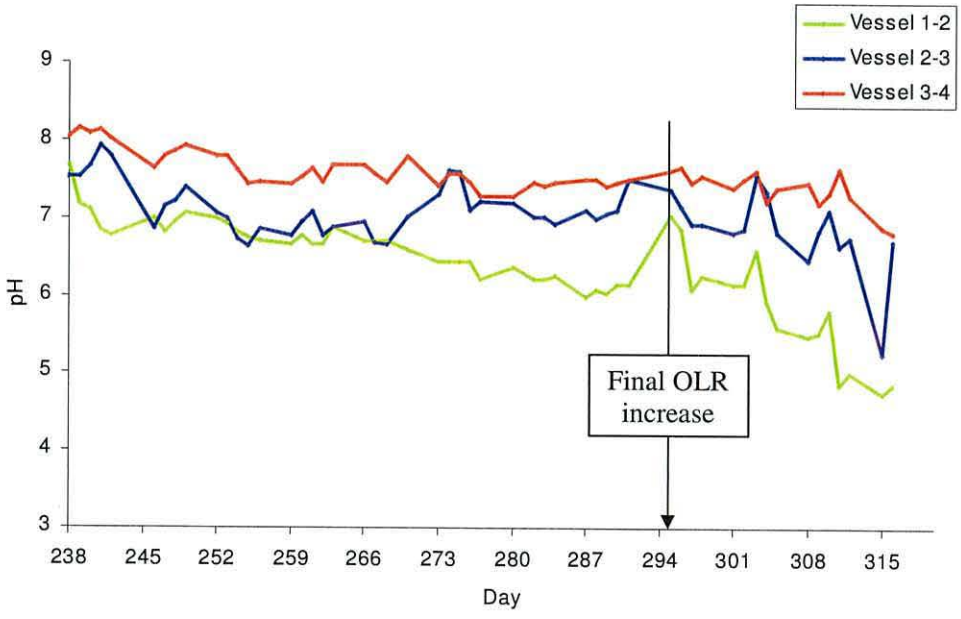

Figure 3.36 pH: system stabilised.

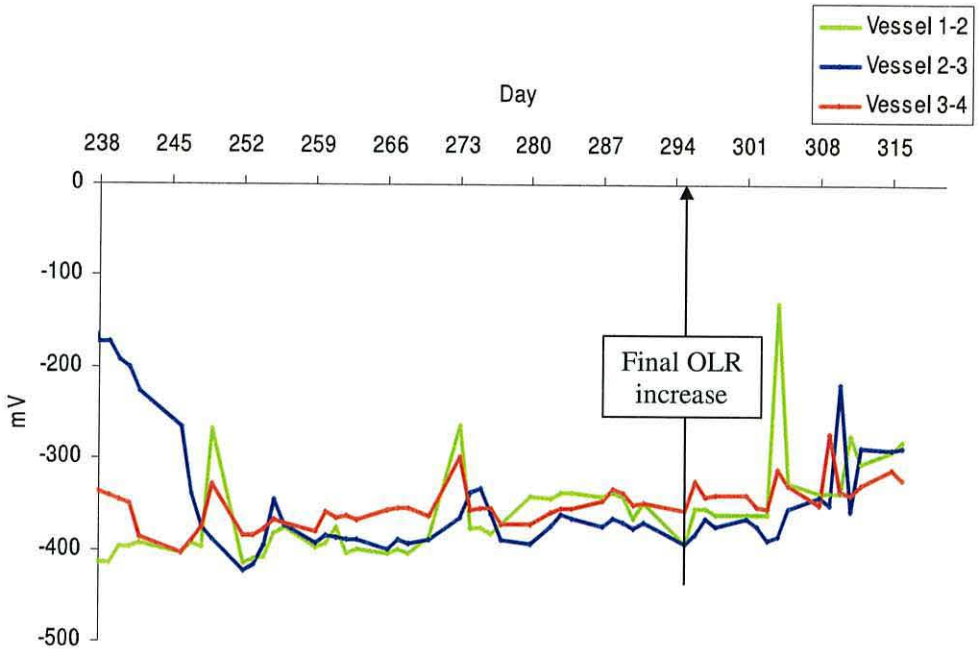

Figure 3.37 Redox potential: system stabilised.

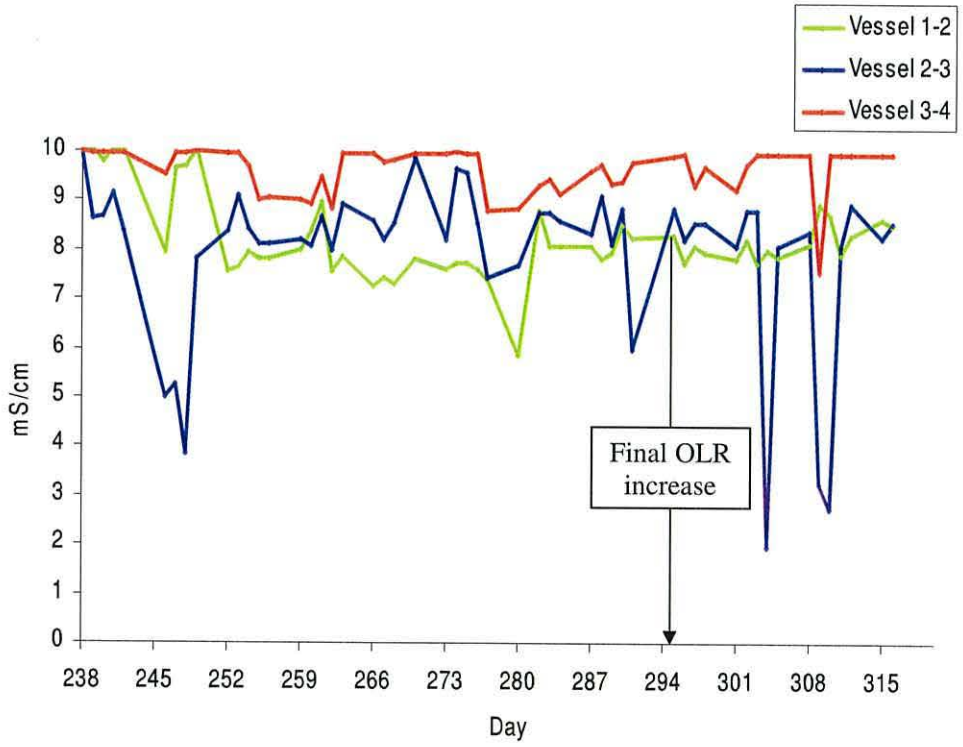

Figure 3.38 Conductivity: system stabilised.

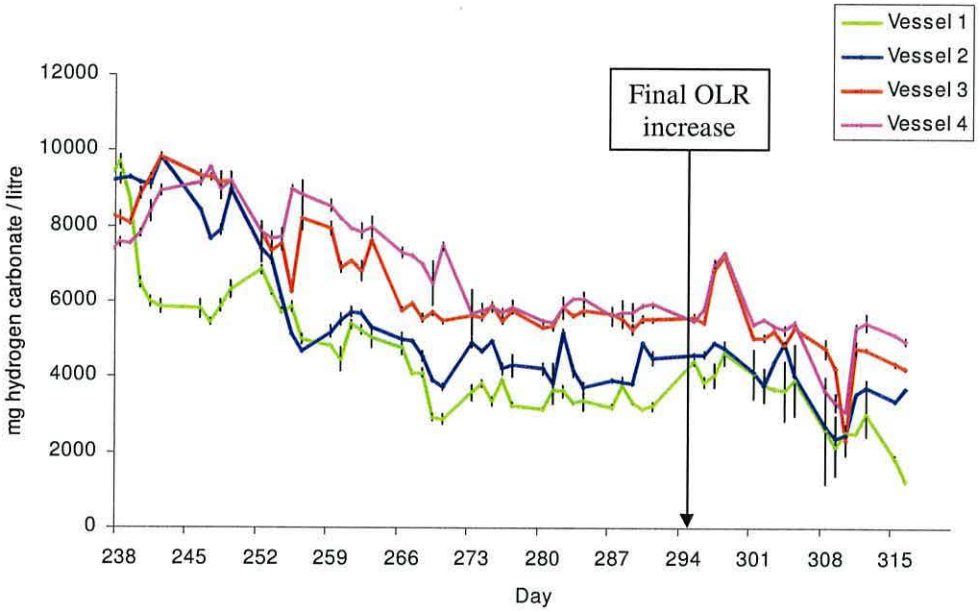

Figure 3.39 Total alkalinity: system stabilised.

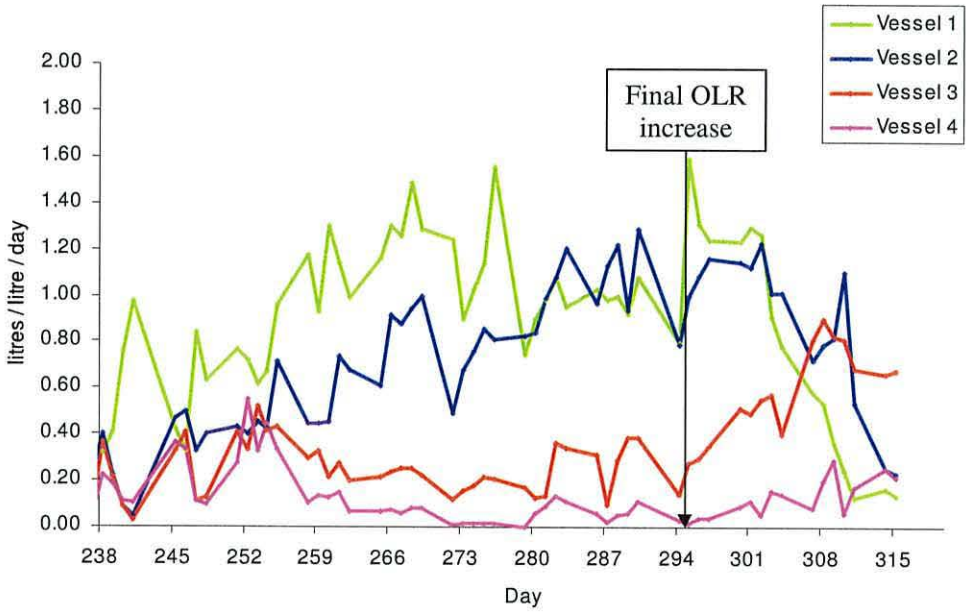

Figure 3.40 Methane production: system stabilised.

The high methane production from vessels 1 and 2 was surprising considering the pH in vessel 1 was low at *ca.* pH 6. The decrease in total methane production as a result of the final organic loading rate increase was unexpected. The data show that an

increase in methane production from vessels 3 and 4 was not sufficient to compensate for the loss in vessels 1 and 2. It was expected that the high-rate methane production from the early stages would be shifted downstream to vessels 3 and 4, perhaps with even greater production rates as the first two vessels would allow more of the feedstock to be hydrolysed. The fact that this did not occur could be partly explained by the nature of the feedstock, as characterised by the batch experiments. The batch experiments were performed after the majority of data had been collected from the continuous process experiment in an attempt to explain the observed pattern of methane production. It would seem that there were two basic components to the feed. Firstly, a rapidly hydrolysable component that was very quickly converted to fatty acids and consequently methane, and secondly a rather recalcitrant component that remained largely un-hydrolysed, even at long hydraulic retention times. This would explain the 'front-heavy' nature of the four stage system for methane production and the rapid but short-lived methane production observed in the batch experiments. However, it should still have been possible to shift the methane production to vessels 3 and 4, thus increasing the maximum stable organic loading rate and the potential income for waste treatment at an industrial scale. It is possible that stages 1 and 2 had a larger population of active organisms, particularly methanogenic types, which had grown as a result of the constant supply of feed. Ironically, later vessels would be expected to have relatively low fatty acid concentrations, as shown by Chanakya *et al.* (1993) where acetate concentrations of between 5000 and 14000 $mg.L^{-1}$ were found in the acid (first) phase of a two phase system whereas acetate concentrations of only 750 to 2500 $mg.L^{-1}$ were found in the methanogenic (second) phase. Thus there would be little scope for growth of acetogenic or methanogenic organisms in later vessels. Increasing the loading rate (and therefore the flow rate) could have increased the fatty acid concentration in vessels 3 and 4, but sufficient organisms may not have been available to use them. It follows that a slower increase in organic loading rate would facilitate a steady increase in active microbial biomass and consequently higher methane production in later vessels, but this was not investigated due to time constraints. Increasing the loading rate depressed the methane production in vessels 1 and 2, but only slightly increased methane production in vessels 3 and 4. Methane yield (Figure 3.41) followed the pattern of methane production as the organic loading rate was constant during this period.

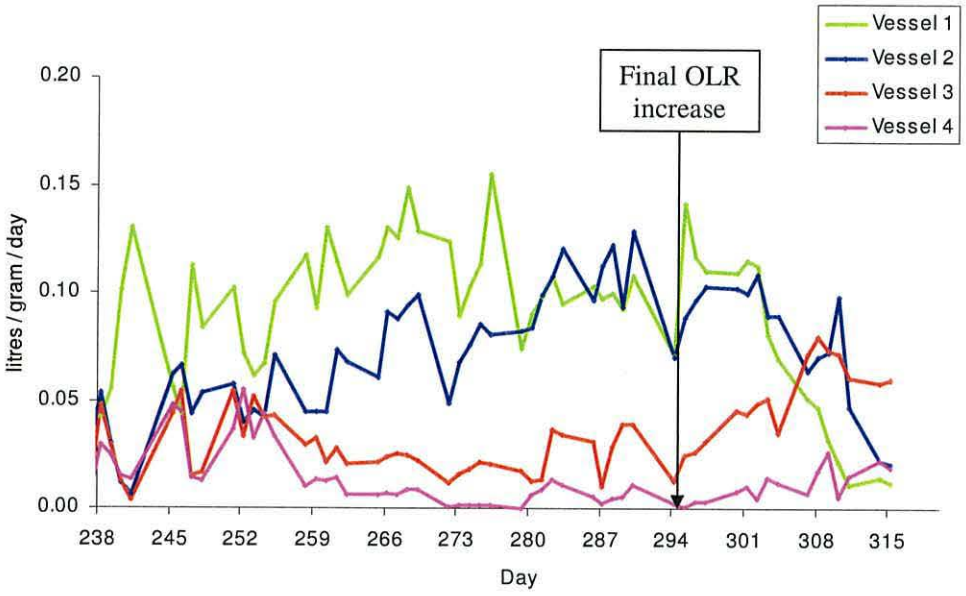

Figure 3.41 Methane yield: system stabilised.

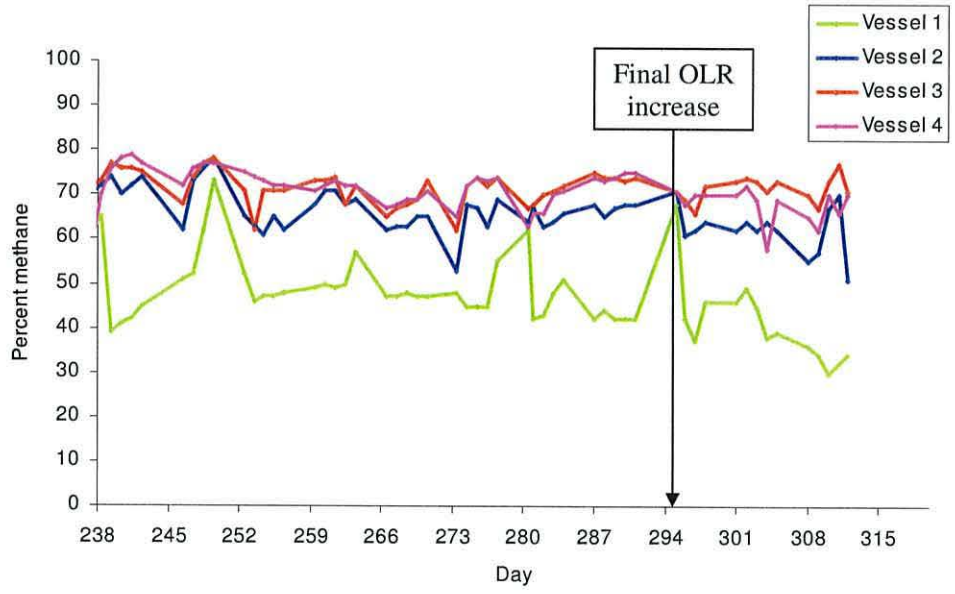

Figure 3.42 Methane percentages: system stabilised.

Although methane production changed in all vessels, the biogas methane percentage (Figure 3.42) remained constant at 45 to 50 % v/v in vessel 1 and between

65 and 70 % v/v in vessels 2, 3 and 4. It was expected that the methane in the biogas would decrease as the pH fell, as seen earlier.

The concentration of hydrogen (Figure 3.43) in the biogas was seen to decrease sequentially through the four stages during the stable period. For example, vessel 1 hydrogen remained above full scale deflection for most of this period, yet was seen to decrease when overloading started again. Vessels 2, 3 and 4 remained below 1000 ppm, with less fluctuation in the later stages of the process. The sudden increase in hydrogen concentration in vessels 2, 3 and 4 on day 273 coincided with a slight decrease in biogas methane concentration, a decrease in methane production in vessels 1 and 2, an increase in redox potential in all vessels and preceeded a decrease in conductivity at all measuring points. This would suggest an increase in fatty acid catabolism causing a temporary inhibition of methanogenic organisms. Any increase in hydrogen concentration was not noticed in vessel 1 as the concentration here was already above the full scale deflection of the measurement instrument. The decrease then increase in vessel 1 H_2 concentration when the loading rate was increased was similar to the pattern noticed during the first failure period (Figure 3.23). However, this experiment did not continue to push the system into complete failure a second time as further experimental duties were required of the digester, so it is not known if the hydrogen concentration would increase again in this case. It is possible that the decrease in H_2 concentration was indicative of a decrease in the metabolism of longer chain fatty acids, perhaps due to product inhibition of the bacteria responsible (Kalyuzhnyi, 1997).

Volatile solids reduction (Figure 3.44) declined slowly from *ca.* 30 % to *ca.* 20 % during the stable period, and decreased further to *ca.* 10 % at the end of the experiment as the system started to fail. The total solids value of the digestate also fell from *ca.* 3 % to *ca.* 2 %, but the results were highly variable. This suggests that the actual concentration of organic matter in the liquid digestate decreased during the stable period. Inspection of the digester at the end of the experiment showed that solids were being retained, particularly in vessel 1.

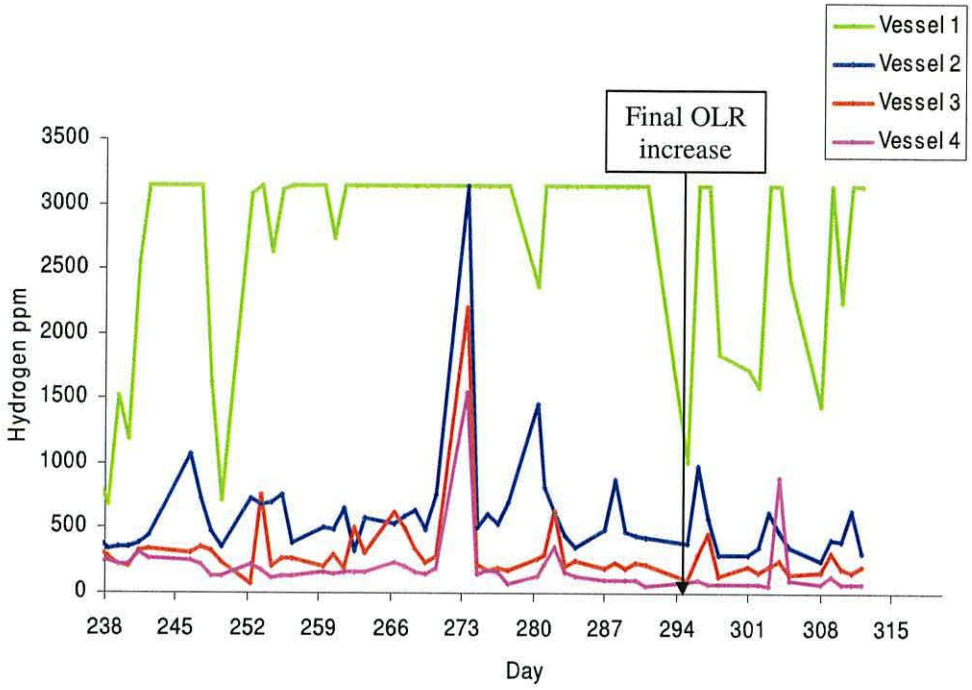

Figure 3.43 Hydrogen: system stabilised.

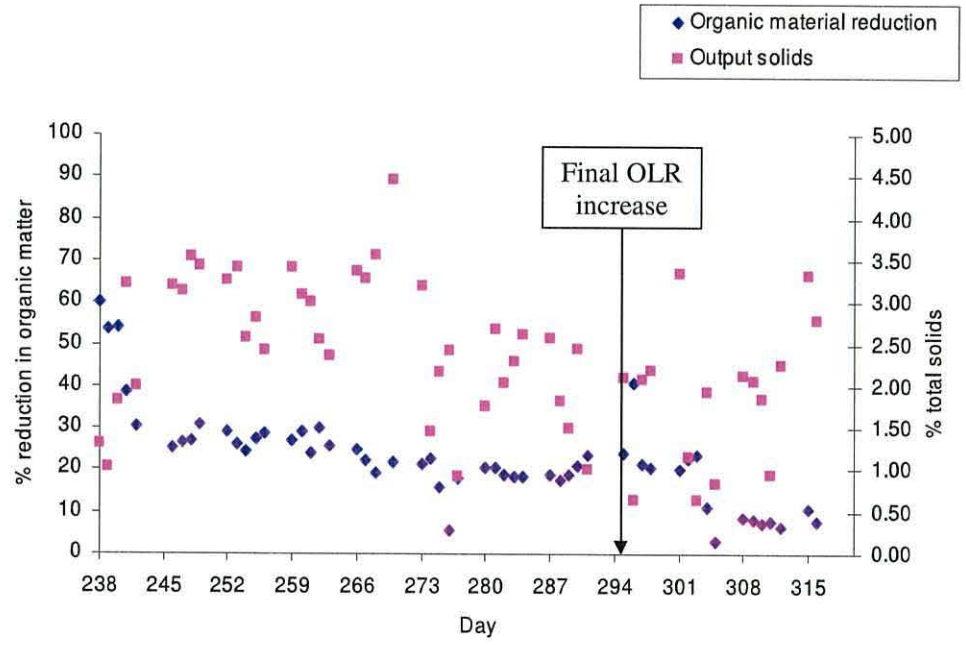

Figure 3.44 Volatile solids reduction and total solids: system stabilised.

3.3.6. Statistical analyses to find the optimum methane production and yield

3.3.6.1. Principal component analysis

The principal component analysis loading plot of all data is shown in Figure 3.45. The data were scaled prior to analysis by multiplying all values by 1/standard deviation. This was a necessary step as the values of different parameters were of different orders of magnitude. Principal component analysis decomposes the data matrix into structure and noise components, the resulting principal components (PC) are a convenient way of viewing complex data relationships that would otherwise exist in three or more dimensions. The clustering of the gas volume related parameters is due to their being related, and it is clear that pH, redox, conductivity, alkalinity and biogas methane concentration all lie opposite the gas volume parameters in relation to the x-axis (PC1). It can be concluded that PC1, the component with maximal data variance, inversely relates the gas production parameters with pH, redox, conductivity, alkalinity and biogas methane concentration. The further the objcts in the loading plot are from the origin, the greater their contribution to that particular PC, in this case alkalinity appears to be the strongest factor relating to the gas volume measurements. PC2 can be examined in a similar way along the y-axis. For example, it can be seen that pH and redox contribute greatly to PC2 and are inversely related. Combining the object positions with respect to PC1 and 2, it can be seen that pH and biogas methane concentration are both directly opposite hydrogen gas concentration, suggesting that both PC1 and 2 affect the inverse relationship between these objects.

A principal component analysis of vessel 1 data was also considered to be of interest as vessel 1 provided the greater production of methane throughout the experiment. The loading plot is shown in Figure 3.46 and shows similar relationships to the combined data objects in Figure 3.45 except that redox potential is now slightly positively related to the gas volume measurements, hydrogen gas concentration now shows little effect on PC2, loading rate is now inversely related to pH and alkalinity and these parameters contribute greatly to both PC1 and 2.

However, the PCA results only give an indication of which factors appear significant and further analysis by regression model curve fitting was conducted to find values for each parameter at which optimal methane production and yield could be determined.

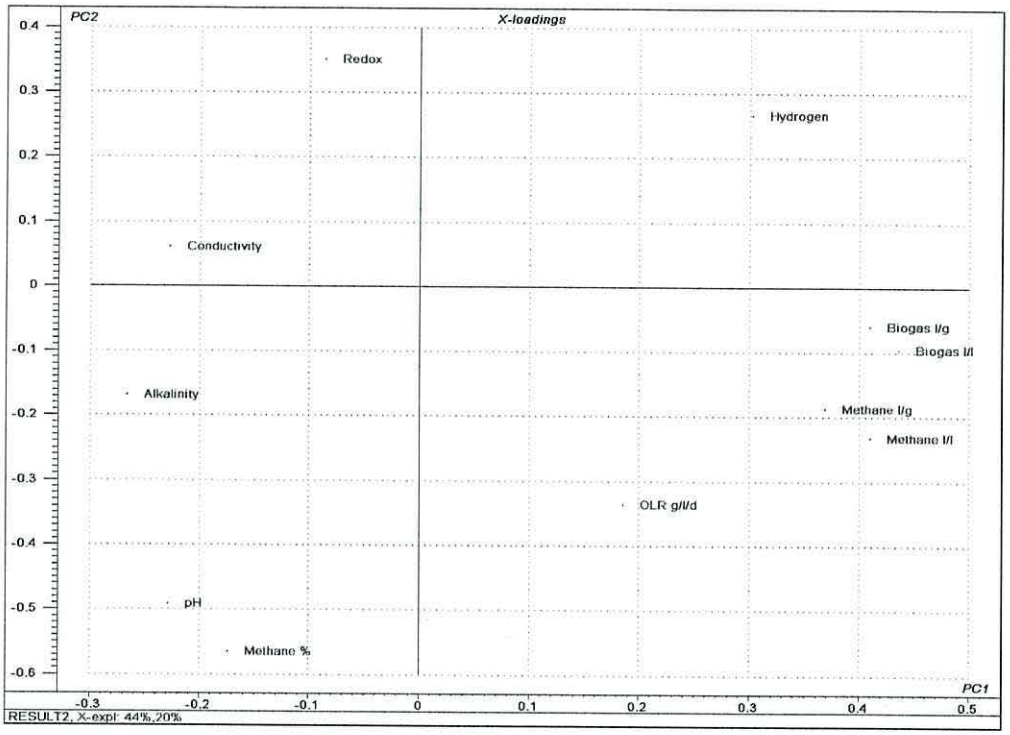

Figure 3.45 Complete PCA analysis loading plot of combined vessels anaerobic digestion data.

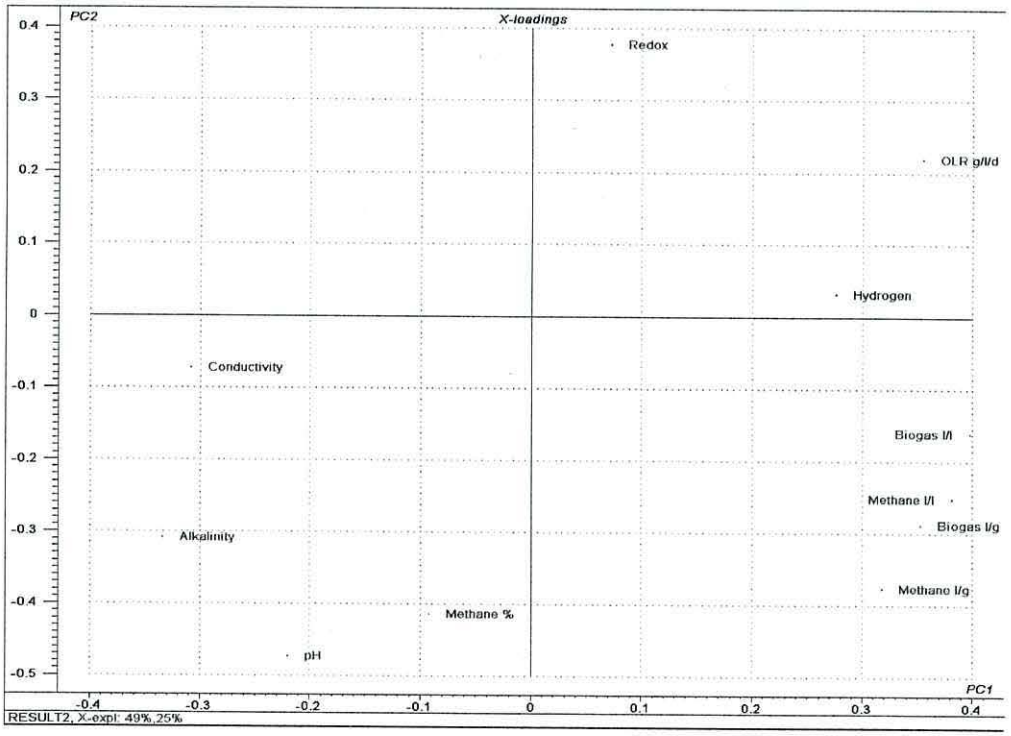

Figure 3.46 PCA analysis loading plot of vessel 1 data.

3.3.6.2. Regression models of methane production and yield

The objectives of this section were to plot methane production and yield data against all other measured parameters. By plotting these data, it was hoped to see if any relationship existed. Models were created by curve fitting non-linear regression using quadratic models as these fitted best in all cases. It must be stressed that these particular models were not intended to be accurate predictors of methane production or yield, but rather to apply a best-fit curve to the data, and where all available curves were seen to fit poorly, the parameter was considered to be a poor predictor of methane production or yield. Models were selected for the shape of the regression line in relation to the data, the maximum percentage R^2 adjusted value (percentage of variance accounted for by model) and the minimum standard error of observations. The models also provided an equation of the curve from which maximum methane production and yield were calculated, giving an ideal value of each parameter where possible. These are listed in Appendix 1.

The limitations of curve fitting non-linear regression was taken into account when building these models, in that some models fitted curves which were not very close to the data. The models were therefore checked for accumulated analysis of variance, and the resulting F-test probabilities were measured. Models are often accepted at a probability of $p < 0.05$, although most in this study were $p < 0.001$.

Models were created using individual vessel data, combined vessel data and non-vessel-specific data such as organic loading rate, total methane percentage and volatile solids reduction to predict the gas outputs of the individual vessels. The individual vessel data and non-vessel-specific data were also used to build models of the total system gas output.

The better models were found to be those that predicted methane output of the whole system rather than individual vessels, based on the R^2 (adjusted) percentage and standard error of observation values. This was unexpected as it was believed the individual vessels would produce methane at a rate that was strongly related to the specific conditions within that vessel. However, this could be explained by the fact that a large proportion of the total methane derived from one or two vessels, although it was expected that these would be the later vessels in the system rather than the first two.

3.3.6.3. Methane production rate models

Methane production rate is the volume of methane produced in litres per litre of digester volume per day, allowing direct comparison between digesters of different sizes.

Table 3.4. Models predicting individual vessel methane production from values of measured parameters.

Rank	Parameter	Source	R^2%	Standard error of observations	Optimum	F test probability
1	Alkalinity	Vessel 1	64.3	0.254	4040 mg/L	<0.001
2	pH	Vessel 1	58.7	0.274	pH 6.38	<0.001
3	Methane %	Vessel 2	53.4	0.241	64.50%	<0.001
4	Redox	Vessel 2	47.8	0.255	-366 mV	<0.001
5	Volatile solids reduction	Vessel 3	46.9	0.161	8.40%	<0.001
6	Loading rate	Vessel 1	44.4	0.317	2.34 g/L/d	<0.001
7	Loading rate	Vessel 4	39.8	0.171	1.19 g/L/d	<0.001
8	Loading rate	Vessel 3	39.8	0.171	2.64 g/L/d	<0.001
9	pH	All vessels	38.2	0.307	pH 6.38	<0.001
10	Loading rate	Vessel 2	37.6	0.278	2.64 g/L/d	<0.001
11	Conductivity	Vessel 1	36.2	0.34	7.08 mS	<0.001
12	Volatile solids reduction	Vessel 2	35.9	0.282	20%	<0.001
13	pH	Vessel 3	35.8	0.177	pH 6.84	<0.001
14	Methane %	Vessel 1	33.5	0.346	47.20%	<0.001
15	Conductivity	All vessels	32.7	0.321	7.1 mS	<0.001
16	Alkalinity	All vessels	32.7	0.326	4180 mg/L	<0.001
17	Methane %	All vessels	31.2	0.329	48%	<0.001
18	Hydrogen	All vessels	27	0.339	High	<0.001
19	Hydrogen	Vessel 4	24.9	0.136	High	<0.001
20	Alkalinity	Vessel 3	24.5	0.192	4720 mg/L	<0.001
21	pH	Vessel 2	24.4	0.306	pH 6.96	<0.001
22	Volatile solids reduction	Vessel 4	21.6	0.139	25.50%	<0.001
23	Hydrogen	Vessel 1	21.3	0.378	High	<0.002
24	Alkalinity	Vessel 2	20.1	0.315	3450 mg/L	0.001
25	Redox	Vessel 1	16.3	0.389	-354 mV	0.005
26	Methane %	Vessel 3	16	0.202	59%	0.006
27	Volatile solids reduction	Vessel 1	15.6	0.391	19%	0.007
28	Hydrogen	Vessel 3	11.6	0.208	Low	0.008
29	Redox	All vessels	11.1	0.368	-375 mV	<0.001
30	Redox	Vessel 3	8.5	0.211	-277 mV	0.054
31	Hydrogen	Vessel 2	6.6	0.348	Low	0.088
32	Methane %	Vessel 4	1.9	0.155	High	0.248
33	Conductivity	Vessel 2	1.5	0.35	N/A	0.302
34	Alkalinity	Vessel 4	0.1	0.157	High	0.404
35	Conductivity	Vessel 3	0.0	0.215	9.35 mS	0.878

Table 3.5. Models predicting total system methane production from values of measured parameters.

Rank	Source	Model	R^2 %	Standard error of observations	Optimum	F test probability
1	Alkalinity	Vessel 1	65.8	0.128	3850 mg/L	<0.001
2	Methane %	Vessel 2	65.5	0.128	64.50%	<0.001
3	Alkalinity	Vessel 3	63.2	0.133	5850 mg/L	<0.001
4	pH	Vessel 3	60.5	0.137	pH 7.54	<0.001
5	Alkalinity	Vessel 4	54.5	0.147	6400 mg/L	<0.001
6	Hydrogen	Vessel 4	54.2	0.15	Low	<0.001
7	Methane %	Vessel 3	54.1	0.148	74.00%	<0.001
8	Conductivity	Vessel 1	53.4	0.149	7.75 mS	<0.001
9	Redox	Vessel 3	52.8	0.15	-360 mV	<0.001
10	pH	Vessel 2	52.3	0.151	pH 6.86	<0.001
11	pH	Vessel 1	47.8	0.158	pH 5.85	<0.001
12	Hydrogen	Vessel2	47.8	0.16	580 ppm	<0.001
13	Hydrogen	Vessel 3	47.4	0.161	225 ppm	<0.001
14	Alkalinity	Vessel 2	45.6	0.161	4690 mg/L	<0.001
15	Loading rate	Complete system	45.1	0.162	2.64 g/L/d	<0.001
16	Redox	Vessel 2	42.8	0.165	-372 mV	<0.001
17	Methane %	Vessel 4	42.4	0.166	72.80%	<0.001
18	Methane %	Vessel 1	41.8	0.167	45.50%	<0.001
19	Redox	Vessel 1	37.1	0.173	-345 mV	<0.001
20	Conductivity	Vessel 2	25.8	0.188	8.52 mS	<0.001
21	Conductivity	Vessel 3	21.4	0.194	9.48 mS	<0.001
22	Total hydrogen	Complete system	17.2	0.202	2590 ppm	<0.001
23	Total CH_4 %	Complete system	12.6	12.1	52.00%	<0.001
24	Hydrogen	Vessel 1	6.2	0.215	1855 ppm	0.034
25	Volatile solids reduction	Complete system	0.0	0.219	26.80%	0.478

The results from the regression models have been tabulated for individual vessel methane production (Table 3.4) and complete system methane production (Table 3.5). The models have been ranked in descending order of the R^2 (adjusted) percentage values, and are the best-fitting model types available for each parameter.

The three highest ranking models from Table 3.4 are displayed graphically in Figures 3.47, 3.48 and 3.49, and those from Table 3.5 for total system methane production in Figures 3.50, 3.51 and 3.52.

Organic loading rate was found to be a good indicator of the methane production rate. A relatively high organic loading rate appears to be best for methane production, with most individual vessel optima in the region of 2.34 – 2.64 g VS l^{-1} d^{-1}. The limited number of loading rate values used makes an exact optimum difficult to predict, but it is

clear that the greatest methane production is found when the system is working close to the overload limit.

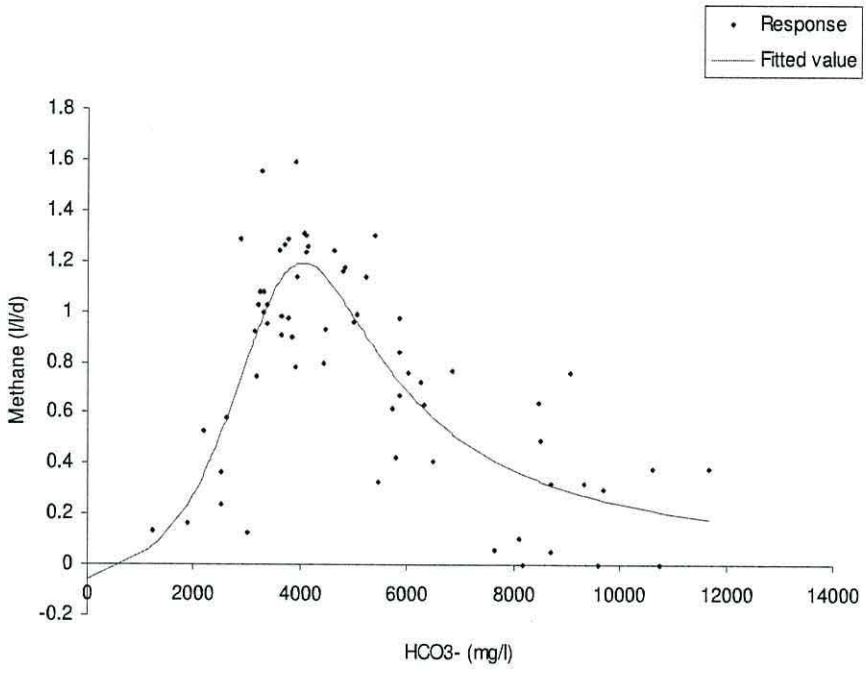

Figure 3.47. Curve fitting model of vessel 1 alkalinity vs. methane production.

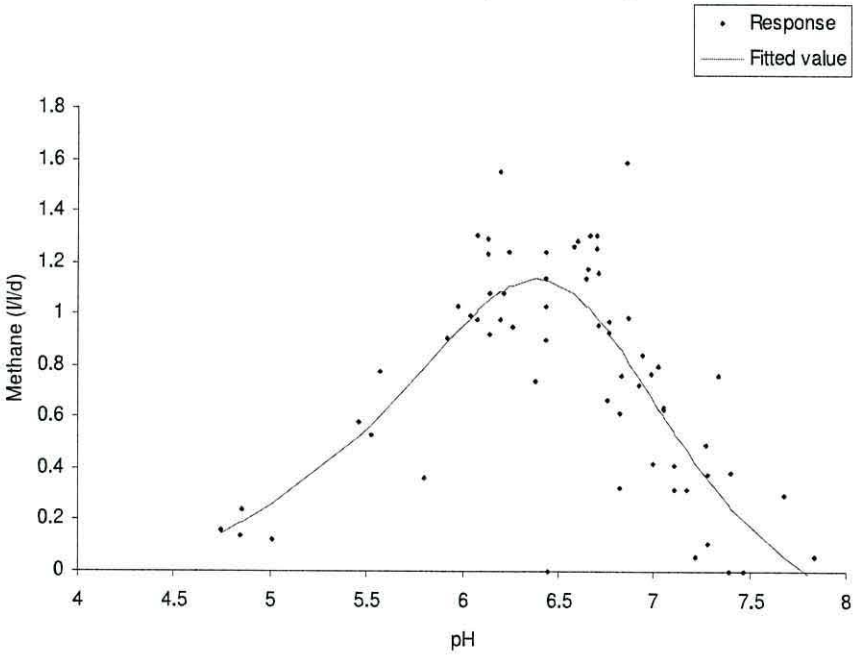

Figure 3.48. Curve fitting model of vessel 1 pH vs. methane production.

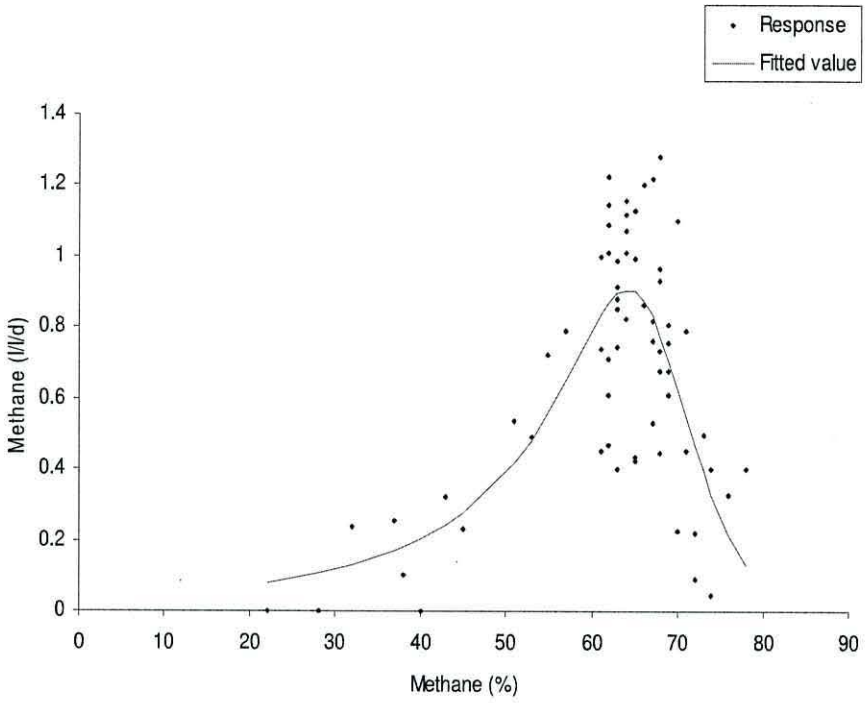

Figure 3.49. Curve fitting model of vessel 2 biogas methane concentration vs. methane production.

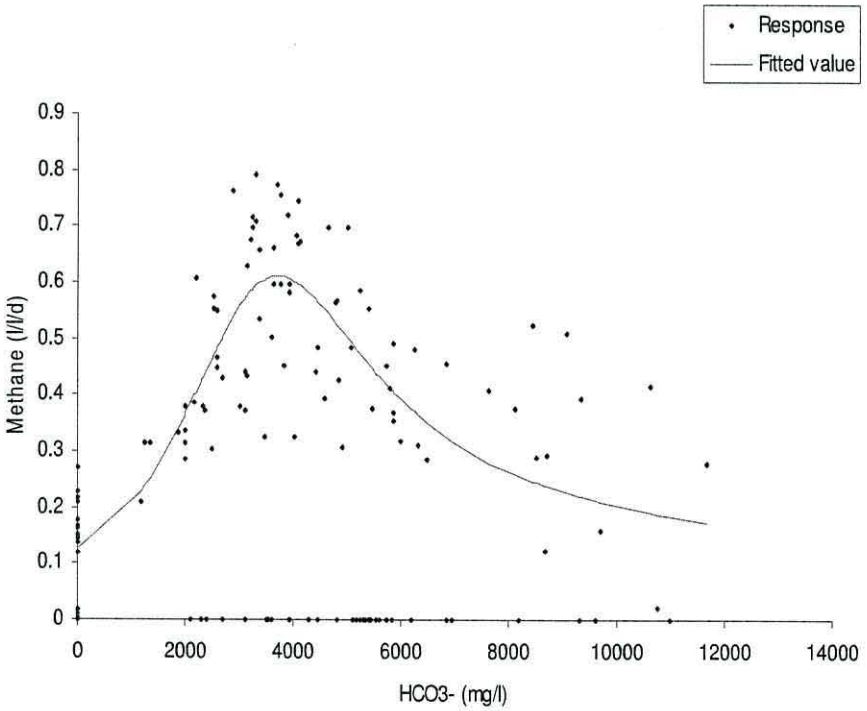

Figure 3.50. Curve fitting model of vessel 1 alkalinity vs. total methane production.

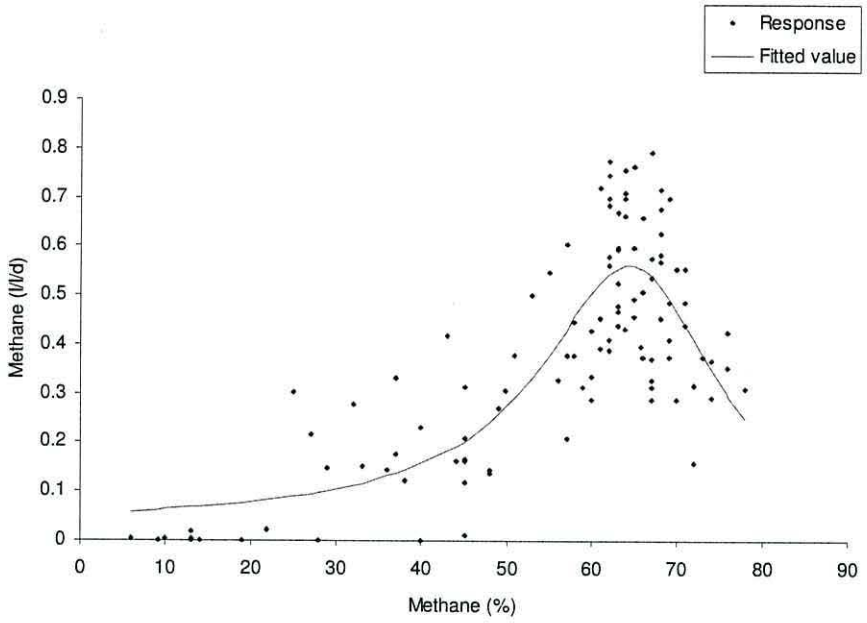

Figure 3.51. Curve fitting model of vessel 2 biogas methane concentration vs. total methane production.

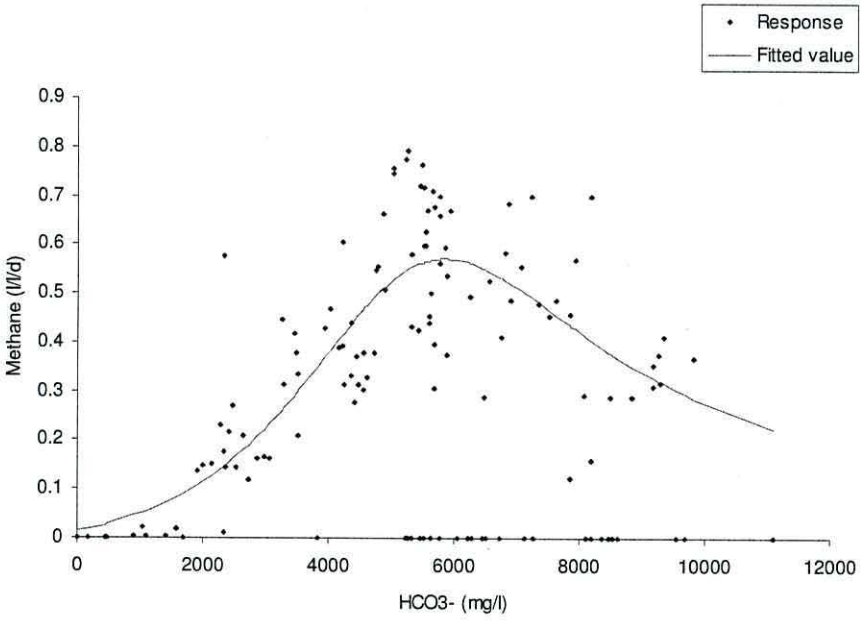

Figure 3.52. Curve fitting model of vessel 3 alkalinity vs. total methane production.

pH was also a consistently good parameter for methane prediction. The predicted optima are quite variable: between pH 6.4 for vessel 1 and pH 7.0 for vessel 2 for the individual vessel data, with the lower of these values also found to be optimal for the combined data from all three measurement points. Total optimal methane

production at a particular pH is even more variable: from pH 5.9 for vessel 1 to pH 7.5 for vessel 3.

As vessel 1 provided the greater part of the methane during recovery and stabilisation periods, it was surprising that this happened in such an acidic environment. It has already been proven in Chapter 2 that vessel 1 had good mixing characteristics, and therefore it seemed unlikely that the methane derived from organisms that were 'protected' from the acidic conditions in large regions of unmixed 'dead space'. It is more likely that the methanogenic organisms were living in a protected micro-environment found within small agglomerations of cells (Vavilin and Angelidaki, 2005). These agglomerations, also known as granules (Liu *et al.*, 2003), are not measured as dead space during hydrodynamic studies as they move freely within the digestate. It can be concluded that pH is an important parameter in predicting methane outputs in anaerobic digestion, but this evidence suggests that methane production can be considerable under acidic conditions, despite previous research showing methane production being severely depressed below pH 6.6 (Mosey and Fernandes, 1989).

Models created using the percentage of methane data produced curves with varying degrees of fit to the observed data, with optima from 47 % to 65 % v/v methane from the individual vessel models, and from 46 % to 74 % v/v methane for the total methane models. The optimum for vessel 1 is similar for models derived from individual and total data, 47 % and 46 % v/v methane respectively. The same is the case from vessel 2 for either model at 65 %, v/v methane but these are obviously very different from each other. This makes a true optimum difficult to find. However, the combined individual vessel data produces a model with an optimum of 48 % v/v methane, which is possibly closest to the true optimum as a larger dataset should provide a more accurate result.

Vessel 1 alkalinity curves prove to be the best fit with the data for both individual and total methane production. The optimum value was also only slightly different for each vessel: 4050 $mg.L^{-1}$ for the individual model and 3850 $mg.L^{-1}$ for the total model. Vessel 1 provided the widest range of values of all and, in line with these assertions, behaved as both a hydrolysis and methanogenesis vessel during the experiment. Models from alkalinity measured in the other vessels provided good models for prediction of total methane production, but with a large variation in the optima. These optima increased through the system from 3850 $mg.L^{-1}$ in vessel 1 to 6400 $mg.L^{-1}$ in vessel 4. The high optima for later vessels can be explained by the fact that the

majority of the methane originated from the first two vessels, where alkalinity was lower than that in later vessels. The later vessels in the system had a high alkalinity throughout the entire experiment except during the latter part of the failure period. This would mean total gas production would be high as a result of vessels 1 and 2, regardless of the environmental conditions in later vessels. Prediction of individual methane production from alkalinity produced models of poor fit, with R^2 values of less than 35 % except for vessel 1 alkalinity, but with optima that are within a tighter range; 3450 $mg.L^{-1}$ to 4700 $mg.L^{-1}$ excluding vessel 4 which did not produce an optimum peak with any model available in the Genstat software used. The combined individual data produced a reasonable model that had an optimum similar to vessel 1 (4200 $mg.L^{-1}$).

Models created from redox data to predict methane production did not score particularly highly in terms of the R^2 or standard error values, but all but one had optima within a close range of -375 mV to -345 mV.

Hydrogen did not predict methane production accurately. The data did not fit any of the curves available well enough to draw any conclusions and the optima from different sources were in total disagreement. Optima were predicted at high levels of hydrogen for vessels 1, 4 and the combined vessels for individual vessel output, and also vessel 1 and total hydrogen for total methane production. All other models predicted an optimum at low hydrogen concentration values. Removing the highest (sensor saturated) values did not improve the quality of the models. It was hoped that the poor results were a result of this misleading data. This was rather disappointing, as observations during the experiment suggested that an increase in hydrogen concentration was indicative of impending system failure. It has been suggested in the literature that dissolved hydrogen in a digester can be linearly correlated to the organic loading rate under normal operating conditions, and has in other studies given a good indication of system overload (Cord-Ruwisch *et al.*, 1997; Guwy *et al.* 1997) although it has also been shown that gas phase hydrogen concentration is not representative of the liquid phase dissolved hydrogen concentration (Pauss *et al.* 1990).

Conductivity models were not accurate methane production predictors, although better results were achieved from total methane production than for individual vessel methane production. The optimal conductivity increased through vessels 1 to 3, from 7.75 mS to 9.48 mS. Conductivity models created without the saturated probe data did not produce better models than those created with it, suggesting that conductivity has little link with methane production.

Volatile solids reduction produced a variety of models with poor curve fitting. The optima ranged from 9 to 25 % with models built from individual vessel data, but the worst model was based on the total methane production data, with an optimum of 27 %.

3.3.6.4. Methane yield models

Methane yield is the production of methane in litres per gram of volatile solids added per day, and provides an indication of the efficiency of a digester in converting organic carbon to methane.

The regression model results are tabulated in Table 3.6 and Table 3.7 for individual vessel and total system methane yields respectively. The three highest ranking individual vessel methane yield models from Table 3.3 are shown graphically in Figures 3.53, 3.54 and 3.55, and those from Table 3.4 are shown in Figures 3.56, 3.57 and 3.58.

Models using alkalinity to predict methane yield were varied in their degree of fit to the data. Those predicting total methane yield were better than those predicting individual vessel methane yield ($p < 0.001$ for all models), but the optima were too widely spaced, at between 4000 $mg.L^{-1}$ and 5600 $mg.L^{-1}$, to make any conclusions. The individual vessel models had a tighter range of optima (3850 $mg.L^{-1}$ to 4800 $mg.L^{-1}$) but only the combined vessel model had $p < 0.01$ at an optimum of 4150 $mg.L^{-1}$.

pH data produced the best models overall based on the statistical results, but the curves in many cases did not appear to fit the data very well. The optima were seen to range from pH 6.1 to pH 7.2 with the individual vessel models, and pH 6.3 to pH 7.7 with the total yield models. The fit of the curve to the data has an optimum point that is visibly too far to the left on the individual yield models for vessel 3, predicting an optimum that is likely to be lower than the true optimum.

Organic loading rate is not a particularly good predictor of methane yield according to the data. Optimal methane yields were generally found at lower loading rates, with 1.16 g VS l^{-1} d^{-1} as the calculated optimum for methane yields of vessels 2, 3 and 4 and a higher optimum of 2.34 g VS l^{-1} d^{-1} for vessel 1 methane yield. Total system methane yield was found at a lower loading rate than that calculated for individual vessels, with an optimum of 0.89 g VS l^{-1} d^{-1}. A lower organic loading rate (and therefore longer hydraulic retention time) being associated with a higher methane yield suggests that the organisms within the digester have more time to hydrolyse the more

recalcitrant components of the feedstock. A better indication of the relationship between organic loading rate and methane yield would require a longer time period at each loading rate, as in this experiment there are many methane yield data points for each loading rate value as the system became acclimatised to a new loading rate, or as the methane yield fell during failure. A longer study period could examine the gas yields once the system had settled under a particular load, and a greater variety of loading rates could also be implemented to increase the definition of the data.

Methane percentage in the biogas appears to be a good indicator of methane yield for vessels 1 and 2 with both individual and total methane yield models, and also for the total system methane percent and all of the vessels combined. Vessels 3 and 4 did not provide such good models. The optima differed greatly, from between 45 % and 68 % for individual vessel models, and from 51 % to 72 % for total methane yield models. The total system methane percentage (optimum 63 %) had the highest R^2 value, but a relatively large standard error of observations, whereas the combined vessels methane percentage (optimum 52 %) had a low R^2 and a high standard error of observations. The variation in optima is too great and the choice between low R^2 with a low standard error and high R^2 with a high standard error makes it difficult to choose a particular model from which to draw any conclusions. Biogas methane percentage was therefore considered to provide a poor indication of methane yield.

Hydrogen concentration produced a poor yield model for vessel 1 but progressively better models for vessels 3, 2 and 4 of the individual vessels. The poor vessel 1 model could be attributed to the saturation of the sensor for the majority of the measurements taken. A similar reason could explain the poor model for the total system. A wide range of optima from the better models, 446 to 910 ppm, again make it impossible to find the true optimum.

Volatile solids reduction was also a poor indicator of methane yield. Volatile solids reduction is a measurement related to the entire system rather than individual vessels, and therefore the total system methane yield data should produce better results. However, this model has an R^2 value of only 8.5 % and a large standard error of observations of 0.118 $L.g.d^{-1}$, in a system where methane yield is often in the region of 0.2 to 0.3 $L.g.d^{-1}$. The optimum for this model is 39.4 % volatile solids reduction, which is unlikely to be a precise estimate but it would be logical that a large methane yield would correspond with a large reduction in volatile solids, as more material is being converted to gas.

Table 3.6. Models predicting individual vessel methane yield from values of measured parameters.

Rank	Source	Model	R^2%	Standard error of observations	Optimum	F test probability
1	Methane %	Vessel 2	43.1	0.0294	65%	<0.001
2	pH	Vessel 1	42.6	0.0312	pH 6.45	<0.002
3	pH	Vessel 3	41.2	0.0205	pH 6.12	<0.003
4	Alkalinity	Vessel 1	35.8	0.0330	3950 mg/L	<0.004
5	Methane %	Vessel 1	33.3	0.0337	45.20%	<0.001
6	pH	All vessels	33.0	0.0388	pH 6.5	<0.001
7	Methane %	All vessels	29.1	0.0363	52%	<0.001
8	Hydrogen	All vessels	29.1	0.0363	High	<0.001
9	pH	Vessel 2	26.4	0.0335	pH 7.2	<0.001
10	Loading rate	Vessel 1	26.0	0.0354	2.34 g/L/d	<0.001
11	Loading rate	Vessel 2	24.8	0.0338	1.16 g/L/d	<0.001
12	Hydrogen	Vessel 1	24.3	0.0359	1846 ppm	<0.001
13	Conductivity	Vessel 1	22.2	0.0363	7.38 mS	<0.001
14	Conductivity	All vessels	21.2	0.0366	6.95 mS	<0.001
15	Volatile solids reduction	Vessel 1	19.4	0.0370	19%	0.002
16	Redox	Vessel 1	16.9	0.0376	-372 mV	0.004
17	Alkalinity	All vessels	16.3	0.0394	4150 mg/L	<0.001
18	Loading rate	Vessel 3	16.0	0.0245	1.16 g/L/d	0.006
19	Methane %	Vessel 3	14.5	0.0247	59%	0.009
20	Redox	All vessels	11.7	0.3670	-375 mV	<0.001
21	Volatile solids reduction	Vessel 4	11.5	0.0254	25.90%	0.023
22	Redox	Vessel 3	11.0	0.0252	-231 mV	0.026
23	Alkalinity	Vessel 3	10.9	0.0252	4790 mg/L	0.027
24	Redox	Vessel 2	10.2	0.0370	N/A	0.033
25	Hydrogen	Vessel 2	10.0	0.0370	675 ppm	0.037
26	Conductivity	Vessel 2	9.9	0.0370	9.321 mS	0.036
27	Loading rate	Vessel 4	9.6	0.0257	1.16 g/L/d	0.039
28	Hydrogen	Vessel 4	9.0	0.0257	High	0.068
29	Hydrogen	Vessel 3	6.6	0.0258	446 ppm	0.088
30	Alkalinity	Vessel 2	5.4	0.0379	3850 mg/L	0.120
31	Volatile solids reduction	Vessel 2	4.6	0.0316	22.50%	<0.001
32	Volatile solids reduction	Vessel 3	3.9	0.0262	Low	0.175
33	Conductivity	Vessel 3	2.4	0.0264	N/A	0.246
34	Alkalinity	Vessel 4	0.1	0.1570	High	0.404
35	Methane %	Vessel 4	0.0	0.0276	68%	0.892

Table 3.7. Models predicting total system methane yield from values of measured parameters.

Rank	Source	Model	R^2 %	Standard error of observations	Optimum	F test probability
1	Alkalinity	Vessel 3	57.6	0.081	5580 mg/L	<0.001
2	Total methane %	Complete system	56.8	0.144	63.50%	<0.001
3	pH	Vessel 2	54.0	0.0834	pH 7.18	<0.001
4	Hydrogen	Vessel 4	53.6	0.0718	910 ppm	<0.001
5	Alkalinity	Vessel 4	52.7	0.0846	5180 mg/L	<0.001
6	Methane %	Vessel 2	48.5	0.0883	66%	<0.001
7	Redox	Vessel 2	45.7	0.0906	-642 mV	<0.001
8	Hydrogen	Vessel 2	42.5	0.0799	550 ppm	<0.001
9	Methane %	Vessel 1	42.1	0.0936	51.00%	<0.001
10	Alkalinity	Vessel 1	42.0	0.0937	4000 mg/L	<0.001
11	pH	Vessel 3	41.1	0.0944	pH 7.68	<0.001
12	Hydrogen	Vessel 3	39.7	0.0819	545 ppm	<0.001
13	Alkalinity	Vessel 2	39.7	0.0955	5100 mg/L	<0.001
14	pH	Vessel 1	38.4	0.0965	pH 6.3	<0.001
15	Loading rate	Complete system	35.5	0.0987	0.89 g/L/d	<0.001
16	Redox	Vessel 1	35.3	0.0989	Low	<0.001
17	Redox	Vessel 3	31.3	0.102	-353 mV	<0.001
18	Conductivity	Vessel 3	25.9	0.106	8 mS	<0.001
19	Methane %	Vessel 3	23.0	0.108	72.00%	<0.001
20	Total hydrogen	Complete system	17.2	0.202	2600 ppm	<0.001
21	Conductivity	Vessel 1	15.2	0.113	6.96 mS	<0.001
22	Conductivity	Vessel 2	13.7	0.114	6.58 mS	<0.001
23	Methane %	Vessel 4	11.5	0.116	62.00%	0.002
24	Volatile solids reduction	Complete system	8.5	0.118	39.40%	0.01
25	Hydrogen	Vessel 1	5.3	0.103	975 ppm	0.05

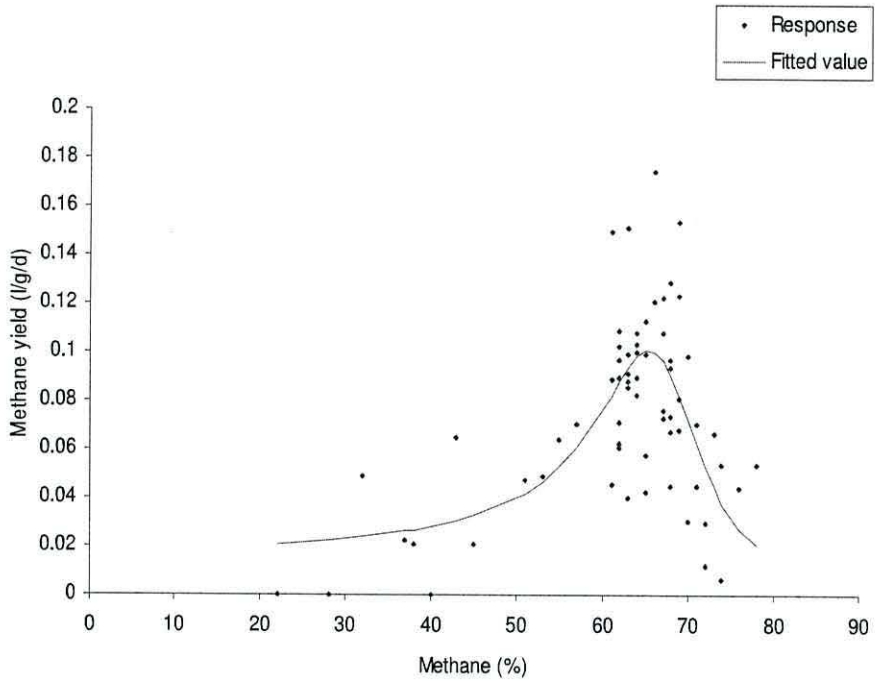

Figure 3.53. Curve fitting model of vessel 2 biogas methane concentration vs. methane yield.

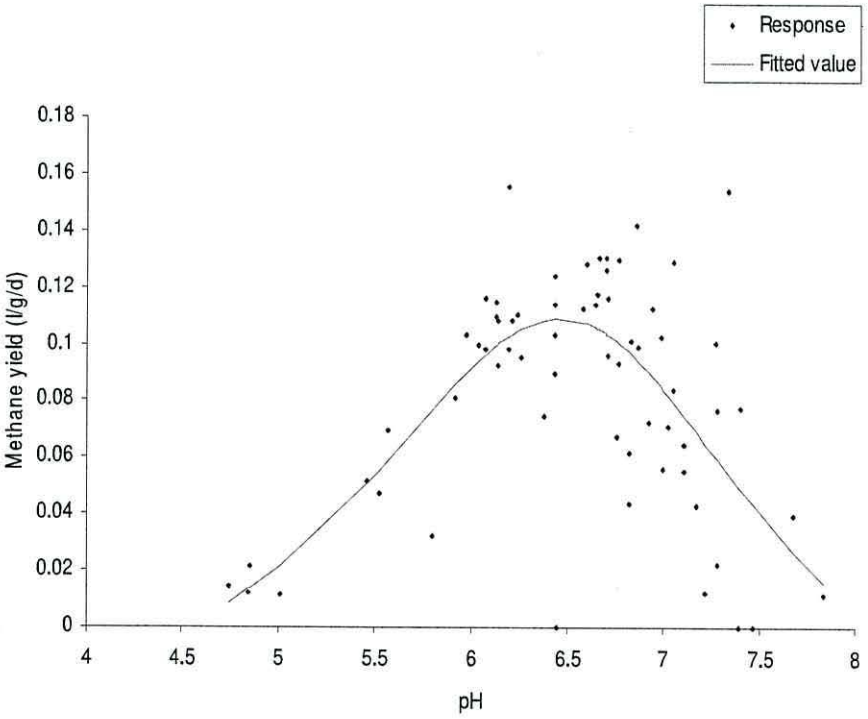

Figure 3.54. Curve fitting model of vessel 1 pH vs. methane yield.

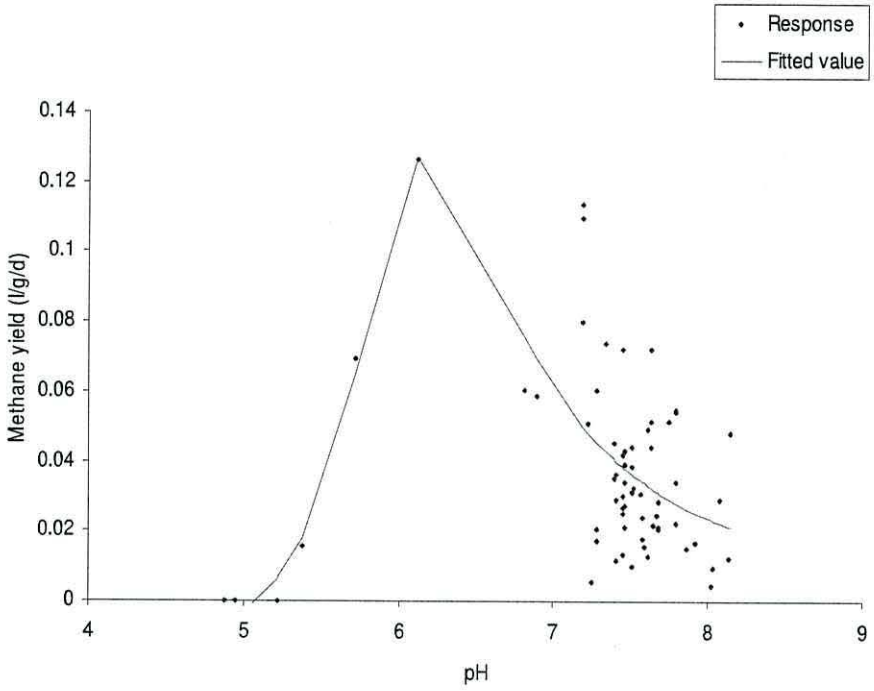

Figure 3.55. Curve fitting model of vessel 3 pH vs. methane yield.

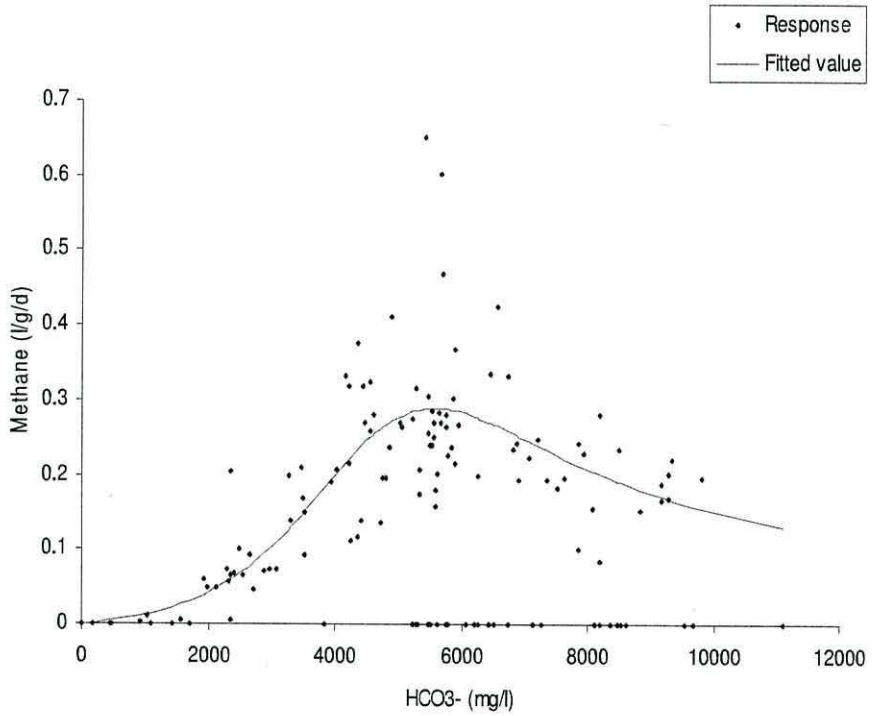

Figure 3.56. Curve fitting model of vessel 3 alkalinity vs. total methane yield.

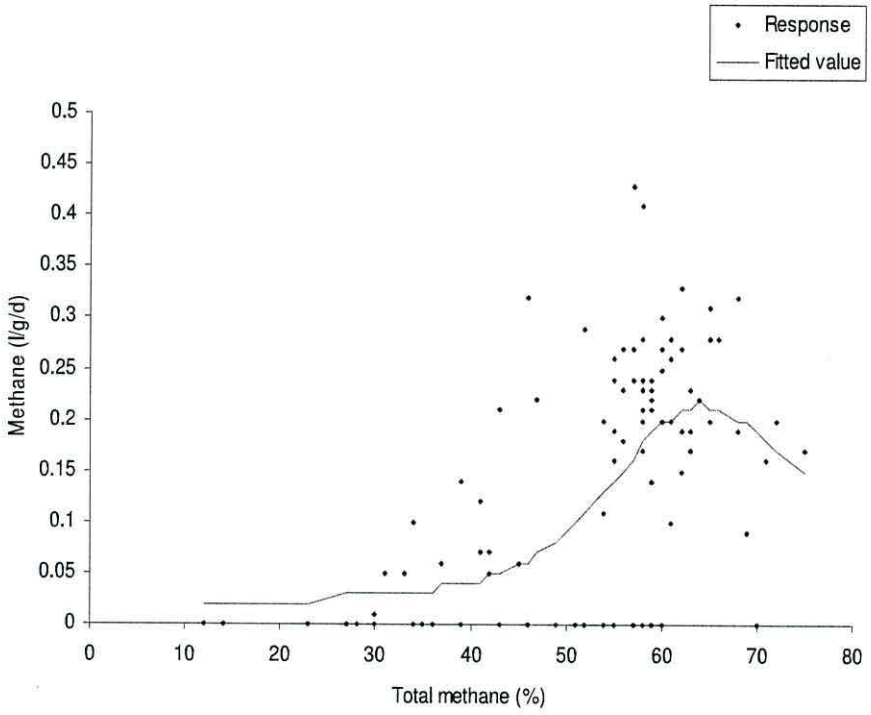

Figure 3.57. Curve fitting model of total biogas methane concentration vs. total methane yield.

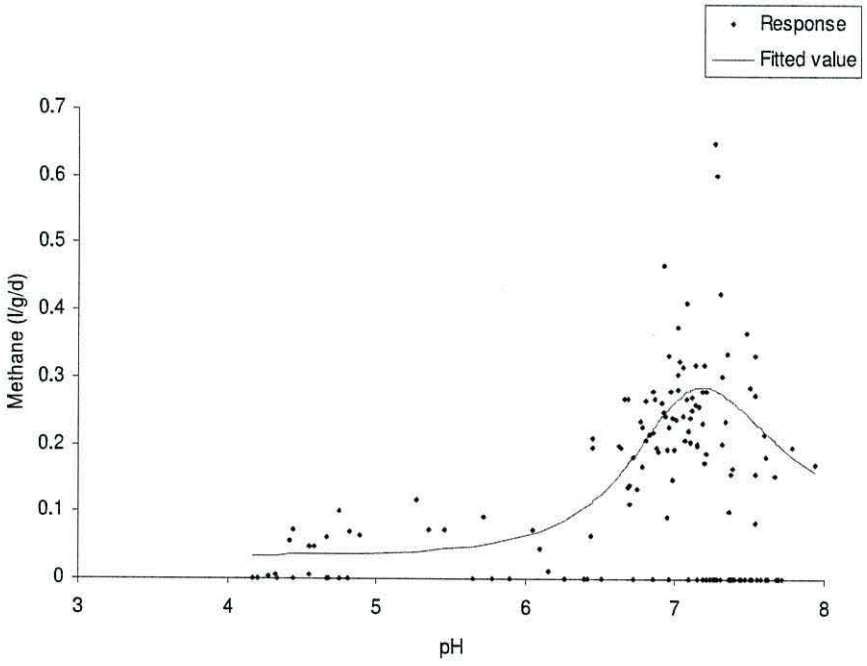

Figure 3.58. Curve fitting model of vessel 2 pH vs. total methane yield.

The models built from redox data do not appear to be useful in the prediction of methane yield. The curves fit the data badly by visual examination for vessels 1 and 2

total methane yield, and for vessels 2 and 3 individual methane yields. The remaining vessel 3 for total yield and vessel 1 for individual yields have optima of -353 mV -372 mV respectively, which are close to that derived from the combined vessels model (-375 mV) and also close to the optimal range found for methane production. Visual observation of the data would suggest that -353 mV to -372 mV would also approximate to an optimum range.

Conductivity produced models with poor curve fitting. The optima derived from these models were, however, within a reasonably narrow range: 6.580 mS to 9.321 mS for all models where an optimum is reached. The models are not of a high enough quality to suggest these optima are correct, but it would seem that a high conductivity measurement, *i.e.* a high concentration of ionised species present occurs concomitantly with a high methane yield. The conductivity measurement is not specific to the species of the ionised compounds, but it is possible that the values are related to HCO_3^- concentrations. Figure 3.59 shows the conductivity values plotted against the HCO_3^- concentrations, and there is a positive correlation of 0.643 ($p < 0.001$) between the data sets. Removal of the larger conductivity values (> 9.900 mS cm^{-1}) that were likely to be beyond full scale deflection when considering slight inaccuracies in the conversion of the 0 – 20 mA variable current data output to mS cm^{-1} values are shown in Figure 3.60 but produced a lower correlation of 0.591 ($p < 0.001$).

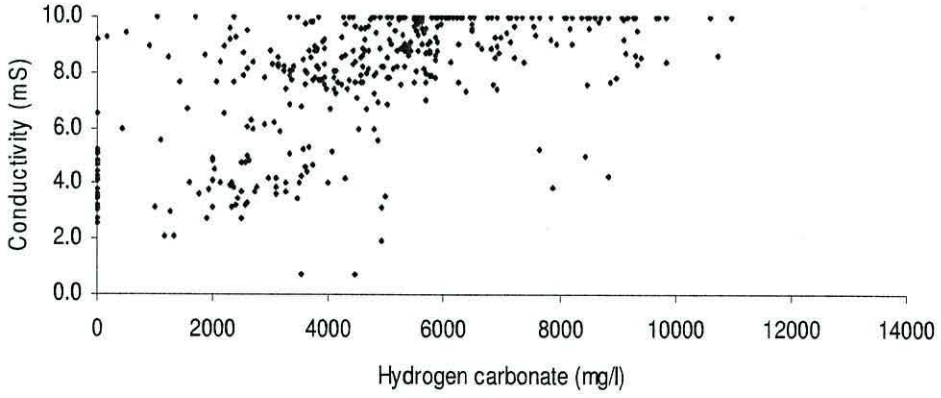

Figure 3.59 Conductivity versus alkalinity values for all vessels combined.

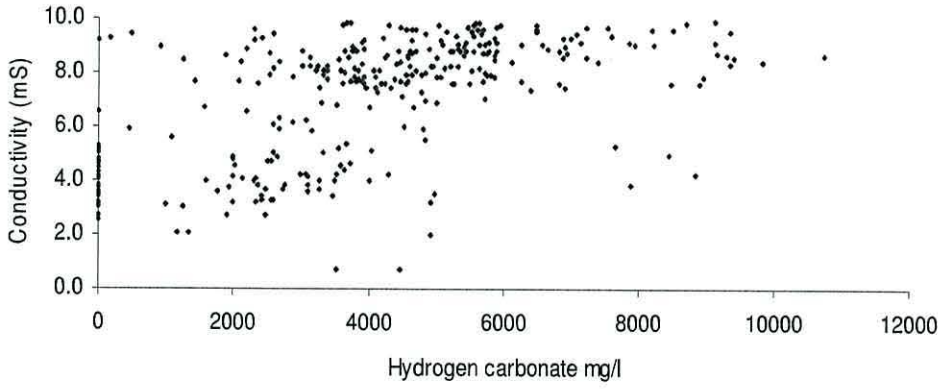

Figure 3.60 Conductivity versus alkalinity values for all vessels combined, minus values greater than FSD of the instrument.

Collection of data in this chapter was complicated by technical problems with the four-stage digester. There were many occasions when digestate tubing became blocked, effectively reducing the organic loading rate of vessel(s) downstream from that point to zero and over-filling the upstream vessel(s) until digestate was drawn into the gas mixer pumps. There was also some concern that biogas was leaking from some vessels. The effect of this was exaggerated during volume measurement, when a small amount of pressure was produced in the system to transfer the water through the measuring vessels. This could explain the very low gas production on certain dates.

The early production of methane seen in this system, particularly at a low pH, is interesting for commercial scale plants. It has been shown that a two-stage system treating cattle manure thermophilically (69° C and 55° C respectively) in which the first stage was 20 % of the entire system volume produced between 7 and 9 % of the whole methane production from the first stage (Nielsen *et al.* 2004). Some two-stage processes, such as that owned by AnDigestion Ltd, do not collect gas from the first stage. The reason for this is unknown as the four main stages of anaerobic digestion are not all necessary for conversion of some feedstock components to methane, *e.g.* hydrogen and carbon dioxide can be produced at early fermentation stages and directly converted to methane, or acetic acid in manure feedstocks could quickly be converted to methane by aceticlastic methanogenesis. Also, even where all the processes of hydrolysis, acidogenesis, acetogenesis and methanogenesis are required, these can take place very rapidly under the right circumstances. This was mentioned earlier in the four-

stage construction section (Chapter 2) in that the four stages were not intended to isolate the four anaerobic digestion processes, rather that they were to see a change through the system. As well as the presence of methane, there was an unknown concentration of hydrogen gas in the early stages. The electrochemical cell used to measure hydrogen was quickly saturated and therefore many concentrations remain unknown, but the saturation occurred very soon after drawing gas through the instrument, suggesting the concentration greatly exceeded the 2000 ppm limit. This is also interesting from an industrial point of view. Thus, if the process can be controlled sufficiently to produce hydrogen from the early anaerobic digestion stage(s) and methane from the latter stage(s) two valuable energy sources could be obtained from a single plant.

3.4. Conclusions

The experiment was considered successful in that a large dataset was obtained and optimal values of several parameters have been found.

The optimum values or ranges of parameters found to be important for maximum methane production and yield in this system are shown in Tables 3.8 and 3.9 respectively.

Table 3.8. Values of key parameters at which optimal methane production was obtained.

Parameter	Optima
Organic loading rate	2.34 to 2.64 g VS l^{-1} d^{-1}
pH	6.8 to 7.0
Biogas methane percentage	48 %
Total alkalinity	3850 to 4050 $mg.L^{-1}$
Redox potential	-375 to -345 mV

Table 3.9. Values of key parameters at which optimal methane yield was obtained.

Parameter	Optima
Organic loading rate	0.89 to 1.16 g VS l^{-1} d^{-1}
pH	6.9 to 7.2
Biogas methane percentage	64 %
Hydrogen concentration	450 to 900 ppm
Redox potential	-375 to -350 mV

The ranges of optima are simply where there are two or more optima which have been deemed to be fairly accurate. The true optimum will cover a larger range in most cases. For example, optimum total alkalinity for methane production: the optimum range of 3850 $mg.L^{-1}$ to 4050 $mg.L^{-1}$ quoted above is very narrow and therefore difficult to maintain in a complex biological process such as anaerobic digestion. The achievable optimum range can be considered to be between 3500 $mg.L^{-1}$ and 4600 $mg.L^{-1}$. These parameters and their optima could all potentially be used to monitor the methane production or yield of an anaerobic digester, and to assess the stability of the system. When a digester is producing methane at a fairly constant rate, as predicted by the above parameters, it is not unreasonable to suggest that this is also a digester that is stable and unlikely to fail under the current operating conditions.

The experimental evidence indicates that a model based on all vessels alkalinity data could be used as a basis of a control strategy for methanogenic reactors. Vessel 1 data also showed promise as a basis for a control strategy because, as mentioned previously, this vessel has been both a hydrolytic and a methanogenic reactor during this experiment and therefore had a greater range of values for most measured parameters.

In Chapter 4, the on-line pH, redox and conductivity values were used to create a software sensor for the prediction of alkalinity through regression models based on the data obtained in this chapter. The software sensor was then used as the basis for a rule based control of the organic loading rate.

4 Development of a software sensor and organic loading rate control system for monitoring and control of anaerobic digesters

4.1. Introduction

The anaerobic digestion process can be unstable, particularly when subjected to changes in the fermentation environment brought about by an increase in the organic loading rate or a change in the nature of the feedstock. For instance, a shock loading of a feedstock which is rapidly hydrolysed will lead to an unstable reactor (Hills and Roberts, 1982; Knol *et al.*, 1978). Such variations often have the effect of reducing the methane production of the digester (Bull *et al.*, 1983; Nachaiyasit and Stuckey, 1997; Robbins *et al.*, 1989). It is therefore common in industrial applications to construct a digester that is larger than optimal to reduce the impact of over-load situations. A larger digester will have a longer hydraulic retention time and therefore a lower specific organic loading rate than a smaller digester with the same input flow rate, although this option is expensive in terms of both construction and maintenance costs. Ideally a more economic alternative would be to continuously monitor the key variables within the process and use this information to control the input feed rate and therefore the buffering capacity *via* an advanced supervisory control system, ensuring optimal methane production at all times. This also makes sound economic sense in terms of increased income through greater material throughput (*e.g.* where gate fees are charged for treatment of wastes), reduced capital costs and improved gas output.

This chapter describes the creation of a software sensor to monitor anaerobic digestion using real-time data obtained from pH, redox and conductivity probes *via* an algorithm derived from regression models. The algorithm was then incorporated into LabVIEW software as the basis for a feedback loop control system.

Chapter 3 identified that the measurement of bicarbonate alkalinity was a good predictive parameter of methane production and yield, and also of assessing process stability. There have been several publications which have also suggested alkalinity as an ideal parameter to monitor and control methanogenesis. Many of these reports have used titration methods (Moosbrugger *et al.*, 1993), spectrophotometric methods (Jantsch and Mattiasson, 2003; Jantsch and Mattiasson, 2004) or acidification of a sample and subsequent measurement of the volume of carbon dioxide produced (Hawkes *et al.*, 1993). However, these analytical procedures all contain several individual steps and the use of various reagents to achieve the desired result. By comparison, simple

instrumentation in the form of probes that contain no mechanical parts to wear out and only require occasional calibration and cleaning (the latter being built into the physical design on many industrial-scale instruments) could provide an alternative monitoring system. Thus, the use of pH, redox and conductivity probes to monitor anaerobic digestion should offer advantages as they are well understood, cheap to buy and are likely to be familiar to operatives.

In this thesis, the effects of combining these three basic probes and creating regression models from large datasets for alkalinity has been studied. The key parameter of total alkalinity, which was normally measured off-line, was then predicted from the on-line data, *i.e.* a software sensor and these parameters compared.

Software sensors have been used in anaerobic digestion previously. For instance Alcaraz-González *et al.* (2002) used a wide variety of inputs including input flow rate, carbon dioxide exhaust flow rate, fatty acid concentration and total inorganic carbon to estimate the unknown parameters of microbial concentrations, alkalinity and chemical oxygen demand in a waste water treatment plant. Furthermore, Feitkenhauer and Meyer (2004) estimated substrate and biomass concentrations from inputs based on titrimetric techniques, and Bernard *et al.* (2000) used a mass balance based model and gaseous measurements to predict fatty acids and inorganic carbon, and a separate software sensor to estimate bacterial biomass. However, the above examples do not take advantage of the simple robust design and easy maintenance of the probes used as inputs in the experiment described in this chapter.

In the experiments described in this chapter, the software sensor was applied to the second (methanogenesis) vessel of each experimental digester. Although Chapter 3 demonstrated that more methane was produced by the first vessel with the feedstock used in these experiments, the alkalinity in the first vessel was usually too low to measure by titration, *i.e.* the start pH was below the titration end-point of pH 4.5. This led to the decision to use the data from the probes located in the second vessel outlet for the prediction of alkalinity and control of the process.

The on-line diagnosis of biological processes is considered a key requirement for efficient operation of anaerobic digestion plants (Lardon *et al.*, 2004). The chosen control system can be best described as a rule-based supervisory system with a feedback loop. This means that the system operates by supervisory commands in the form of 'if → then' rules, and data from the process digestate output can be fed back to the input feed pump. Rule based systems are considered better than conventional proportional

integral derivative (PID) controllers in dealing with the non-linear and time-varying data often associated with bioreactors (Babuska *et al.*, 2003). In addition, they have previously been successfully used in anaerobic digestion control, (Liu *et al.*, 2004) with inputs of pH and biogas flow rate to control the organic loading rate *via* modulation of the feed flow rate. This system showed good control performance and rejection of disturbances but the on-line measurement of biogas production and use of waste water as a feedstock prevent a direct comparison with the control system described in this chapter. The control system can, however, be compared to a PID type controller in that both use a measurement of the error in relation to a set-point to determine the proportional component, *i.e.* the amount of error and therefore the amount by which to increase or decrease the value of an actuator. However, the rule based supervisory system presented in this thesis produced one of only four broad output values from the proportional component at any one time. These four output sets were as follows: i) large increase, ii) small increase, iii) no change and iv) large decrease in organic loading rate. Thus, the inclusion of a 'no change' set where there was no error-based change to organic loading rate meant the controller was expected to be more stable and less prone to oscillations caused by noisy or imperfect input data once the predicted alkalinity was within this set. It should however be noted that feedback systems have been criticised in the past for waiting for a disturbance at the input to take effect before reacting to the problem (Luyben, 1990). In practice, this means that there is some time delay between the problem occurring and the system responding to it. This should be less of a problem with the two-stage systems which were used to test the control systems described in this thesis, as this arrangement tends slightly away from a CSTR model and more towards a plug-flow model (Levenspiel, 1999) because the fresh feedstock is not directly mixed with the methanogenic organisms. This is because a CSTR model assumes that incoming feedstock is immediately and completely mixed with the vessel contents, whereas a plug flow model will not mix fresh and existing feedstock at all. Thus, two CSTR stages effectively use the first stage as a buffer zone for fresh feedstock before entering the second stage. Therefore, a reduction in the feed flow rate when the alkalinity is low will immediately reduce the flow of acidic organic material from the first (hydrolytic / acidogenic) stage to the second (methanogenic) stage. This should, in turn, allow the acetogenic and methanogenic organisms in the second vessel time to metabolise the fatty acids, which should allow alkalinity to increase to the set-point level relatively quickly. Monitoring the vessel output rather than the vessel directly was

initially considered to be a potential problem of reactor / experimental design in this thesis. However, because the individual vessels exhibit CSTR characteristics (Chapter 2 section 2.4.2), the output material will theoretically be representative of the material at every spatial point within the vessel. However, it could not be guaranteed that the contents of the flow cells were representative of the vessels at all times because the flow through them was not continuous and they were not heated.

4.2. Materials and methods

4.2.1. Test digesters

The software sensor and control system were applied to two two-stage digesters, whose construction was described in Chapter 2 section 2.3. The digesters were not identical replicates as one digester had biomass support media in the methanogenic stage as described later in Chapter 6. However, this was seen as a good opportunity to test the sensor and control systems on different digesters, which were both different from each other and also from the original four-stage digester used to collect the data and develop the software sensor. The addition of a fourth set of probes, similar to those already used, allowed complete monitoring of the pair of two-stage digesters.

4.2.2. Regression models and statistical analyses

On-line data from pH, redox and conductivity probes were fitted to titration alkalinity data (as recorded in Chapter 3) through multiple linear regression models of the combined probe data, and also simple linear and non-linear regression models of individual probe data. Models were constructed from data from individual vessels and combinations of vessels 1 and 2, vessels 2 and 3 and vessels 1, 2 and 3. Vessel 4 did not have a set of probes on the output during data collection, so was not included. It is not believed that the lack of vessel 4 data had significant consequence on the regression models as the alkalinity of this vessel was rarely at a critically low level, as shown in Chapter 3. All statistical models and tests were created using Genstat v.9.2 software.

4.2.3. Testing of potential control systems using a process model

The control system was tested using a model created with LabVIEW software. The model was a replica of the intended control systems, but had been designed to test the control system response to an artificial alkalinity curve but in a shorter time span. In the model used, one hour of real time equals five seconds. This reduced the overall

testing period without the danger of potentially overloading the real digesters. The alkalinity curve in the model was created by plotting data produced by an equation chosen simply to produce a curve that was considered a good test of the control system response. The controllers were used in conjunction with this artificial alkalinity curve to calculate an organic loading rate based on the curve as if it were real predicted alkalinity data from the software sensor. The curve was designed to have a gentle positive gradient followed by a larger negative gradient, representing a situation where alkalinity increases steadily then falls rapidly (Figure 4.1). This simulated data was used to model three types of controllers that were considered suitable for feed pump control of an anaerobic digester, examining the controllers in terms of speed of response and potential over-shoot above the set-point.

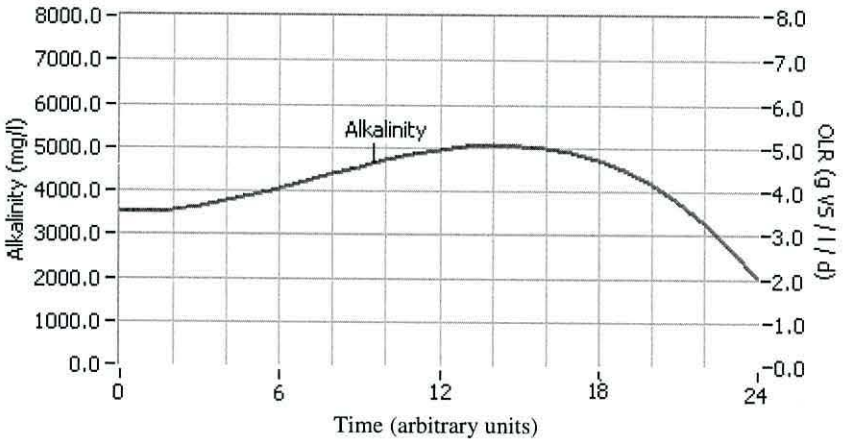

Figure 4.1. Artificial alkalinity curve constructed to test controller responses in process models (OLR = organic loading rate).

The controller types were an error based percentage increase controller, an error based constant increase controller and an error based constant increase with derivative controller. These were implemented within the LabVIEW software and were extensions of the system described by Liu *et al.* (2004). The error based percentage increase controller alters the loading rate by a set percentage, the error based constant increase controller uses constant values to alter the loading rate, and the error based constant increase with derivative controller is the same as the error based controller but adds a derivative component to use the rate of change of the alkalinity in addition to the error component.

4.2.4. LabVIEW architecture

4.2.4.1. General description

Construction of an anaerobic digestion control system led to a complete overhaul of the LabVIEW virtual instrument. In previous work in this thesis (Chapters 2 and 3), the software simply collected the probe data, displayed it graphically on the screen and stored it in data files. By comparison, this updated version was designed to also control the digester feeding cycles *via* the software sensor predicted alkalinity values, and the mixing cycles *via* simple numerical controls that determined the duration of the mixing time in an hourly cycle. The predicted alkalinities and the calculated organic loading rates based on these predictions were also stored as data files; the former stored every thirty minutes and the latter every hour (*i.e.* the feeding frequency). In addition to the extended capabilities of the virtual instrument, a comprehensive user interface was included. A schematic diagram of the entire process is shown in Figure 4.2 divided into the three main parts of process, hardware (data I/O) and software (LabVIEW).

4.2.4.2. Front panel design

The front panel consisted of several 'tabs' which could be selected to view the various displays. An example of these, the 'Schematic' tab, is illustrated in Figure 4.3. These included a 'Controls' tab which contained the mixing timing and the alkalinity limits that determined the borders of the sets. The control tab also showed numeric displays of the flow rate in litres per day, the retention time in days, the organic loading rate in g VS l^{-1} d^{-1} and the timing of the feed pump per hourly cycle in seconds. The 'Schematic' tab contained a diagram of the layout of the digesters with pH, redox, and conductivity and the predicted alkalinity as numeric displays on each relevant vessel. The 'Organic loading rate' (OLR) tab displayed the loading rates of the two digesters as XY graphs. This tab also gave access to the constants by which the organic loading rate was varied depending on which set the alkalinity value belonged to and also the derivative weighting. The latter determined how much leverage the derivative component had on the controller. A weighting of '1' is equivalent to a change in the organic loading rate of 0.01 g VS l^{-1} d^{-1} for every 100 $mg.L^{-1}$ difference between the current alkalinity and the alkalinity measured sixty minutes previously, as shown in Equation 4.1. The final number in the equation is to bring the change in OLR to the correct order of magnitude.

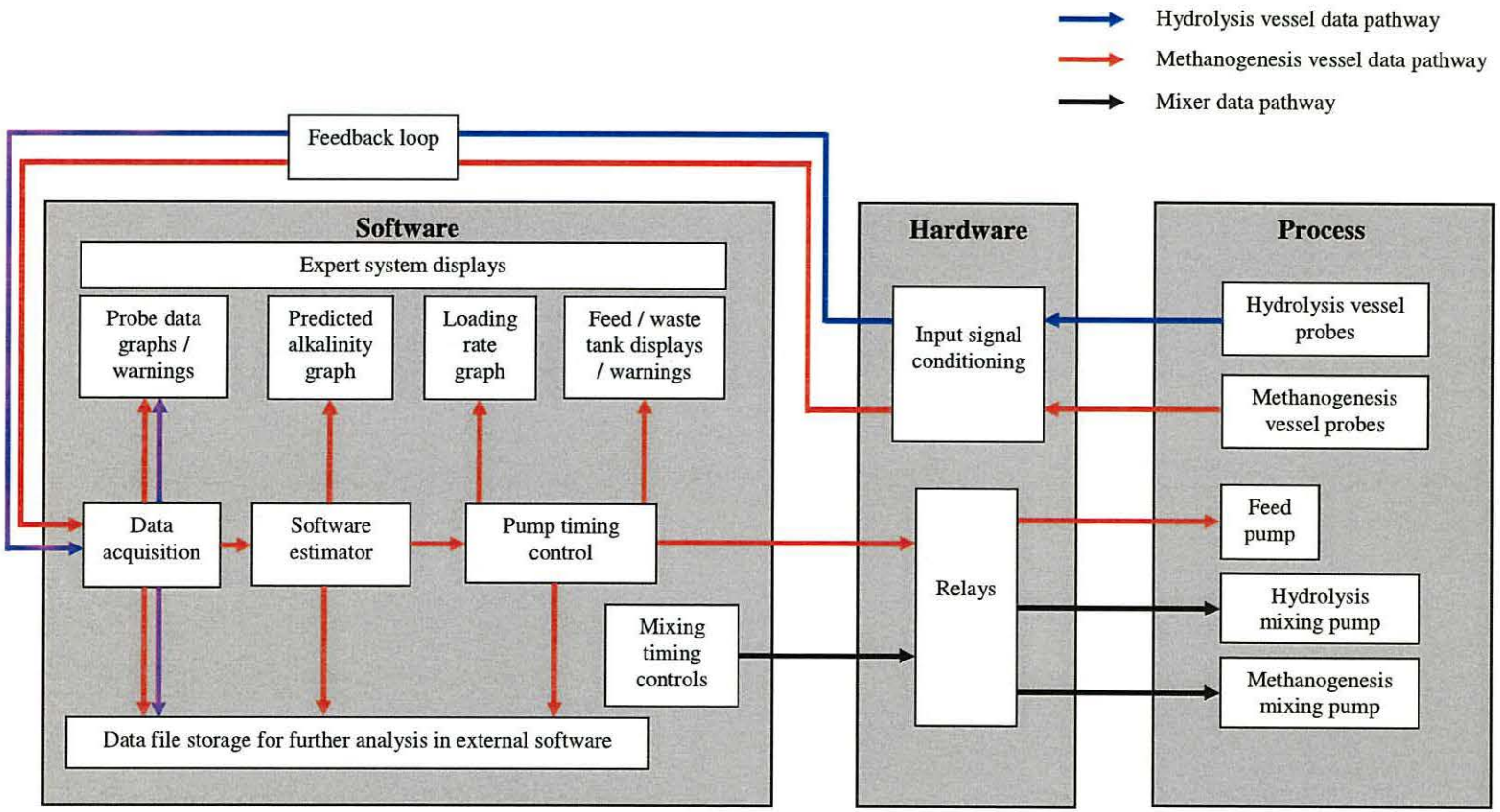

Figure 4.2 Monitoring and control schematic diagram, one of each controls each two-stage digester separately.

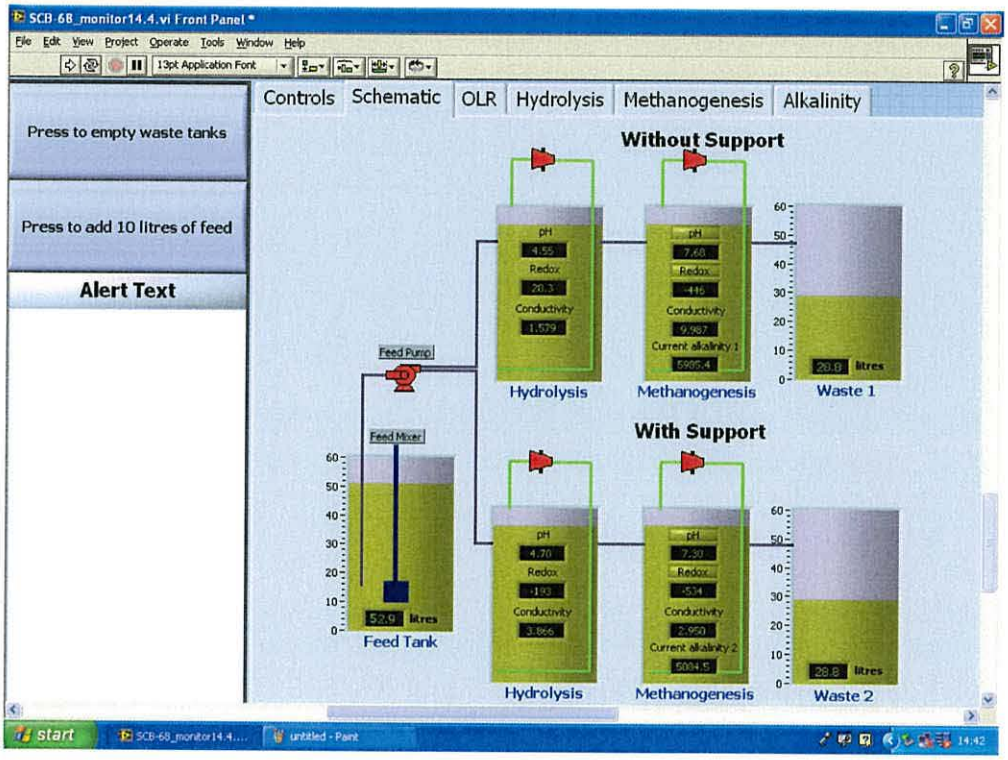

Figure 4.3. LabVIEW front panel view of 'Schematic' tab, showing the probe readings for each vessel.

Equation 4.1

$$OLR_{current} = OLR_{previous} + (alkalinity_{previous} - alkalinity_{current} \times \text{weighting value} \times 0.0001)$$

The remaining tabs were for hydrolysis, methanogenesis and alkalinity and displayed XY graphs of the relevant probe values from the vessels or the alkalinity values.

4.2.4.3. Control system implementation

The control strategy was to assign predicted alkalinity data into one of four sets, one set was for very high alkalinity values, one for fairly high alkalinity values, one for middle alkalinity values and one for low alkalinity values. The borders of each set were adjusted *via* the front panel during the experiment, therefore no values are mentioned in this section. The controller then modified the feed pump operating time at every feeding event by an amount which depended on the particular set the current predicted alkalinity

belonged to. The previous predicted alkalinity (from an hour earlier) was also compared with the current predicted alkalinity to determine the direction and rate of change. This result was multiplied by a constant to bring the value to the correct order of magnitude for making a suitable change in the organic loading rate (Equation 4.1). These limits and constants were displayed on the LabVIEW virtual instrument front panel tabs as controls, thus allowing changes to be made quickly and easily to fine tune the control system as the experiment progressed, and as such are not referred to in the following description as specific values.

The control system underwent several modifications to the original basic design during the experiment. The three basic flow charts are illustrated in Figures 4.4, 4.5 and 4.6. Figure 4.4 shows the original design, which included the placing of the predicted alkalinity value into one of four sets, but had a separate section for checking the feed tank level. The 'empty' level was set at *ca.* 50 mm above the draw pipe to the feed pump to prevent solid deposits blocking the tube before the feed tank mixing system had time to homogenise the tank contents. If this value was considered 'empty', the organic loading rate calculated from the predicted alkalinity was subtracted from itself to equal zero. This proved unsatisfactory as the software did not behave as negative values were displayed. For this reason, the calculation order was altered to follow the series of events shown in Figure 4.5.

In the modified system (Figure 4.5), the process was divided into a more logical order of checks on the various parameters. This first step checked the feed tank level and, if 'empty', the remaining steps in the calculation were by-passed and the organic loading rate was set to zero. If the tank level was not zero, the next step in the process was to check if the pH was below a lower limit. This was intended as a 'safety net' to help prevent acidification, which would have increased the time required to complete the experiment as a recovery period would have been necessary. If the pH was below the lower limit, the organic loading rate was decreased by a set percentage of the current value and the pump timing calculated on this value alone. The organic loading rate was then converted to a pump 'on' time per hour using pump calibration data (Chapter 2). As in the original design, in this scenario the rest of the steps were then by-passed.

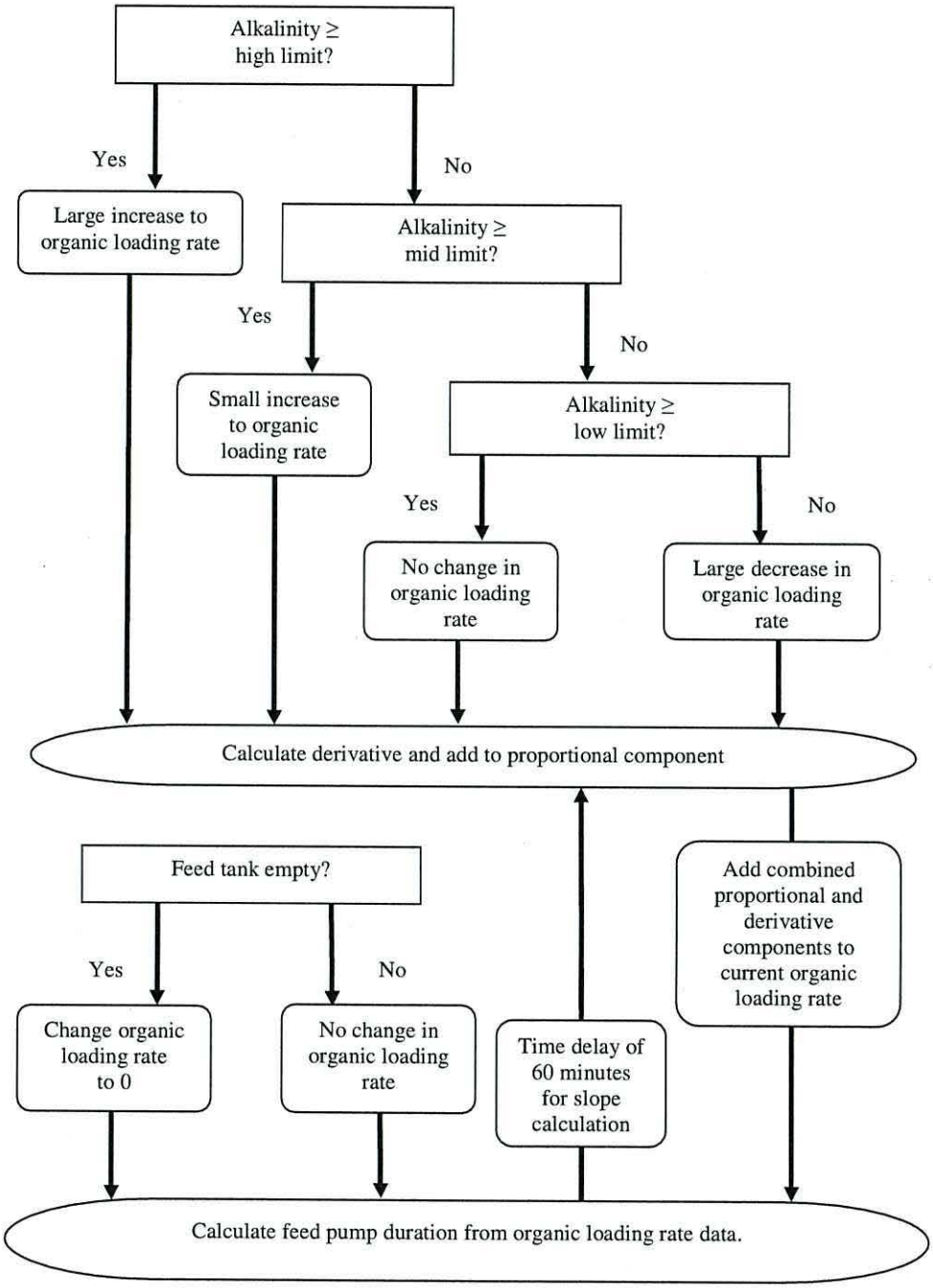

Figure 4.4. Flow chart of controller logic, from 30/12/2006 to 4/1/2007, with 'feed tank empty' check conducted after other calculations.

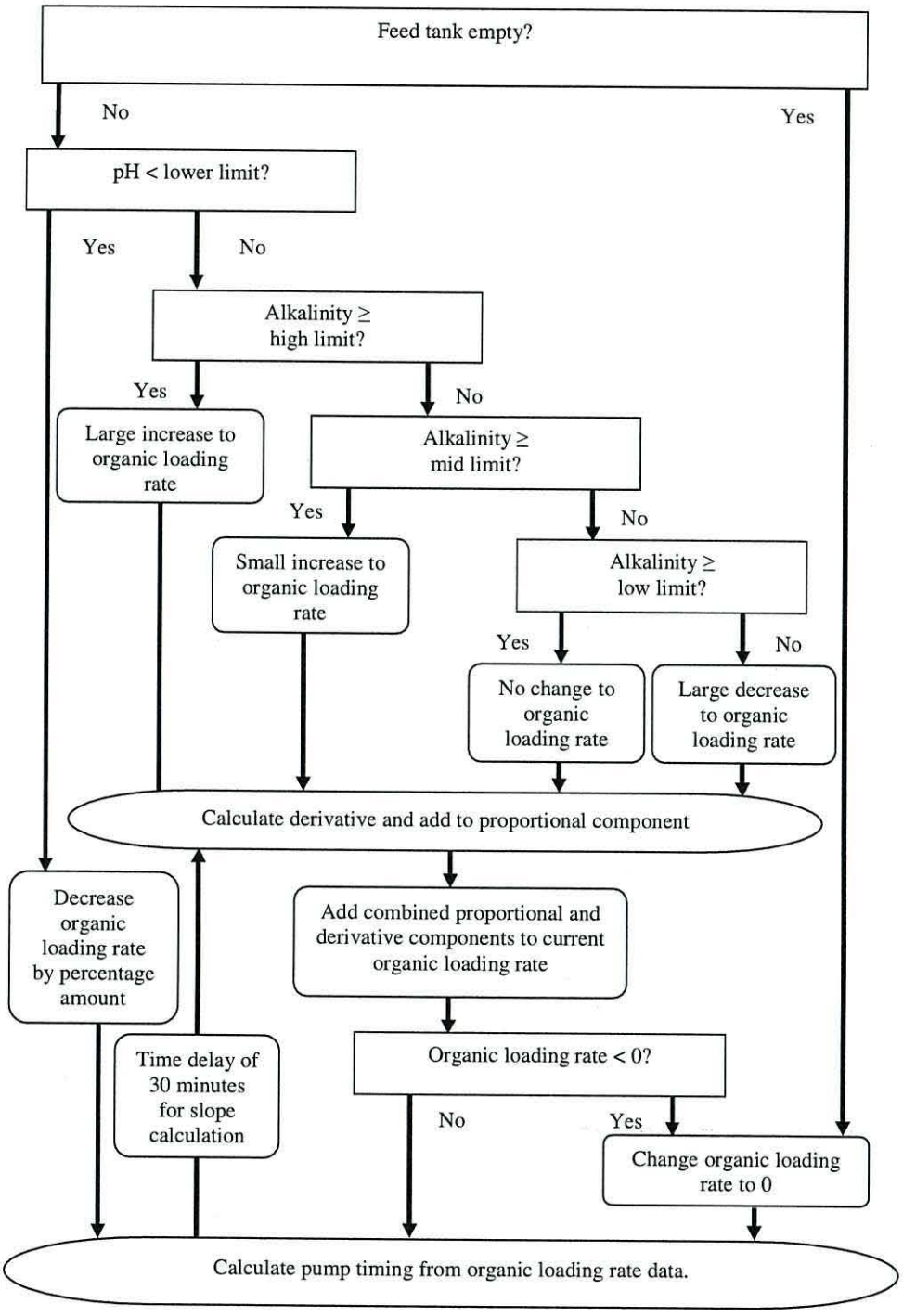

Figure 4.5. Flow chart of controller logic, from 4/1/2007 to 8/1/2007, with 'feed tank empty' check conducted before other calculations.

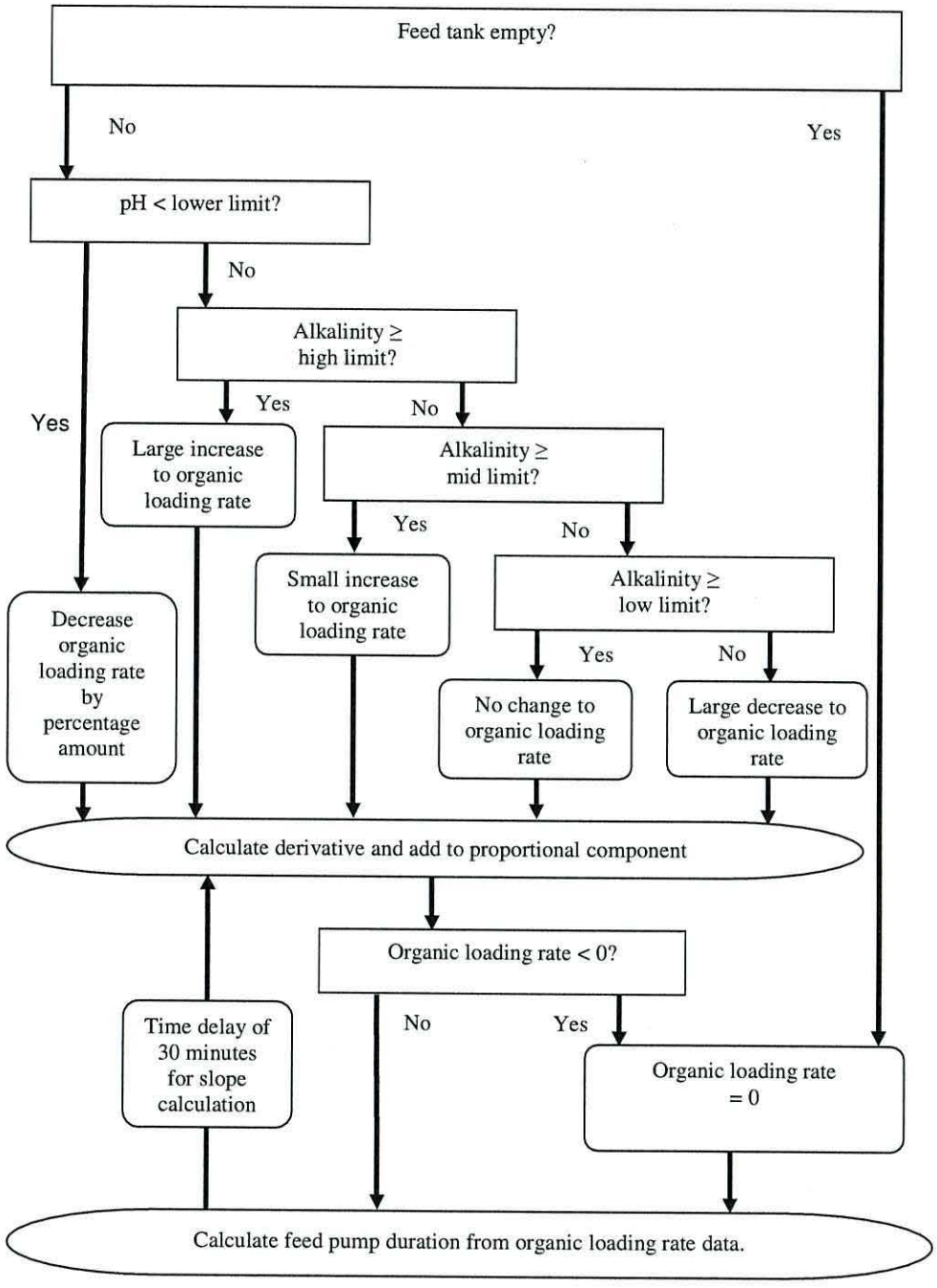

Figure 4.6. Flow chart of controller logic, from 8/1/2007, where a derivative calculation is included in 'pH below low limit' conditions.

However, this method also proved unsatisfactory in performance. The reason was that when the pH was below the 'low pH' limit, the software also by-passed the derivative calculation. As a result, the organic loading rate was depressed for longer periods than was believed necessary as the control system failed to respond to an increasing alkalinity in these circumstances. These observations led to the final design (Figure 4.6) which included the organic loading rate calculated during low pH warning periods in the derivative calculation. This allowed sudden increases (or decreases) in predicted alkalinity to make a difference to the organic loading rate when pH was below the low limit. It was expected that this would improve the recovery speed of the organic loading rate.

The complete sequence of events undertaken by the software can be described as follows:

1. Data was collected from each of the four sets of pH, redox and conductivity probes connected to each vessel (12 sets of data in total). These were recorded in a text data file at 100 second intervals, thus reducing the quantity of data stored to manageable file sizes. The data was also put through a series of calculations to measure the moving average. The data averaged over five minutes was then displayed in both graphical format and numerically on the screen representations of the relevant vessels. All graphs used in the software had the X axes set to show 24 hours, and were automatically scaled to fit elapsed time up to 24 hours when first started. The Y axes were set to a maximum and minimum range that covered all expected operational data values. This was chosen instead of auto-scaling the Y axes as it allowed graphs of the same type (*e.g.* methanogenesis pH) to be scaled equally, which allowed for "at-a-glance" comparisons.
2. Warnings were created by case structures which checked if pH in the methanogenesis vessels was below a specific value, or redox was above 0 mV (these were considered necessary as they would suggest digester acidification or an oxidising environment, respectively). Case structures were used in LabVIEW for determining alternative outcomes based on two or more inputs. For the pH example mentioned above, the inputs were either true or false for the question "is pH below [specific value]?" The output was different for each of the true or false cases. When these cases were true, the relevant numerical display turned red, as did a larger warning light on the left portion of the screen with a string of characters describing what and where the specific problem was. The left portion

of the screen was visible at all times and the representations of the vessels and the various graphical displays were viewed individually by selecting the tab at the top of the screen. These warnings created a fully developed expert control system.

3. The averaged probe values were also used as inputs to a formula node. This contained the algorithm for the prediction of alkalinity. The alkalinity values were recorded in a data file every sixty minutes and also presented graphically on screen.
4. The control system was accomplished through the use of nested case structures which checked all necessary information before making a decision to modify the feed pump timing.
5. The first case structure asked whether the feed tank was below its minimum level. If this case was 'true', the organic loading rate was subtracted from itself to produce an organic loading rate of zero and the control system proceeded no further until the next feeding time one hour later. The reason here was a potential hazard arising from a low feed tank level which would allow air to be pumped into the first vessel which would create an aerobic environment and possibly an explosive gas mix of methane and oxygen. A 'false' case here allowed the following case structures to be considered and ultimately for feeding to commence.
6. The second case structure was a safety net for maintaining the system stability, and asked if the pH of the methanogenesis tank was below a preset value set on the front panel. A 'true' case would reduce the organic loading rate by a percentage value rather than a numeric constant and bypass the proportional increase case structures but still calculate the derivative. This was chosen as it reduced the organic loading rate at a proportional rate, i.e. a large reduction at high organic loading rate and a small reduction at low organic loading rate. A 'false' case allowed the alkalinity proportional case structures below to be considered.
7. The next series of case structures considered the alkalinity value predicted by the software sensor and decided which of the four sets or decision making categories the value was placed into. These sets were i) large increase, ii) small increase, iii) no change and iv) large decrease in organic loading rate sets described previously. The set boundaries were determined *via* the control panel, and consisted of high, middle and low alkalinity values, respectively. The first of these case structures

asked if alkalinity was greater or equal to the high limit. If 'true' this returned a relatively large increase in the organic loading rate. If 'false' the software moved on to the next case structure, which asked if alkalinity was greater or equal to the mid limit. An answer of 'true' increased the organic loading rate by a smaller amount than the previous case and an answer of 'false' moved on to the next case structure, which asked whether alkalinity was greater or equal to the low limit. If 'true' was the outcome, the organic loading rate was increased by zero, and 'false' decreased the organic loading rate by a relatively large amount.

8. The organic loading rate, after modification by one of the above cases, was then altered further by the inclusion of the derivative value. This was calculated from the current alkalinity value at feeding time and the alkalinity value from the previous feeding time 60 minutes earlier.
9. The final organic loading rate was checked for being a value less than zero. If 'true', the organic loading rate was increased to zero. A 'false' value here did nothing to the organic loading rate. The resultant organic loading rate was used to calculate the feeding time using the pump rate calibration data.
10. Finally, the organic loading rate was also represented as an XY graph and as a numeric display on the left part of the front panel. The data was automatically stored at hourly intervals.

4.3. Results and discussion

4.3.1. Software sensor regression models

The results of the regression models are shown in Table 4.1, and include percentage variance accounted for (a percentage value equivalent to the R^2 adjusted value) and the standard error of observations in $mg.L^{-1}$. The six most important models both in terms of high percentage variance accounted for (R^2) and low standard error of observations are shown graphically within this chapter as observed *versus* predicted alkalinity data. The models regarded as less important had lower percentage variance accounted for and higher standard errors of observations. All the graphs of the models feature a 1:1 gradient line to demonstrate the 'perfect' model of predicted *versus* observed alkalinity data. It must be stressed that these are not lines of best fit to the data.

From the results, the pH probe appears to be the most important factor within the models as the four data sets that include pH data are ranked as the best four models (see Table 4.1). It is not surprising that pH is important in a software sensor predicting

alkalinity, as the main reason for maintaining an optimal alkalinity is to maintain a neutral pH. It is, however, interesting that combining the pH probe with any of the other probes produces better models than pH alone, suggesting that redox potential and conductivity play some part in predicting alkalinity. The conductivity probe appears to better predict alkalinity alone than the redox probe alone, with R^2 (%) of 60 %. It was hoped that conductivity would correlate well to alkalinity, as mentioned in Chapter 3, although a poor correlation was seen.

Examination of the observed *versus* predicted alkalinity graphs reveals that the best models are those that use all three probes (Figures 4.7 to 4.12), with between 68 and 81 % of variance accounted for, and 1187 to 1487 $mg.L^{-1}$ standard error of observations.

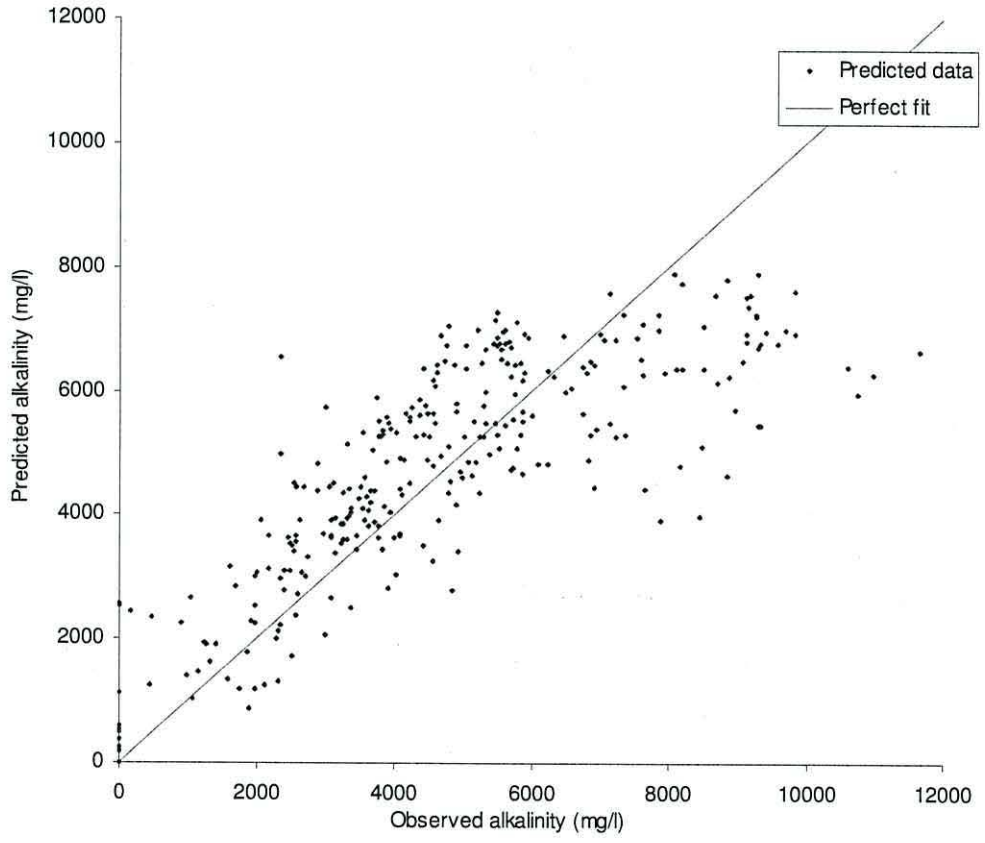

Figure 4.7. Regression model using all pH, redox, conductivity data.

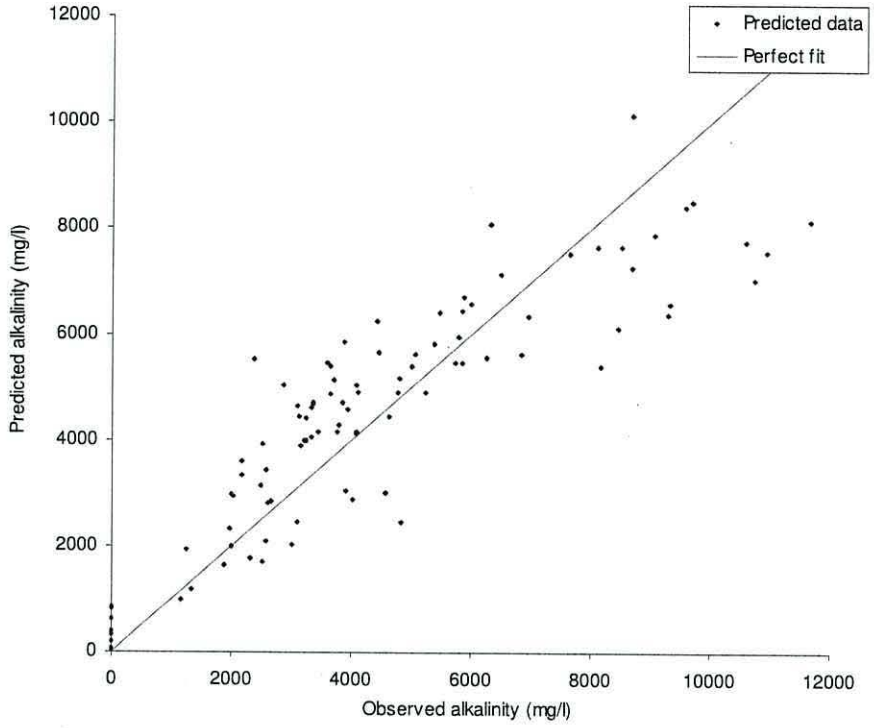

Figure 4.8. Regression model using vessel 1 pH, redox, conductivity data.

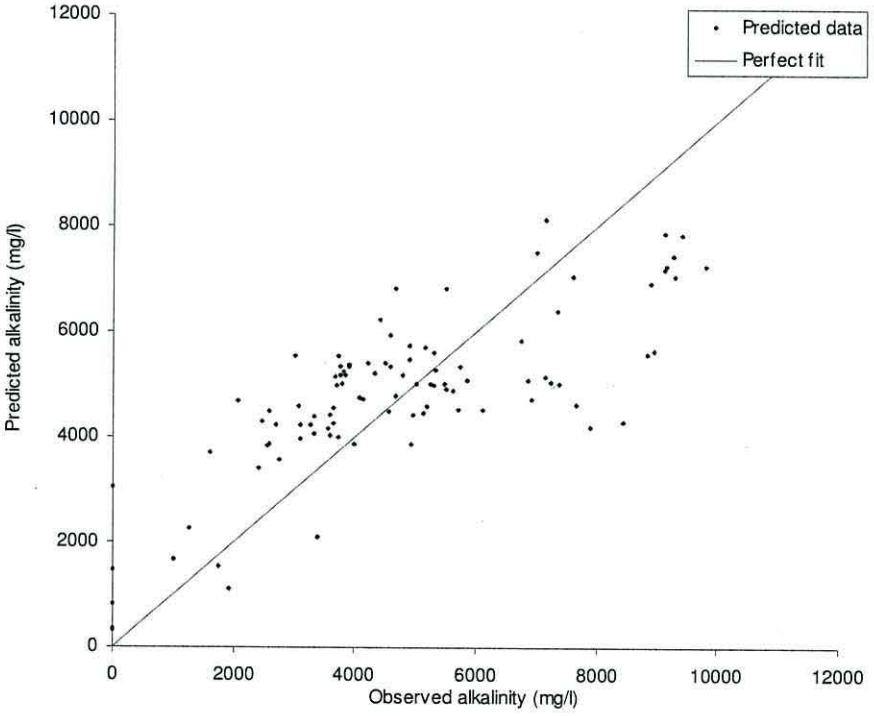

Figure 4.9. Regression model using vessel 2 pH, redox, conductivity data.

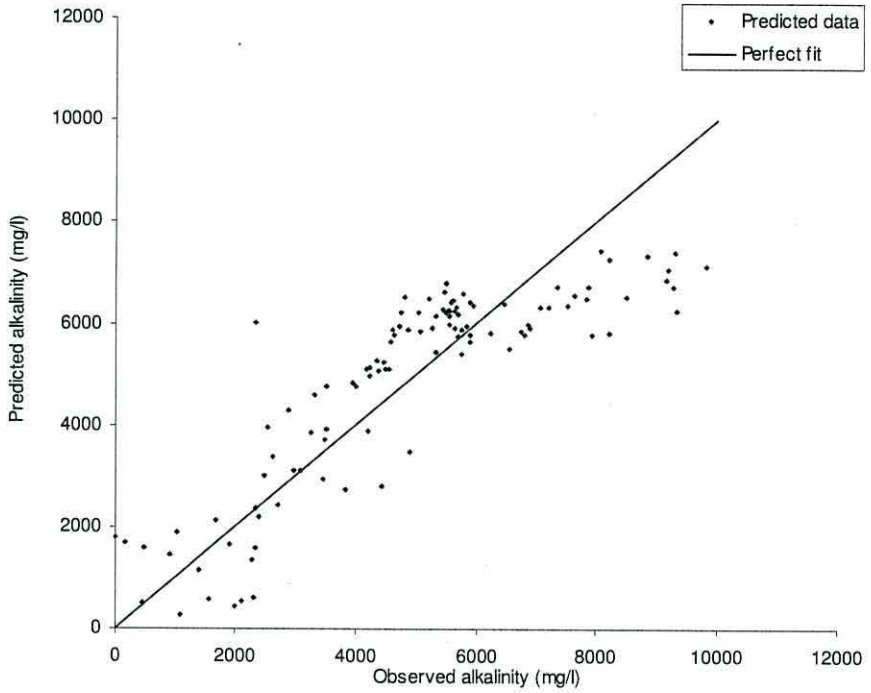

Figure 4.10. Regression model using vessel 3 pH, redox, conductivity data.

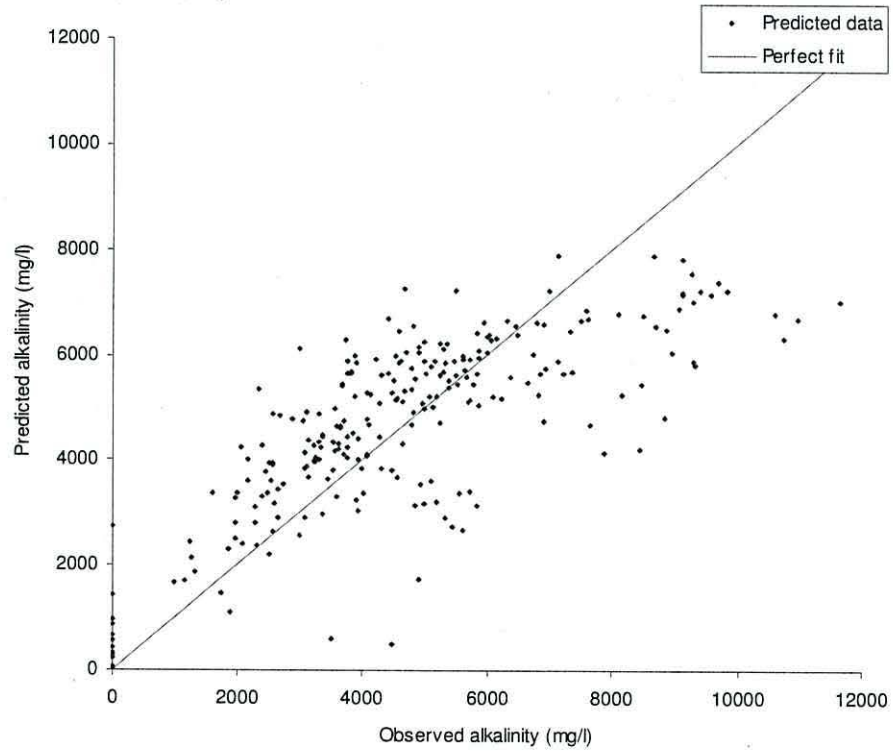

Figure 4.11. Linear regression model using vessels 1 and 2 pH, redox and conductivity data.

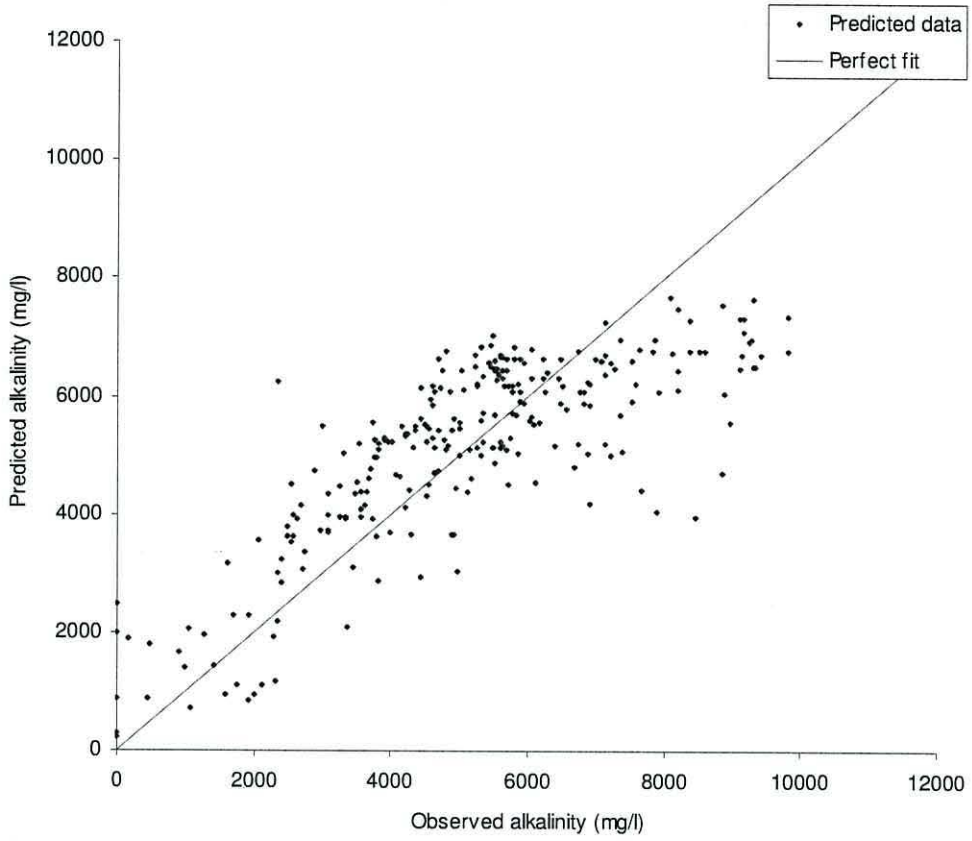

Figure 4.12. Linear regression model using vessels 2 and 3 pH, redox and conductivity data.

The other combination / single probe models are ranked in the following descending order of R^2 value: pH-conductivity, pH-redox, pH, redox-conductivity, conductivity and finally redox. Regression models using non-linear curve fitting generally fitted the data less well than the multiple linear regression models, but produced better redox and conductivity models than simple linear regression. Based on the R^2 and RMSEP values, the decision of which model to use was restricted to the three-probe models, of which there were six types depending on which data was used.

The single vessel datasets produced models with higher percentages of variance accounted for and lower standard errors than the combined vessel datasets, but examination of the graphs shows that the model using all data (71 % variance accounted for, 1441 $mg.L^{-1}$ standard error) is actually a better fit to the data, particularly over the critical range of alkalinity between 3600 $mg.L^{-1}$ and 4600 $mg.L^{-1}$.

Table 4.1. Percentage variance accounted for (percentage R2 adjusted) and standard errors of observations of regression models.

Type of regression model and data source	Model percentage variance accounted for / standard error of observations of regression models for all combinations of probes													
	pH, redox, conductivity		pH, redox		pH, conductivity		redox, conductivity		pH		redox		conductivity	
	R^2 (%)	S.E. $mg.L^{-1}$	R^2 (%)	S.E. $mg.L^{-1}$	R^2 (%)	S.E. $mg.L^{-1}$	R^2 (%)	S.E. $mg.L^{-1}$	R^2 (%)	S.E. $mg.L^{-1}$	R^2 (%)	S.E. $mg.L^{-1}$	R^2 (%)	S.E. $mg.L^{-1}$
All data linear	71	1441	62	1637	70	1939	47	1456	61	1659	11	2008	43	2512
Vessel 1 linear	81	1310	72	1568	77	1417	65	1774	66	1743	27	2544	60	1890
Vessel 2 linear	68	1487	63	1602	64	1577	34	2148	58	1714	0	2651	34	2141
Vessel 3 linear	73	1187	62	1399	73	1186	61	1426	63	1393	51	1595	32	1879
All data non-linear	N/A	N/A	N/A	N/A	N/A	N/A	N/A	N/A	61	1580	17	2290	43	1901
Vessel 1 non-linear	N/A	N/A	N/A	N/A	N/A	N/A	N/A	N/A	59	1720	39	2113	56	1796
Vessel 2 non-linear	N/A	N/A	N/A	N/A	N/A	N/A	N/A	N/A	59	1596	13	2325	35	1967
Vessel 3 non-linear	N/A	N/A	N/A	N/A	N/A	N/A	N/A	N/A	76	1097	60	1391	37	1785
Vessels 1 and 2 linear	68	1469	56	1711	67	1485	41	1981	56	1714	8	2474	40	1999
Vessels 2 and 3 linear	69	1296	62	1441	69	1314	39	1821	61	1455	11	2209	36	1867
Vessels 1 and 2 non-linear	N/A	N/A	N/A	N/A	N/A	N/A	N/A	N/A	58	1677	13	2405	43	1959
Vessels 2 and 3 non-linear	N/A	N/A	N/A	N/A	N/A	N/A	N/A	N/A	64	1395	16	2146	37	1863

It must be noted that none of the models featured here appear to be linear above approximately 6000 $mg.L^{-1}$. This was ascribed to the fact that the models are heavily dependant on pH, for models where pH is part of the model data, and pH increased only slightly when the alkalinity doubled from *e.g.* 5006 $mg.L^{-1}$ at pH 7.15, vessel 2, 16/12/05, to 10477 $mg.L^{-1}$ at pH 7.50, vessel 2, 23/11/05, whereas pH will change rapidly when alkalinity is below approximately 3000 $mg.L^{-1}$, *e.g.* alkalinity was 3089 $mg.L^{-1}$ at pH 6 in vessel 2 on 6/3/06, but on 24/4/06 pH fell to 5.64 at an alkalinity of 2076 $mg.L^{-1}$, also in vessel 2. Thus the HCO_3^- buffering capacity and the logarithmic pH scale are reflected here. The non-linearity above alkalinities of 6000 $mg.L^{-1}$ was not considered to be of great importance as this is well above the critical (optimal) range established in Chapter 3. The effect on the models illustrated in Figures 4.7 to 4.12 when titrated alkalinity values above 6000 $mg.L^{-1}$ were removed was also investigated. The results are tabulated in Table 4.2.

Table 4.2. Comparison of R2 percentage values of full range alkalinity prediction models and models only using alkalinity data below 6000 $mg.L^{-1}$.

Model	Full range R^2 %	<6000 $mg.L^{-1}$ R^2 %	Slope and offset
All data pH, redox, conductivity	71 %	82 %	y = 1.0777 x + 269.2
Vessel 1 pH, redox, conductivity	81 %	83 %	y = 1.1129 x + 28.8
Vessel 2 pH, redox, conductivity	68 %	77 %	y = 1.0049 x + 527.2
Vessel 3 pH, redox, conductivity	73 %	80 %	y = 1.0664 x + 181.3
Vessels 1 and 2 pH, redox, conductivity	68 %	71 %	y = 0.9376 x + 647.1
Vessels 2 and 3 pH, redox, conductivity	69 %	81 %	y = 1.031 x + 426.4

The models show better R^2 values when titrated alkalinity values above 6000 $mg.L^{-1}$ are removed, although the R^2 values required a slope and offset correction (as shown in the table) to reach these improved values. It was decided not to repeat the regression calculations without alkalinity values above 6000 $mg.L^{-1}$ as the full data range better represented possible process states and therefore produce a more robust model.

Genstat provided a formula for the calculation of alkalinity from the probe data as a result of the regression models. The choice of algorithms constructed from all three sets of probe data were as follows: Equation 4.2 shows the model derived from all data, Equation 4.3 from vessel 1 data, Equation 4.4 from vessel 2 data, Equation 4.5 from vessel 3 data, Equation 4.6 from vessels 1 and 2 data and Equation 4.7 from vessels 2 and 3 data.

Equation 4.2

$$Alk_p = -8906 + (1678 \times V_p) + (1.998 \times V_r) + (384.2 \times V_c)$$

Equation 4.3

$$Alk_p = -11785 + (2416 \times V_p) + (7.44 \times V_r) + (479.3 \times V_c)$$

Equation 4.4

$$Alk_p = -9284 + (1922 \times V_p) + (4.05 \times V_r) + (295.9 \times V_c)$$

Equation 4.5

$$Alk_p = -10059 + (1766 \times V_p) + (2.01 \times V_r) + (381.7 \times V_c)$$

Equation 4.6

$$Alk_p = -8428 + (1612 \times V_p) + (1.791 \times V_r) + (416.3 \times V_c)$$

Equation 4.7

$$Alk_p = -9318 + (1784 \times V_p) + (1.916 \times V_r) + (312.8 \times V_c)$$

Where

Alk_p = predicted alkalinity

Vp = pH value

Vr = redox value

Vc = conductivity value

4.3.2. Model validation

The alkalinity algorithms were initially examined by using them to calculate alkalinity values based on the four-stage digester pH, redox and conductivity data obtained in Chapter 3, *i.e.* the data sources for the algorithms. This was done for the three individual vessels (1 – 3) with probes on the outlets and for all the data combined. Correlations of the calculated alkalinity predictions to the observed data are shown in Table 4.3 (all correlations were $p > 0.001$). The correlations were calculated as in equation 4.8.

Equation 4.8

$$Correlation = \frac{\sum (x-\bar{x})(y-\bar{y})}{\sqrt{\sum (x-\bar{x})^2 \sum (y-\bar{y})^2}}$$

The correlations of predicted data to observed data were quite similar for each model derived from a particular model data source when tested against a particular test data source, for instance 'all vessel' data gave consistently high R^2 values in the region of 0.8, whereas 'vessel 3' data gave consistently low R^2 values in the region of 0.5.

Table 4.3. R2 correlations (fit towards 1.0) of modelled data to data obtained during Chapter 3 experiment.

Test data source	Model data source R^2 values					
	All vessels	**Vessel 1**	**Vessel 2**	**Vessel 3**	**Vessels 1 and 2**	**Vessels 2 and 3**
All data	0.820	0.788	0.804	0.822	0.822	0.820
Vessel 1	0.649	0.652	0.647	0.648	0.649	0.643
Vessel 2	0.655	0.690	0.676	0.658	0.659	0.643
Vessel 3	0.578	0.488	0.468	0.502	0.520	0.482

The best correlations were therefore for the 'all data' source, and the worst were for the 'vessel 3' data source. The reason for vessel 3 being the worst data source is uncertain. It was hoped that the model would work well at this later point in the process, as it was the second stage of the two-stage digesters which were to be monitored for stability and control purposes. It is possible that the dataset for vessel 3 was less varied than the others, as vessels 1 and 2 were both closer to failure at any time than vessel 3 and thus a less accurate model was produced. The data suggest that the best all round model was constructed from all vessel data, as this model correlates to all the test data reasonably well. It was decided that this model would be incorporated into the LabVIEW software as an on-line monitor of alkalinity and the basis of an organic loading rate control system.

The digesters were run under the control of the algorithm for *ca.* three months before the system was set at a constant organic loading rate for experimental work described in Chapter 6. Comparisons of observed and predicted alkalinity data are shown in Figures 4.13 and 4.14. It should be noted that the period of missing data after day 73 for the 'with support' digester predicted alkalinity was due to repair of the respective probes and modification of the control system to include independent pump drives.

The models were calibrated each month; the differences between the predicted and titrated alkalinities were used to modify the constant which features as the first number in the model equation used for each digester (Equation 4.2). This calibration was in addition to the normal probe calibrations conducted every two months.The model calibrations were minimal. Changes were made on day 32, when the constant was decreased by 480 units (therefore the predicted alkalinity decreased by 480 $mg.L^{-1}$) for the digester without support media, and by 375 units for the digester with support media. Such monthly changes, involving duplicate titration of a sample, were not considered to be a problem.

The predicted alkalinities were correlated to the observed (titrated) alkalinity with r values of 0.82 for the with support digester but only 0.20 for 'without' support digester ($p < 0.001$).

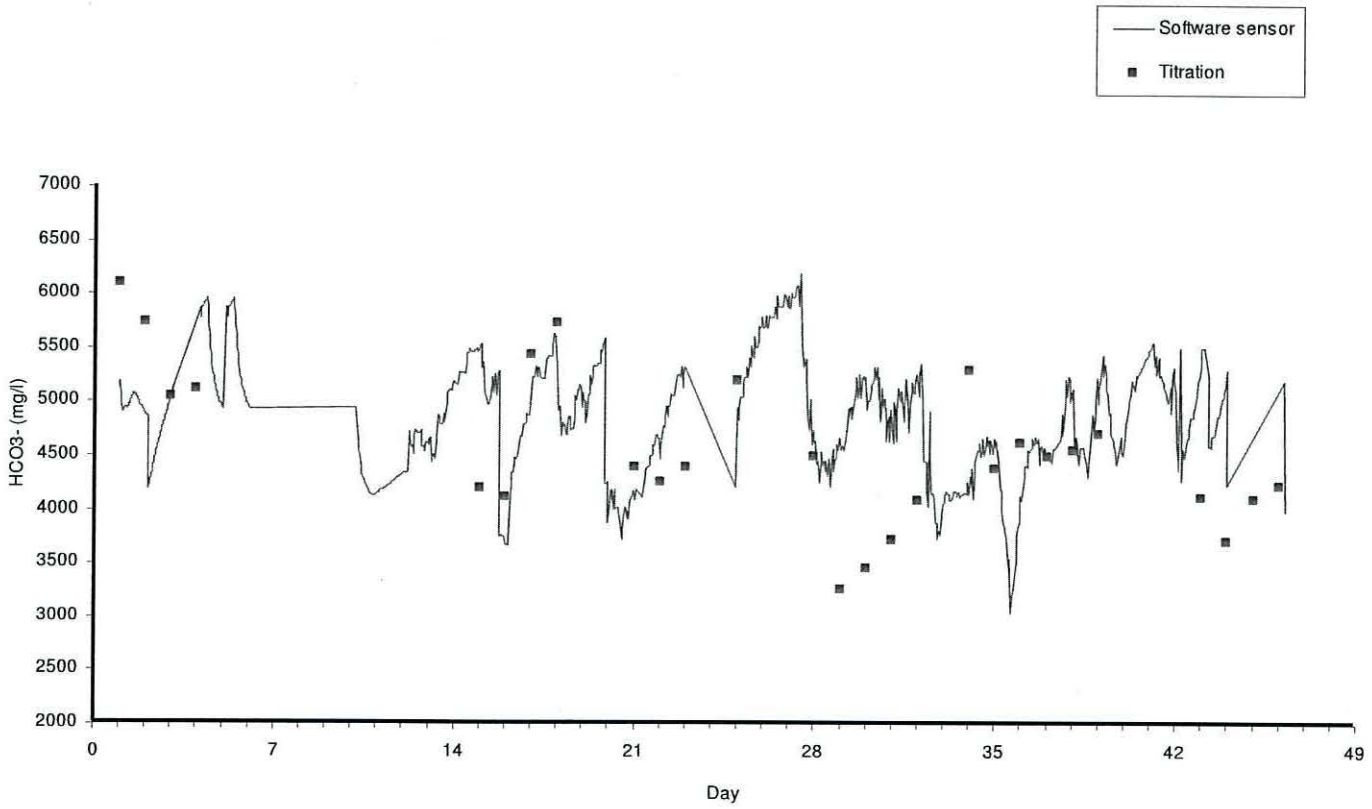

Figure 4.13. Predicted and observed alkalinity for digester without support media.

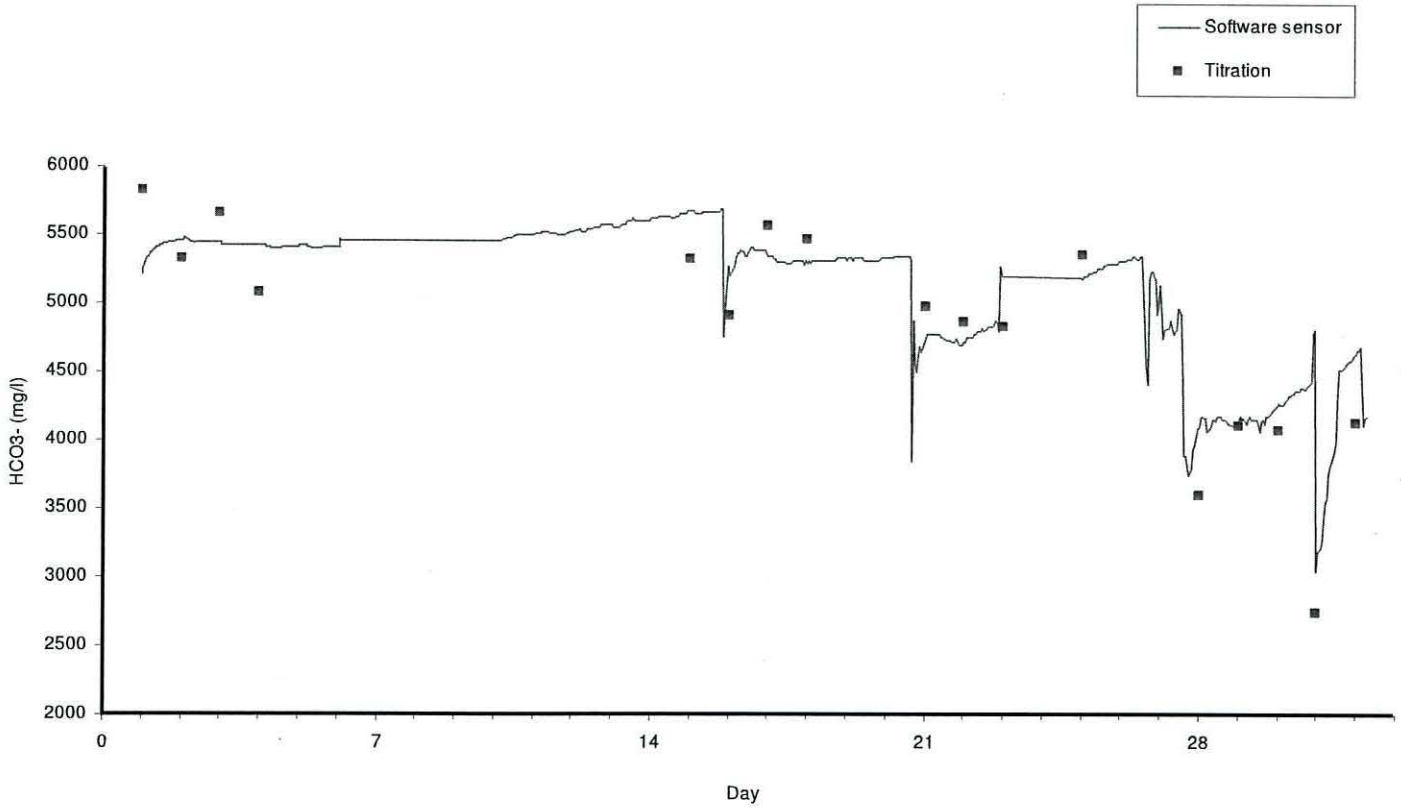

Figure 4.14. Predicted and observed alkalinity for digester with support media.

Linear regressions of predicted and observed alkalinities are shown in Figure 4.15 for the digester with support media and Figure 4.16 for the digester without support media. The digester with support media regression line had a reasonable R^2 value of 0.6713 whereas the digester without support media had a very poor R^2 value of 0.0393. Both regression lines required slope and offset corrections to achieve these values. The lower R^2 values for the without support digester was ascribed to the very noisy predicted alkalinity seen in Figure 4.13. The source of the noise was traced to the redox probe but the definite cause was unknown, as the probe appeared to be performing well when calibrated.

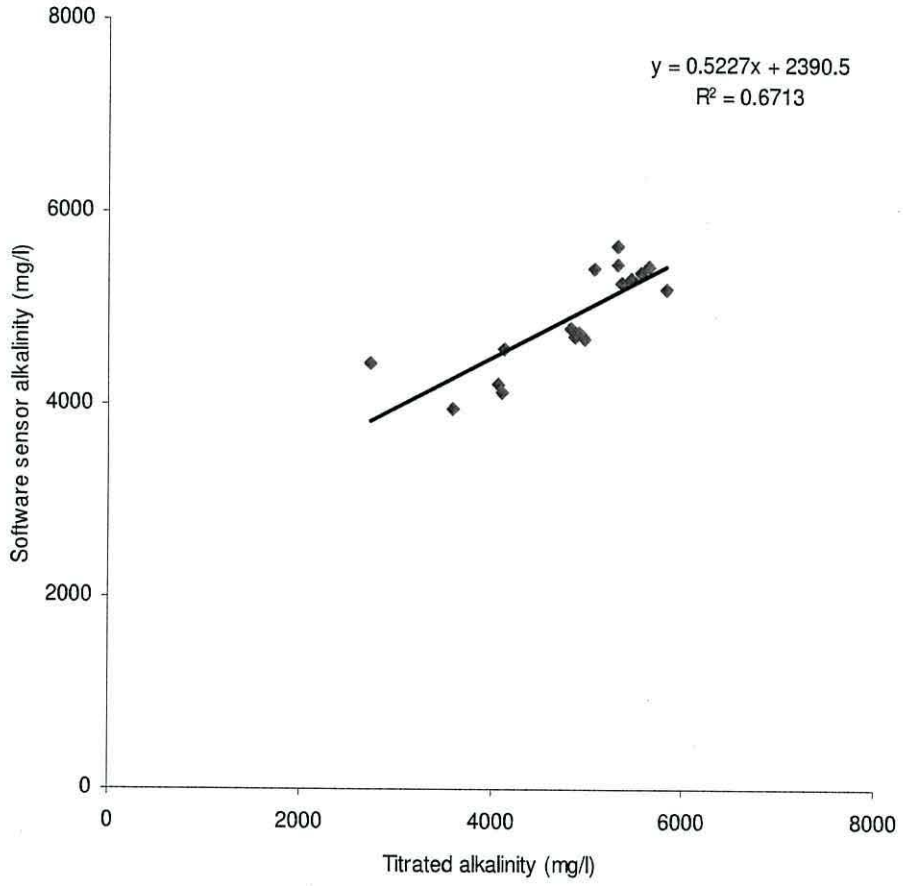

Figure 4.15. Regression of predicted and observed alkalinities for digester with support media.

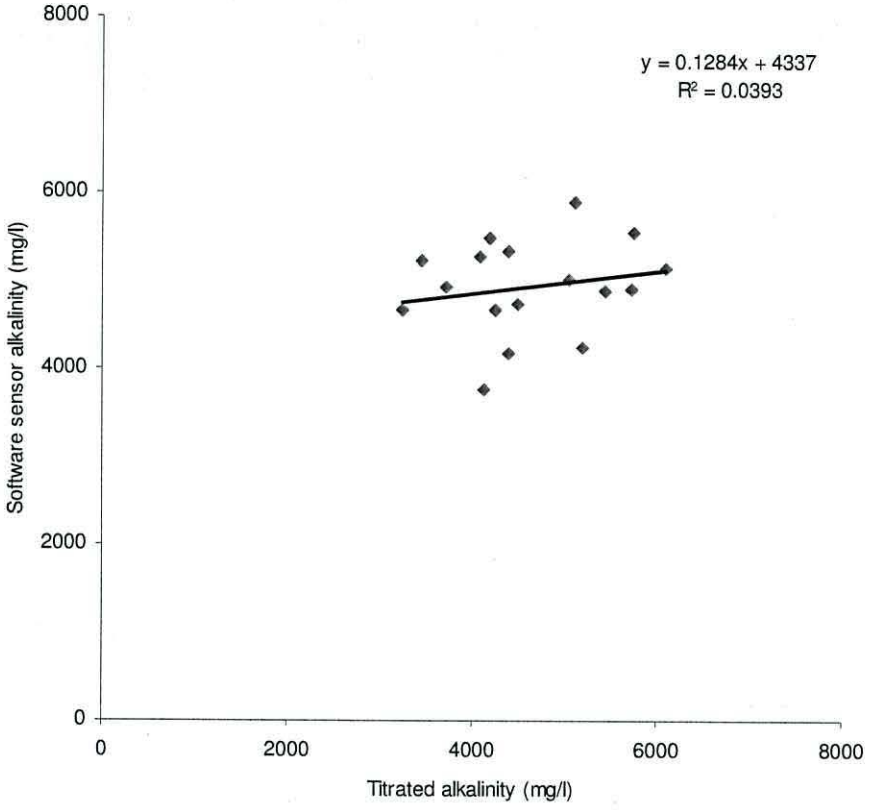

Figure 4.16. Regression of predicted and observed alkalinities for digester without support media.

4.3.3. Control system test models

The results of the responses of the test models based on three variations of the control system are displayed in Figures 4.17, 4.18 and 4.19. These responses were ultimately used for deciding which were to be used in the full scale experiment. Initially, it was thought that using a percentage increase or decrease of the OLR would be suitable for control purposes. The OLR was controlled by modulating the timing of the feedstock pump operating period. The percentage increase type of controller would have an advantage in that the OLR would always remain positive, *i.e.* constantly decreasing an OLR value by a percentage would tend towards zero but would never reach zero. However, a high predicted alkalinity would increase the OLR at an increasing rate every hour, which was considered undesirable.

Table 4.4. Control settings for percentage increase in OLR for proportional-type controller in response to alkalinity values shown.

Alkalinity value (HCO_3^-)	Organic loading rate change
>4500 $mg.L^{-1}$	+ 10 %
3800-4500 $mg.L^{-1}$	+ 5 %
3600-3800 $mg.L^{-1}$	0
<3600 $mg.L^{-1}$	- 20 %

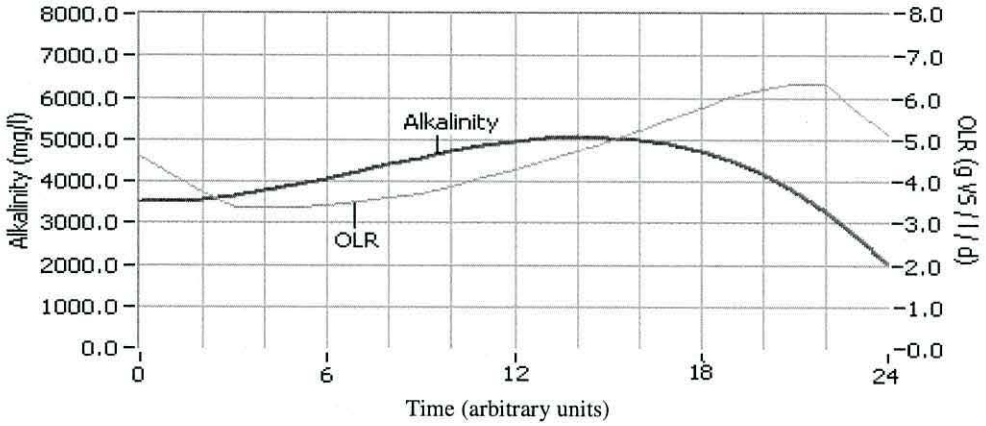

Figure 4.17. LabVIEW model of organic loading rate response to an error based percentage increase controller, using simulated alkalinity data.

The settings for the control system are shown in Table 4.4, and the response to the artificial alkalinity curve is shown in Figure 4.17. The ranges of alkalinity values were chosen to be quite narrow for the test models to see if the controllers could maintain the optimal value (the value at which there is minimal change in OLR). All control models used the same preset alkalinity curve, the X axes are in arbitrary time units and there was no feedback from the loading rate to alter the curve in any way.

The percentage control graph (Figure 4.17) shows that the loading rate is slow to respond to the increasing alkalinity at first, but continues to increase at a high rate even when the alkalinity is falling from t = 14 onwards. It was felt that the slow response relative to the rate of decrease in the modelled alkalinity curve could be improved by creating greater increase percentages but this would also increase the over-shoot seen in the latter part of the graph. Such an over-shoot is a serious problem, and is a result of the control system responding to the alkalinity error only, which is still positive until *ca.* t = 20.5.

A solution to the slow response problem was to use constants for the increase and decrease steps to keep a tighter control of the loading rate, but to also finish the control system routines with a check on the positive or negative status of the organic loading rate. Thus, a case structure was added to ask the question 'is the organic loading rate less than zero?', and if so the organic loading rate was simply subtracted from itself to produce a zero output.

The modified control settings are shown in Table 4.5 and the model response to these changes is shown in Figure 4.18.

Table 4.5. Control settings for constant increase in OLR error-only type controller.

Alkalinity value (HCO_3^-)	Organic loading rate change
>4500 mg.L^{-1}	+ 0.1 g / l / d.
3800-4500 mg.L^{-1}	+ 0.05 g / l / d.
3600-3800 mg.L^{-1}	0
<3600 mg.L^{-1}	- 0.2 g / l/ d.

Figure 4.21 shows an improved loading rate response to the alkalinity increase, but the fall in alkalinity from t = 14 is still not recognised by the controller. Therefore the organic loading rate continues to increase until the alkalinity has fallen below 3800 mg.L^{-1}. Such a delayed response would not maintain a stable system and therefore the proportional-type control was augmented by a derivative component to take into account the rate of change of the alkalinity values.

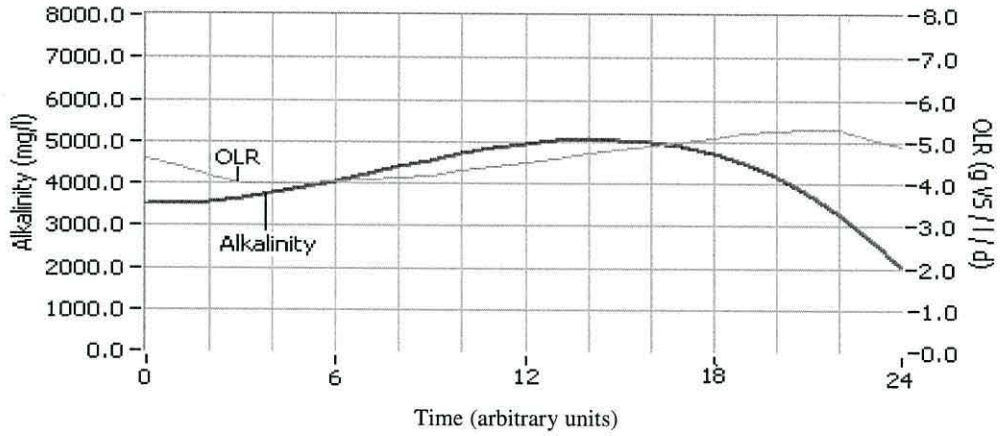

Figure 4.18. LabVIEW model of organic loading rate response to an error based constant increase controller, using simulated alkalinity data.

This additional derivative control was added to the front panel with a weighting value, so adjustments could be made to determine how much difference the derivative would make. The derivative was measured over two points, by taking the predicted alkalinity value for the previous feeding cycle and subtracting it from the alkalinity predicted at the current feeding cycle to measure the rate of increase or decrease. This value was divided by a constant (10,000 in the model) to bring it to an acceptable order of magnitude for loading rate manipulation. This value was then multiplied by the weighting value and finally added to the organic loading rate as a positive or negative value. The settings for the error model with derivative were the same as with the error-only controller (Table 4.5).

Figure 4.19 shows the predicted outcome of these modifications and it is clear from the results that the derivative component greatly improves the response to the fall in alkalinity seen after 14 hours. The sudden fall and rise in the organic loading rate at the beginning ($t < 2$) is due to there being no previous value to use in the derivative calculation. The organic loading rate decreases as the alkalinity starts to decrease, showing a rapid response to the rate and direction of change.

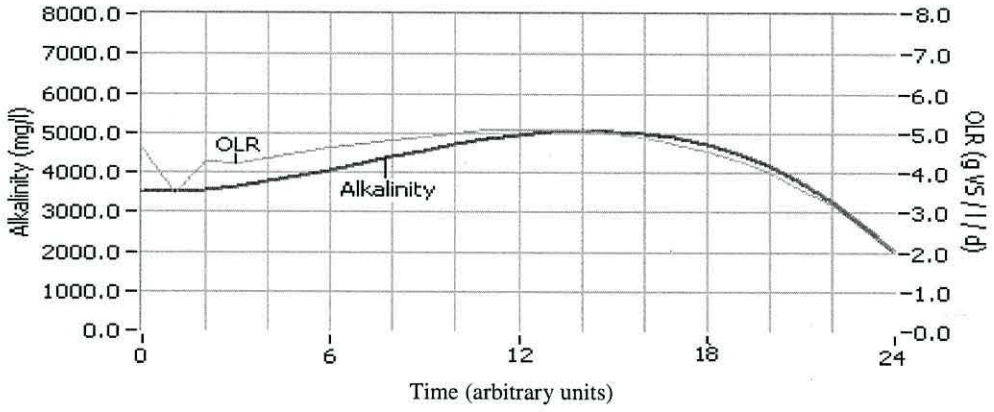

Figure 4.19. LabVIEW model of organic loading rate response to an error based constant increase controller with derivative, using simulated alkalinity data.

As mentioned previously, the model used an alkalinity curve equation that simply produced a curve with a shallow positive gradient and a steeper negative gradient. This was intended to mimic a real system becoming steadily overloaded from an under-loaded starting point. However, the real system

alkalinity predicted by the software sensor did not only control the loading rate, but was itself subject to change as a result of an increased loading rate. This was because an increased loading rate should produce more fatty acids which, in turn, would decrease the buffering capacity. For this reason, a fast response to changes in alkalinity, as seen with the addition of the derivative component, was necessary.

4.3.4. Control system development

Based on the control system test model results shown above, the chosen control system was the constant increase with derivative type. This was added to the LabVIEW virtual instrument and the automatic control system started operating on the 30th December 2006 day 12 following the conversion of the system into two-stage digesters, but was modified on days 18 and 21, as explained in section 4.2.4. Initially, until 29th January 2007 (day 42), the two digesters were fed *via* a single pump motor equipped with two pumping heads, thus linking the organic loading rates of the parallel digesters. These digesters were part of an experiment explained in Chapter 6, and are described as 'with' and 'without' support media, with the predicted alkalinity of the 'without' support digester controlling the feed to both digesters when a single pump was used. Possibly as a result of variation in manufacture, the pump heads feeding the two digesters were not exactly equal in their feed delivery. Thus, calibration of the pump heads found that one pump head regularly delivered 2.4 % more volume than the other. The pump head with the greater flow was used with the 'with support media' digester and the organic loading rate data are adjusted to account for this difference. From 29th January 2007 onwards, a second pump drive was obtained and the two digesters were then fully independent in operation. The results for the predicted alkalinities are displayed with the organic loading rates and the control system alkalinity threshold levels for the digester without support in Figure 4.20 from 30th December 2006 to 29th January 2007 (Days 12 to 42) and Figure 4.21 from 29th January 2007 to 25th March 2007 (Days 42 to 93). The methane production rates for the digester without support media are shown in Figure 4.22. Results from the digester with support media are shown in Figure 4.23 from day 42 to day 93. The loading rate data for the digester with support before day 42 is not shown as the two digesters were linked

at this time. The methane production rates for the digester with support media is shown in Figure 4.24. Data from 25th March (day 93) for both digesters has been omitted here as during this time the digesters were not under automatic control, but were subject to experimental conditions described in Chapter 6. The gas production data in this section are referred to where most relevant. The gas data are discussed more fully in Chapter 6.

The control system was continuously fine-tuned during the period of the experiment (Table 4.6). This included changes to the threshold alkalinity levels which defined the borders of the sets that made the proportional part of the controller *via* the Controls tab. The constant values by which the organic loading rates were increased or decreased and the weightings of the derivatives were also varied to improve the response of the controller and to reduce over-shooting and oscillation of the organic loading rate. These variables were controlled *via* the OLR tab. The experiment was also subject to numerous problems, mainly from blockages in the tubing but also from power failures. The gas production was also very erratic, possibly due to the great variability of the organic loading rate as the control system was adjusted. There follows an account of the various changes made and the problems encountered, with reference to the graphs combining organic loading rate and predicted alkalinity and those showing methane production rate (Figures 4.20 – 4.24).

Table 4.6. Development of control system settings, including predicted alkalinity set limits, proportional control increases and derivative weighting constant.

Date / day	Low set		Mid set	High set		Very high set		Derivative weighting constant
	Limit ($mg.L^{-1}$)	Inc ($g.L^{-1}d^{-1}$)	Limits ($mg.L^{-1}$)	Limits ($mg.L^{-1}$)	Inc ($g.L^{-1}d^{-1}$)	Limit ($mg.L^{-1}$)	Inc ($g.L^{-1}d^{-1}$)	
30/12/06 (Day 12)	<4600	-0.1	4600-4700	4700-4900	0.05	>4900	0.1	2
5/1/07 (Day 18)	<4600	-0.1	4600-4700	4700-5250	0.05	>5250	0.1	2
8/1/07 (Day 20)	<4600	-0.1	4600-5000	5000-5250	0.05	>5250	0.1	2
24/1/07 (Day 47)	<4600	-0.1	4600-5000	5000-5250	0.03	>5250	0.06	4

The period up to day 42 will be discussed in terms of the digester without support only, as during this time both digesters had linked organic loading rates. The digester without support was the source of the predicted alkalinity which controlled the organic loading rate of both digesters. The settings for the system were aimed at maintaining an alkalinity at the higher end of the optimum range found in Chapter 3 as it was thought better to keep the system away from failure as much as possible whilst the controls were set up. The set limits, proportional increases and derivative weightings are shown in Table 4.6 from 30/12/06. In addition, the low pH limit was set at pH 6.8 and a pH reading of less than or equal to this would decrease the organic loading rate by 25 % at each hourly feeding interval. The system was also set to have a minimum organic loading rate of 0.2 g VS l^{-1} d^{-1} unless the feed tank was empty.

The experiment started well, with HCO_3^- concentrations maintained in the region of 4550 to 4750 mg.L^{-1} during days 12 and 13 with an organic loading rate of 1.7 to 1.85 g VS L^{-1} d^{-1}. This was acceptable as the control system was set to maintain an alkalinity at the high end of the optimum found in Chapter 3, therefore an organic loading rate lower than the maximum sustainable was expected. Methane production rate (Figure 4.23) was low at this time at *ca.* 0.15 L L^{-1} d^{-1} for the whole system.

A blockage upstream of the feed pump occurred sometime on day 14, although the problem was not rectified until late day 16. This caused a cessation of feeding to both digesters. The results of this can be seen in Figure 4.21 as an increase in alkalinity due to no feeding, and the consequent increase in organic loading rate. Clearing the blockage resulted in the system suddenly being operated at high organic loading rates of 6.75 and 6.59 g VS l^{-1} d^{-1} for the 'with' and 'without' digesters respectively. It was known from previous experience in Chapter 3 that these values were well beyond the capability of the system. Hence, the sudden decrease in alkalinity and organic loading rate in both digesters during the following period of 12 hours or more. The heavily loaded system produced an increasing amount of methane during this period (alkalinity was still above the optimal value found in chapter 3), reaching a peak of 0.4 l l^{-1} d^{-1} on day 22 for the total system. It was also noticed on day 16 that the low pH warning was not connected to the proper terminal in the LabVIEW virtual instrument, and so was not functioning. This was corrected immediately. The

minimum organic loading rate limit of 0.2 g $VS.L^{-1}$ d^{-1} was also changed to 0 at this time, as the system somehow became stuck at the initial lower limit. No explanation of this behaviour was realised at that time, other than some glitch in the LabVIEW coding, but it is possible that it was due to a similar problem found and solved later in the experiment, which is described below.

Examination of the data showed that the organic loading rate was increasing too rapidly, from 1.5 to 4.5 g $VS.L^{-1}.d^{-1}$ during the 24 hours between days 14 and 15. For this reason, the upper alkalinity limit was increased from 4900 $mg.L^{-1}$ to 5250 $mg.L^{-1}$ on day 15 to slow the increase of organic loading rate when alkalinity is only slightly above the desired level (Table 4.5). However, the increase in organic loading rate remained rapid during that morning, and further investigation revealed a problem with the 'without support' hydrolysis vessel mixing system, which had led to a build up of solids in this vessel. The effective volume of the hydrolysis vessel was estimated to have been reduced to less than 10 % of its original volume. Thus, an important role of the hydrolysis vessel, the buffering of shock loads, was lost. The vessel was emptied of the majority of solids, the mixing system repaired and the vessel diluted with water. This caused a delay in the acidification of the feedstock entering the methanogenesis vessel, and so the system alkalinity increased until a sudden fall on day 17, with a corresponding fall in the organic loading rate.

The lack of stabilisation of the organic loading rate was attributed to the narrow range of alkalinity values within which the organic loading rate would remain constant. The range of the mid set was therefore increased as shown in Table 4.5 on day 20. A low pH warning was triggered during day 21, which caused the rapid decline in organic loading rate seen at this time. Methane production decreased in line with the reduced loading rate. The system eventually settled into a an oscillating predicted alkalinity (and therefore the loading rate behaved similarly) from day 28 to day 45. Methane production at this time was low (*ca.* 0.1 – 0.3 $L.L^{-1}$ d^{-1}) but more stable than the earlier part of the experiment. The stability achieved during this period was still not considered satisfactory, therefore on day 47 the proportional increase constants were decreased and the derivative weighting increased as shown in Table 4.6. The new derivative weighting meant that a change in the current predicted alkalinity of +/-

100 $mg.L^{-1}$ when compared to that calculated sixty minutes previously would result in a change in the organic loading rate of +/- 0.04 g $VS.L^{-1}$ d^{-1}. These changes were intended to reduce the amount of over-shooting and oscillation seen in the organic loading rate response. As a result, the. predicted alkalinity and loading rate oscillations reduced in amplitude until day 89. The loading rate was low at this time, between 1 and 2 g $VS.L^{-1}.d^{-1}$ which gave a very low methane production of *ca.* 0.08 $L.L^{-1}$ d^{-1}. The combination of stable organic loading rate and methane production proves the hypothesis of loading rate control being capable of regulating methane production. The experiment was stopped a few days later.

The system was subject to many problems during the course of the experiment.

The sudden decrease of the organic loading rate to zero seen on day 50 was the result of the feed tank running empty. This mechanism described earlier to prevent continued additions in this event worked well in preventing the feed pump adding air to the primary vessels, but once the problem had been rectified the organic loading rate was at zero and therefore needed to build up to a suitable level slowly. A better method would have been to stop the feed pump when the feed tank was empty but to retain the last organic loading rate value for when the system was re-started, but this would have required extensive modification to the LabVIEW architecture.

A low pH warning on day 66 caused a rapid decrease in organic loading rate for the digester without support, and in addition to this, the feed tank ran low and the 'empty' warning was again triggered. The organic loading rate was manually increased to 2 g $VS.L^{-1}$ d^{-1} when the feed tank was re-filled, as the predicted alkalinity had increased to *ca.* 5000 $mg.L^{-1}$.

Blockages in the transfer tubing between the hydrolysis and methanogenesis vessels often led to an increase in the predicted alkalinity as there was no feedstock input to the methanogenesis vessel during these occurrences. Consequently, the apparent organic loading rate was increased to levels that would be impossible to sustain. When the blockage was removed, the system was suddenly operating at the elevated organic loading rate and therefore alkalinity fell very quickly. Such problems occurred between days 58 and 59 and days 72 and 73 for the digester without support media.

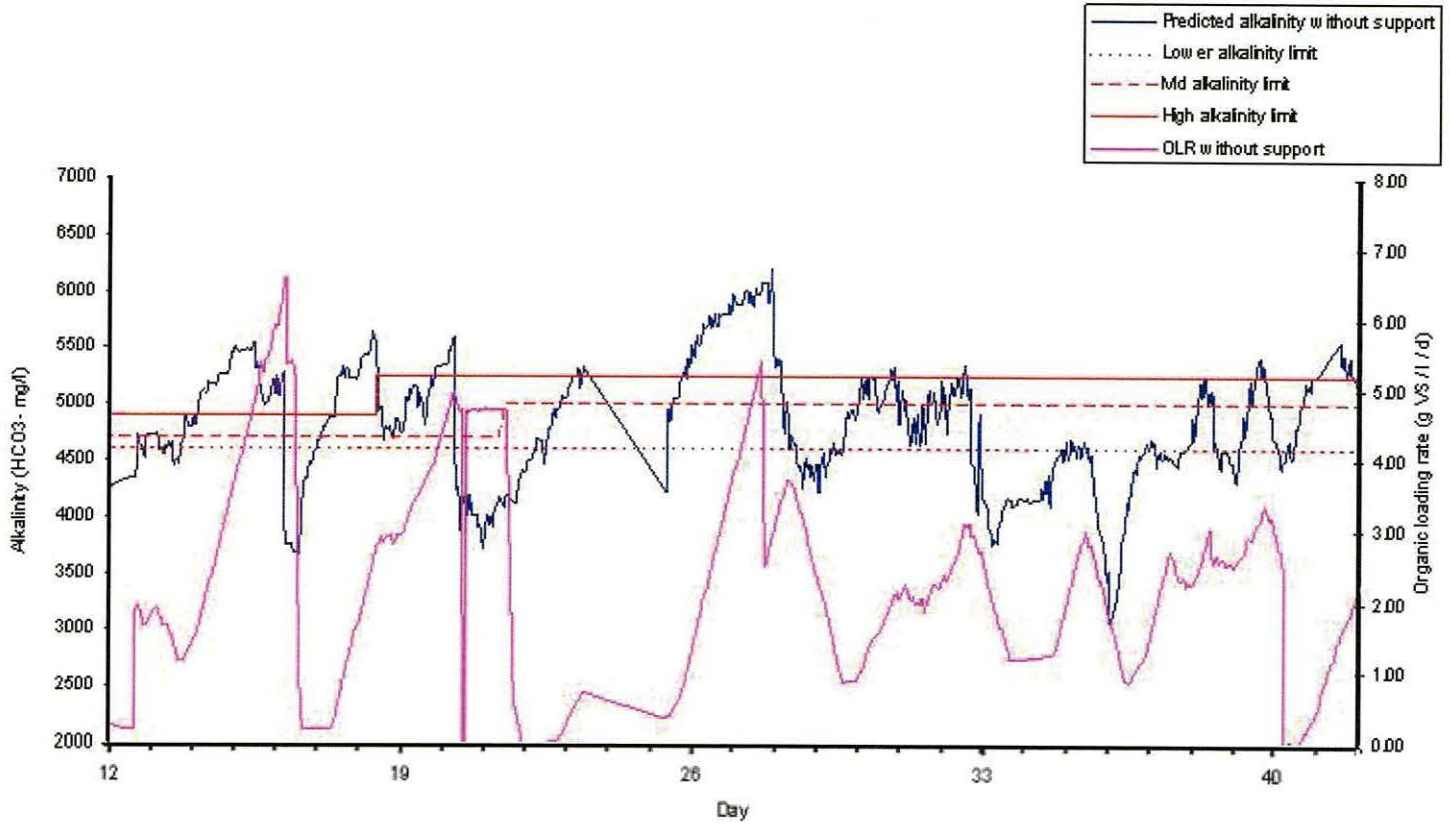

Figure 4.20. Predicted alkalinity and organic loading rate from 30/12/06 – 29/1/07 (days 12 – 42) for digester without support media

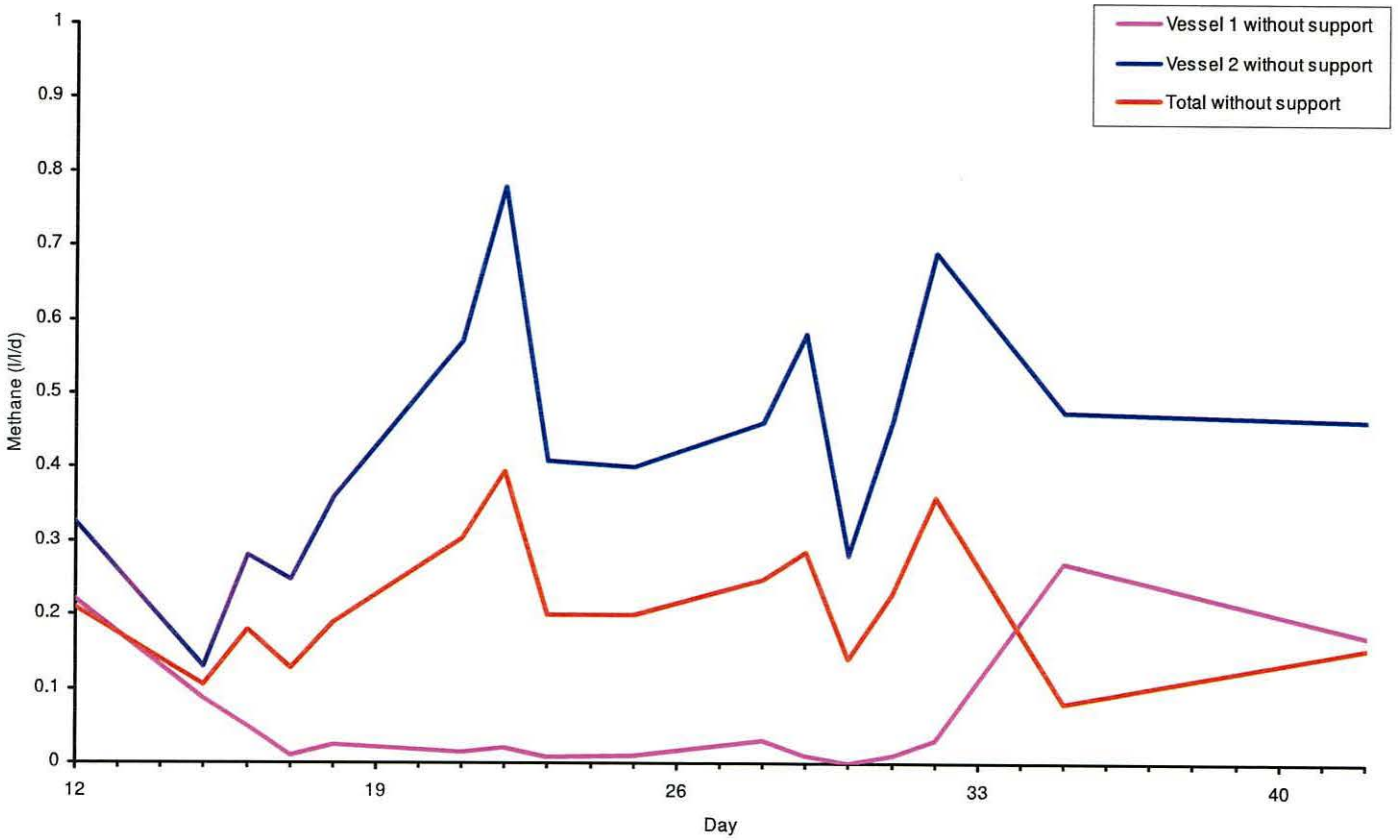

Figure 4.21. Methane production rate for digester without support media from 30/12/06 - 29/1/07.

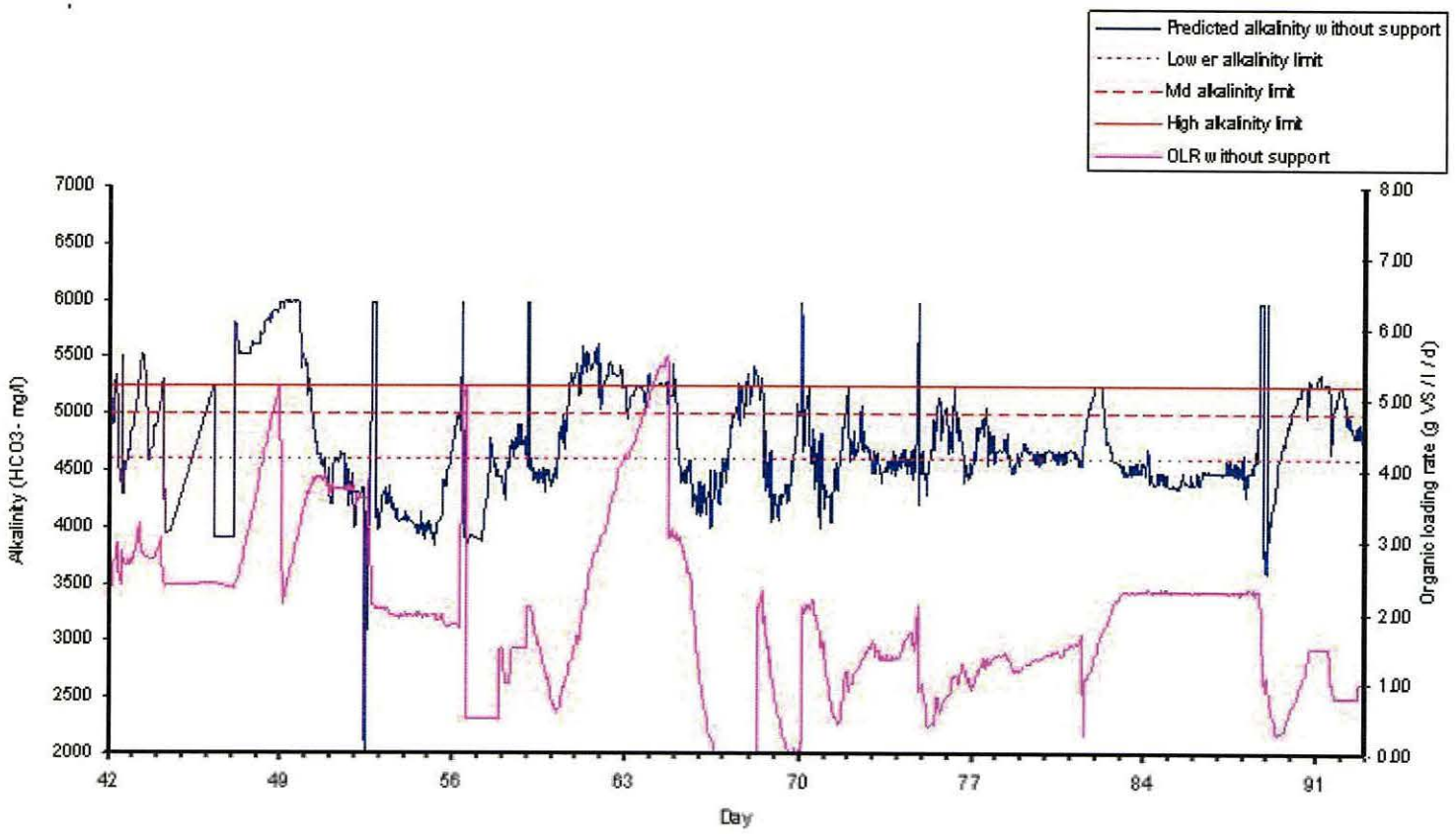

Figure 4.22. Predicted alkalinity and organic loading rate from 29/1/07 – 25/3/07 for digester without support media.

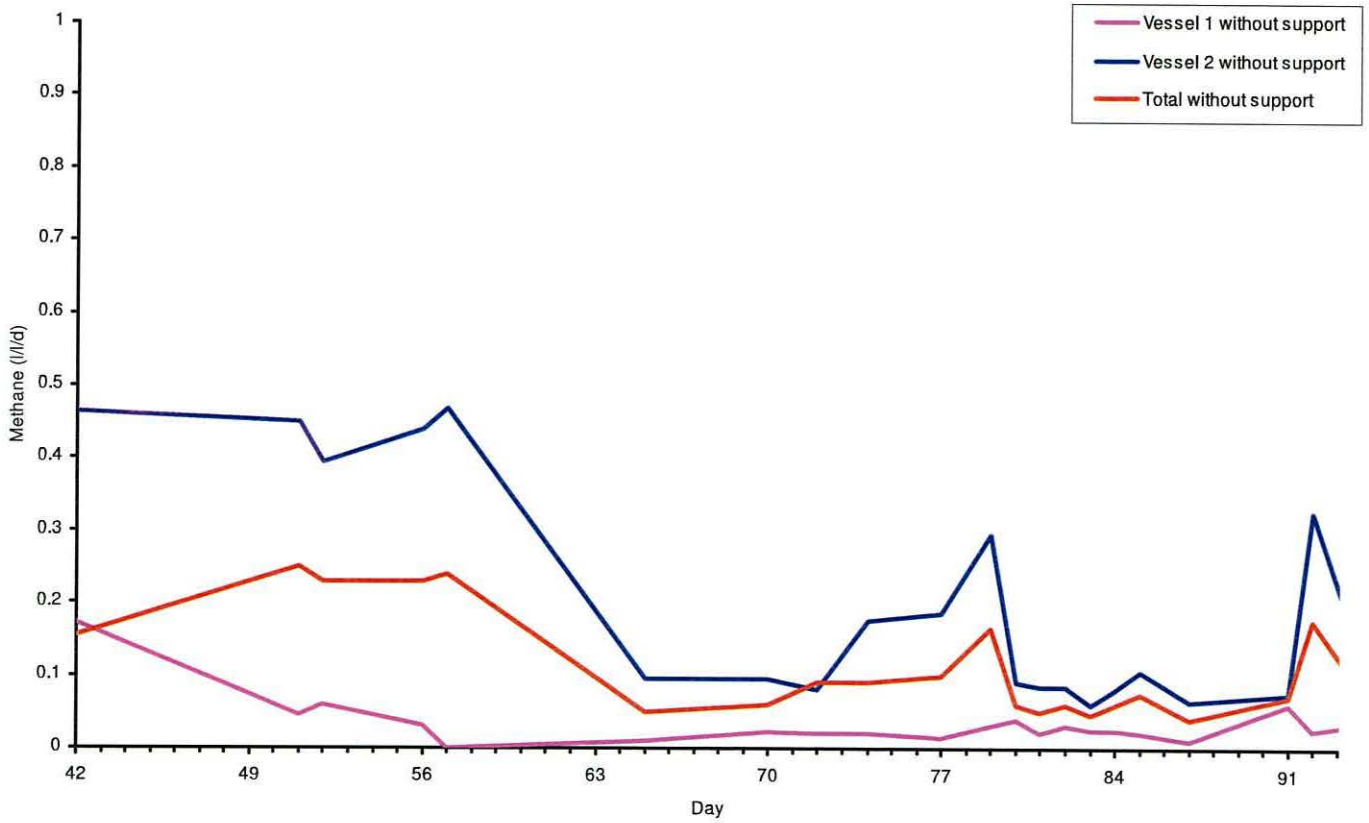

Figure 4.23. . Methane production rate for digester without support media from 29/1/07 - 25/3/07.

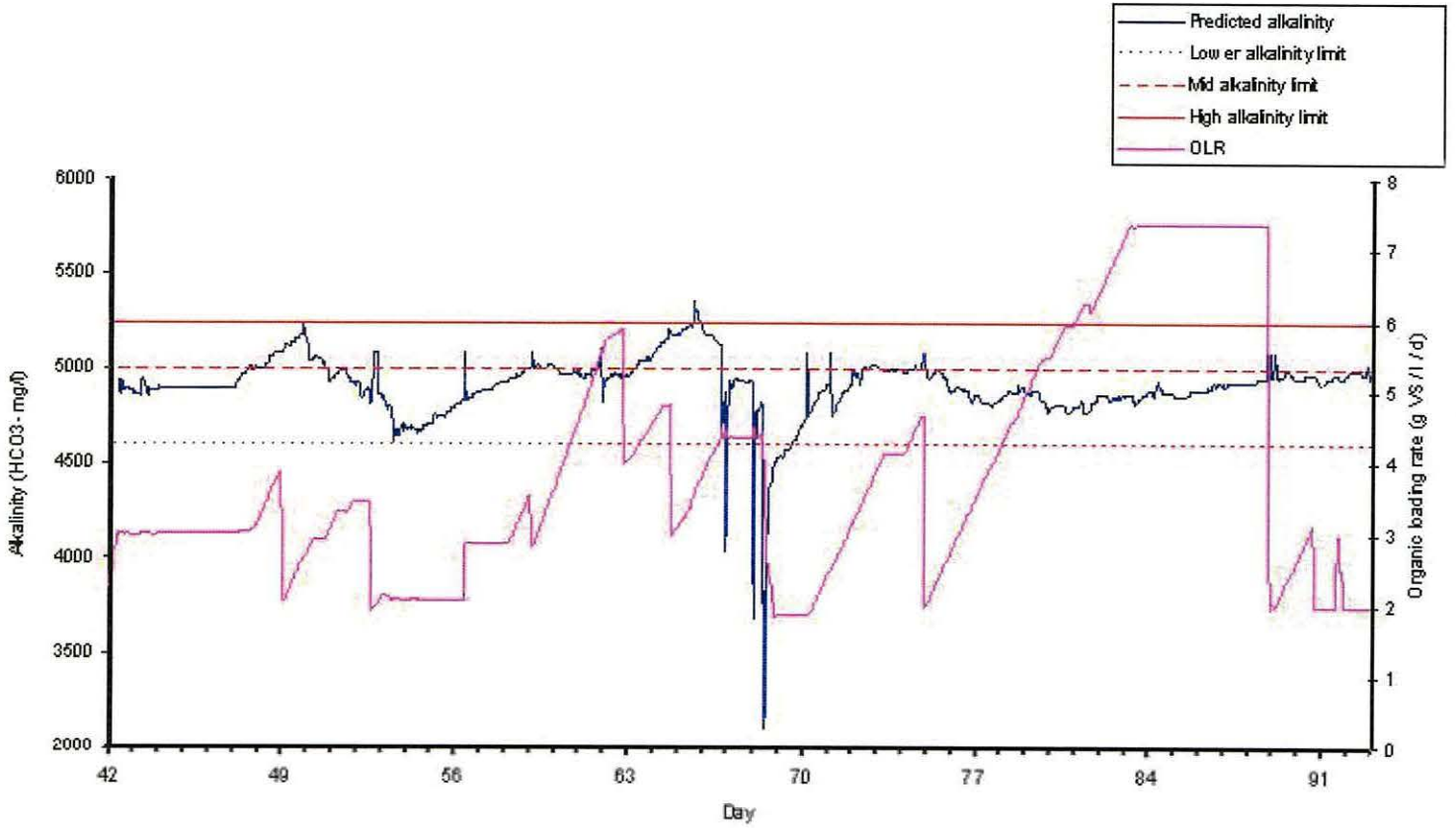

Figure 4.24. Predicted alkalinity and organic loading rate from 29/1/07 – 25/3/07 for digester with support media.

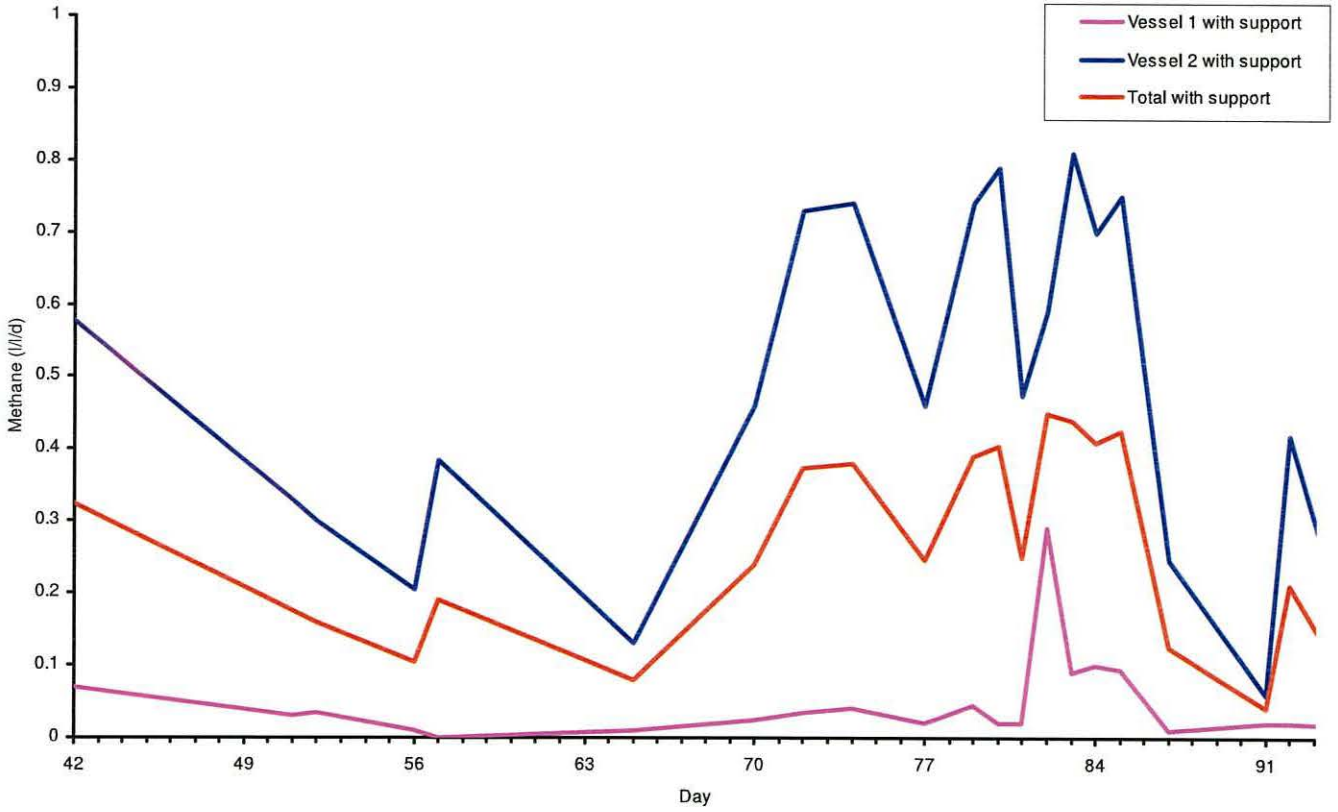

Figure 4.25. Methane production rate for digester with support from 29/1/07 - 25/3/07.

As mentioned above, from day 42 the digesters were able to operate completely independently. The digester with support media suffered fewer blockages in the digestate transfer tubing than the digester without support media and generally appeared more stable in terms of predicted alkalinity and loading rate. Methane production was less stable, as between days 42 and 60, the loading rate was *ca.*3 g $VS.L^{-1}$ d^{-1} and the predicted alkalinity was 4600 – 5200 $mg.L^{-1}$, yet methane production fell from 0.32 $L.L^{-1}$ d^{-1} to 0.2 $L.L^{-1}$ d^{-1}.The increase in loading rate from day 60 to 62 was not expected, based on the predicted alkalinity, The software seemed to have an unknown flaw. It was believed that this also caused the large increase in organic loading rate seen between days 70 and 83, with a consequently high methane production rate of *ca.* 0.35 $L.L^{-1}$ d^{-1} from the whole system. This production rate fell to *ca.* 0.15 $L.L^{-1}$ d^{-1} when the loading rate fell to *ca.* 2.5 g $VS.L^{-1}$ d^{-1}. At this point in the experiment the hypothesis of loading rate controlling methane production was proven again as the loading rate controlled the amount of available substrate to the organisms. It has already been shown in chapter 3 that methane production was high at a high loading rate, although constant operation at a high rate risked failure of the system. The software should have not produced an error-based organic loading rate increase during this period as the predicted alkalinity was within the 'no change' zone. The automatic control system was disabled shortly after this as both digesters were required to be maintained at constant OLRs for experiments described in Chapter 6. Shortly after the Chapter 6 experiments, both digesters were found to have excessive solids in the first vessels due to failure of the mixing systems preventing further experimentation.

It should be noted that the software sensor described in this chapter could be specific to the feedstock used. This may be particularly the case for the conductivity probe, as the exact mechanism by which conductivity affects alkalinity in largely unknown (the sensor has a 'black box' quality). The measurement of electrical conductivity in the water industry is known to be impossible to compare between different sample sources and, as such, is used only for comparative measurements from the same water source (HMSO, 1978). It has been shown that conductivity can change during batch anaerobic digestion experiments of animal manures with olive industry wastes (Al-Masri, 2001), where conductivity was found to increase up to day 28 from *ca.* 5000 $\mu S\ cm^{-1}$ to *ca.* 6500 $\mu S\ cm^{-1}$ and then decrease to *ca.* 5200 $\mu S\ cm^{-1}$ by the end of the (40 day) experiments. Similarly, conductivity was found to increase through the four stages of the process described in chapter 3, the latter stages of the multi stage

system can in be compared to a batch digestion experiment after several weeks digestion. However, in another study of the anaerobic digestion of cattle dung with brackish waters of conductivities between 1000 μS cm^{-1} and 15000 μS cm^{-1}, waters with conductivity above 5000 μS cm^{-1} was found to be inhibitory to the process (Yeole *et al.* 1997), in this case it was suggested that the conductivity variation was due to ions such as Na^+, Cl^- and NO_3^- in high concentrations. The conflicting information about the relationship between electrical conductivity and process state suggest the software sensor is very specific to the feedstock used as conductivity does not differentiate between different ions present in solution.

The control system used in this chapter was not ideal. Modifications to improve the controller could include more case structures to increase or decrease the organic loading rate at specific alkalinity values, allowing for a smoother transition between the error-based components of the controller. However, care must be taken to avoid too many case structures as this would produce a system that was little different from a simple PD controller. Creating a maximum organic loading rate limit for the system, based on experience gained during non-automatic control operation in Chapter 3 could also assist in reducing the oscillations of the controller output. It may be worth considering fuzzy logic as an alternative to the rule based system, as controllers based on this principle are in some ways similar in that noisy or inaccurate data is managed by assigning values to sets. Fuzzy logic uses a system whereby an input or output value can have partial membership of a set, so there are no sudden changes between sets. The derivative component in a fuzzy system would also be put into sets of *e.g.* 'large positive change' or 'small negative change' and the overall change to the organic loading rate would be based on the combination of the error based and derivative set memberships. However, it should be noted the anaerobic digestion process will always be subject to some degree of time lag between increasing the input and the consequent increase in fatty acids due to it being a biologically driven process. Thus any control system will be likely to always have some degree of over-shoot.

4.4. Conclusions

The software sensor was considered a success in that alkalinity was predicted accurately enough to provide an early warning of process failure. The best model for predicting alkalinity was found to be a multiple linear regression model using all three probes and the combined data from all vessels. This model had an R^2 value of 71 % (p

< 0.001) and a standard error of 1441 $mg.L^{-1}$. The model subsequently produced correlations with R^2 values of as much as 0.82 ($p < 0.001$) when validated with new data.

This Chapter dealt with one of the two constantly variable actuators available in anaerobic digestion, that of the organic loading rate (which is related to the feed flow rate). The use of basic off-the-shelf sensors to monitor the anaerobic digestion process was a success. However, a more advanced yet still low-maintenance sensor system is examined in Chapter 5, using Near Infrared Reflectance Spectroscopy (NIRS) to measure key process variables. The other actuator available in anaerobic digesters is the mixing frequency. Mixing speed is a far more difficult variable to change in existing anaerobic digesters. This is because it requires expensive motor speed controllers which are unlikely to be found on full-scale biogas plants. By comparison, simply controlling the on–off action of a mixing device is far simpler. An investigation into mixing frequency is discussed in Chapter 6.

5 Prediction of key anaerobic digestion parameters by Fourier Transform Near-Infrared Reflectance Spectroscopy

5.1. Introduction

5.1.1. Overview

Near infrared reflectance spectroscopy (NIRS) is proving itself to be a valuable tool for many industrial and scientific applications (Reich, 2005). Because the technique is spectroscopic, it is essentially instantaneous and can in theory operate continuously. It is also non-destructive, and provides multi-constituent analysis of virtually any matrix (Reich, 2005). It also requires no sample preparation or reagents (Givens *et al.*, 1997).

Near infrared radiation occurs in the region of the electromagnetic spectrum which, according to the American Society of Testing and Materials (ASTM), lies between visible light and the mid infrared region, of wavelengths 780 – 2526 nm, although infrared spectra are usually described by wave numbers ($\bar{\nu}$) instead of wavelength, with the reciprocal centimetre as the unit, as this is proportional to the energy of vibration (Reich, 2005). The NIRS range therefore corresponds to wave numbers between 12821 cm^{-1} and 3959 cm^{-1}. The relationship between $\bar{\nu}$ (the number of waves per centimetre), ν (the frequency), λ (the wavelength) and c (the speed of light *in vacuo*), can be expressed as in Equation 5.1 (Reich, 2005).

Equation 5.1

$$\bar{\nu} \propto \frac{1}{\lambda} \propto \frac{\nu}{c}$$

The often narrow peaks of mid infrared spectroscopy make this technique suitable for the identification of organic compounds. However, low signal to noise ratios makes it less suitable for quantitative analysis. This is a particular problem when dealing with aqueous matrices where the intense IR absorption by water often masks and / or interferes with signals from target analytes. In reality quantitative, mid-infrared analysis is only possible for thin film aqueous samples. By comparison near infrared instruments have a typical signal to noise ratio of 10,000:1 (Givens *et al.*, 1997). In addition, NIRS is appropriate for water based substrates such as in fermentation processes because the water signal is relatively less intense than in the mid-IR range

The signals in NIR spectra are generally composed of absorption bands dominated by overtones and combinations from the vibrational modes of C-H, O-H and

N-H bonds of organic molecules due to the low mass of the hydrogen atom (Givens *et al.*, 1997). A combination of all these factors makes NIRS an interesting candidate for studying biogas processes.

Light scattering can be used to measure particle size. In addition, light absorption can be used to quantify target analytes (Givens and Deaville, 1999). However, it is not possible to measure both these parameters simultaneously unless different parts of the electromagnetic spectrum are used for each parameter. Thus, there are no mathematical laws to describe the interaction of radiation with a scattering medium of absorbing species, so calibration of the instrument is required with a large number (particularly in a complex media such as anaerobic digestates) of known samples whose concentrations have been determined by standard methods of measurement (Givens and Deaville, 1999).

The majority of bands in the near infrared range tend to be overtones when λ is less than 1800 nm and combinations when it is greater than 1800 nm of the fundamental vibration frequencies found in the mid-IR region (MIR, 4000-400 cm^{-1}) and consist of broad peaks at a much lower amplitude than the fundamentals (Pons *et al.*, 2004). Because of the weakness of NIR bands (typically 10 -100 times weaker than MIR) and their overlapping nature, the information within the spectra is multivariate and data processing is required to relate spectra to the sample properties (Reich, 2005).

5.1.2. Infrared spectroscopy

Infrared radiation absorbed by organic molecules at frequencies between 10,000 and 100 cm^{-1} is converted into molecular vibration energy, whilst frequencies of less than 100 cm^{-1} tend to be converted into molecular rotation energy. Absorptions are resonant and quantised. However, because a single vibrational energy change is accompanied by several rotational energy changes (Figure 5.1), vibrational spectra appear as bands rather than discrete lines (Silverstein *et al.*, 2005).

The quantised energy levels, of which there are number of stacks in a molecule, are a function of the quantum number, and when a molecule is subjected to radiation a photon is emitted or absorbed. The energy of the photon must be equivalent to the gap between the quantised energy levels for resonant absorption and this is related to the frequency as shown in Equation 5.2.

Equation 5.2

$$\Delta E = h\nu$$

Where E = energy, ν = frequency and h is the Planck constant (6.626 x 10^{-34} J.s). It follows that the frequency of emission or absorption between two energy states can be calculated by Equation 5.3 (Stuart, 1997).

Equation 5.3

$$\nu = \frac{(E_1 - E_0)}{h}$$

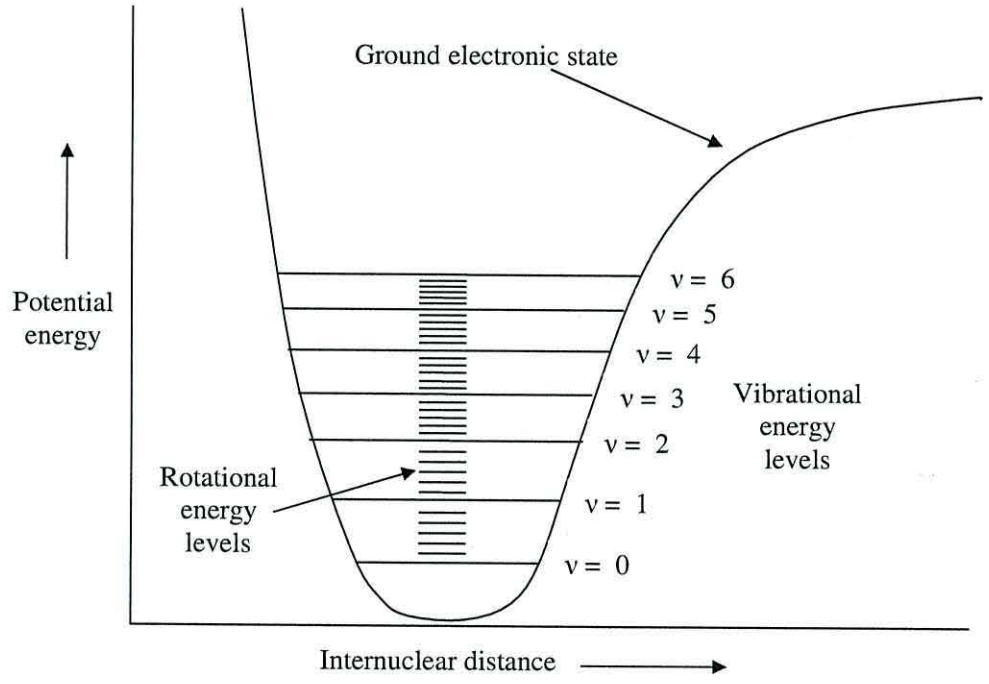

Figure 5.1. Potential energy diagram of vibrational and rotational energy levels, redrawn from Smith (1998).

Atoms or molecules return to their original state after quantised absorption by a deactivation mechanism, *i.e.* the vibration (Figure 5.2).

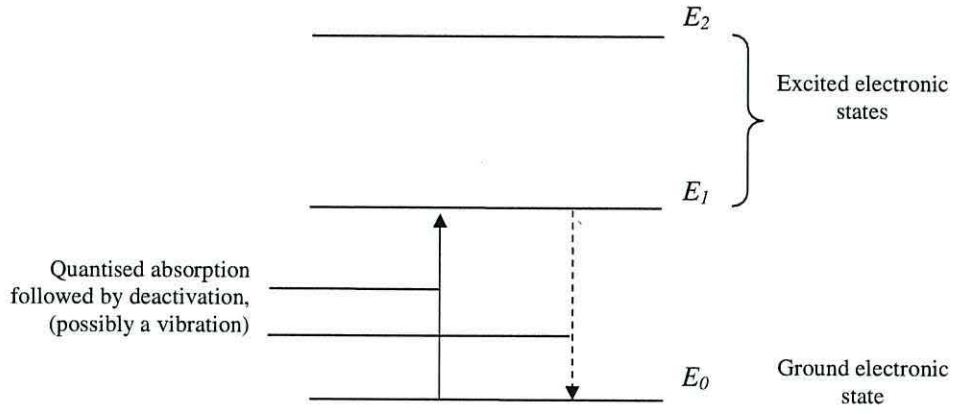

Figure 5.2. Energy levels of an atom or molecule, redrawn from Stuart (1997).

The potential energy diagrams shown in Figures 5.3 and 5.4 show how the rotational energy levels relate to overtones and combination bands (respectively) which dominate the NIR spectrum.

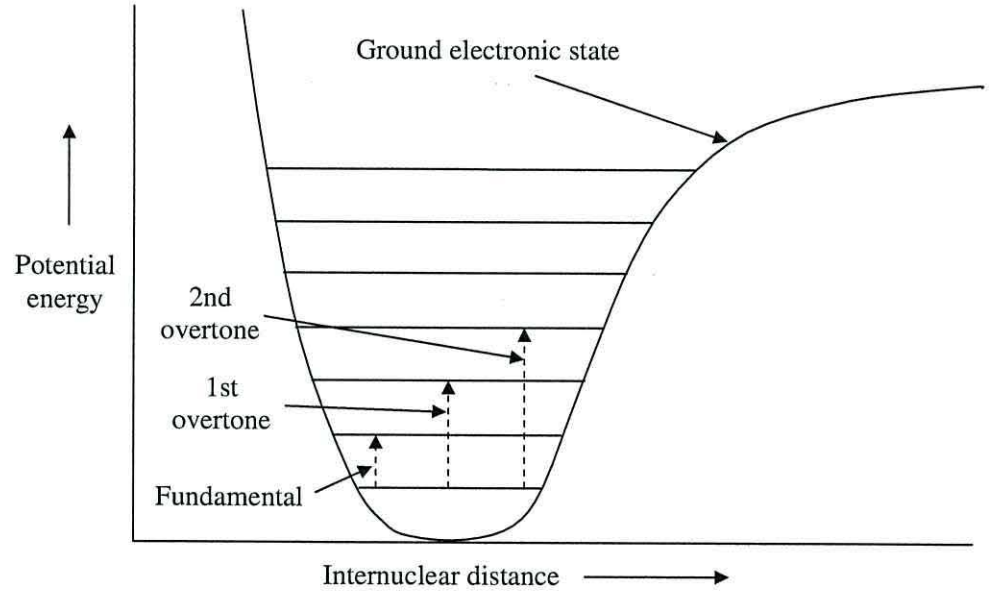

Figure 5.3. Potential energy diagram showing jumps between vibrational energy levels which are represented by 1st and 2nd overtones of the fundamental vibrational frequency, redrawn from Smith (1998).

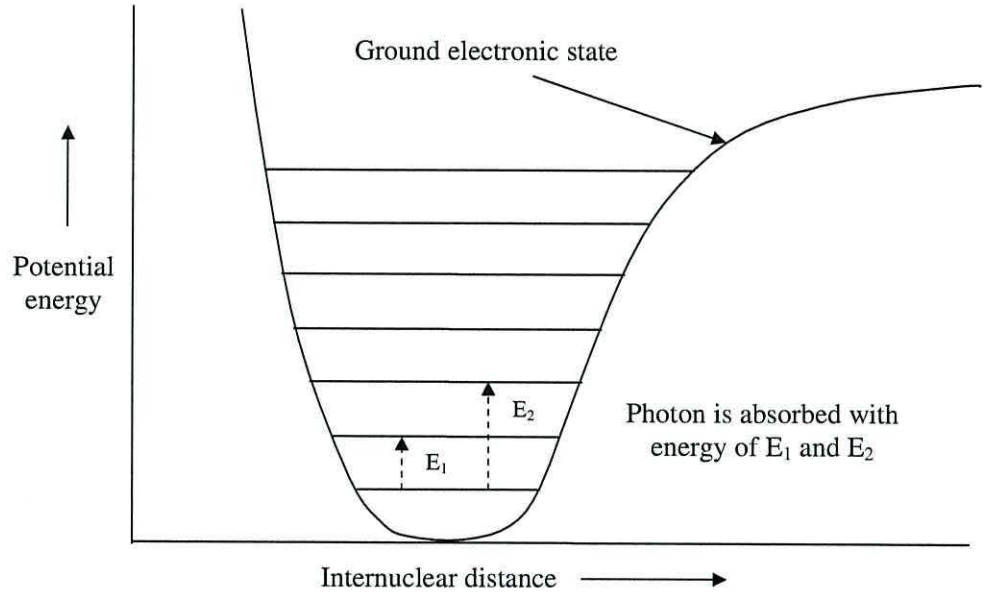

Figure 5.4. Potential energy diagram showing jumps between vibrational energy levels which are the result of absorption of a photon, producing a combination band of infrared spectra, redrawn from Smith (1998).

The atoms in a molecule can move in relation to each other, either by stretching or bending movements known as vibrations. A simple diatomic molecule can only vibrate by stretching and compression of the bond and therefore has one degree of vibrational freedom. A polyatomic molecule containing N atoms will have $3N$ degrees of freedom in total, of which there are $3N - 5$ degrees of vibrational freedom for linear molecules such as carbon dioxide and $3N - 6$ degrees of freedom for non-linear molecules such as water. This is because both linear and non-linear molecules have three degrees of translational freedom but non-linear molecules have three degrees of rotational freedom whereas linear molecules have only two degrees of rotational freedom because there is no energy involved in rotation around the O=C=O axis or that of other linear molecules. Subtracting the translational and rotational degrees of freedom from the total therefore gives the number of vibrational degrees of freedom.

A molecule absorbs infrared radiation of the same frequency as one of the fundamental modes of vibration. The molecular bond vibrations associated with a CH_2 group are shown in Figure 5.5 as an example. Stretching vibrations are movements of bonded atoms towards and away from each other (Figure 5.5 a-b), and bending vibrations are where the distance between bonded atoms remains constant but their angle in relation to the rest of the molecule changes (Figure 5.5 c-f).

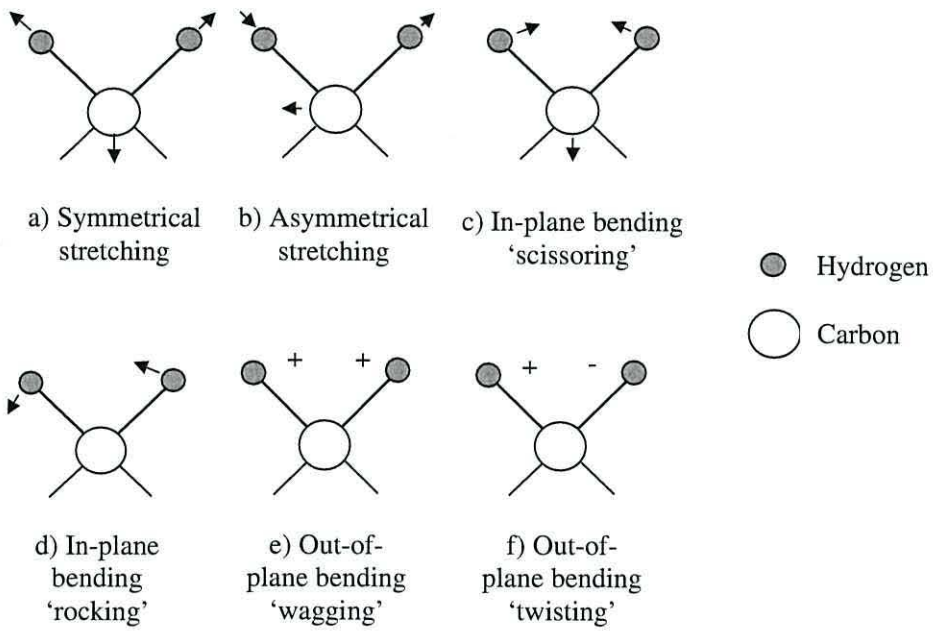

Figure 5.5. Vibrational models for CH2 group, + and – indicate movement perpendicular to the plane of the page, redrawn from Silverstein et al. (2005). Bonds are shown below the C atoms which would connect the CH2 group to other atoms as part of a larger molecule.

In order for an infrared mode to be active, there must be a change in the dipole during transition. A larger change in dipole moment will give a more intense absorption band. An example of this can be shown with a C=O double bond. The large difference in electronegativity between carbon (δ^+) and oxygen (δ^-) means that stretching of the bond will increase the dipole moment (*i.e.* change it during vibration) giving rise to an intense absorption. With a CO_2 molecule, symmetrical stretching (Figure 5.6 a) of both of the C=O bonds equally but in opposite directions produces no net dipole so this is IR inactive, but asymmetrical stretching (Figure 5.6 b) of the molecule will have a dipole and is therefore infrared active. Symmetrical molecules will have fewer vibrations which are infrared active than unsymmetrical molecules. Also, vibration of bonds between atoms in widely separated groups on the Periodic Table will give more intense absorption bands as the change in dipole moment is greater (Stuart, 1997).

a) Asymmetric stretching of CO_2 molecule.
Net change in dipole during transition.

b) Symmetric stretching of CO_2 molecule.
No net change in dipole during transition.

Figure 5.6. Vibration of a CO2 molecule showing how a) asymmetrical stretching produces a net dipole and is IR active, and b) symmetrical stretching does not, redrawn from Smith (1998).

Fourier transform infrared spectrometers measure all frequencies simultaneously, unlike the older dispersive instruments which do not and required a longer time period to scan across all frequencies. The interferometer used in FT-IR instruments which allows simultaneous measurements is quite simple and is shown as a diagram in Figure 5.7.

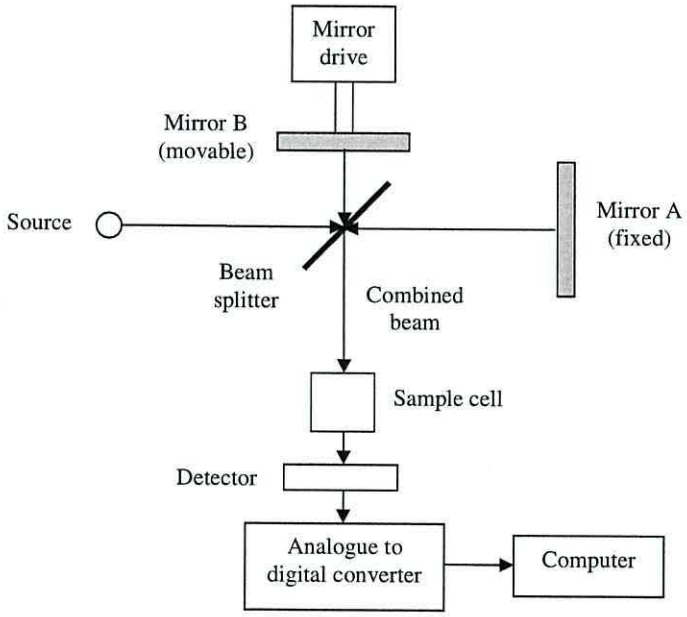

Figure 5.7. Diagram of an FT-infrared spectrometer during transmission measurement. Reflection measurements are similar but the detector is fitted next to the emitted combined beam (Silverstein et al., 2005).

The beam splitter divides the incoming beam towards both a fixed and a moving mirror, which reflect the beams back to the splitter where they recombine. The small difference in path length of the two beams causes interference. The resulting signal is called an interferogram which contains signal information about every frequency which came from the source. The interferogram cannot be interpreted directly and requires

decoding by Fourier transformation to produce the spectral information. The benefits of FT-IR over dispersive machines can be summarised as the Felgett Advantage which is the high speed scanning of all frequencies simultaneously, the Jacquinot Advantage, meaning the optical throughput is higher with higher detector sensitivity and also signal averaging of several scans to reduce noise (Ferrec *et al.* 2006).

5.1.3. NIRS of manures and anaerobic digestion processes

NIRS has been successfully used in the analysis of components of complex organic substrates such as manures and digestates from anaerobic processes, as summarised in Tables 5.1 and 5.2 respectively. The R^2 (%) obtained in the following examples have been graded as follows: Excellent (R^2 (%) $\geq$ 0.95), very good (R^2 (%) $\geq$ 0.90), good (R^2 (%) $\geq$ 0.85), reasonable (R^2 (%) $\geq$ 0.80) and poor (R^2 (%) $<$ 0.80). These grades were believed to be more descriptive of accurate prediction than those suggested previously (Williams, 2003).

Huang *et al.* (2007) collected manures from twenty two Chinese provinces to compare total organic carbon, total nitrogen and volatile solids of fresh and dried samples with NIR reflectance spectra over the wavenumber range 4000 – 10,000 cm^{-1}. The calibration results are shown in Table 5.1, with an excellent prediction of wet sample moisture content and of total N in both wet and dry samples, very good predictions of organic carbon, volatile solids and electrical conductivity of wet samples and good predictions for organic carbon and volatile solids of dry samples. Poor calibrations were obtained for pH, C:N ratio and total phosphorous. The authors concluded that NIRS was a useful tool for rapid evaluation of manure quality. Malley *et al.* (2005) used a portable VIS NIR (visible / near infrared) spectrometer over a wavenumber range of 27778 – 5917 cm^{-1} and found that NIRS of raw, stockpiled (not turned) and composted (turned in windrows) beef feedlot manure produced calibrations for measurement of the constituents shown in Table 5.1. Very good predictions were obtained for organic and total carbon, reasonable prediction of K and poor predictions of total N, S and P. The poor prediction of total N and the good predictions of both pH and C:N ratio was contradictory to the results obtained by Huang *et al.* (2007) mentioned above. It is possible that the use of different instruments had an effect on the results as the two instruments ranges are very different, with the Malley group using the visible spectrum in addition to the NIR. The same researchers also found that using classification analysis software on the spectra alone showed that stockpiled manure did

not significantly change in composition upon drying whereas composted manure was significantly different and less variable than the raw or stockpiled manures. Saeys *et al.* (2005a) also used a VIS NIR spectrometer, in the range 23474 to 5942 cm^{-1}, measuring reflectance. Very good predictions of organic and dry matter were found but predictions of P, Ca and Mg were poor.

Summarising the information in Table 5.1, it is clear that organic matter, dry matter, N and C are the most popular and accurately predicted constituents of manures. These may be of interest in anaerobic digestion as organic and dry matters are fundamental properties of feedstocks and digestates. N and C are also useful parameters for estimation of potential inhibition by ammonia and for an approximate estimation of ultimate methane yield.

NIRS of anaerobic digestion processes has shown some success, as shown in Table 5.2. Propionate has been suggested as an effective parameter for indicating process imbalance (Nielsen *et al*,. 2007). Hansson *et al.* (2002; 2003) found very good and good prediction of propionate in two separate studies involving the anaerobic digestion of municipal solid waste. The good prediction was from the latter study which included more data. The spectral range in these studies was 800 to 2000 nm (12500 to 5000 cm^{-1}). In addition to the quantitative determination of propionate, the authors found that principal component analysis of the NIR spectra showed dynamic changes in microbial biomass by phospholipid fatty acid (PLFA) and phospholipid ether lipid (PLEL) predictions upon over loading in the 2002 publication. Also spectral changes relating to overloading, excessive foaming, failed stirring and changes in substrate C:N ratio were seen in the 2003 paper.

Holm-Nielsen *et al.* (2006) examined volatile solids, total solids and COD as part of a study in representative sampling of biological slurries, with NIRS predictions that were very good, good and poor respectively. A later study by the same authors (Holm-Nielsen *et al.* 2008) concentrated on measuring VFAs for process monitoring and also glycerol as a feedstock. Predictions of VFA were quite variable, with excellent predictions of acetate, iso-butyrate, iso-valerate and total VFA, very good prediction of valerate and poor prediction of butyrate and propionate, the latter with an R^2 (%) of just 0.37. The technique used in both Holm-Nielsen studies was transflexive NIRS (described below), the 2006 study as an off-line analysis and the 2008 study as an in-line analysis using a flow cell with a path length of 3 mm within a sampling loop.

Table 5.1. Examples of recent NIRS analyses of manures.

Measured constituent	Malley *et al.* (2005)	Huang *et al.* (2007)		Saeys *et al.* (2005a)
	Cattle manure	Dry composted manure	Wet composted manure	Pig manure
Total C	$R^2 = 0.91$, RMSEP = 23.4 mg/g	N/A	N/A	N/A
Organic C	$R^2 = 0.91$, RMSEP = 22.6 mg/g	$R^2 = 0.85$, RMSEP = 2.56	$R^2 = 0.91$, RMSEP = 3.17	N/A
Nitrogen	$R^2 = 0.74$, RMSEP = 1.2 mg/g (TN)	$R^2 = 0.97$, RMSEP = 6.9 (TN)	$R^2 = 0.97$, RMSEP = 6.11 (TN)	$R^2 = 0.86$ / 0.76, RMSEP = 1.225 / 1.125 (TN / NH_4 N)
C:N ratio	$R^2 = 0.87$, RMSEP = 1.59 mg/g	N/A	N/A	N/A
K	$R^2 = 0.83$, RMSEP = 2.9 mg/g	N/A	N/A	$R^2 = 0.69$, RMSEP = 1.148 g/L
S	$R^2 = 0.73$, RMSEP = 0.44 mg/g	N/A	N/A	N/A
P	$R^2 = 0.61$, RMSEP = 0.7 mg/g	N/A	N/A	$R^2 = 0.75$, RMSEP = 1.12 g/L
pH	$R^2 = 0.89$, RMSEP = 0.29	N/A	N/A	N/A
VS / organic matter	N/A	$R^2 = 0.85$, RMSEP = 2.6	$R^2 = 0.94$, RMSEP = 4.05	$R^2 = 0.9$, RMSEP = 9.292
Moisture / dry matter	N/A	N/A	$R^2 = 0.98$, RMSEP = 7.48	$R^2 = 0.91$, RMSEP = 12 g/L
Electrical Conductivity	N/A	N/A	$R^2 = 0.9$, RMSEP = 3.1	N/A
Ca	N/A	N/A	N/A	$R^2 = 0.59$, RMSEP = 1.49 g/L
Mg	N/A	N/A	N/A	$R^2 = 0.8$, RMSEP 0.502 g/L

Table 5.2. Examples of recent NIRS analyses of biogas processes.

Measured constituent	Holm-Nielsen *et al.* (2006)	Holm-Nielsen *et al.* (2008)	Hansson *et al.* (2002)	Hansson *et al.* (2003)
	AD of biomass	AD of manure	AD of municipal solid waste	AD of municipal solid waste
VS / organic matter	$R^2 = 0.91$, RMSEP = 0.23	N/A	N/A	N/A
Moisture / dry matter	$R^2 = 0.81$	N/A	N/A	N/A
COD	$R^2 = 0.77$	N/A	N/A	N/A
Glycerol	N/A	$R^2 = 0.96$, RMSEP = 3037 mg/L	N/A	N/A
Acetate	N/A	R = 0.98, RMSEP = 1476 mg/L	N/A	N/A
Propionate	N/A	R = 0.37, RMSEP = 1364 mg/L	$R^2 = 0.94$, RMSEP = 0.21 g/L	$R^2 = 0.85$, RMSEP = 0.53 g/L
Iso-butyrate	N/A	R = 0.95, RMSEP = 26.46 mg/L	N/A	N/A
Butyrate	N/A	R = 0.74, RMSEP = 271.9 mg/L	N/A	N/A
Iso-valerate	N/A	R = 0.97, RMSEP = 55.83 mg/L	N/A	N/A
Valerate	N/A	R = 0.93, RMSEP = 24.31 mg/L	N/A	N/A
Total VFA	N/A	R = 0.98, RMSEP = 2096 mg/L	N/A	N/A

The most commonly measured parameter for NIRS prediction in anaerobic digestion processes (Table 5.2) is propionate concentation, although monitoring relative concentrations of volatile fatty acids has been suggested to be more indicative of process stability (Ahring *et al.* 1995; Pullammanappallil *et al.* 2001; Pind *et al.* 2003). However, VFAs were not measured in this study but it was believed that alkalinity, which was found to be a good indicator of process in Chapter 3, could be predicted by

NIRS. Steyer *et al.* (2002) have shown that mid infrared spectroscopy (MIRS) can be used to predict partial and total alkalinity in anaerobic digesters, and this method appeared to accurately predict alkalinities when compared to a titrimetric sensor and off-line analyses, although an R^2 value was not stated. However, the MIRS system required an ultrafiltration membrane to treat samples before analysis and this was found to be a weak point in the system. It is also difficult to compare NIRS against MIRS calibrations as the former use complex multivariate analysis to create a calibration because of the overlapping peaks obtained in the spectra, whereas the latter uses the Beer-Lambert law as MIRS peaks are considerably better defined (Reich, 2005).

Saeys *et al.* (2005a) encountered problems in the NIR region of the spectra in that an unusual representation of a broad peak found at 1450 nm (6897 cm^{-1}). This peak is the result of the O-H bonds in water, but was found to be less clear at lower dry matter (*i.e.* higher water) values. This was attributed to the reduced number of scattering particles at lower dry matter values causing less light to be reflected back to the detector and therefore is not due to absorption by molecular bonds. Attempts have been made to overcome this problem. Malley *et al.* (2002) used a modification to reflection spectroscopy procedure known as transflectance, where samples were scanned through a narrow (1 mm) path length with a gold reflector opposite the instrument window. The transflectance method has recently been repeated as mentioned above as an in-line method (Holm-Nielsen 2007, 2008). Transflectance has been compared directly with reflectance the former was found to give better results for constituents directly related to dry matter (organic matter, P, Ca and Mg) in hog manure (Saeys *et al.*, 2005b). This was attributed to the loss of light in reflectance measurements complexing the relationship between dry matter and absorbance. However, the transflection methods are of little interest here as many particles present in typical feedstocks used in anaerobic digestion are much larger than the flow cells used (European Union Animal By-Products Regulation stipulates a maximum particle size of 12 mm). In this context, using such instruments for on-line or in-line measurement would be hampered by blockages (Saeys *et al.*, 2005b). There are also potential problems in the form of collinearity between parameters. For instance, Saeys *et al.* (2005) found that organic matter, P, Ca, and Mg were strongly correlated to dry matter, with R^2 (%) of 0.97, 0.82, 0.74 and 0.84 respectively. Such collinearities prevent the accurate model prediction of these parameters separately. It should also be noted that the predictions of P, Ca, Mg, S and K are not actually as a result of the components themselves as these are not

spectrally active. Such calibrations rely on 'surrogate' measurements of other components which possess spectrally active bonds such as C-H, O-H or N-H. The correlation of P, Ca and Mg to dry matter found by Saeys *et al.* (2005a) would be a likely explanation of these surrogate predictions.

5.2. Materials and methods

All samples were analysed with a Bruker Vector 22/N FT-NIR spectrometer with OPUS v. 5.0 software for spectral analysis and OPUS Lab software as a user interface for measurement of multiple sample sets (Bruker Optics Limited, Banner Lane, Coventry CV4 9GH, England). In a typical analysis, 20 ml of each fresh sample was measured in triplicate at room temperature and added to 40 ml glass vials for reflectance measurements. Reflectance spectroscopy was considered a better choice for highly scattering materials such as slurries, based on manufacturer's recommendations. The maximum spectrometer range was from 12,800 to 4000 cm^{-1} (780 to 2500 nm). The resolution of the spectrometer was set at 16 cm^{-1}. The spectrometer used an internal integrating sphere to collect a greater proportion of the reflected energy by concentrating the diffuse reflected photons.

The OPUS software quantitative analysis determined the property Y from an experimentally observed X using a calibration function b. Values of Y in this case were the reference measurements of alkalinity determined by titration, and X values were the calibration spectra which formed the row vectors. From these, b was determined as in Equation 5.4. Equation 5.5 shows this for a simple three-spectrum matrix (Bruker, 2004).

Equation 5.4

$$\bar{Y} = X.\bar{b}$$

Equation 5.5

$$\begin{bmatrix} Y_1 \\ Y_2 \\ Y_3 \end{bmatrix} = \begin{bmatrix} Spectrum1 \\ Spectrum2 \\ Spectrum3 \end{bmatrix}.\bar{b}$$

The software used a PLS 1 (Partial least squares) regression which is commonly used in NIR spectral analysis (McCarty *et al.* 2002; Viscarra Rossel *et al.* 2006). The matrices were broken down into their Eigenvectors, known as factors or principal

components. This allowed the minimal number of factors to be used to produce the calibration model, thereby simplifying the model. The first factor was a relatively simple correlation between component values and the raw data of spectral intensities. If the values of Y were reproduced consistently (helped by calibration function b) the regression analysis could be stopped, reducing the amount of calculation required to calibrate the instrument. If not, subsequent PLS factors were arranged according to their relevance to predict the component values, with the ability to stop the regression after the factor with which values of Y could be consistently reproduced. The maximum number of factors was determined by the maximum rank setting, therefore a higher maximum rank required a greater amount of calculation but may have been necessary for large and complex datasets. However, there was a danger of using a rank that was too high, leading to overfitting of the model. Overfitting is the use of a model that is too complex, *i.e.* it has too many variables and not enough samples. Overfitting models can lead to idiosyncrasies of the sample data which may not appear in subsequent samples analysed using the model, whereas underfitting or bias is the term used for a model which is too simple and may miss meaningful data (Gershenfeld, 1999). The software recommended an ideal rank, based on either the minimum root mean square error of prediction (RMSEP) or the root mean square error of cross validation (RMSECV). The RMSEP or RMSECV provided an error based on spectra which were not part of the calibration set when a test set validation was performed or based on the entire validation when cross validation was performed, respectively. Thus, overfitting or underfitting were easily avoided as data independent of the validation were used to test the model. However, the software did recommend a ratio of calibration spectra to factors of 20:1 (Bruker, 2004). This was not a problem with the combined data from all vessels as there were a total of 316 separate samples for alkalinity data, allowing a theoretical maximum of > 15 factors. This number was reduced for pH, redox and conductivity data as there were only three points at which these data could be collected, therefore the number of spectra was 237 and the maximum number of factors was > 11. The numbers were reduced still further for individual vessel data to barely 4 factors from 79 spectra.

Residuals (*Res*) were the difference between true and fitted values, and the sum of squared errors (SSE) was calculated as Equation 5.6 (Bruker, 2004).

Equation 5.6

$$SSE = \sum [\mathrm{Re}\, s_i]^2$$

The *SSE* was then used to calculate the root mean square error of estimation (*RMSEE*) as Equation 5.7 with *M* being the number of standards and *R* the rank (Bruker 2004).

Equation 5.7

$$RMSEE = \sqrt{\frac{1}{M-R-1}SSE}$$

The determination coefficient or R^2 (as a percentage) was also calculated from *SSE*, as Equation 5.8.

Equation 5.8

$$R^2 = \left(1 - \frac{SSE}{\sum (y_i - y_m)^2}\right) \times 100$$

The detection of outliers relied on complex mathematical manipulation of the matrices, in that the matrix X needed to be inverted and bi-diagonalised. This allowed calculation of the leverage value (h_i) by the software as Equation 5.9 (Bruker, 2004).

Equation 5.9

$$h_i = diag(UU^T)$$

Where *U* represents orthonormal matrices. The leverage was a measure of how much influence a particular spectrum had on the PLS model for a particular component. Leverage values are always less than 1 and the sum of all leverages was equal to the rank (*R*) as Equation 5.10 (Bruker, 2004).

Equation 5.10

$$\sum h_i = R$$

From this, the mean leverage value, *R/M* can be calculated, where *M* is the number of calibration samples. It was recommended that 5 *R/M* was a suitable limit for determining outliers (Bruker, 2004).

5.3. Results and discussion

5.3.1. Visual examination of the spectra

An example of a typical spectrum from the anaerobic digester is shown in Figure 5.8, this particular example being taken from vessel 1 on January 6th 2006. The spectrum has been marked at the dominant peaks and possible sources of these peaks have been added to the figure. The approximate regions are marked A) Combination bands region, B) First overtone region, C) Second overtone region and D) Third overtone region. Possible molecular bond sources of peaks have also been added (Bruker, 2004). It is impossible to pinpoint particular species in a mixture as complicated as that found in anaerobic digesters, but some of the peaks do match with the water first overtone and combination bands at 6900 and 5190 cm^{-1}, respectively. Similarly, the CH first overtone is somewhat aligned with the 5600 cm^{-1} peak, as are the CH, CH_2 and CH_3 second overtones with the 8380 and 8580 cm^{-1} peaks. The CH bonds could be from a number of compounds such as organic acids or alcohols. The RCO_2H second overtone, indicative of organic acids, is found between 5260 and 5320 cm^{-1} and is obscured by the H_2O peak in the same area.

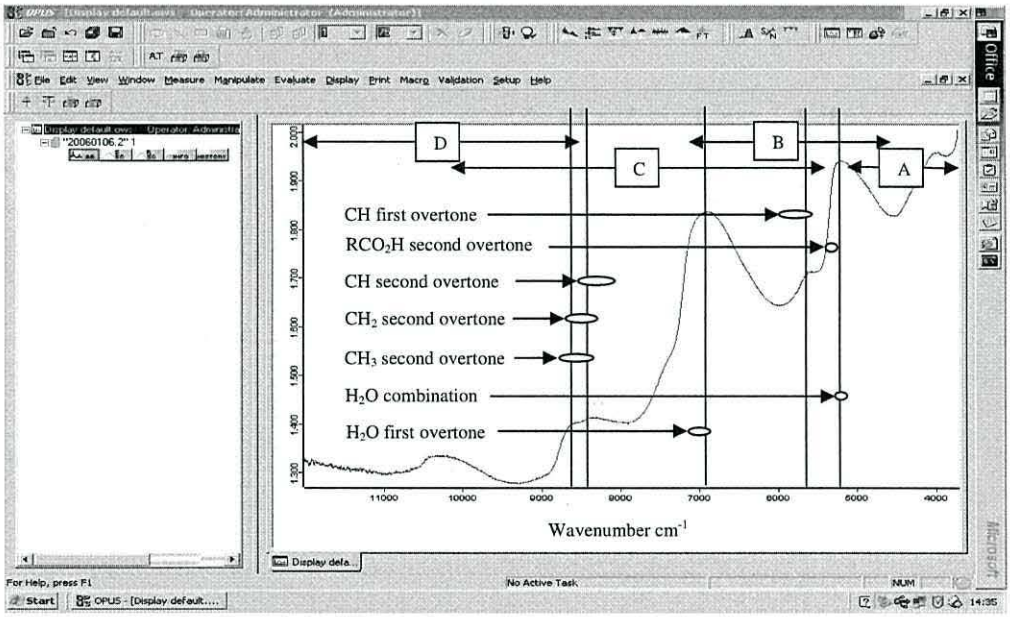

Figure 5.8. Single spectrum, from January 6th 2006, displayed by OPUS software.

Figure 5.9 shows a three dimensional plot of wavenumbers *versus* absorbance, calculated as $\log_{10}$ 1 / (% reflection) (Blanco *et al.* 1999), with the sample numbers (from vessel 1) plotted along the Z axis in chronological order from start up through to

failure only. The plot shows a clear change in the overall shape of the spectra during failure, which occurred from *ca.* point 40 along the Z axis, particularly in terms of the scale of the absorbance peaks. The blue coloured marker on this axis represents the 12th March 2006, a date when alkalinity became too low to measure by titration and pH had fallen to below 5, *i.e.* conditions which suggested acidification and failure of that particular vessel.

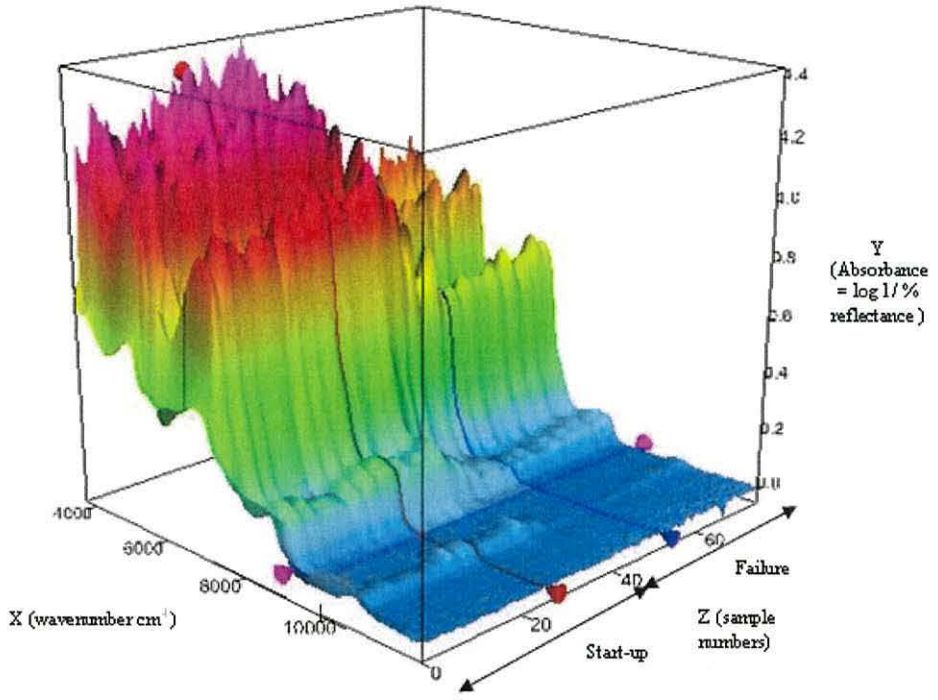

Figure 5.9. Three dimensional plot of infrared reflectance in vessel 1 during start up (Z = 0 – 40) and failure (Z > 40).

Figure 5.10 shows the first derivative values of the reflectance spectra shown in Figure 5.9. This highlights the rate of change, showing the greatest values at the point at which failure occurred (*ca.* Z = 40). This was more pronounced at *ca.* 5300 cm^{-1}, suggesting changes in concentrations of different chemical species, although as mentioned above these are impossible to fully identify without the use of powerful statistical analyses.

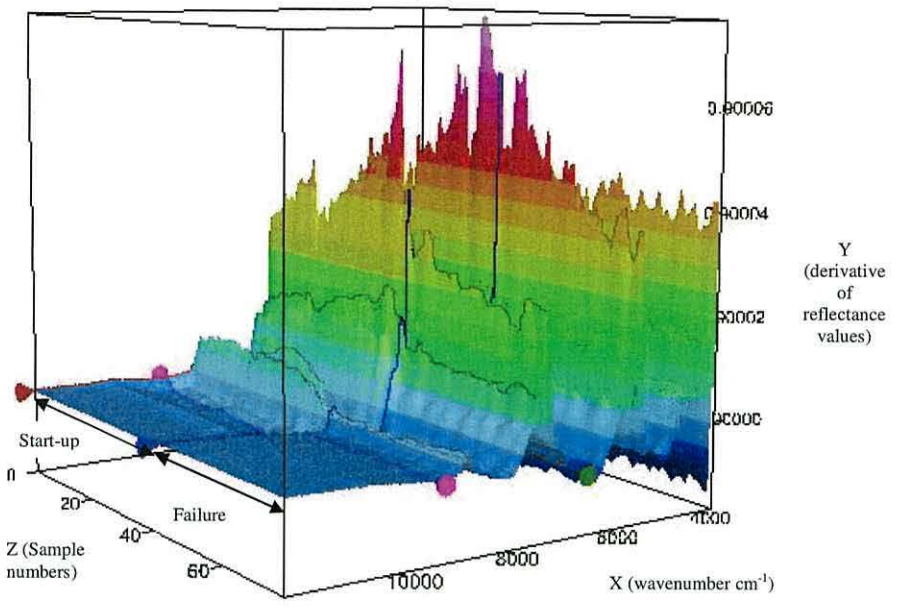

Figure 5.10. Three dimensional plot of the first derivatives of the values from vessel 1 versus wavenumber and chronologically ordered sample numbers during start up (Z = 0 – 40) and failure (Z > 40).

Figures 5.8, 5.9 and 5.10 provide only a visual representation of a change in a non-specific way, although the later two figures show that the process state of anaerobic digestion is a measurable quality. To make a full calibration with FT-NIRS requires the use of computer software to analyse the vectors, choose spectral regions of importance and to recommend spectral pre-processing such as straight line subtraction or multiplicative scattering correction to improve the calibration model (Bruker, 2004). In this work, the important spectral regions and pre-processing were then used to produce a PLS model, with R^2 (percentage of variance accounted for) and root mean square error of cross validation (RMSECV, the average error) for cross validated models and a root mean square error of prediction (RMSEP) for test set validated models, which provided a quantitative assessment of the method.

5.3.2. Optimisation of partial least squares models

Initial optimisations were conducted at a maximum rank of 10 PLS components as this was recommended by the spectrometer user manual as suitable for most applications (Bruker, 2004). All available data were used to make models. The individual vessel data model ranking, R^2 (%) and RMSECV are tabulated in Tables 5.3 to 5.6 for vessels 1 to 4, respectively, and have been sorted to list the data in descending

order of R^2 (%). It was believed best to initially sort by R^2 (%) as these are more directly comparable. The RMSECV values on the other hand are not immediately noticeable as better or worse between different parameters, for example vessel 1 alkalinity has an RMSECV of 1270 $mg.L^{-1}$, whereas vessel 1 total methane yield has an RMSECV of 0.101 $L.g^{-1}.d^{-1}$. These values are very different in their orders of magnitude yet it is not immediately obvious which is smallest in relation to the mean value. It has been suggested that a better parameter to examine than RMSECV is the RPD (residual prediction deviation) which is the ratio of the standard deviation of the reference data to the RMSECV or RMSEP, RPD values ≥ 3 were considered a good model (Williams, 2001). All parameters were checked for collinearity, a built-in option with the OPUS software which warns against R^2 values of > 0.7 between datasets. A high R^2 between data makes a true prediction of individual collinear parameters impossible (Bruker, 2004). No significant collinearity was found between any pairs of parameters used in these experiments.

The data was validated for the individual vessels using cross validation. This validation removed one (random) sample and built the calibration model with the other samples, then checked the omitted sample against the model. The process then repeated itself using a different omitted sample until all samples had been omitted and validated against the others. This process is slow and is better suited to smaller sample sets such as the individual vessel data.

Table 5.3. NIR prediction model rank, R2 (%) and RMSECV using vessel 1 data of all parameters.

Component	Rank	R^2 (%)	RMSECV	RPD
pH	3	55.04	0.384	3.07
Organic loading rate ($g\ VS.l^{-1}.d^{-1}$)	5	37.77	0.39	2.15
Alkalinity ($mg.L^{-1}$)	3	31.60	1270	2.70
Total CH_4 production rate ($L.L^{-1}.d^{-1}$)	4	24.16	0.187	1.01
Individual vessel CH_4 yield ($L.g^{-1}.d^{-1}$)	2	23.89	0.173	0.23
VS reduction (%)	2	23.18	8.97	1.13
Total CH_4 yield ($L.g^{-1}.d^{-1}$)	2	23.16	0.101	1.39
Individual vessel CH_4 production rate ($L.L^{-1}.d^{-1}$)	4	17.86	0.327	1.28
Redox (mV)	3	15.78	53.2	2.93
CH_4 (%)	2	-0.57	11.3	1.72
Hydrogen (ppm)	1	-6.15	357	2.71
Conductivity ($mS\ cm^{-1}$)	1	-7.17	0.407	6.61

Table 5.4. NIR prediction model rank, R2 (%) and RMSECV using vessel 2 data of all parameters.

Component	Rank	R^2 (%)	RMSECV	RPD
pH	3	47.55	0.694	1.52
CH_4 (%)	4	37.80	9.52	2.01
Alkalinity ($mg.L^{-1}$)	4	32.64	2190	1.39
Total CH_4 production rate ($L.L^{-1}.d^{-1}$)	4	28.87	0.201	0.95
Organic loading rate ($g\ VS.L^{-1}.d^{-1}$)	2	25.57	0.645	1.30
Hydrogen (ppm)	4	24.14	887	1.33
Redox (mV)	10	20.91	117	1.31
VS reduction (%)	2	15.91	9.01	1.12
Individual vessel CH_4 yield ($L.g^{-1}.d^{-1}$)	2	14.76	0.0401	1.25
Total CH_4 yield ($L.g^{-1}.d^{-1}$)	3	14.36	0.132	1.06
Conductivity ($mS\ cm^{-1}$)	4	8.08	2.25	1.08
Individual vessel CH_4 production rate ($L.L^{-1}.d^{-1}$)	3	4.64	0.41	0.68

Table 5.5. NIR prediction model rank, R2 (%) and RMSECV using vessel 3 data of all parameters.

Component	Rank	R^2 (%)	RMSECV	RPD
Alkalinity ($mg.L^{-1}$)	3	31.60	1270	2.06
pH	4	20.33	0.864	1.28
Redox (mV)	4	12.35	103	1.19
Individual vessel CH_4 production rate ($L.L^{-1}.d^{-1}$)	4	10.57	0.342	0.49
VS reduction (%)	2	8.87	9.16	1.10
Conductivity ($mS\ cm^{-1}$)	2	8.46	1.95	1.17
Total CH_4 production rate ($L.L^{-1}.d^{-1}$)	4	7.65	0.207	0.19
CH_4 (%)	3	5.04	11.7	0.92
Individual vessel CH_4 yield ($L.g^{-1}.d^{-1}$)	2	4.30	0.194	0.15
Total CH_4 yield ($L.g^{-1}.d^{-1}$)	2	3.36	0.113	1.24
Organic loading rate ($g\ VS.L^{-1}.d^{-1}$)	2	1.47	0.743	1.13
Hydrogen (ppm)	1	-3.72	1040	1.15

Table 5.6. NIR prediction model rank, R2 (%) and RMSECV using vessel 4 data of all parameters.

Component	Rank	R^2 (%)	RMSECV	RPD
Individual vessel CH_4 yield ($L.g^{-1}.d^{-1}$)	2	18.19	0.179	0.17
Total CH_4 yield ($L.g^{-1}.d^{-1}$)	2	14.59	0.107	1.31
Alkalinity ($mg.L^{-1}$)	3	13.28	1960	1.23
CH_4 (%)	1	-1.30	12.2	1.38
Organic loading rate ($g\ VS.L^{-1}.d^{-1}$)	2	7.47	0.72	1.17
Individual vessel CH_4 production rate ($L.L^{-1}.d^{-1}$)	2	3.67	0.355	0.54
Total CH_4 production rate ($L.L^{-1}.d^{-1}$)	1	3.23	0.212	0.90
Hydrogen (ppm)	1	-4.28	1040	1.20
VS reduction (%)	1	-6.96	9.95	1.02

The individual vessel models show that pH and alkalinity are consistently the best predicted parameters from those available, with R^2 (%) of between 20.33 to 55.04 % and 13.28 to 32.64 % respectively. This is important in that although measurement of pH is better by a simple probe, both in terms of expense and degree of error (minimum pH RMSECV is 0.38 units, an error easily bettered by a probe), alkalinity measurement had already been found to be a key parameter in predicting the process state in Chapter 3 and was used as a predicted parameter by the software sensor in Chapter 4. However, the maximum alkalinity R^2 (%) of 32.64 % and 31.60 % for vessels 1 and 3 were very low. These were accompanied by large RMSECV values of 2190 $mg.L^{-1}$ for vessel 2, although the RMSECV value of both vessels 1 and 3 were smaller at 1270 $mg.L^{-1}$. Other parameters were not of a consistently high R^2 (%) or low RMSEP to be considered useful from the individual vessel data, and were also not singled out as particularly useful parameters for monitoring of the process in Chapter 3.

The combination of low R^2 (%) and fairly high RMSECV values of the individual vessel datasets led to the modelling of parameters using the much larger combined datasets of all vessels combined. This was a difficult option as there were a large number of samples, each measured in triplicate, from which to perform the optimisation procedure. The complex nature of the PLS analysis of the spectral matrices was made clear by the time taken to complete optimisation of the combined vessels data. This took approximately 10 days with a fairly modern PC computer. The optimisation using the pH, redox and conductivity data had to be performed separately as these data were only available for vessels 1 to 3. The use of a greater number of samples allowed for the use of test set validation of the calibration model. The test set validation required that all spectra be put randomly in equal numbers into either a calibration or validation set (Bruker, 2004). The calibration set was used to build the model and the validation set validated the model. The minimum number of samples required for test set validation was not stated in the operation manual supplied with the software, but the use of 237 and 316 individual samples for the combined datasets, with and without probe data respectively, was considered enough, and reduced the validation time considerably.

Examination of the larger datasets provided by the combined vessels data using a maximum rank of 10 (*i.e.* a maximum of 10 PLS vectors or factors to be used to build the calibration model) produced an alkalinity model superior to those obtained with individual vessel data, and is shown in Figure 5.11. The dark shaded data points are

considered outliers by the software, as described in section 5.2. A better model was expected compared to the individual vessel datasets, as random sampling error or variance is often reduced with a larger number of samples (Esbensen *et a.*, 2007) and this also gave a more global range of sample values and hence a better fit for the model.

The OPUS Quant optimisation software recommended that specific bands of spectra found at 9751.2 - 7498.5 cm^{-1} and 6102.2 - 4246.8 cm^{-1} were most informative. This is a very broad range of NIR spectra, which can be clearly seen by examination of the raw spectra in Figure 5.8. No spectral information is available at wavenumbers much greater than 9500 cm^{-1} or below 4000 cm^{-1}, these regions being only noise. Therefore the calibration set removed a spectral band between 6102.2 and 7498.5 cm^{-1} from the analysis, which included the large water 1st overtone peak found at *ca.* 7000 cm^{-1}. The software also suggested that spectral pre-processing was required in the form of straight line subtraction. This process subtracts a straight line from the spectrum, thus removing any tilt in the absorbance values across the range of wavenumbers due to differing energy absorbance over such a large energy range. This affects reflection too as absorbance = $\log_{10}$ 1 / reflectance %. The resulting model had an R^2 (%) of 83.70 % and a RMSEP of 1390 $mg.L^{-1}$ after test set validation. The calculated RPD was 2.92, just below the recommended minimum of 3, suggesting the RMSEP was too large.

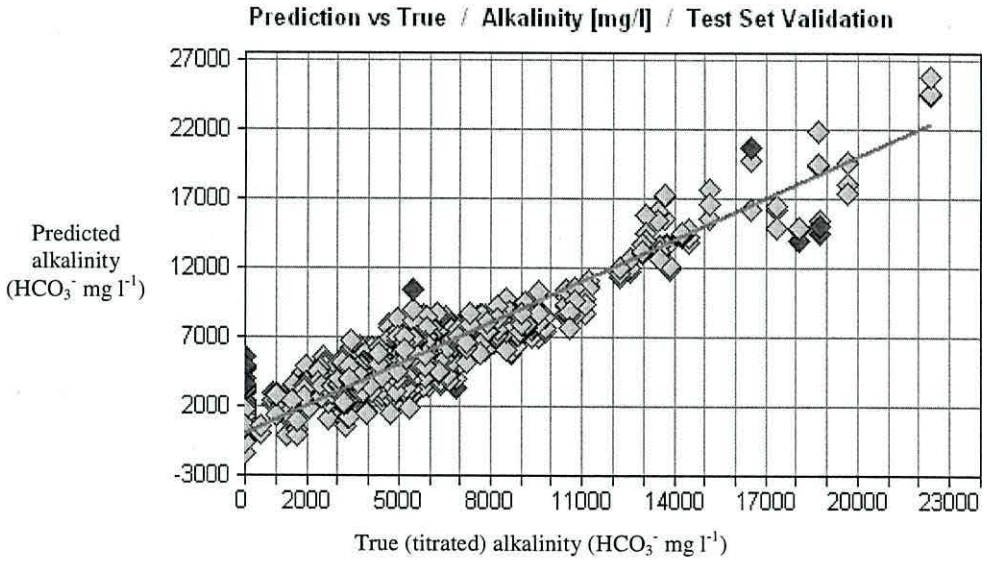

Figure 5.11. Prediction versus true graph of alkalinity optimised at rank 10.

The optimisation procedure recommended a model with an optimum rank of ten from a maximum of ten. This would suggest that there may have been a higher optimum rank and therefore a better model, so optimisation was tried again with a maximum rank

of fifteen. The results of validating the data against a test set of the data are shown in Figures 5.12 and 5.13, plotting rank against R^2 (%) and RMSEP respectively. These plots show that a rank thirteen model has both the highest R^2 (%) and the lowest RMSEP value, although this is not a huge improvement over a model with ranks as low as 8.

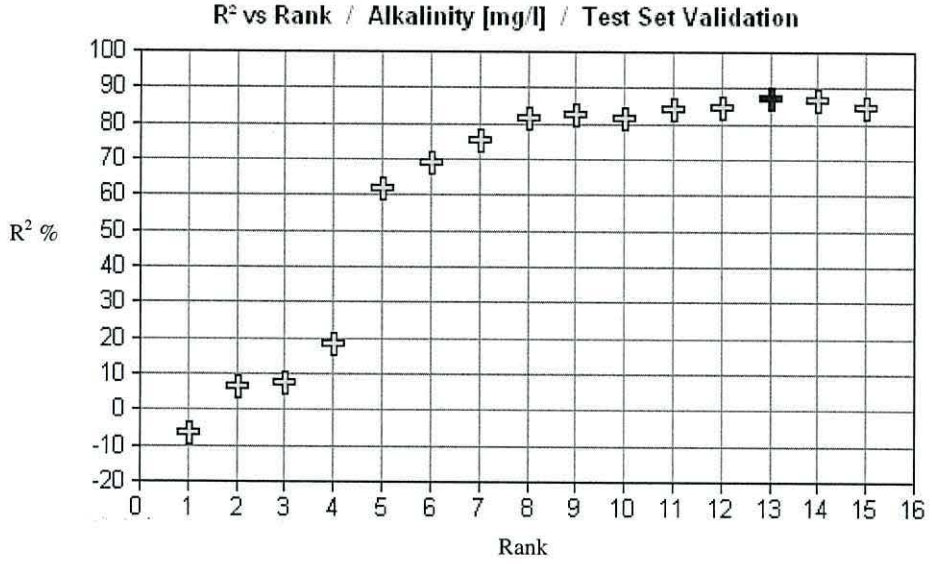

Figure 5.12. R2 (%) versus rank of all vessel data alkalinity after test set validation. The dark shaded data point shows the rank recommended by the OPUS software.

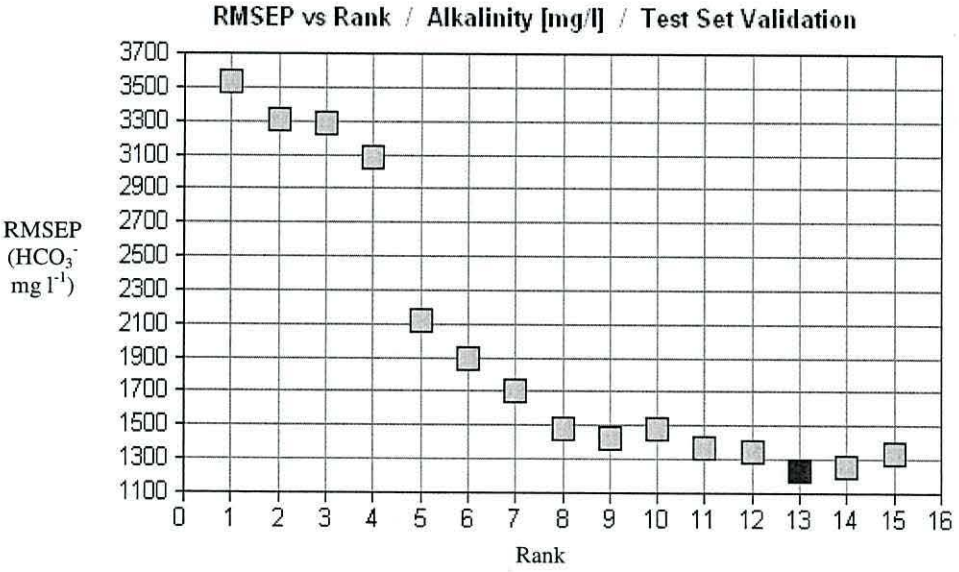

Figure 5.13. RMSEP versus rank of all vessel data alkalinity after test set validation. The dark shaded data point shows the rank recommended by the OPUS software.

The rank recommended by the software is shown as the darker shaded points in Figures 5.12 and 5.13, and it was decided to follow this recommendation. Above rank 13 the R^2 (%) can be seen to decrease (Figure 5.12) whilst RMSEP increases (Figure 5.13) suggesting overfitting of the model.

Figure 5.14 shows the prediction *versus* true plot of the rank thirteen model. The model had an improved R^2 (%) of 87 % and a lower RMSEP of 1230 $mg.L^{-1}$ with only one outlier highlighted by the software, shown in darker shading. The RPD for this model was 3.3, which was above the minimum recommended by Williams (2001), therefore the model was acceptable. The optimisation procedure that produced this model did so by only considering wavenumbers between 7502.4 and 4246.8 cm^{-1} and vector normalisation as spectral pre-processing. This was unusual as this region included both the water combination band and water 1st overtone band at *ca.* 5200 and 7000 cm^{-1}, respectively. Normally, such large absorbance bands are avoided (Bruker 2004). Vector normalisation calculates the average intensity value of the chosen spectra and subtracts this value from the entire section(s) of the spectrum. The sum of the squared intensities is then calculated and the spectrum is divided by the square root of this sum (Bruker, 2004). This method can be of use when samples are of a different thickness or depth. It should be noted that in this experiment each sample volume and therefore depth was measured precisely. However, the nature of reflectance measurement means that path lengths can vary due to varying particle size and nature scattering protons differently.

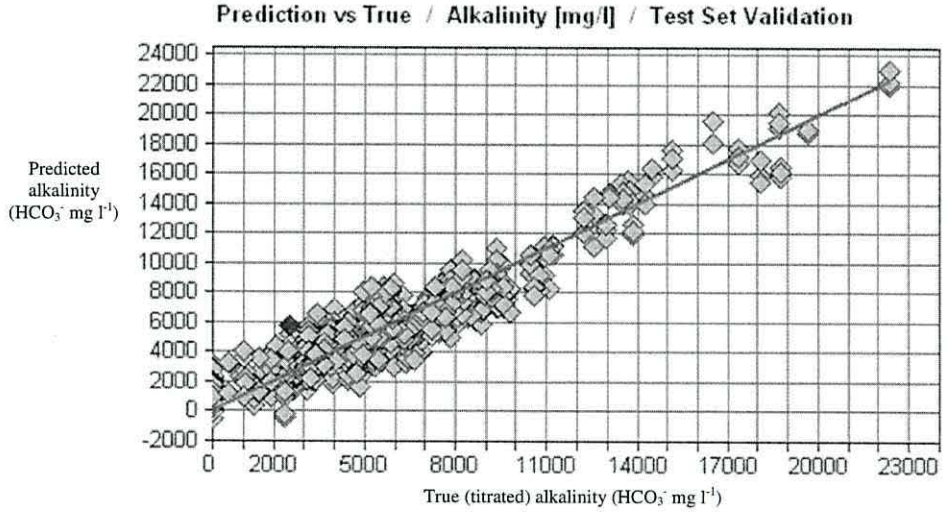

Figure 5.14. Prediction versus true graph of alkalinity optimised at rank 13.

Table 5.7. NIR prediction model rank, R2 (%) and RMSEP using all vessels data of all parameters.

Component	Rank	R^2 (%)	RMSEP	RPD
Alkalinity ($mg.L^{-1}$)	13	87.02	1.23 E+003	3.3
pH	6	62.96	0.674	1.69
Redox (mV)	7	59.34	93.9	1.58
Methane (%)	7	52.3	9.21	.071
Conductivity ($mS\ cm^{-1}$)	11	36.68	1.96	1.29
Total CH_4 production rate ($L.L^{-1}.d^{-1}$)	7	36.33	0.172	1.1
Total CH_4 yield ($L.g^{-1}.d^{-1}$)	7	21.59	0.114	1.23
Individual vessel CH_4 yield ($L.g^{-1}.d^{-1}$)	2	14.76	0.0401	0.1
VS reduction (%)	3	8.322	10.9	0.93
Individual vessel CH_4 production rate ($L.L^{-1}.d^{-1}$)	3	4.635	0.41	0.82
Hydrogen (ppm)	1	4.1	1.07E+003	1.17

Although the R^2 (%) for both rank 10 and rank 13 models are quite high, the RMSEP values are too large to accurately predict alkalinity for control purposes. Experimental work in Chapter 3 found that optimum alkalinity was *ca.* 3600 to 4600 $mg.L^{-1}$. Attempting to maintain this optimum with a possible difference between predicted and observed alkalinity of +/- 1200 $mg.L^{-1}$ could lead to a failed digester, whilst setting the alkalinity threshold higher would result in non-optimal operation.

The rank 15 (maximum) models for all other data are tabulated in Table 5.7. This again shows pH to be a reasonably well predicted parameter, as was the case with the individual vessel data. All parameters are clearly improved over those obtained from the individual vessel data shown in Tables 5.3 to 5.6. However, apart from alkalinity, these models were of poor fit to the data (R^2 (%) < 80 %, RPD < 3) and were therefore of limited value for prediction of process stability and were not examined further.

5.3.3. Validation of the models against new data

The rank ten and rank thirteen models were validated further with data collected after the models were constructed. The sources of these data were the two stage digesters with or without biomass support media, the construction of which was described in Chapter 2. The results are shown in Figure 5.15 for the digester with support media and Figure 5.16 for the digester without support media.

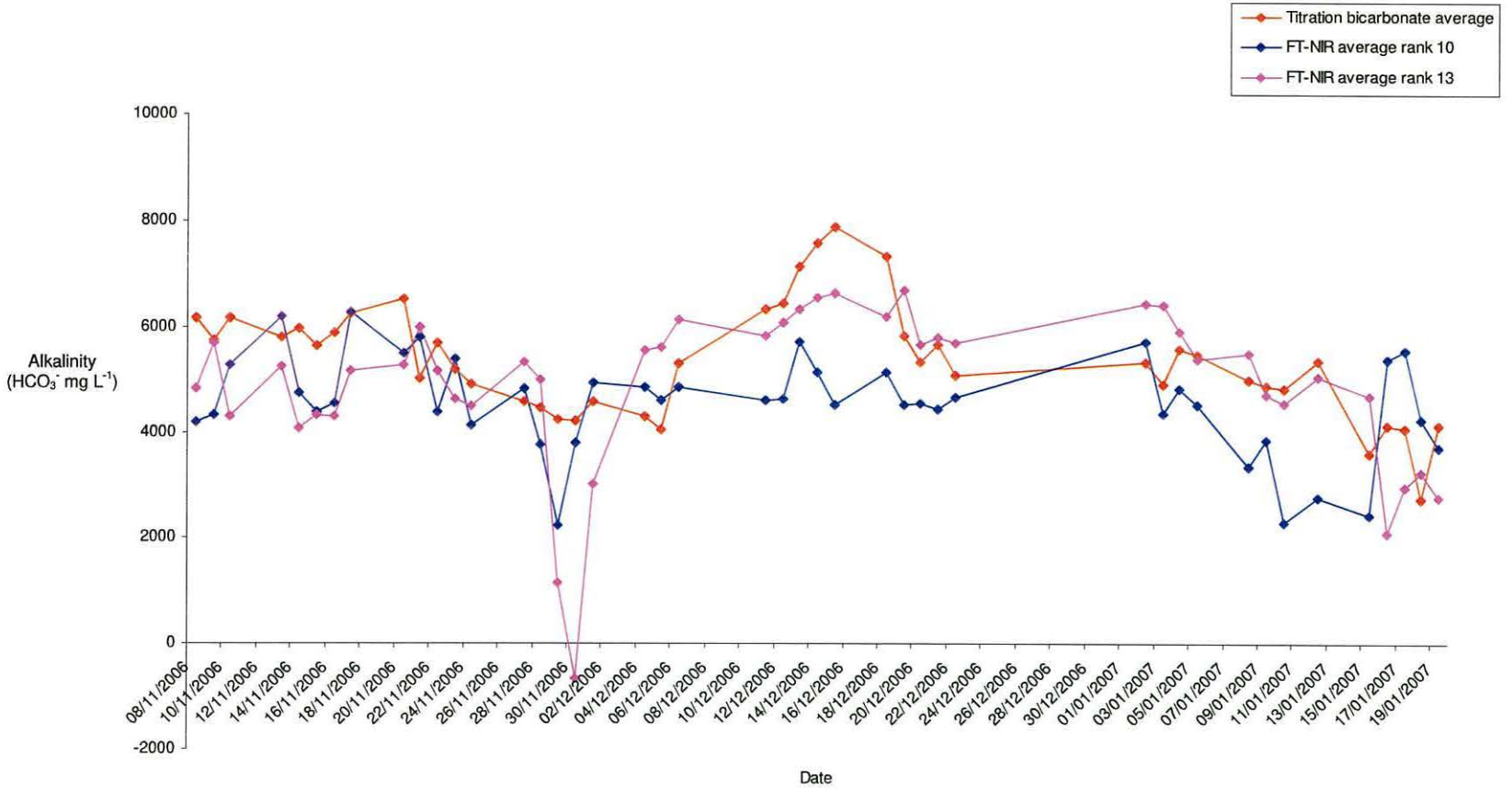

Figure 5.15. Alkalinity predicted by rank 10 and rank 13 models compared to titrated alkalinity of vessel 2 of a two-stage digester with support media.

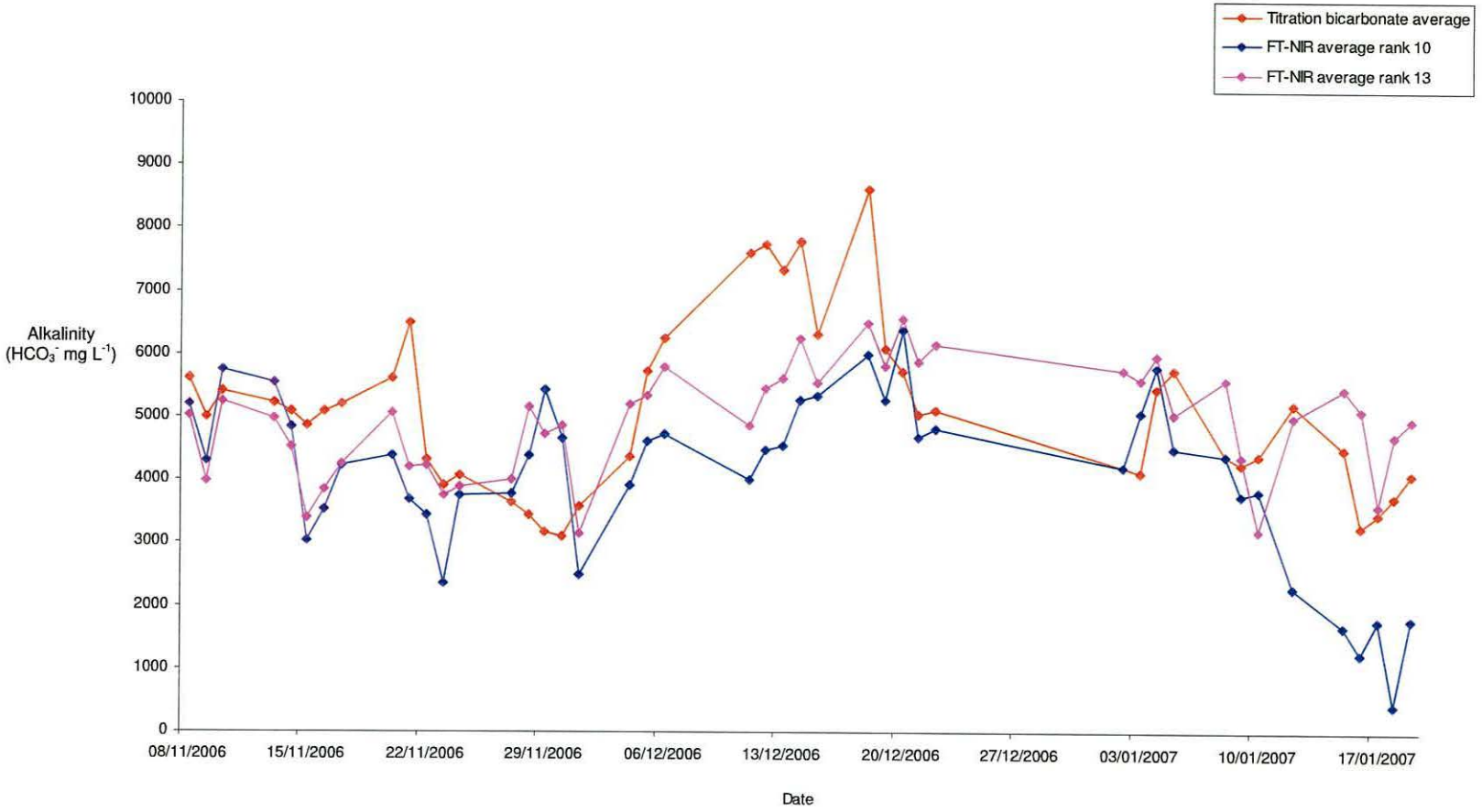

Figure 5.16. Alkalinity predicted by rank 10 and 13 models compared to titrated alkalinity of vessel 2 of a two-stage digester without support media.

All samples were again measured in triplicate, with standard deviations between replicates of less than 10 % of the mean. The NIRS and titration data were correlated against each other as equation 4.8.

The best correlation of the alkalinity new sample validation data set against the rank 13 results was $r = 0.56$ ($p < 0.001$) for the digester with support, whereas the digester without support correlation was only $r = 0.49$ ($p < 0.001$). The three low values at the end of November and beginning of December for the digester with support media coincided with a blockage problem within the system. The samples taken on these days were very pale in colour and appeared to be low in total solids by visual examination of sedimentation after analysis. Removing these three data points increases the rank 13 correlation slightly to $r^2 = 0.565$ ($p < 0.001$).

The rank 13 NIRS model validation data were also regressed as shown in Figures 5.17, 5.18 and 5.19 for the digester with support media, the same data with the three outliers mentioned above removed and for the digester without support media respectively.

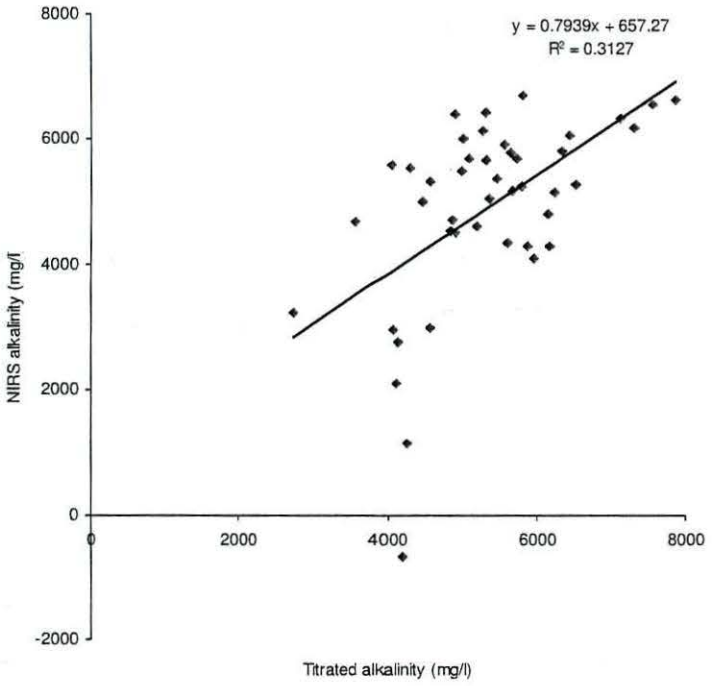

Figure 5.17. Regression of NIRS predicted alkalinity against titrated alkalinity for digester with support media.

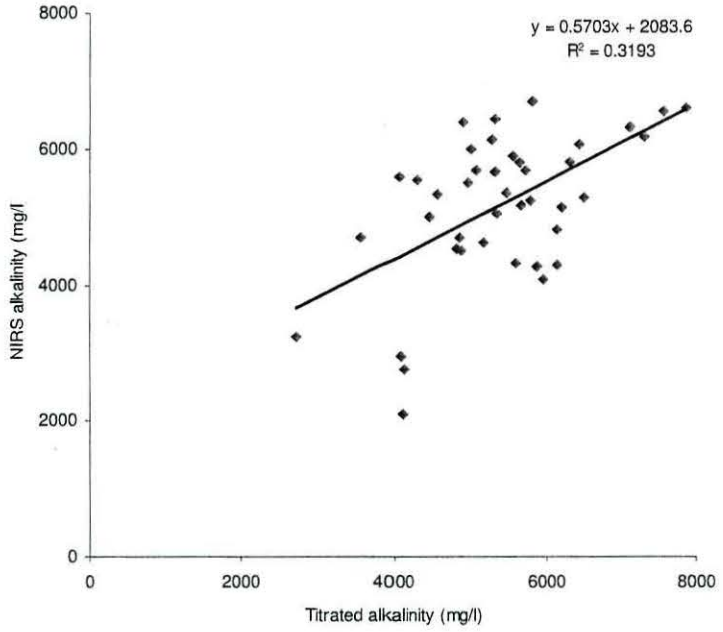

Figure 5.18. Regression of NIRS predicted alkalinity against titrated alkalinity for digester with support media with outliers removed.

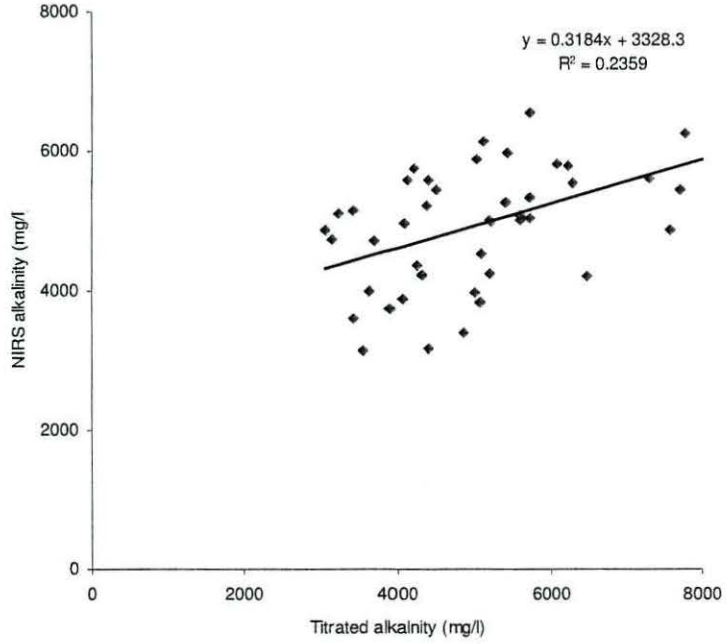

Figure 5.19. Regression of NIRS predicted alkalinity against titrated alkalinity for digester without support media.

The digester with support media had better R^2 values, with R^2 = 0.3127 and a slight improvement to R^2 = 0.3193 with the outliers removed. The digester without support media had an R^2 value of only 0.2359. The regression lines also required slope and offset corrections to achieve these results, as displayed on the relevant Figure. The validation regressions were therefore of poorer quality than the correlations between titrated and NIRS predicted data. However, the validation dataset had limited titrated alkalinity values when compared to the original calibration dataset and it had been shown during the calibration that the RMSEP was relatively high at 1230 $mg.L^{-1}$.

A validation method including MDL (method detection limit), LOQ (limit of quantification) and PQL (practical quantification limit) tests to produce a reliable method is also required, and the ability to transfer this method to different laboratories and instruments is also desirable. Transfer is relatively easy because the Fourier Transform function eliminates instrument effect on the spectra. The validation of a measurement method for use with anaerobic digesters is more complicated than that found in, say, the manufacturing industry, as to make a truly universal monitoring device for use with any anaerobic digester would also require validation using samples from many different digesters. The highly variable feedstocks used in different and indeed a single digester would inevitably have some effect on measurement derived from a PLS model. Validation methods necessary for a new laboratory method are recommended by the International Union of Pure and Applied Chemistry (Thompson *et al.*, 2002). The MDL is the minimum concentration which can be analysed with 99 % confidence that it is greater than zero. The LOQ is often taken as a fixed multiple (2 is typical) of the detection limit, although it is often believed that useful information can be found below this limit. The PQL, which is typically 3 to 5 times the MDL, is an accurate measurement which is routinely achievable in laboratories. A range of validation samples near the limit of detection would be required in future experiments to find MDL, LOQ and PQL. These validation methods will be affected by the relatively large RMSEP of 1230 $mg.L^{-1}$ found in the calibration set. Thus, although the calibration set included several samples at 0 $mg.L^{-1}$, the limit of detection can only be considered reasonably accurate to +/- the RMSEP.

Intermediate precision and reproducibility tests of the method were not possible due to a lack of alternative equipment and laboratory facilities. However, manufacturers of modern FT-NIR spectrometers claim that the instruments are built with sufficient

accuracy to reproduce measurements and calibrations made on different machines (ABB, 2004).

A validation of the method was also limited by the range of alkalinity values available in the post method development samples. These were in the range of *ca.* 3000 to 9000 $mg.L^{-1}$, and therefore did not cover the range of calibration set samples used to create the model, which were between 0 and 23000 $mg.L^{-1}$. However, the new dataset covered a range of alkalinities deemed more than adequate for monitoring of anaerobic digesters for prevention of failure purposes, the cut-off point for alkalinity having been established in Chapter 3 as *ca.* 3600 $mg.L^{-1}$.

There was some concern with the effect of sedimentation of samples during analysis. It was impossible to guarantee that solid particles in the samples were consistently maintained in suspension during analysis, despite shaking of the sample vials prior to analysis. The source NIR beam used with the Bruker Vector 22/N instrument passed upwards *via* a mirror, with the reflected beam passing to a mirror adjacent to the source mirror. This was therefore likely to be subject to interference from settled solids. A sampling method which provided a more representative sample of the digestate was required but difficult to implement on the instrument used. Since these experiments have taken place, work has been published involving the in-line monitoring of anaerobic digestion by FT-NIRS (Holm-Nielsen *et al.*, 2008) using a method for the provision of representative samples. Levels of VFA in digestate were measured with *ca.* 90 % of variance accounted for with FT-NIRS transflection measurements in a sample loop taken semi-continuously from three digesters. The transflection method showed potential for fitting to existing biogas plants, although the short (3 mm or less) path length required for transmission or transflection methods may prove to be too narrow for digestate that has not been prepared in some way. Some sample preparation such as filtering or centrifugation may have improved the results obtained in this chapter, as these techniques would both have removed solid material that was prone to settling. It was decided not to do either of these as any sample preparation would calibrate the instrument for in-line or at-line measurements (*via* a sample loop or a laboratory test conducted separately, respectively), rather than the on-line technique this work aimed to ultimately achieve. It is understood that the methods of sampling and analysis used in this chapter are indeed at-line, but it was hoped that this would lead to an on-line system.

5.3.4. Future research

Future work would involve dealing with the problem of representative sample measurement in terms of both sample collection and maintaining homogeneity during measurement. Rotating sample holding devices are available for Bruker machines amongst others, but such a device was not fitted to the machine used. This would reduce the settling of solid particles and would therefore be likely to produce a better result. Many instruments are now available with an optional reflectance probe constructed from high quality stainless steel with scratch-resistant quartz or sapphire optics (Bruker Matrix-F, Q-Interline Flex). These probes are connected to the spectrometer by optical fibre cables of many metres in length, allowing safe isolation of the instrument from hazardous conditions such as liquid spillage or vibration which may be found near the tank. Such probes can easily be located in an aperture fitted to the side of a digester, with powered gas-tight removal-replacement apparatus for easy cleaning and maintenance. This arrangement provides a representative sample of the digester contents, similar to the sample loop method mentioned in section 5.3.3, but with no tubing or small path length to cause problems with blockages the method is likely to be more reliable.

Quantitative analysis of components within the chosen matrix is not the only possible use for FT-NIRS. Certain types of software, such as Thermo PLSplus IQ (Thermo, 2005) offer discriminate analysis of spectral data. This allows samples to be classified into categories and is sometimes referred to as pattern recognition. This is of interest here as it was immediately noticeable from the three dimensional spectral plots in Figures 5.3 and 5.4 that there was a change in the basic spectral shape when the system failed. If the discriminate analysis is trained on a set of samples which can be classified into various 'good' or 'bad' states of the process, the software can detect when a change from one state to another is occurring. Thus, the software can produce a relevant output to a process control system. In addition, the use of NIRS as one of multiple outputs that could be used in a fuzzy logic system may provide an alternative means of quality data for process control. These outputs could include the individual pH, redox and conductivity probes or the software sensor based on these on-line measurements as described in Chapter 4. The addition of on-line gas analysis could also be added to this system.

5.4. Conclusions

This chapter demonstrated that near infrared reflectance spectroscopy can be used to measure alkalinity and therefore be a means of quantifying the state of an AD process. The PLS analysis produced a model requiring 13 factors. This number of factors suggests that the data is complex. The PLS model had an R^2 (%) value of 87 % and a RMSEP of 1230 $mg.L^{-1}$. The model was not subject to overfitting as the number of samples used exceeded the recommended minimum of twenty per PLS factor. The R^2 (%) value is indicative of a 'good' model according to the criteria chosen in Section 5.1.2. Although the model was complex, this was not a problem as further investigations with more data samples demonstrated. The calculation of the alkalinity from the samples took a fraction of a second in addition to the scanning. The instrument scanned triplicate samples with reference scans before each in a total time of six minutes. This is a very short time in relation to the overall process and was considered practically instantaneous.

Overload is only one potential problem which may lead to failure of the anaerobic digestion process; toxicity can also be a problem. It must be noted that the NIRS method described in this chapter is only capable of detecting overload situations and not toxicity.

6 Investigation into the effect of mixing frequency on anaerobic digesters with biomass support media

6.1. Introduction

6.1.1. Overview

There are many reasons for mixing an anaerobic digester. For instance, mixing the fresh feedstock with the partially digested feedstock will subject the fresh material to active microbial biomass. This is important for inoculation and will also increase the rate of microbial action. Mixing can dilute high levels of toxins, for example metals (Wong and Cheung, 1995) and inhibitory substances such as high levels of volatile fatty acids present in the feedstock by spreading them throughout the reactor whilst also ensuring homogeneous temperature within the reactor. In addition, larger particles in the feedstock are broken up by mixing, creating a greater surface area for hydrolytic bacteria to work on. It follows that biogas is also released more efficiently when the medium is stirred, as bubbles can sometimes stick to granules and flocs, or may become trapped in viscous digestates.

Mixing also prevents the build-up of floating scum layers and sediments of heavy material. The floating scum is derived largely from fibre in the feedstock and can dry out, thus becoming very difficult to remove, and it can also impede the release of biogas from the surface. With inefficient mixing, heavy portions of the feedstock, which are often refractory materials like grit, will sink to the bottom. This will gradually reduce the volume of the digester, and will damage stirring equipment if the layer is deep enough to come into contact with any moving parts. Adequate mixing will incorporate these layers into the digestible feedstock, and will therefore be expelled from the digester as part of the digestate.

There is some evidence to suggest that mixing by hydrodynamic forces is important in the formation of biofilms and granules in that more compact, stable and denser biofilms and granules were formed in reactors that were subjected to higher shear forces (Liu and Tay, 2002).

An acceleration of suspended chemical oxygen demand degradation with increased agitation has also been reported in laboratory scale batch reactors containing 3 cm polyurethane foam particles as a support media for bacterial growth (Pinho *et al.*, 2004). This increase was attributed to shearing of particulate matter by the mixing action and the resulting increased solubilisation of suspended particles. They also found an overall increase in organic matter consumption with agitator velocities up to 900

rpm. It was stated that it may have been possible that the support media reduced the possibility of disruption of the syntrophic communities that were important to methane production, whilst the agitation provided a ready supply of volatile fatty acids for conversion into acetate in addition to the shear effect.

Although the benefits of mixing which are listed above are valid, there is also evidence that excessive mixing has a detrimental effect on performance. For instance, if a mixing system completely homogenises the entire contents of a reactor, then there will be a small portion of fresh feedstock that has exited the digester in somewhat less time than the average hydraulic retention time. This compares to a plug flow reactor which has a very narrow exit age distribution, as was discussed in Chapter 2.

In experiments using batch reactors for the anaerobic digestion of cattle manure, non-mixing was found to produce higher gas yields than mixing (Ong *et al.*, 2002). It was found that the mixed reactors suffered from a loss of volatile solids, and a decrease in extracellular polymeric substances (EPS). These are a major component of the granule matrix material, assisting aggregation and adhesion to support media. Low quantities of EPS are considered to be an indicator of reduced agglomeration of biomass. This is important as agglomerated cells settle well and are therefore less susceptible to washout from the digester.

Stroot *et al.* (2001) reported an experiment where four reactors were started on a continuous mixing regime on a shaker table and fed municipal solid waste. The reactors were switched to minimal mixing (hand shaken for two minutes per day) after two weeks. Minimal mixing showed an improvement in reactor performance over continuous mixing. In a second experiment, six reactors were set up and results suggested that continuous mixing led to instability at high organic loading rates, whereas minimal mixing did not (Stroot *et al.*, 2001). It was also found that an unstable continuously-mixed reactor could be stabilised when changed to minimal mixing. It was suggested that this may have been because the high levels of volatile fatty acids which often characterise an unstable digester did not immediately come into contact with the methanogens when minimally mixed, allowing time to build up a suitable population able to degrade excess substrates.

In a reactor operating at a high organic loading rate and intensive mixing, acidification and subsequent failure occurred (Vavilin and Angelidaki, 2005). These workers came to the conclusion that intensive mixing prevented methanogenic zones becoming established. Thus there were areas within the reactor where methanogenesis

dominated, protecting methanogens from acid inhibition. The authors also found large irregular cocci type cells at minimal mixing rates and many dead cells after high mixing rates, when analysed by fluorescence *in-situ* hybridisation (FISH).

Mixing also affects hydrogen partial pressure which must be at a low level for some of the reactions in an anaerobic digester to be thermodynamically feasible. To ensure a low hydrogen partial pressure, the diffusion distance between hydrogen producers such as propionate oxidising bacteria and hydrogenotrophic methanogens must be small. It has been suggested that propionate oxidisers and methanogens live in close proximity in granules (de Bok *et al.*, 2004). There is evidence that excessive agitation may disrupt the micro colonies in these densely-packed granules, thus inhibiting the oxidation of volatile fatty acids (McMahon *et al.*, 2001).

Further evidence of the detrimental effects of mixing is that excessive flow of feedstock or gas in upflow anaerobic sludge blanket reactors has been shown to produce sufficient shear forces to detach biomass from the support media, resulting in washout of the organisms (Smith *et al.*, 1996). Schink (1992) stated that the spatial juxtaposition of syntrophic organisms is just as important as a good substrate uptake system, but also that a minimal amount of mixing is required to assist cell clones in separation after replication, enabling close contact with their syntrophic partners.

It would seem from the evidence above that only minimal agitation is beneficial unless support media is used, and that a more gentle method of mixing should be better than a more aggressive one.

6.1.2. Types of mixing equipment used in anaerobic digesters

Four types of mixing apparatus typically used in anaerobic digesters are illustrated in Figure 6.1. The vertical paddle stirrer (Figure 6.1a) is a slow-rotating device that homogenises the digester contents with little shear force. The paddle can be subject to a build-up of microbial growth, increasing the weight and therefore the energy required for turning, or even causing damage.

Recycling biogas for mixing by bubbling from the bottom of the reactor (Figure 6.1b) is a method used in many types of anaerobic digesters. These have the maintenance advantage of having no moving parts inside the reactor, although they can sometimes be subject to blockage of the gas jets. This type of agitation is gentle and shear forces are minimal, reducing the damage to flocs of bacterial biomass. This

method of mixing was chosen for use in these experiments partly for these reasons and partly because it requires no gas-tight rotational seal.

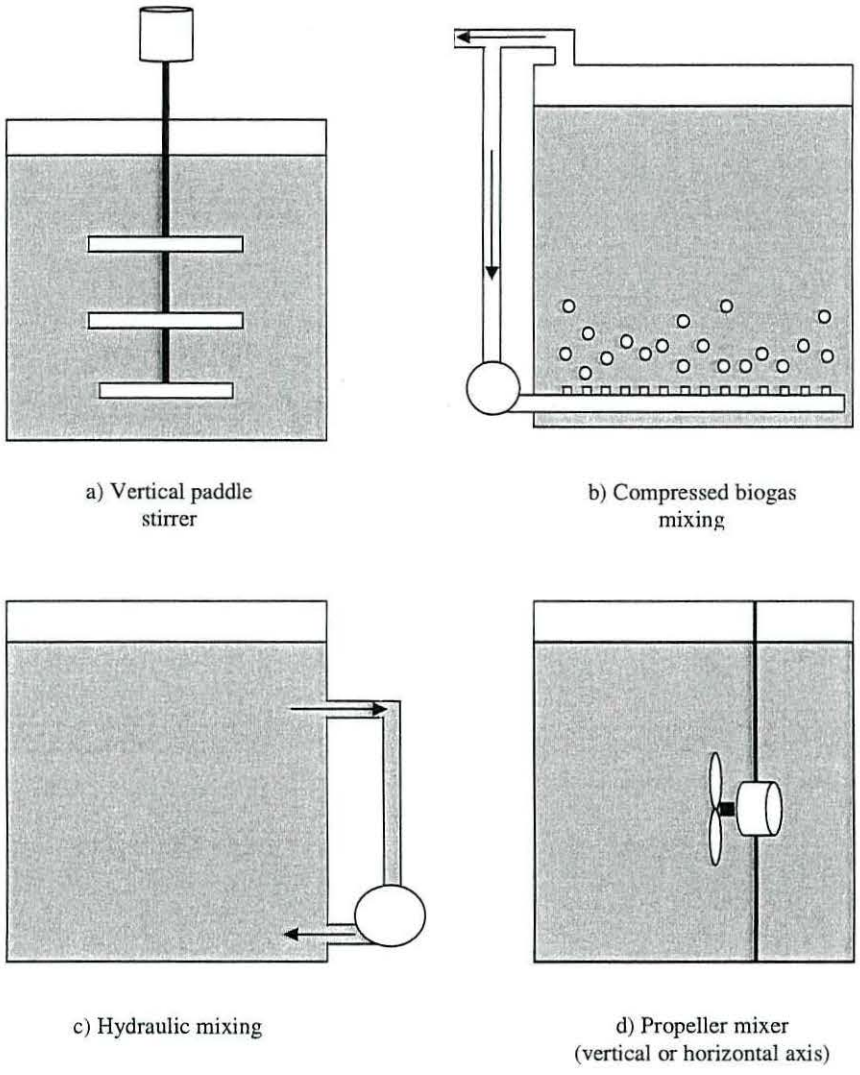

Figure 6.1. Types of mixers used in anaerobic digestion.

Hydraulic mixing (Figure 6.1c) involves drawing out the actively degrading feedstock and pumping it back in. This can cause damage to bacterial flocs from the shear forces generated by the fluid flow if the velocity is high enough, but most damage is by the pump itself. For example, many pumps used in slurry handling are of the centrifugal-type that operate at high speed. Propeller mixing (Figure 6.1d) is also common in anaerobic digestion. The rate can be fast or slow, with some degree of shear forces involved depending on speed.

6.1.3. Microbial aggregation

Microbial aggregates consist of micro-organisms in association with each other and varying quantities of extracellular polymeric substances. There are two main types of aggregation: firstly, granules or flocs and secondly biofilms. The size of granules and flocks in anaerobic digesters can vary in the region of 0.25 to 3.75 mm in diameter (Huang *et al.*, 2006), and have been shown in different studies to be ellipsoidal (Baloch *et al.*, 2006) or symmetrical (Wimpenny, 2000) and show spatial differentiation and metabolic co-operation. The second type of microbial aggregate is a biofilm, where an aggregate forms on a phase interface, most commonly between a solid and a liquid (Wimpenny, 2000).

The events in the formation and subsequent detachment of a microbial biofilm are described below and shown in Figure 6.2. Initially, biofilms are generally thought to start with a covering of organic molecules (the conditioning film) onto a previously clean surface (Figure 6.2a), which can occur within a few seconds of exposure. Diffusional mass transfer is greater for macromolecules than microbial cells as they are much smaller in size (Van der Mei *et al.*, 1994), so it is unlikely that a cell will contact a surface which is not already coated with a conditioning film. The substratum surface properties dictate the composition and conformation of the conditioning film. For example, mucin molecules have been shown to adsorb with their carbohydrate end to hydrophilic substrata, and with their protein end to hydrophobic substrata (Busscher and Van der Mei, 2000).

Microbial mass transport (Figure 6.2b) has been reported as being important in biofilm formation and can be performed by a number of mechanisms including diffusion, convection and sedimentation (Van der Mei *et al.*, 1994). It has been shown that convective mass transport is greater when towards a surface than when parallel to a surface (Yang *et al.*, 1999).

Microbes initially adhere (Figure 6.2c) by non-specific attractive Lifshitz-van der Waals forces when cells are within several hundred nanometres of the conditioning film (Rutter and Vincent, 1980), adhering by physisorption. Irreversible adhesion or anchoring (Figure 6.2d) occurs at distances of less than 5 nm when adhesion receptors become effective (Busscher *et al.*, 1992).

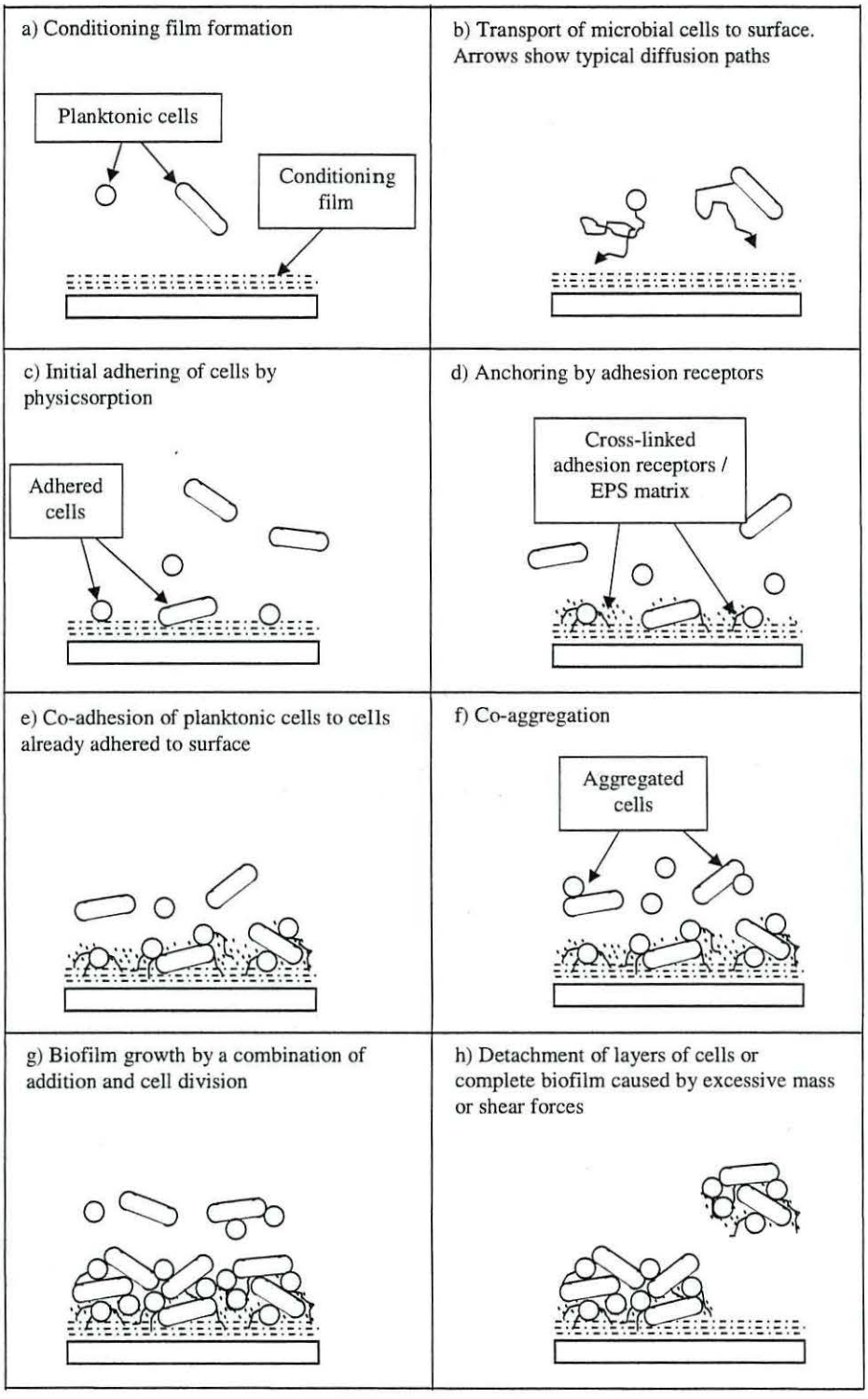

Figure 6.2. Processes involved in biofilm formation, redrawn from Busscher and Van der Mei (2000).

Co-adhesion (Figure 6.2e) is the interaction of a planktonic and an adhering organism (Bos *et al.*, 1995). This can create a niche in which growth of both partners is optimal (Bradshaw *et al.*, 1994). By comparison, co-aggregation (Figure 6.2f) is the interaction between two planktonic cells. Such an event is less likely than co-adhesion due to the low densities of the microorganisms. The irreversibly adhering organisms are free to grow and increase the thickness of the biofilm (Figure 6.2g). The thickness of the biofilm depends largely on shear forces and the strength of the EPS matrix, as it is now subject to detachment (Figure 6.2h). In an anaerobic digester, this is likely to be a result of hydrodynamic forces from mixing or the ingress of fresh material. A weakness in the internal cohesivity of the biofilm could cause partial detachment of outer layers, whereas a weakness in the biofilm to substratum bonding could detach the whole biofilm.

6.1.4. Biomass support media in anaerobic digestion

To encourage the formation of a biofilm and to increase the surface area available for biofilm bonding, biomass support media has been widely used in anaerobic digestion, with reported improvements in start-up time, methane production and COD removal of the effluent (Andersson and Bjornsson, 2002; Arnaiz *et al.*, 2003; Bertin *et al.*, 2004; Buchholz *et al.*, 1992). The biomass support medium used in these experiments was reticulated polyurethane foam. This material has been used as a support medium in anaerobic filters (Lima *et al.*, 2005), fixed bed reactors (Britz and Van Der Merwe, 1993; Yang *et al.*, 2004a) and fluidised bed reactors (Damasceno *et al.*, 2007; Yang *et al.*, 2004b), and has been found to quickly develop highly-retained biomass concentrations (Fukuzaki *et al.*, 1990; Fynn and Whitmore, 1982; Gijzen *et al.*, 1988). Upon examination of biofilms grown in brewery waste water, the biofilms formed on polyurethane foam were up to 2 mm thicker than those formed on ceramic foam and glass sponge media (Stadlbauer *et al.*, 1994).

The use of polyurethane foam in anaerobic digesters is not without problems. For instance, experiments using support media in anaerobic digestion have largely been conducted with artificial substrates or highly soluble substrates that are low in total solids (Britz and Van Der Merwe, 1993; Fynn and Whitmore, 1982; Zellner *et al.*, 1991). This is principally because the substrate passes through the media, whilst a high percentage of suspended solids or large particles would be expected to quickly block the pores (Dugba and Zhang, 1999). However, low-solids substrates such as waste waters or

fatty acid solutions also suffer as the formation of biofilms have been reported to impede flow through the media, leading to channelling and a gradual deterioration of performance (Gijzen and Kansiime, 1996; Lima *et al.*, 2005). Fynn and Whitmore (1984) reported a rapid loss of biomass from reticulated polyurethane foam when subjected to hydrodynamic forces, possibly as a result of weak bonding between the biofilm and the substrata. The loss was independent of pore size. The exact bonding mechanism of the anaerobic biofilm to the support media is unknown, but scanning electron microscopy of biomass retained within polyurethane foam has shown the development of microbial aggregates in three distinct patterns: micro-granules of 270 μm to 470 μm were found entrapped in the pores, multi cellular films were found on the inner surfaces and the support also held individual cells (Varesche *et al.*, 1997). This would suggest that the cell aggregates are partly retained by the support media by simply being trapped in the polyurethane foam matrix.

In addition, Hill and Bolte (1992) reported physical degradation of polyurethane foam leading to 98 % loss of the material during three six month runs using swine waste, and suggested the use of polypropylene felt as this did not show physical damage and had comparable bio-retentive properties. The type of foam additive used was not stated, and it is possible that an ester additive rather than a polyether additive was used. Polyurethane foams with an ester additive have good solvent resistance but are more easily hydrolysed than foams with a polyether additive (Altaf *et al.*, 2006). In a more recent study it has been shown that polyether PU foam suffered no change in weight, tensile strength or infrared signature, or any utilisation of the foam as a carbon or nitrogen source when exposed to anaerobic biological processes over a ten week period (Urgun-Demirtas *et al.*, 2007).

There are some examples of the use of biomass support media with higher total solids values. Calzada *et al.* (1984) used non-reticulated polyurethane foam packed bed reactors to treat coffee pulp juice with total solids values of 3 to 4.5 %. In addition, Demirer and Chen (2005) used a floating layer of commercially available support medium to treat cattle manure at 9.87 % volatile solids.

This chapter investigates the effect of the frequency of mixing by biogas recycling in laboratory scale single-stage digesters and pilot scale two-stage digesters in the presence and absence of reticulated polyether polyurethane foam. A pig-feed feedstock (as described in Chapter 3) of particle size $\leq$ 2 mm at 5 % total solids was used. To avoid any potential problems arising through blockages, the feedstock was not

passed through cubes of the media, as is the case with fixed and fluidised beds and anaerobic filters, but instead was circulated by the mixing system across the surface of suspended polyurethane foam sheets. It has been shown previously that high organic loading rates can cause washout of microorganisms (Denac *et al.*, 1988), but this chapter addresses the possibility of washout due to mixing, specifically the frequency of mixing cycles at a constant input energy per second when mixers are active.

Making a decision on the pore size of the polyurethane foam was not straightforward. Fynn and Whitmore (1984) have shown that pore densities of 60 pores per linear inch (*ca.* 24 per linear cm) yielded the highest density of methanogenic organisms when compared to polyurethane foam with pore densities of 20, 30 and 45 pores per linear inch (*ca.* 8, 12 and 18 pores per linear cm respectively). Yang *et al.* (2004b) reported similar results in that they found polyurethane foam with a pore density of 20 pores per linear inch (8 per linear cm) retained more microbial biomass than polyurethane foam with a pore density of 10 pores per linear inch (4 pores per linear cm). It must be mentioned that both the above publications used synthetic feedstocks which contained no suspended solids. In this thesis, it was decided that using polyurethane foam with a pore density of 10 pores per linear inch (*ca.* 2.5 mm pore diameter) could minimise clogging by either feedstock or EPS and yet possibly still demonstrate an improved performance over a digester containing no support media.

Two of the four single-stage digesters and the methanogenic (second) stage of one of the two-stage pilot scale digesters used in this work contained reticulated polyurethane foam as a microbial biomass support media. The hypothesis was that a more frequent mixing cycle would transport materials more effectively through the digester vessels, although excessive shear forces created by mixing could be detrimental to the agglomerated colonies of microbial cells. However, it was postulated that the cells attached to the polyurethane support as biofilms would be protected to some degree from the direct mixing shear forces so that digester methane production was expected to be better at higher mixing frequencies than digesters that did not contain the support media. The digesters using support media were also expected to be more stable at higher mixing frequencies, *i.e.* less likely to fail under a high organic loading rate. Mixing frequency was chosen over mixing power as frequency is far more easily controlled in existing biogas plants. Increasing or decreasing the power of mixing would require expensive replacement of motors or the inclusion of motor speed controllers.

6.2. Materials and methods

6.2.1. Single-stage digester feeding

The single stage digesters were fed at approximately 9 a.m. Monday to Friday only, due to laboratory safety regulations. The feeding process involved drawing a volume of digestate equal to the intended volume of mixed feed by siphoning *via* the submerged feed tube. The siphon tube was made of flexible rubber and was held in a 'U' shape after drawing off digestate to retain anaerobic conditions within the digesters. It was realised that, when the digestate was drawn off, there would be a reduction in pressure in the digester and this could lead to air being drawn into the digesters through the outlets. To minimise the volume of air entering the digesters, the gas outlet of each digester was fitted to a one litre bottle to act as a reservoir of biogas. Feedstock (as defined in Chapter 3) was weighed (15 g) and tap water (300 mL per digester at 38° C) was measured to give a prepared feed of 5 % total solids. This produced a loading rate of 3.13 g $VS.L^{-1}$ d^{-1} when averaged over a seven day week, and a hydraulic retention time of 21 days. The feed was mixed by adding *ca.* 60 % of the water to the feed, stirring vigorously, and fed carefully *via* a funnel ensuring no air was pushed through the tube and into the digester vessel, where it would compromise the anaerobic environment. The remainder of the water was used to rinse the feed mixing vessel into the digester to ensure all feedstock had entered.

6.2.2. Collection of single-stage digester samples

Sample collection was part of the feeding process. The drawn digestate was used as a sample, part of which was used for pH measurement (Orion 720A) and extraction of EPS. The remaining digestate sample was used to fill a 25 m.L universal container, which was stored at -20° C for later TS and VS determination.

6.2.3. Gas volume measurement

The gas volume measurement apparatus of the single stage digesters (Figure 6.3) was similar to that used for the multi-stage digesters (described in Chapter 2) in that water was displaced from one bottle to another by gas pressure. Differences were limited to the use of single two litre bottles for gas collection, with water being displaced into an identical two litre bottle, and the use of a three way valve to switch gas flow from the vent (normal setting) to the gas collection bottle (measurement setting).

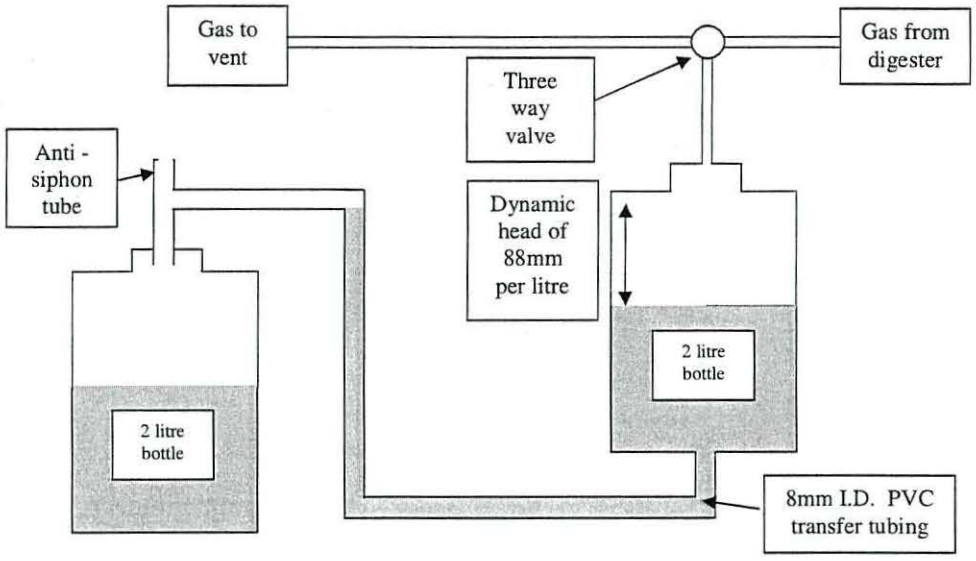

Figure 6.3. Water displacement gas volume measurement apparatus for single-stage digesters.

6.2.4. Gas composition measurement

Gas composition was measured using a Crowcon Triple + plus IR gas monitor, similar to that used in Chapter 3 but measured methane lower explosive level and methane percentage volume only. A gas drying tube identical to that described in Chapter 3 was also constructed. Gas composition was measured after gas volume measurements were complete. The process of returning the water to the gas collection bottle displaced the gas in the collection bottle which was directed through the monitor and from there to the vent. This provided an adequate flow of gas across the sensors for compositional determination.

6.2.5. Two-stage digesters

The four-stage digester used for data collection in Chapter 3 was modified as described in Chapter 2 to form two, two-stage digesters. These were used to run the software sensor and control system described in Chapter 4, but one was also fitted with the same polyurethane foam support media (in the second stage only) as used in the single-stage experiments. The support media foam was only fitted to vessel two of the two-stage experiment because it was intended to assist the methane-producing microbes rather than hydrolytic and acidogenic microbes. The mixing experiment was run at a manually controlled constant organic loading rate of 2 g $VS.L^{-1}$ d^{-1}. This was low in

comparison to both the single-stage experiments and the maximum sustainable organic loading rate established in Chapter 3 for the four-stage system, but digester instability problems during the period directly before the mixing experiment led to the choice of the lower organic loading rate. The gas flow rate of the mixers was five litres per minute as used previously, effectively cycling the entire vessel headspace of five litres during each one minute mixing cycle. This was proportionally less than that used in the single stage digesters, where gas flow rates of two litres per minute were used with vessels of *ca.* 800 ml headspace. The difference was as a result of availability of suitable pumps for use with biogas, the single-stage digester pumps having been modified by the manufacturer to reduce the flow rate as much as possible.

6.2.6. Analysis of extracellular polymeric substances (EPS)

6.2.6.1. Extraction

The method of extraction was based on that published by Liu and Fang (2002). Each sample was washed by centrifuging 25 mL at 4300 x g for ten minutes at 4° C. The supernatant was removed and the pellet re-suspended in 8.5 % w/v NaCl solution. The washing step was repeated to ensure effective removal of unbound EPS. 150 µL of 37 % formaldehyde, in 7-8 % methanol (Avocado) was added to each sample, shaken and left for one hour at 4° C. Then 10 ml of 1 M NaOH (Merck) was added, shaken and left for three hours at 4° C. The samples were then centrifuged at 20,000 x g for twenty minutes at 4° C and initially attempts were made to filter through 0.2 µm syringe filters. This was found to be impossible due to blocking of the filter membrane, so two earlier filtering steps were taken to remove larger particles. In detail, the samples were first filtered through Whatman 542 filter paper (2.7 µm pore size) and then through Whatman GF/F paper (1.6 µm pore size) before finally passing through the 0.2 µm syringe filters. 22 mL of the filtered EPS extract was then poured into a 3500 Da cut-off dialysis membrane (Pierce SnakeSkin), and placed in 220 mL ultra pure water for twenty four hours at 4° C to remove much of the methanol and formaldehyde.

3.1.1.1. Total and volatile solids and total EPS

Determination of total and volatile solids of the raw samples was carried out to the same method as described in Chapter 3. The dry weights of EPS extracts were also found this way and this was considered to be the total EPS per gram of total solids.

3.1.1.2. Determination of carbohydrates

Carbohydrates in the extracted EPS were determined by the Anthrone method (Gaudy, 1962). This method measures sugars and polysaccharides, even when chemically combined. Anthrone in strong sulphuric acid reacts with carbohydrates to produce a green colour. In a typical measurement, 2 g of 97 % anthrone (Avocado) was dissolved in strong sulphuric acid. 0.2 mL of the anthrone reagent was then added to 0.2 mL of sample and chilled in an iced water bath for five minutes, and then 1 mL of anthrone reagent was added and mixed rapidly by swirling in the iced water. Samples were then transferred to boiling water for ten minutes before returning to the iced water bath.

The green colour that developed was measured for absorbance at 625 nm (Unicam UV / Vis UV2) using glucose standards to produce a standard curve. All samples and standards were analysed in triplicate. The standards were prepared from glucose (Fisher) at concentrations of 0, 10, 20, 30, 40, 50, 60, 70, 80, 90, 100, 110, 120 and 130 $mg.L^{-1}$ after preliminary measurements of samples showed this to be a suitable range.

3.1.1.3. Determination of proteins

Protein in the extracted EPS was determined by a modification to the Lowry method (Lowry *et al.*, 1951) as described by Frolund *et al.* (1995). This method relies on the reaction of peptide nitrogen atoms with copper [II] ions in an alkaline environment, and reduction of the Folin-Ciocalteu reagent (containing phosphomolybdate and phosphotungstate) to heteropolymolybdenum blue by the copper-catalyzed oxidation of aromatic amino acids (Dunn, 1992).

Reagents were made up for protein determination as follows:
Reagent 1. 2 % Na_2CO_3 in 0.1 M NaOH.
Reagent 2. 1 % NaK tartrate in H_2O
Reagent 3. 0.5 % $CuSO_4.5H_2O$ in H_2O.
Reagent 4. 48 mL of reagent 1, 1 mL of reagent 2 and 1 mL of reagent 3.

2 ml of reagent 4 were added to the samples and the sample tubes were then incubated for ten minutes at room temperature. 0.2 mL of dilute Folin phenol solution was added to each sample, mixed and incubated at room temperature for thirty minutes.

Absorbance was then measured at 600 nm (Unicam UV / Vis UV2) and the concentrations calculated from a standard curve. The standard was made from 1 $\mu g\ \mu l^{-1}$ bovine serum albumin (BSA) solution (Fisher) diluted in reagent grade H_2O to a total volume of 200 μL at 0, 0.01, 0.02, 0.03, 0.05, 0.05, 0.06, 0.07, 0.08, 0.09, 0.10, 0.11, 0.12, 0.13, 0.14, and 0.15 $\mu g.\mu L^{-1}$ concentrations.

6.3. Results and discussion

6.3.1. Single-stage digesters

The results for the methane production, biogas methane percentage, pH and total solids and volatile solids of the single-stage digesters are shown in Figures 6.4, 6.5, 6.6 and 6.7 respectively. The results for methane yield are not shown as the curves are identical in shape to those obtained for methane production, due to the constant organic loading rate of 3.13 g $VS.L^{-1}\ d^{-1}$ throughout the experiment. The organic loading rate was chosen to be deliberately high (based on Chapter 3 data) so that any instability caused by the mixing frequency changes would be more likely to push the digesters to failure.

The data at first appears to be very variable, but the principal reason for this is the feeding schedule, which only took place on weekdays. The result of not feeding every day is that on the first day of the week methane production is low, the methane percentage is high and the pH is high. The rapid production of methane from this feedstock, as characterised in Chapter 3, explains the low production after two or more days without feeding, and it was also established in Chapter 3 that the alkalinity of the system would rise when the digesters were not fed. Daily feeding throughout the week increased the production rate (as long as the organic loading rate was sustainable) whilst decreasing the methane percentage and pH. Again these variations were to be expected, based on the response to increased and decreased loading rates recorded in Chapter 3.

The first set of data was recorded for the digesters operating at one minute per hour mixing frequency. Approximately twenty five days after measurements began the methane production rates stabilised at *ca.* 0.8 $L.L^{-1}d^{-1}$ and the methane percentage at *ca.* 52 %. The pH measurements had also stabilised from the beginning of the measurement period, but appeared to be a little more erratic after the twenty five day stabilisation period mentioned above. However, pH remained at *ca.* pH 7.2. The pH was simply used as an indication that the experimental digesters were either operating well or were failing.

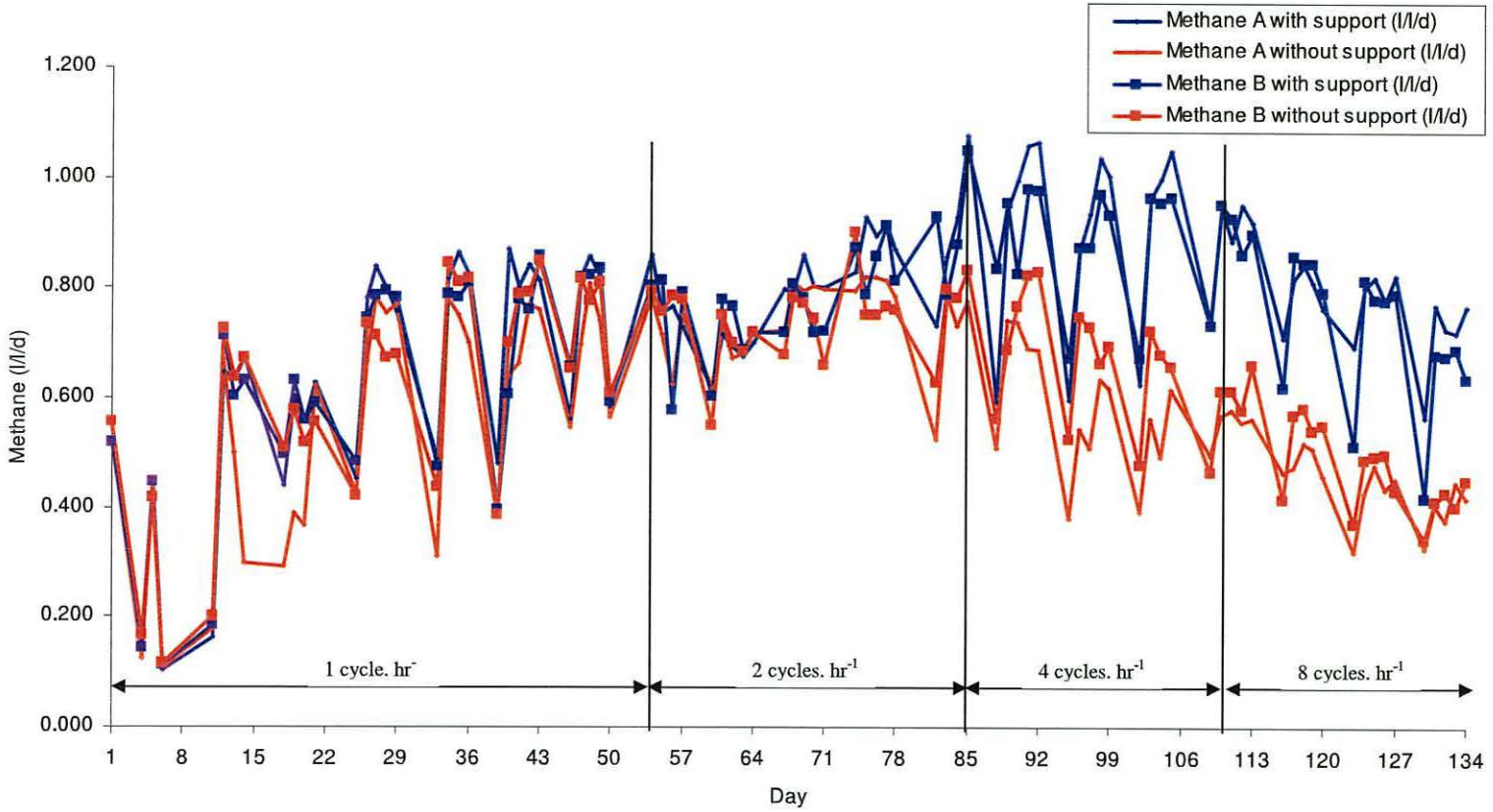

Figure 6.4. Methane production rates of single-stage digesters with different mixing frequencies.

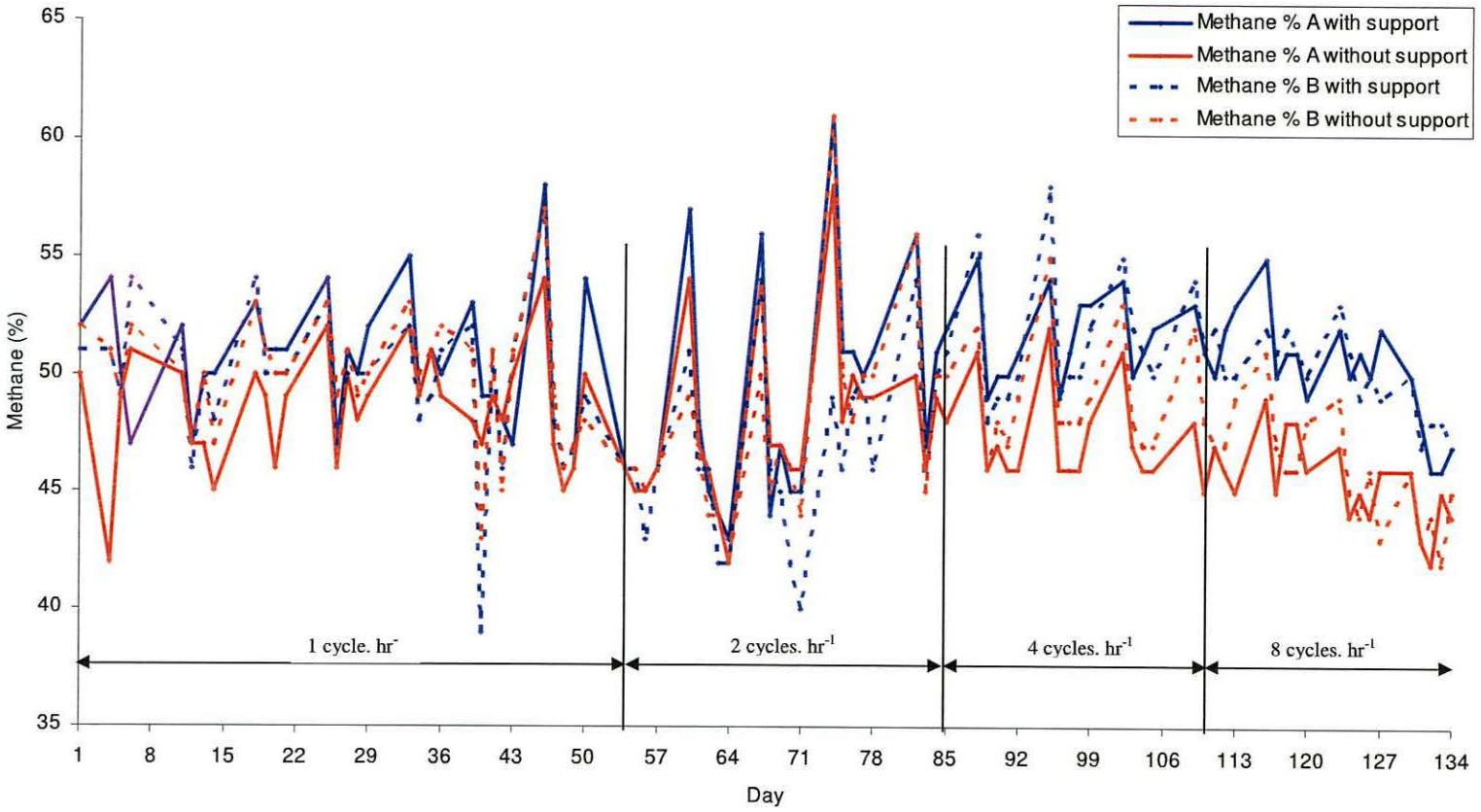

Figure 6.5. Biogas methane percentages of single-stage digesters with different mixing frequencies.

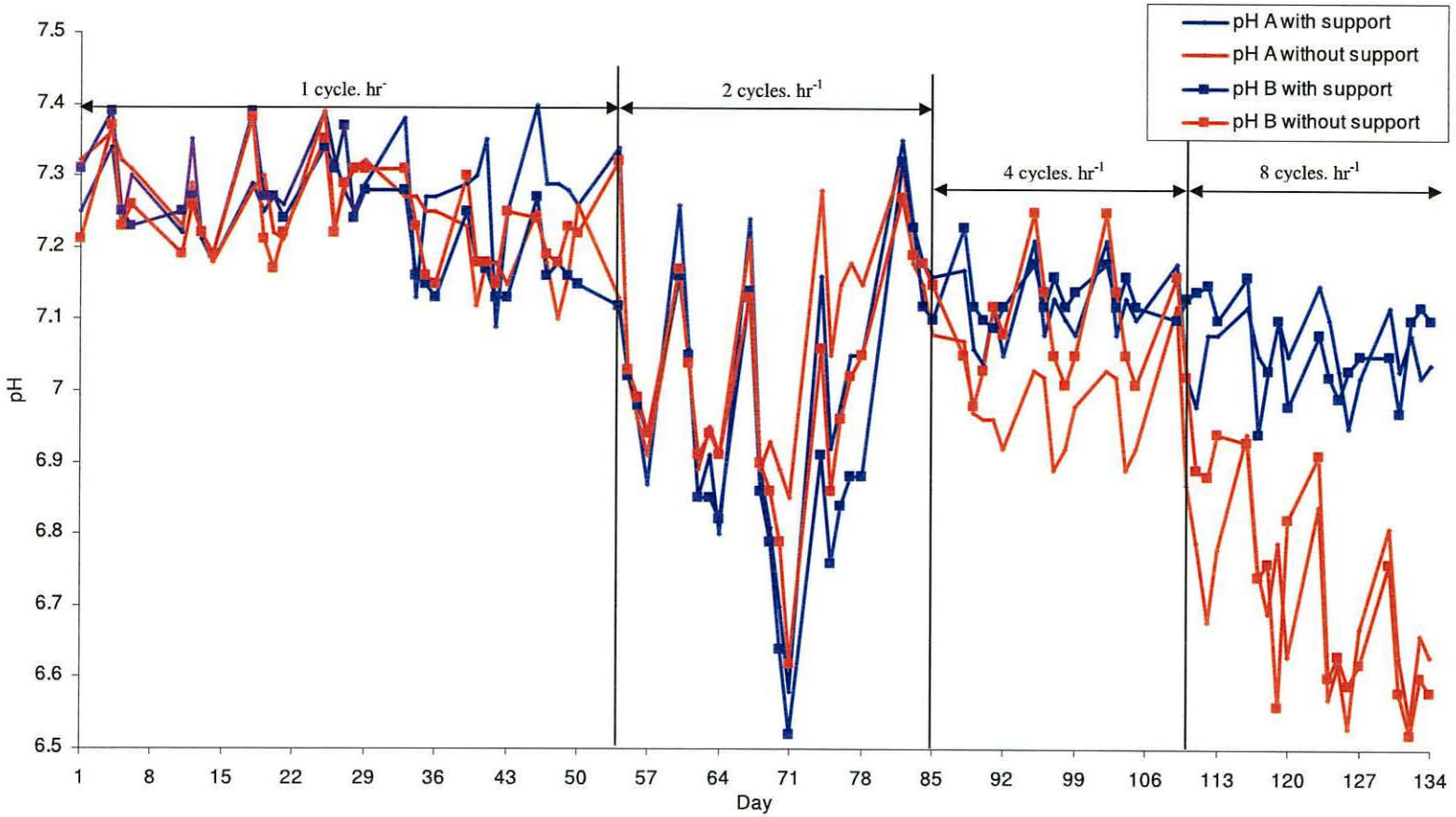

Figure 6.6. Digestate pH of single-stage digesters with different mixing frequencies.

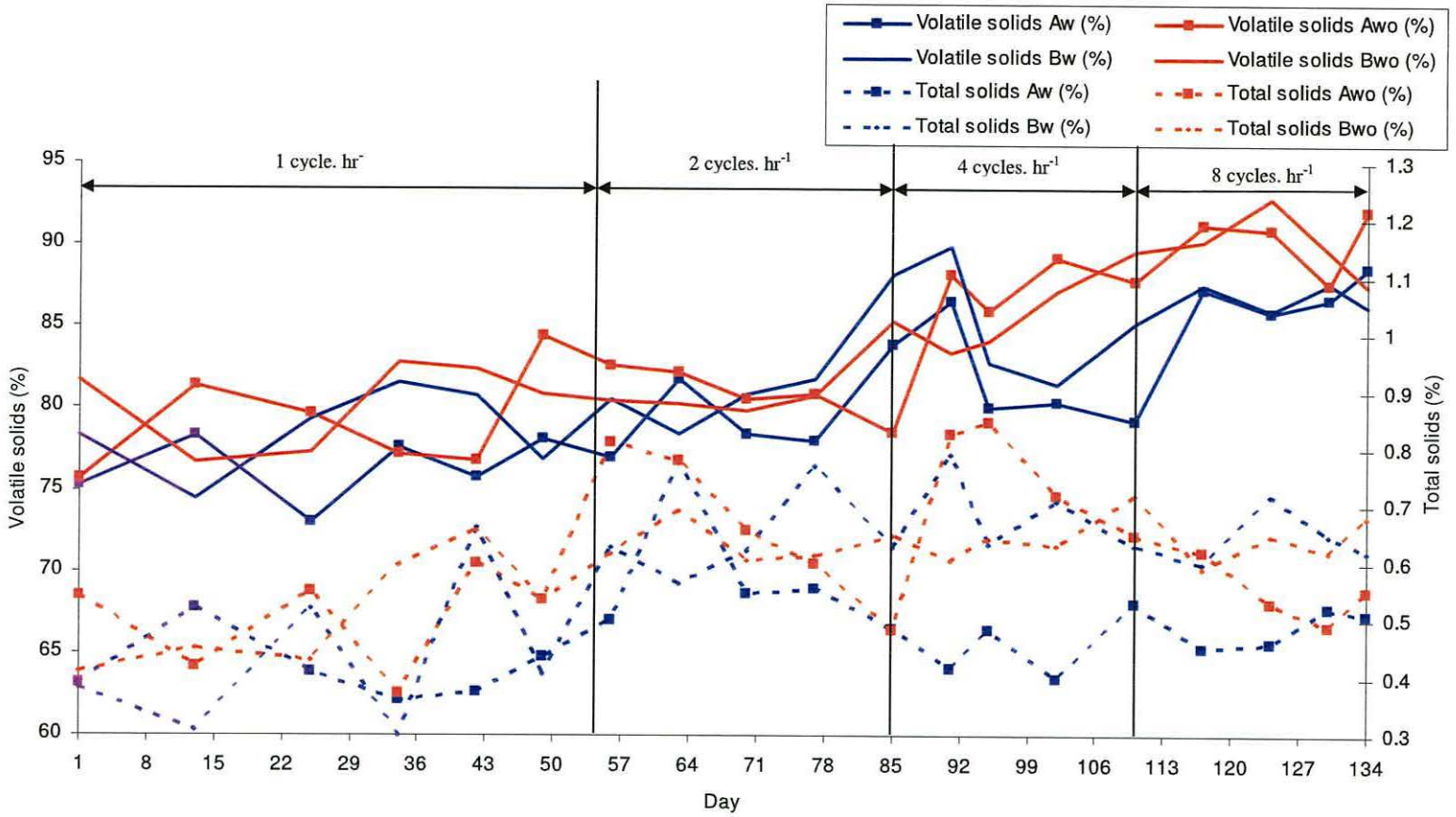

Figure 6.7. Total and volatile solids of single-stage digester outputs with different mixing frequencies.

The mean methane production rates of the digesters with support media during this period was 0.633 $L.L^{-1}$ d^{-1}, which was 8 % higher than the 0.587 $L.L^{-1}$ d^{-1} mean production rate of digesters without support media. However, the results for the first week showed nearly identical production rates from all four digesters, which was attributed to slow development of a biofilm on the support media. Methane production stabilised from day 25, with mean production rates of 0.74 and 0.69 $L.L^{-1}$ d^{-1} for digesters with support media and without support media respectively. The total solids values of the digesters without support were slightly larger than the digesters with support, with overall means of 0.62 % TS and 0.55 % TS respectively. This was noticed during sample collection, when the digesters without support samples were seen to have a darker colour. It is possible that either a greater proportion of the solids were converted to gas (as seen in the methane production data) or that a portion of the dry matter was being retained in the digesters either by sedimentation or material trapped within the pore spaces of the polyurethane foam. However, no evidence was seen of an abnormally large build-up of solids in the digesters, either through the glass digesters during the experiment or when the vessels were emptied upon completion of the experiment. The support media also did not contain large quantities of feedstock when examined after the experiment. Mean volatile solids of the digestate samples were 77.4 % VS for the digesters with support and 84.8 % VS for the digesters without support, suggesting a more efficient conversion of organic material in the former.

Doubling the mixing frequency to two cycles per hour (each one minute in length) caused an immediate reduction in the methane production rate to *ca.* 0.70 $L.L^{-1}$ d^{-1} for a period of *ca.* two weeks for all digesters. This period also saw a reduction in pH of all the digesters to less than pH 7.0 and a decrease in the biogas methane percentage to *ca.* 47 %. However, after two weeks of reduced performance, the digesters all appeared to become acclimatised to the increased mixing frequency and production rates increased above the stable 1 cycle per hour mixing rate methane production rate by 6.75 % to 0.79 $L.L^{-1}$ d^{-1} for the digesters with support and by 7.2 % to 0.74 $L.L^{-1}$ d^{-1} for the digesters without support. The improvement was therefore more pronounced for the digesters without support, although they still produced less methane than the digesters with support. The performance of the digesters with support continued to increase throughout the twenty nine day period at this mixing frequency, whilst the digesters without support appeared to reach a maximum at *ca.* day 68. The volatile solids results showed little change from those obtained during one cycle per hour mixing, but the total

solids increased to 0.62 % and 0.67 % for digesters with and without support, respectively. The increased solids content of the samples was attributed to improved homogenisation of the digesters, thus reducing the sedimentation of feedstock. It was, however, difficult to retrieve an entirely homogenised digestate sample as it was considered unwise to draw digestate off during mixing, as it would increase the possibility of air entering the head space.

Increasing the mixing frequency to four cycles per hour did not have the immediate effect of reducing the methane production rate and percentage which was seen when the frequency was changed from one to two cycles per hour. In the digesters without support methane production fell by *ca.* 36 % from *ca.* 0.75 $L.L^{-1}$ d^{-1} to *ca.* 0.55 $L.L^{-1}$ d^{-1} but this was over the twenty five day period at this mixing frequency. The mean of the two replicates was brought down by the poor performance of the digester A without support, although digester B without support still produced less methane during this period than the digesters which were fitted with the support media. However, the pH of the digesters without support did fall immediately after the change in mixing frequency, to *ca.* pH 7.0 for 'A' and *ca.* pH 7.1 for 'B'. The reduced pH and methane production would suggest an accumulation of fatty acids. This could possibly be attributed to improved transport of substrates and products to and from acidogenic bacteria or an improved hydrolysis rate increasing fatty acid production. More efficient hydrolysis could also have been because of improved transport of substrates or the longer period during which shear forces were acting on the digestate, breaking up particulate matter. An increase in fatty acids due to reduced consumption by acidogenic and / or methanogenic bacteria can be attributed to mixing shear forces preventing the formation of cellular agglomerates, either granular or as surface biofilms. This process of accumulation of fatty acids in the digesters without support can be further validated by examining the data for digesters with support. These digesters show an immediate improvement in performance when the mixing frequency is increased. Methane production increases to *ca.* 0.9 $L.L^{-1}$ d^{-1} with no significant change in the methane content of the biogas, and the digestate pH remained stable at *ca.* pH 7.1. The reason why this reinforces the idea of fatty acid accumulation in the digesters without support is that the support media could have provided a greater area for the development of surface biofilms and provided physical protection against shear forces, thus reducing the washout of microorganisms. In turn, this could increase the metabolism of fatty acids, assuming the biofilms consisted of fatty acid degrading organisms and methanogenic

organisms, as suggested by de Bok *et al.* (2004). The four cycles per hour mixing frequency was therefore too much for the digesters without support, but the protection offered by the biomass support media appeared to reduce washout and thus allowed increased methane production at this mixing frequency.

The four cycles per hour mixing frequency did not make much difference to the total solids of the samples, but there was an increase in the digestate volatile solids results. These increased to means of 83.8 % and 85.9 % volatile solids for digesters with and without support, respectively. This was indicative of a lower rate of conversion of organic carbon to methane. This would have been expected for the digesters without support as methane production fell during this period, but the digesters with support showed that maximum methane production was attained during this part of the experiment.

Increasing the mixing frequency to eight cycles per hour reduced methane production and the methane percentage of the biogas from all digesters. Methane percentage fell only by a small amount to *ca.* 45 % and 43 % methane for the digesters with and without support, respectively. However, methane production in all digesters fell from *ca.* 0.95 $L.L^{-1}$ d^{-1} during the four cycles per hour mixing frequency to 0.7 $L.L^{-1}$ d^{-1} for the digesters with support, and from *ca.* 0.60 to 0.45 $L.L^{-1}$ d^{-1} for the digesters without support. This would suggest that eight cycles per hour was too much mixing for all the digesters used in this experiment. The reduced methane production of digesters without support media was accompanied by a fall in pH from *ca.* pH 6.9 during four cycles per hour mixing to *ca.* pH 6.6 after 25 days at eight mixing cycles per hour. This would suggest that the methanogenic bacteria are more susceptible to mixing rates, as a reduction in methanogenic activity would be expected to lead to an increase in fatty acid concentration and therefore a decrease in pH.

Statistical analysis of the data using analysis of variance (ANOVA) techniques with Genstat v.9.2 software proved that the mixing frequency and the use of support media were both significant factors determining methane production.

The mean methane production over the whole experimental period for single-stage digesters with support was 0.75 $L.L^{-1}$ d^{-1}, compared with 0.61 $L.L^{-1}$ d^{-1} for digesters without support, an increase of 23 %. However, this increase includes the poor production data obtained at four and eight mixing cycles per hour for digesters without support, so mean production data at each frequency of mixing cycles are shown in Figure 6.8. The data show that digesters with support outperformed digesters without

support at all frequencies of mixing, with an 8 % increase at one cycle per hour, a 6.5 % increase at two cycles per hour, a 43 % increase at four cycles per hour and a 62 % increase at eight cycles per hour. However, the eight cycles per hour mixing frequency also reduced the methane production of the digesters with support. The mean methane production data affected by the frequency of mixing (Figure 6.9) were 0.61 l l^{-1} d^{-1} at one cycle per hour, 0.76 $L.L^{-1}$ d^{-1} at two cycles per hour, 0.77 $L.L^{-1}$ d^{-1} at four cycles per hour and 0.62 $L.L^{-1}$ d^{-1} at eight cycles per hour, a maximum difference of 26 %. The optima are found at two and four cycles per hour for digesters without and with support media respectively, as shown in Figure 6.8. This was in line with the predicted effect of the support in that increased mixing improved biogas production and that the support media appeared to protect the micro-organisms allowing a higher mixing frequency. All ANOVA analyses of the methane production data in this section were significant at $p < 0.001$.

Examining all the data, it was interesting to note that the methane production in the single-stage digesters fell when the first change from one cycle per hour to two cycles per hour was implemented. However, there was no such immediate effect after subsequent changes in mixing frequency (although there was a steady decrease in output after four and eight cycles per hour were tried for digesters without and with support respectively).

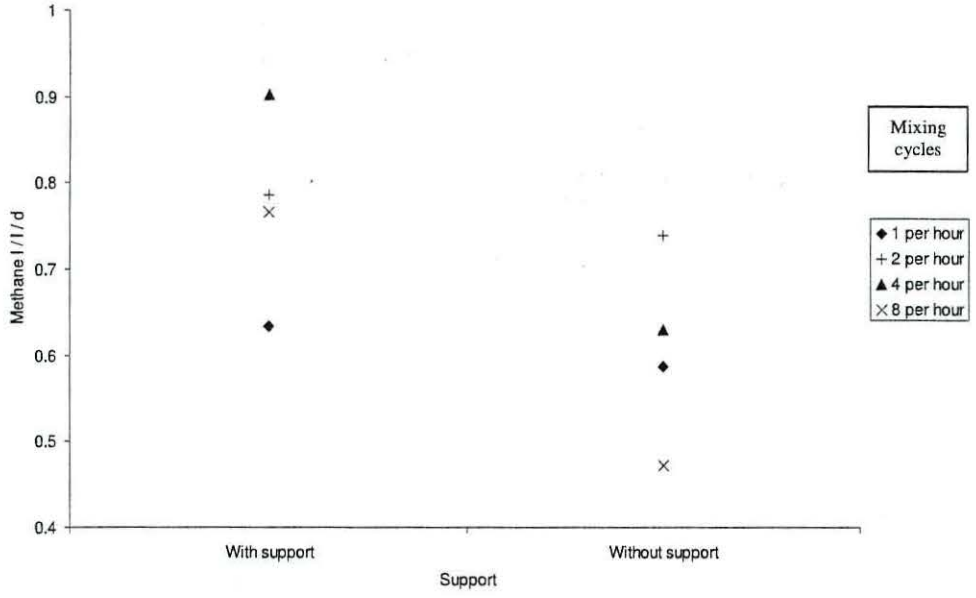

Figure 6.8. Mean methane production of single-stage digesters with and without support media at the various mixing cycles used in this experiment.

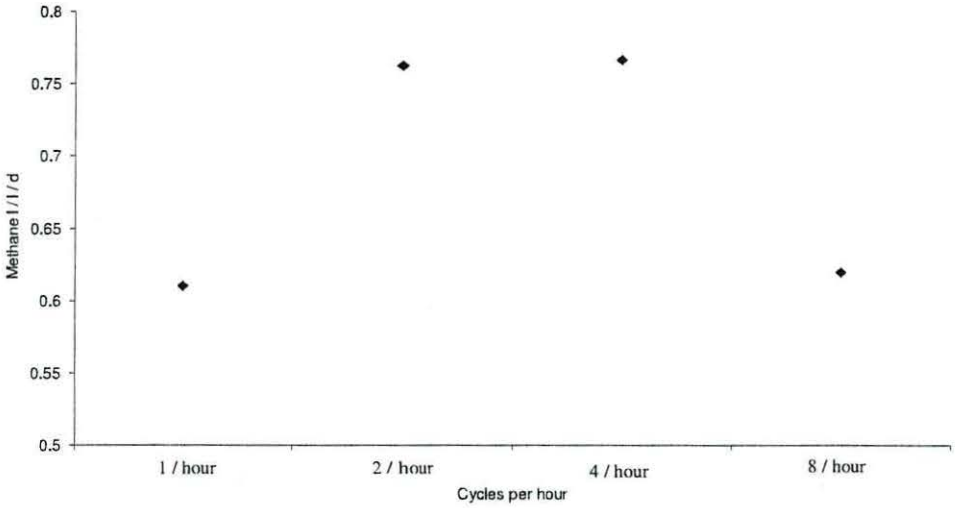

Figure 6.9. Mean methane production of single-stage digesters combining both the means of the support media factor and mixing cycle factors.

The decrease in methane production after the first change in mixing frequency could be related to the suggestion by Liu and Tay (2002) that shear forces can improve biofilms and granules. They found that shear forces affected mass transfer, EPS production and the genetic and metabolic behaviour of biofilms and also that more stable biofilms were produced when subjected to shear forces. Thus, the increased shear forces generated upon the first change in mixing frequency could have been responsible for an initial disruption in the free granular colonies structure, but the formation of denser granules attributed to the shear forces could have been responsible for the improved gas production noticed after a recovery period of *ca.* two weeks (Figure 6.4). The greater increase in methane production recorded for the digesters with support can also be linked to the principal of shear forces improving biofilms. The formation of a biofilm requires first the transport of organic molecules to form a conditioning film and then the transport of cells to adhere (Busscher and Van der Mei, 2000). It is possible that the improved mass transfer rate at a higher frequency of mixing cycles could build biofilms more rapidly. The further improvement in methane production seen at four mixing cycles per hour for the digesters with support can also be attributed to the increase in mass transfer of substrates and products to the microbial colonies bound to the support media. It would seem that the increased shear forces can act as a selecting mechanism for granules and biofilms, with those that are bound weakly being removed to make way for the more robust. The fall in methane production seen at four or more mixing cycles per hour for the digesters without support and at eight mixing cycles per

hour for the digesters with support can only be explained by disruption of the colonies due to shear forces which were too great for the adhering properties of the EPS.

The EPS data are shown in Figures 6.10, 6.11 and 6.12 for total, carbohydrate and protein EPS components respectively, and the probabilities of significance produced by ANOVA analysis are shown in Table 6.1.

Table 6.1 shows that the mixing cycle variation had a greater effect on EPS than did the presence or absence of support media. Mixing had a significant ($p < 0.05$) effect on total EPS, carbohydrate EPS and protein EPS, but the support media variable only had a significant effect on total EPS. The total EPS produced the most significant results, the means of which are shown in Figures 6.13 and 6.14.

Table 6.1. Significance probabilities of support media and mixing cycle's effect on EPS and total and volatile solids in single-stage digesters.

	Variable		
	Support	**Mixing cycles**	**Support and mixing cycles**
Total EPS	$p < 0.001$	$p < 0.001$	$p = 0.086$
Carbohydrate EPS	$p = 0.125$	$p = 0.028$	$p = 0.764$
Protein EPS	$p = 0.285$	$p = 0.002$	$p = 0.967$
Total solids	$p = 0.003$	$p < 0.001$	$p = 0.622$
Volatile solids	$p < 0.001$	$p < 0.001$	$p = 0.759$

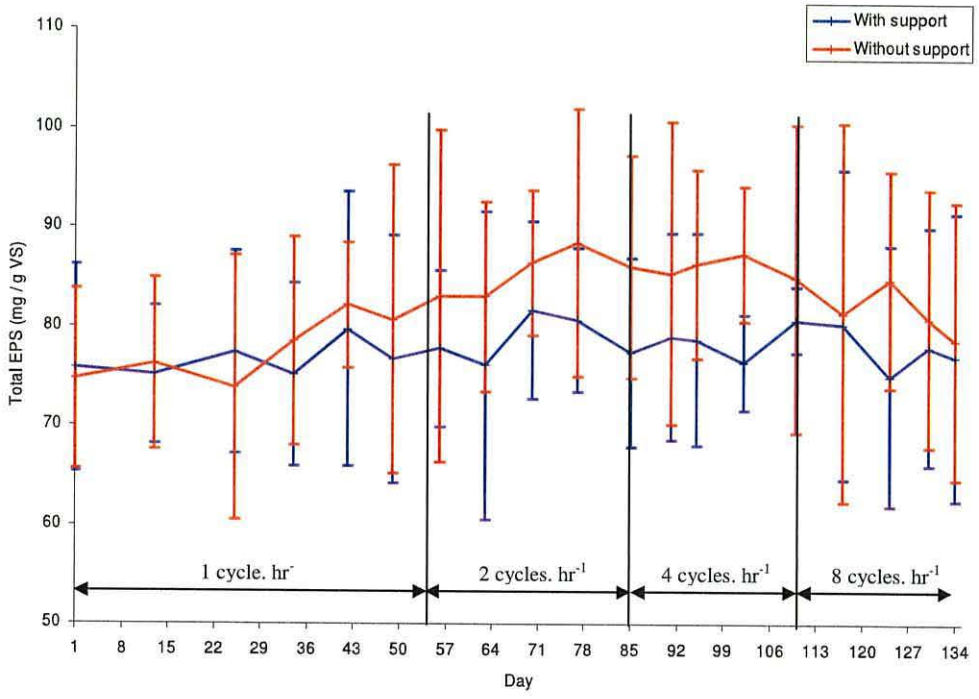

Figure 6.10. Total EPS from single-stage digesters at various mixing frequencies.

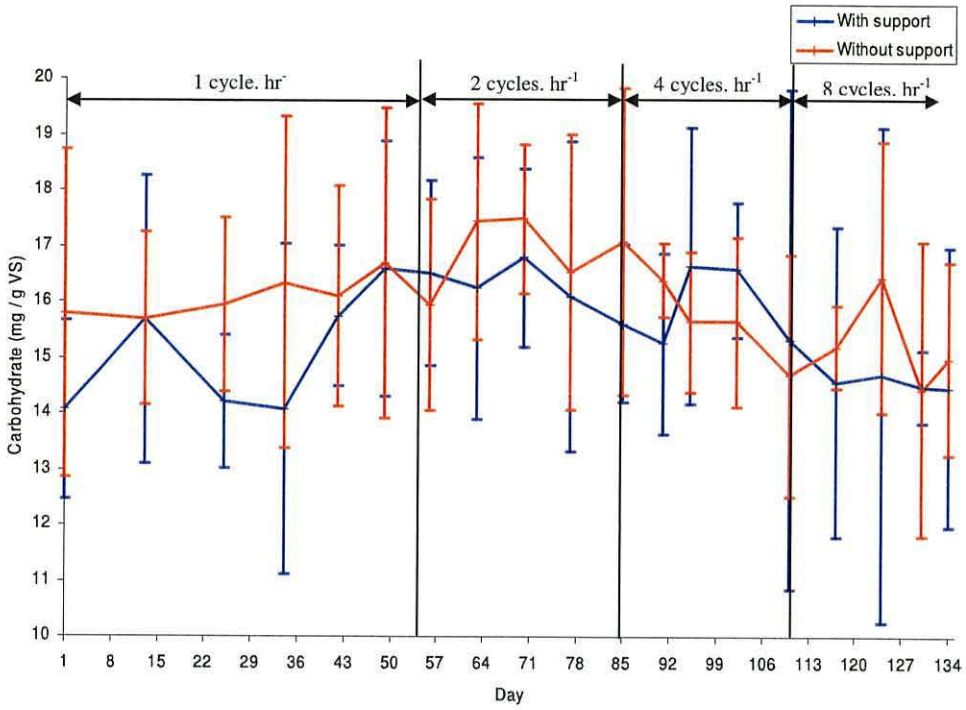

Figure 6.11. Carbohydrate EPS from single-stage digesters at various mixing frequencies.

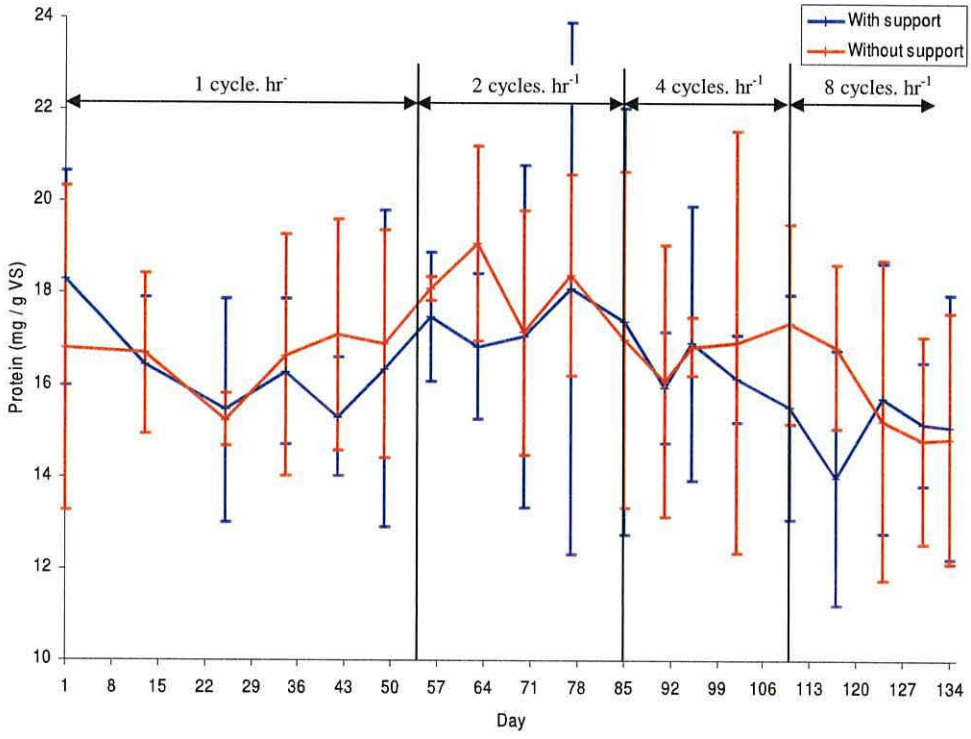

Figure 6.12. Protein EPS from single-stage digesters at various mixing frequencies.

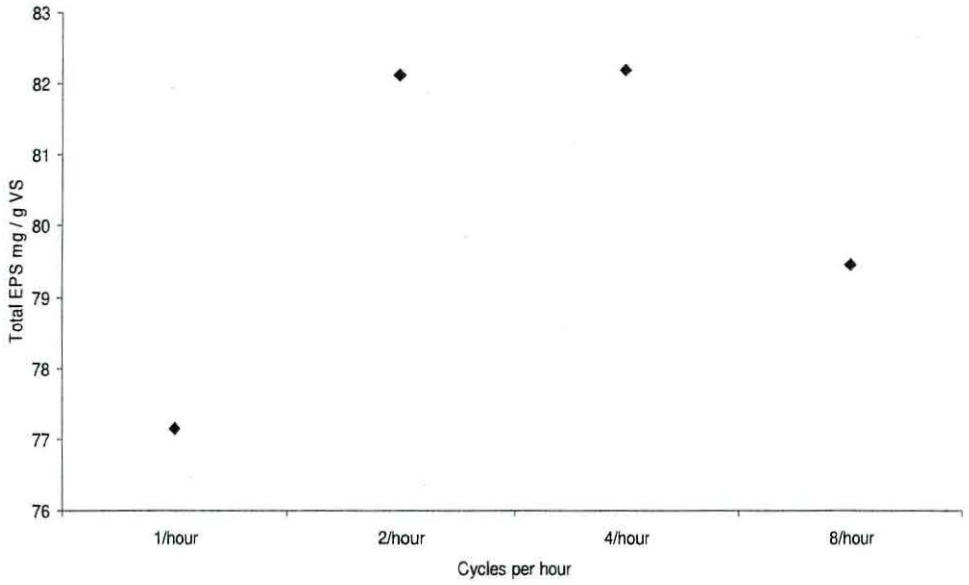

Figure 6.13. Means of total EPS in relation to mixing frequencies.

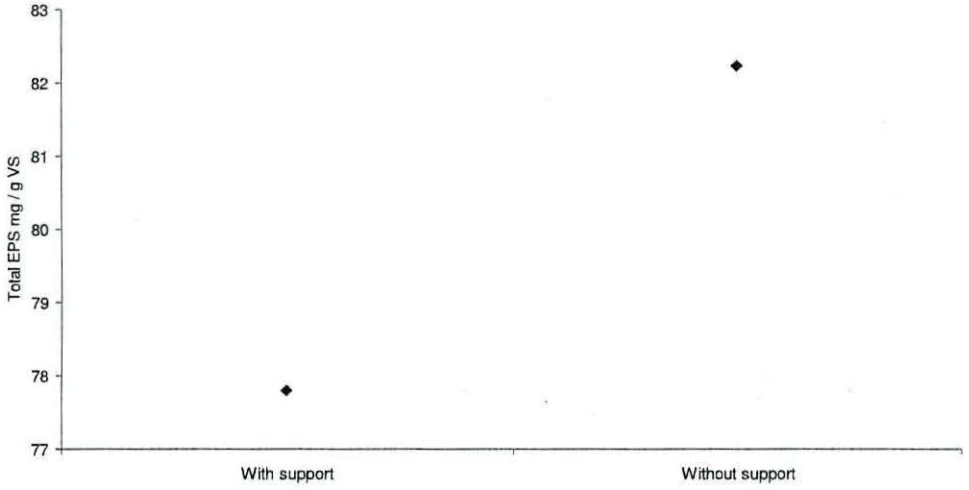

Figure 6.14. Means of total EPS in relation to the presence or absence of support media.

The mean of total EPS of digesters both with and without support media shown in Figure 6.13 assumes a similar shaped graph to that for the mean methane production of digesters with and without support media at the various mixing frequencies (Figure 6.9). This suggests that the quantity of total EPS was proportional to the methane production. This was to be expected as larger quantities of EPS have been shown to be indicative of larger and more stable granules, which are important for methane production (Ong *et al.,* 2002). However, the data correlate poorly, with R^2 values of

0.37, 0.08, 0.24 and 0.49 for digsters A with support, A without support, B with support and B without support respectively. The reduction in EPS found at the highest mixing frequency is likely to be a result of the disruption of the freely moving granules in the digester leading to a reduced oxidation of VFA and subsequent acidification of the reactor (McMahon *et al.*, 2001). However, the greater quantity of total EPS found in the digesters without support media than was found in digesters with support media (Figure 6.14) does not agree with the previous statement linking total EPS to methane production. It has already been shown that digesters with support media produced more methane (Figure 6.8). Thus, the greater volume of methane produced can most likely be attributed to colonies of methanogenic cells which are bound to the support media. The EPS of the bound cells were not present in the samples taken and therefore not measured in this study.

Examination of the data graphs (Figures 6.10, 6.11 and 6.12) shows that there was a large error between replicates for all EPS components, including both replicate digesters and EPS measurements. The large errors may have originated in the measurement process, possibly due to the interference of substances in the extracted samples. This was believed to be possible because of the evidence provided by the glucose and BSA standards, which all produced good quality linear standard curves but were simply mixtures of glucose or BSA in water and therefore had no other compounds present to interfere with the absorbance values when measured. Also, some of the measured EPS may have been undigested feedstock in the samples, which became hydrolysed during the extraction process, thus providing poor quality results.

6.3.2. Two-stage digesters

The two-stage digesters used in this experiment were under automatic control between 20th December and 25th March 2007. However, the control system was linked between the two digesters until 29th January as described in Chapter 4. The two-stage digesters were later subjected to variations in the mixing frequency, with experimental frequencies of a single one-minute mixing cycle per hour (this was also the frequency used with the two and four-stage digesters in all previous experimental work), two one-minute cycles per hour, four one-minute cycles per hour and finally eight one-minute cycles per hour. The automatic control system was not operating during the mixing frequency experiment.

It is worth noting that the greater part of the methane production in this experiment was from the second of the two-stages. This is unlike the data found in Chapter 3, which showed a decrease in methane production through the four-stages of the digester, from vessel 1 having the highest production to vessel 4 having the lowest. It was discovered at the end of the experiment described in this chapter that the first stages of both digesters were almost completely filled with solidified feedstock as a result of mixing failure, which significantly reduced the effective volume of the first stages and decreased the true total hydraulic retention time by an estimated 45 %, assuming only 10 % of the first stage remained as mixed volume.

The organic loading rates of the two digesters (as shown in Chapter 4, Figures 4.23, 4.24 and 4.25) were examined to find if the support media made any difference to loading rates as controlled by the software sensor. The mean organic loading rates were 2.38 g $VS.L^{-1}$ d^{-1} for the digester with support and 1.59 g $VS.L^{-1}$ d^{-1} for the digester without support, a considerable increase of *ca.* 50 % in loading rate attributed to the addition of support media. Methane production during automatic control is shown in Figure 6.15, and during manual control (constant organic loading rate of 2 g $VS.L^{-1}$ d^{-1}) in Figure 6.16. It is clear that the digester with support (solid line) had a greater methane production rate than the digesters without support (dotted line). The increase in methane production rate can be measured by the means obtained for the automatic control experiment, the mixing experiment and both experiments combined, which are shown in Table 6.2.

Table 6.2. Mean methane production from two-stage digesters with and without support media.

Experiment	Vessel 1	Vessel 2	Total system (mean)
With support media, automatic control experiment	0.033 $L.L^{-1}$ d^{-1}	0.427 $L.L^{-1}$ d^{-1}	0.230 $L.L^{-1}$ d^{-1}
Without support media, automatic control experiment	0.029 $L.L^{-1}$ d^{-1}	0.413 $L.L^{-1}$ d^{-1}	0.221 $L.L^{-1}$ d^{-1}
With support media, mixing experiment	0.041 $L.L^{-1}$ d^{-1}	0.581 $L.L^{-1}$ d^{-1}	0.311 $L.L^{-1}$ d^{-1}
Without support media, mixing experiment	0.024 $L.L^{-1}$ d^{-1}	0.277 $L.L^{-1}$ d^{-1}	0.151 $L.L^{-1}$ d^{-1}
With support media, all data	0.037 $L.L^{-1}$ d^{-1}	0.498 $L.L^{-1}$ d^{-1}	0.268 $L.L^{-1}$ d^{-1}
Without support media, all data	0.026 $L.L^{-1}$ d^{-1}	0.350 $L.L^{-1}$ d^{-1}	0.188 $L.L^{-1}$ d^{-1}

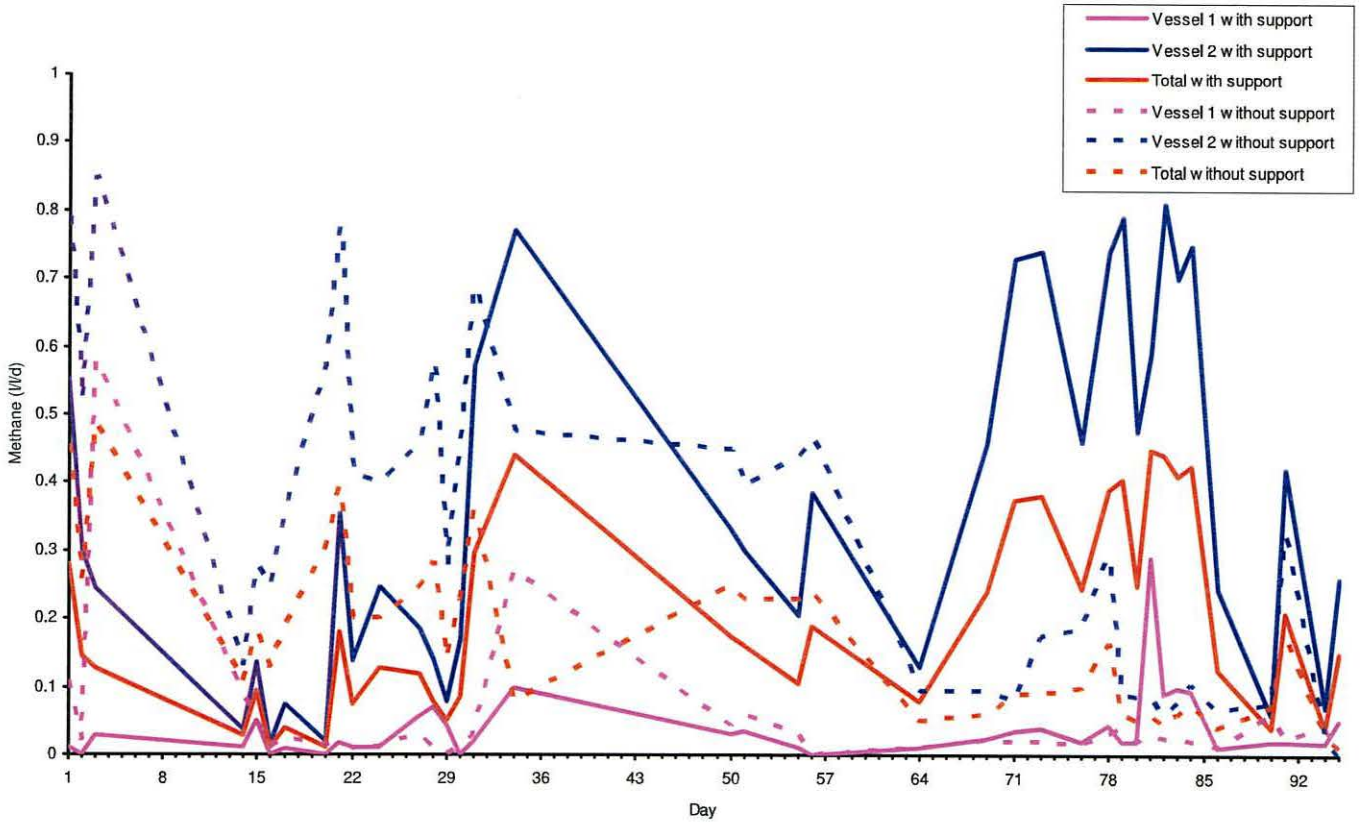

Figure 6.15. Methane production rates of two-stage digesters under automatic loading rate control.

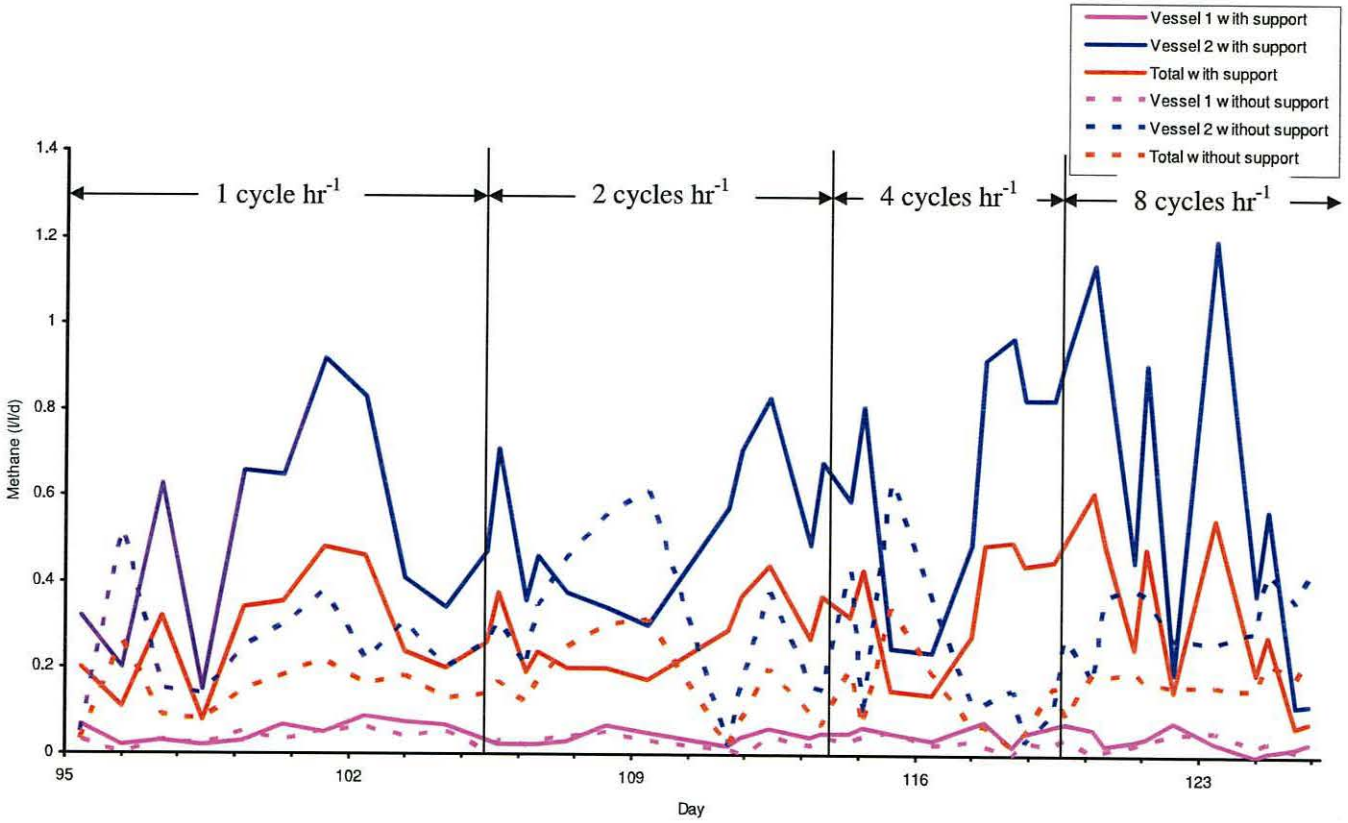

Figure 6.16. Methane production rates of two-stage digesters under manual loading rate control and different mixing frequencies.

During the automatic control experiment described in Chapter 4, the methane production was 14 % greater in vessel one of the digester with support media in the second stage than the methane production of vessel one of the digester which did not contain support media. However, methane production of the digester with support media was only 3 % greater in vessel two and 4 % greater for the total methane production than was found in the digester without support media. This would suggest that the digester that did not contain support media was under-performing, possibly as a result of the build up of solid material in the primary vessels which was discovered at the end of the experiment. The small increases in vessel 2 methane production and total methane production of the digester with support media was less than was expected considering the 50 % greater average organic loading rate applied to the digester with support media.

During the mixing experiment, the mean methane production rates of the digester with support media were 71 %, 110 % and 106 % greater from vessels 1, 2 and the mean of the total system (respectively) than the comparable mean methane production rates of the digester without support data. These data indicate a greater difference was made by the variations in mixing frequency.

When the combined mixing and support experimental data were examined, the digester with support media had a total mean methane production rate which was *ca.* 43 % greater than that obtained from the digester without support media. However, the individual methane production rate of vessels one and two for each digester also increased by *ca.* 43 %, although only vessel 2 contained the support media, *i.e.* there should have been no difference between the two first stages. This would suggest the increase in methane production from the digester with support was for reasons other than the presence of the support media. It is possible that the clogging of the first vessels (as mentioned above) could have happened to the first vessel of the digester without support media at a much earlier time than with the vessel with support media.

All data were investigated for variance using one or two-way ANOVA as necessary. The F-test probabilities for all two-stage experimental data presented in this chapter are shown in Table 6.3.

Combining all the data used in this chapter shows significant differences ($p < 0.05$) in vessels one, two and total methane production rate. However, splitting the data into the automatic control and mixing experiments shows that neither was significant alone. The fact that there was a significant difference between all data obtained from

vessels one of digesters with and without support media (vessel one contained no support media) reinforces the point made earlier that there were other factors responsible for the difference in methane production rates. The variation in organic loading rate between digesters with and without support can partly explain the difference in methane production during the auto-control experiment, but organic loading rates were constant during the mixing experiment. However, mixing frequency had a significant effect ($p < 0.001$) on methane production rate in both vessels one and two and total gas output.

Table 6.3. F-test probabilities of support media and mixing frequency two-stage experiments.

Experiment	Vessel 1	Vessel 2	Total
Auto control (support)	$p = 0.642$	$p = 0.862$	$p = 0.833$
Mixing (frequency)	$p < 0.001$	$p < 0.001$	$p < 0.001$
Mixing (support)	$p = 0.191$	$p = 0.645$	$p = 0.666$
Mixing (frequency and support)	$p = 0.202$	$p = 0.067$	$p = 0.052$
All data (support)	$p = 0.036$	$p = 0.036$	$p = 0.003$

The mean methane production rates for the two-stage digesters during the mixing experiment are tabulated in Table 6.4.

Table 6.4. Mean methane production for two-stage digesters at various mixing frequencies.

Mixing frequency	Vessel 1	Vessel 2	Total
1 cycle / hour	0.037 $l l^{-1} d^{-1}$	0.383 $l l^{-1} d^{-1}$	0.210 $l l^{-1} d^{-1}$
2 cycles / hour	0.028 $l l^{-1} d^{-1}$	0.429 $l l^{-1} d^{-1}$	0.229 $l l^{-1} d^{-1}$
4 cycles / hour	0.037 $l l^{-1} d^{-1}$	0.471 $l l^{-1} d^{-1}$	0.254 $l l^{-1} d^{-1}$
8 cycles / hour	0.028 $l l^{-1} d^{-1}$	0.438 $l l^{-1} d^{-1}$	0.233 $l l^{-1} d^{-1}$

The data were first examined in terms of mixing frequency alone. The mean methane production rates for vessel one are either unchanged or 32 % lower than the base frequency production rate when the mixing frequency was above the base frequency. Base frequency being defined as one cycle per hour, the frequency at which all previous two and four-stage digesters were operated. However, the second vessel and the total combined vessel mean methane production rates are improved at higher mixing frequencies. Two mixing cycles per hour increased mean methane production above that found at the base frequency by 11 % and 8 % for vessel two and total gas

output respectively. It increased further above the base frequency production by 19 % and 17 % at four cycles per hour and 13 % and 10 % at eight cycles per hour, each for set of figures for vessel 2 and total system mean methane production respectively. This would suggest that the optimum mixing frequency was four one-minute cycles per hour for the two-stage digesters in terms of methane production rate.

Combining the support and mixing frequency data did not produce significant results (*i.e.* $p > 0.05$) as shown in Table 6.3. However, the total combined vessels methane production rate was close to being significant, with a probability of $p = 0.052$. The means of methane production rates for combined support and mixing data are also shown in Table 6.5. The total methane production rate increases in relation to mixing frequency in the order eight, two, one and four cycles per hour for the digester with support. For the digester without support, total methane production increases in the order of two, four, eight and one cycles per hour. The digester with support showed an increase in methane production from 0.280 l l^{-1} d^{-1} at the least efficient mixing frequency of eight cycles per hour to 0.396 $L.L^{-1}$ d^{-1} at the most efficient frequency of four cycles per hour.

Table 6.5. Means of methane production rates ($L.L^{-1}d^{-1}$) at various mixing frequencies in two-stage digesters with and without support media.

Mixing frequency	Support	Vessel 1	Vessel 2	Total
1 cycle / hour	without	0.027	0.259	0.143
2 cycles / hour	without	0.020	0.301	0.161
4 cycles / hour	without	0.021	0.202	0.111
8 cycles / hour	without	0.025	0.345	0.185
1 cycle / hour	with	0.047	0.506	0.276
2 cycles / hour	with	0.036	0.557	0.297
4 cycles / hour	with	0.053	0.740	0.396
8 cycles / hour	with	0.031	0.530	0.280

The digester without support showed an increase in methane production from 0.111 $L.L^{-1}$ d^{-1} at four cycles per hour to 0.185 $L.L^{-1}$ d^{-1} at eight cycles per hour. The increase in methane production was proportionally greater for the digester without support, although the digester with support had a greater quantitative increase. Therefore it can be said that the digester without support was more sensitive to variations in the mixing frequency. However, the digester without support produced

more methane at one, two and eight cycles per hour than at the intermediate frequency of four cycles per hour. It was assumed that the mixing power and frequencies used in these experiments were not close to eliminating mass transfer limitations, which is close to being achieved in fluidised bed reactors commonly used for waste water digesters (Perez *et al.*, 2001; Moletta, 2005). It was expected that there would be a balance between mass transfer and shear forces playing a role in methane production, in that mass transfer and the duration of the shearing action of the mixing process increase with mixing frequency until the benefits of increased mass transfer are outweighed by the negative effect of the shear forces on the microbial colonies.

The work requires further investigation into the true optima, now that a rough approximation of the mixing frequency optima has been established. The results are also very subjective in that they are based on specific laboratory scale digesters, using specific gas flows for mixing through certain types of spargers or bubblers. This information is very difficult to scale up or even to transfer to another laboratory scale digester, but it clearly proves that methane production can be improved by adding biomass support media and particularly by optimisation of mixing frequency. It would also be of interest to investigate optimum mixing frequencies in separate stages of two-stage digesters. This could be based on gas production for both vessels or possibly by measuring the hydrolytic efficiency or VFA production of the first vessel and gas production from the second.

The support media would be most difficult to apply to an existing digester, as it would require considerable modification to the vessels to add a supporting frame for the media, not to mention the need to shut down and empty the tank(s). The media appeared to exhibit neutral buoyancy when immersed in the digestate, but any collapse of the polyurethane sheeting would be disastrous for an industrial process, with the potential blocking of pipes and damage to mixing apparatus. Mixing optimisation, however, would be very easily implemented into most digesters; those that use constant mixing could even be modified into an intermittent system. The plant operators would simply need to make some simple gas output measurements over a period of a few months and could find their own optima from these data quite easily. This, in many cases, could reduce site running costs as it may well be that a reduced mixing frequency is optimal, but where it is found that increasing the mixing frequency produces more gas, the increased energy (and possibly maintenance) costs of using the mixer more often would

have to be compared with the energy output gained from the increased methane production.

The 26 % increase in methane production found in the single stage experiment can be compared to a full scale system. The 1100 m^3 reactor treating agricultural manures and silages found at Aarhus University Research Centre Foulum, Denmark, has a single central mixer of 7 kW which operates continuously. The optimal methane production rate found in the single stage reactors in this chapter was in the region of 0.95 $L.L^{-1}$ d^{-1} which equates to 1045 m^3 per day in a 1100 m^3 reactor, whereas the least optimal methane production found in th single stage experiment would equate to approximately 770 m^3 per day, a difference of 275 m^3. Methane has an energy yield on combustion of 39500 kj m^{-3} (Suzuki *et al.*, 2007), which is equivalent to 10.97 kWh per m^3. The increased energy production from optimal mixing is therefore approximately 3 MWh per day, and assuming a conservative 30 % electrical conversion efficiency, would equal 0.9 MWh per day as saleable electricity. The current UK renewable energy payment for renewable generators is approximately £0.09 per kWh, which in this case would mean £81 of extra income to the biogas plant per day. This assumes that the biogas plant is not selling heat energy, a potential further source of income. In addition to this, the current UK system ensures an additional reward to renewable energy producers in the form of Renewable Obligation Certificates (ROCs), a single ROC given for every Mwh of energy produced, which can be sold for at least £45 to electricity supply companies. The ROC scheme has recently been changed for new biogas plants to ensure two ROCs per MWh. This would mean a ROC payment to the biogas plant of between £40.50 and £81 per day, plus the electricity sale of £81 per day, totalling at least £121.50 per day. Assuming the biogas plant buys electricity at the same price it sells for (£0.09 per kWh), halving the mixing operating time would save 84 kWh or £7.56 per day.

6.4. Conclusions

The data obtained during this experiment suggest that biomass support media and mixing frequency had significant effects on the production of methane. The single-stage support media digesters produced at least 6.5 % more methane than those that had no support media fitted, and the optimal mixing frequency with these digesters was shown to increase methane production by as much as 26 %. The two-stage data was less clear due to proportionally similar increases in methane production in vessel 1 as well

as vessel 2, although vessel 1 contained no support media. Also, the order of mixing frequencies which increased methane production of the two-stage digesters without support media was difficult to explain *i.e.* frequencies of one, two and eight cycles per hour were better than four cycles per hour. However, the optima found here are only the optima of the frequencies used in the experiment, *i.e.* the true optima may be a frequency that was not used in this experiment, for example two cycles every forty minutes.

7 Final conclusions and future research

The literature review in Chapter one revealed several areas that required further research. These included the development of a monitoring system which was both robust and simple yet also gave useful and timely information on key process variables. Such a monitoring system would be at its most useful when used to control the feedstock influent, with the potential to develop a fully automatic system. Existing research has indicated that mixing in the anaerobic digestion of solid materials is far more complex than just mass transport. Minimal shear forces are needed to maintain active biofilms or granular microbial communities which are important to ensure good methane production. The literature appeared to contain no research which combined variations in mixing power or frequency with the use of microbial support media.

Chapter two describes the construction of a four-stage anaerobic digester suitable for research purposes. The hydrodynamics of the system demonstrated that the mixing model within a single reactor vessel was very close to the CSTR model. This meant that the contents of the vessel were homogenised rapidly providing good mass transport in terms of moving substrates and products to and from microbial cells as well as diluting any potentially toxic materials. The experimental data shows that the use of four of these CSTRs in series reduced the risk of hydraulic bypass, where a portion of fresh material leaves the reactor after a very short retention time. This meant that a sample taken at a specific point in the system, for example vessel 2 outlet, would be largely composed of material which had spent a known amount of time in the digester. In this case, the age of the material would be half the hydraulic retention time as the sample point was mid-way in the system.

Chapter two data also show that the four-stage digester was reasonably reliable in operation after a few modifications were made during running, and produced a large amount of information on process monitoring and control. However, it would be preferable in the future to construct larger digestate transfer tubing as blockages in these were the source of many problems. The system would also have benefited from the addition of float switches to stop pumping operations when a vessel was overfull.

Data analysed in Chapter 3 demonstrated that it was possible to predict methane production and yield from both the individual vessels from which the data was sourced and the system as a whole using non-linear regression models which fitted curves to the data to. Based on the best curve fitting models, methane production for this specific

feedstock was optimal at an organic loading rate of 2.34 to 2.64 g $VS.L^{-1}$ d^{-1}, pH 6.8 to 7.0, redox potential of -376 to -345 mV, alkalinity between 3850 and 4050 $mg.L^{-1}$ and biogas at 48 % v/v methane. By comparison, methane yield was optimal at a much lower organic loading rate range of 0.89 to 1.16 g $VS.L^{-1}$ d^{-1}, a slightly higher pH of 6.9 to 7.2, a similarly low redox potential of -375 to -353 mV and biogas with hydrogen and methane concentrations of between 446 and 910 ppm and 63.5 % v/v respectively. It was expected that methane yield would be higher at a lower organic loading rate. This is because this corresponded with a longer hydraulic retention time and therefore a greater time to metabolise more of the feedstock. It also follows from this that pH and methane percentage would be higher as the under-loaded system produced fatty acids at slower rate meaning less depletion of buffering capacity and less CO_2 in the biogas.

The four-stage system demonstrated a progression through the stages. It was seen that, during stable operation, pH, alkalinity, biogas methane concentration and conductivity increased through the system, whereas methane production, redox potential and biogas hydrogen concentration decreased. It would be interesting to further explore the variations of hydrogen gas concentration variations which would suddenly fall then rise before the system began to fail. This occurred on two occasions but was not detected by the statistical methods used here, although PCA analysis suggested hydrogen concentration was an important parameter.

It was found that bicarbonate alkalinity gave a good prediction of both methane yield and production by examination of the curve-fitted models. This led to the development of a robust software sensor using the available on-line pH, redox and conductivity probes. Multiple linear regression models were built using all combinations of the probe data from different vessels. It was found that the best model was based on using all three probes and the largest dataset from all the individual vessels combined. This model was of reasonably good fit to the data, with an R^2 (%) of 71 % ($p < 0.001$) and 1441 $mg.L^{-1}$ alkalinity as a standard error. The model was correlated to new titrated alkalinity data with a maximum r^2 of 0.82 ($p < 0.001$) and was therefore considered successful as long as the probes were well maintained.

Potential improvements to the software sensor include changes to both the probes themselves and the data collected. Probes mounted directly into the digester vessels would give a more representative sample of the contents, although the alkalinity titration data used to make the regression models used samples collected from points adjacent to the probes and was therefore representative of the digestate presented to the

probes at that time. Regular cleaning and calibration would still be necessary to ensure reliable operation, although modern industrial probes for use in the waste water industry are self-cleaning. In addition to these modifications, a conductivity probe with a higher maximum value would also be necessary to provide accurate data.

It is also unknown how the software sensor algorithm used here would behave if a different feedstock was used. However, it is believed that the anaerobic digestion intermediates present in the second stage of a two-stage system would be very similar for most feedstocks, after hydrolysis and acidification in the first stage.

Using the software sensor data as the basis of a control system was the ultimate objective of this thesis. The choice of a constant increase / decrease proportional controller with a derivative component was based on the responses seen with artificial alkalinity values in a test version of the control system. The rule based supervisory control system provided a reasonably stable control of the organic loading rate after careful tuning to set the boundaries of the alkalinity sets as well as the correct balance of proportional and derivative components. The system stabilised at organic loading rates of *ca.* 1.5 and 2.0 g $VS.L^{-1}$ d^{-1} for digesters without and with support media respectively, although the latter proved to be the most stable. The relatively low organic loading rates were attributed to the decision to set the desired alkalinity at between 4600 and 5000 $mg.L^{-1}$ HCO_3^-, considerably above the optimal alkalinity range of *ca.* 3800 to 4000 $mg.L^{-1}$ HCO_3^- found in Chapter 3. In addition, the control system would probably benefit from an increased number of sets to make the transitions between organic loading rate increases and decreases less abrupt.

Chapter five showed that the calibration of an FT-NIR spectrometer to predict alkalinity provided a better correlation to the training data than the software sensor, with an R^2 (%) value of 87 % and RMSEP of 1230 $mg.L^{-1}$. Correlating the predicted alkalinity to new data could only give a maximum r^2 correlation of 0.56 ($p < 0.001$). However, the use of NIRS to monitor the anaerobic digestion process was still considered a success. The low correlation with new data was misleading in some ways as the graphical evidence in Figures 5.15 and 5.16 suggest the predicted bicarbonate alkalinity curves followed the shapes of the titrated curves reasonably well. It is acknowledged that the work of Steyer (2002) may have produced a better prediction of total alkalinity when using mid infrared spectroscopy of ultrafiltrated digestate although no R^2 value was quoted in the work.

Further development of the NIRS method of measuring digester stability is required. This would primarily be the development of a better method of presenting samples to the machine. This could be either by using on in-line system where a loop of digestate is pumped past a NIR spectrometer window or an on-line system using a transmittance probe fitted directly through the digester tank. The latter method is preferable as there are likely to be problems with sample tubes blocking or building up a layer of settled solids on the bottom, particularly if the sample loop is constructed from small bore tubing or has a low flow rate. Both methods are suitable for either reflectance or transmission measurements, although transmission measurements require a fixed pathlength of a few millimetres which is generally unsuitable for the relatively large particle sizes common in digester feedstocks without some form of sample preparation.

An increase in the number of measured parameters could also improve the NIRS method of process monitoring. It is possible that a single NIR spectrum (or at least averaged multiple spectra) could be used to measure, for example, VFA, ammonia, alkalinity and total solids for full system monitoring. Thus, in operation, VFA, ammonia and alkalinity could estimate process state and the total solids measurement could be used to indicate problems with mixing equipment.

It is also possible that the NIR spectra be used for discriminate analysis by a chemometric approach rather than direct measurement of specific parameters. Spectra could be obtained for good and bad digester process states, these values then being grouped as sets. New spectra could then be compared with these standards and the Mahalanobis distance between sets calculated to estimate the digester state as good, bad or some specific point between. Mahalanobis distance differs from traditional Euclidean distance in that the three-dimensional shape of the sets are taken into account when calculating distance between sets, rather than just the distance between the set centres.

The method also needs full validation as if it were any other method, particularly if it is to be used for industrial processes where a great deal of responsibility is placed on the accuracy and precision of measurements. It is possible that the data from the NIR spectra may be specific to the digester and feedstock used. This also requires further research for validation. A worst case scenario may be that a calibration needs to be created for each individual digester and feedstock and repeated when the feedstock changes.

So far, research into the use of NIRS in anaerobic digestion has not investigated changes in the feedstock composition. As NIRS measures a variety of parameters in a

sample any changes to the feedstock composition are likely to affect the prediction ability of the model.

Using the parameters measured in Chapter 3, the software sensor developed in Chapter 4 and the NIRS system described in Chapter 5 could potentially lead to full monitoring of the anaerobic digestion process. From Chapter 3, it can be stated that a decrease in pH, an increase in redox potential, a decrease in alkalinity (measured by the software sensor and / or NIRS), an increase in hydrogen concentration and a decrease in the concentration of methane in the biogas are all indicative of process failure. Such inputs would be ideal for a control system such as fuzzy logic, which could add weightings to the various parameters and respond to both the parameter values and the rates of change. Any sudden fluctuations in the above parameters are a cause for concern. A complete control system would respond to such changes by decreasing the loading rate or providing a warning for plant operators. Many full scale plants use separate feed tanks for various feedstocks, and a plant with a wide variety of feedstocks will be more vulnerable to overloading than a plant fed on an largely unchanging supply of feed. If a new feedstock was introduced to a plant, those plants with separate feedstock tanks could reduce the proportion of the new feedstock if addition of this caused a shift towards failure.

The mixing and microbial biomass support media experiments showed that both changes in mixing frequency and the presence of support media affected the production of methane from anaerobic digesters significantly. Methane production increased by over 6.5 % when support media was fitted to single stage digesters, and optimisation of mixing frequency increased methane production by up to 26 %. The optimal mixing frequencies of two and four one minute mixing cycles per hour for single stage digesters without and with support media respectively and frequencies of eight and four cycles per hour for two-stage digesters without and with support media respectively show that the mixing results are important and specific to each system. This is not a problem when transferring the technology to full scale systems, as the experiments only show that optimisation of mixing frequency has a significant effect. A full scale plant could quite easily run similar experiments for a few months to find the optimum frequency of mixing for that specific system. If a reduced mixing frequency increases methane production then the plant benefits from the improved energy output, reduced energy input and reduced maintenance due to limiting the use of the mixer motors. Thus, finding that increasing the mixing frequency produced more methane would have to be

balanced against the increased plant running costs resulting from more use of the mixers.

The addition of support media used in this experiment had less effect than the optimisation of mixing frequency, and therefore the difficulty and cost of fitting an existing plant with the media is unlikely to be worthwhile. It may however be of interest in the construction of new plants, although studies of the optimal material for use and the long term stability of this material need to be carried out.

References

ABB Bomen Inc. 2004. FTLA2000 Series Laboratory FT-IR Spectrometers users guide, ABB Bomen Inc, Québec, Canada.

Ahring, B.K., Sandberg, M., Angelidaki, I., 1995. Volatile fatty acids as indicators of process imbalance in anaerobic digesters. *Applied Microbiology and Biotechnology*, 43, 559-565.

Alatriste-Mondragon, F., Samar, P., Cox, H.H.J., Ahring, B.K., Iranpour, R., 2006. Anaerobic co-digestion of municipal, farm and industrial organic wastes: A survey of recent literature. *Water Environment Research*, 78, 607-636.

Alcaraz-Gonzalez, V., Harmand, J., Rapaport, A., Steyer, J.P., Gonzalez-Alvarez, V., Pelayo-Ortiz, C., 2002. Software sensors for highly uncertain waste water treatment plants: a new approach based on interval observers. *Water Research*, 36, 2515-2524.

Al-Masri, M.R., 2001. Changes in biogas production due to different ratios of some animal and agricultural wastes. *Bioresource Technology*, 77, 97-100.

Altaf, K., Harman, D., McIntyre, S., O'Hara, M., Waite, H., Carney, I., Hillier, K., Melia, A., Thurman, N., Cookson, P., King, D., Munshi, I., Waite, D., 2006. Flexible polyurethane foam, a UK user's guide. British Plastics Federation.

Alvarez-Ramirez, J., Meraz, M., Monroy, O., Velasco, A., 2002. Feedback control design for an anaerobic digestion process. *Journal of Chemical Technology and Biotechnology*, 77, 725-734.

Alzate-Gaviria, L.M., Sebastian, P.J., Perez-Hernandez, A., Eapen, D., 2007. Comparison of two anaerobic systems for hydrogen production from the organic fraction of municipal solid waste and synthetic wastewater. *International Journal of Hydrogen Energy*, 32, 3141-3146.

Amon, T., Amon, B., Kryvoruchko, V., Machmuller, A., Hopfner-Sixt, K., Bodiroza, V., Hrbek, R., Friedel, J., Potsch, E., Wagentristl, H., Schreiner, M., Zollitsch, W., 2007. Methane production through anaerobic digestion of various energy crops grown in sustainable crop rotations. *Bioresource Technology*, 98, 3204-3212.

Amon, T., Amon, B., Kryvoruchko, V., Zollitsch, W., Mayer, K., Gruber, L., 2007. Biogas production from maize and dairy cattle manure - Influence of biomass composition on the methane yield. *Agriculture Ecosystems & Environment*, 118, 173-182.

Anderson, G.K., Campos, C.M.M., Chernicharo, C.A.L., Smith, L.C., 1991. Evaluation of the inhibitory effects of lithium when used as a tracer for anaerobic digesters. *Water Research*, 25, 755-760.

Andersson, J., Bjornsson, L., 2002. Evaluation of straw as a biofilm carrier in the methanogenic stage of two-stage anaerobic digestion of crop residues. *Bioresource Technology*, 85, 51-56.

Andrasik, A., Meszaros, A., de Azevedo, S.E., 2004. On-line tuning of a neural PID controller based on plant hybrid modeling. *Computers & Chemical Engineering*, 28, 1499-1509.

Angelidaki, I., Ahring, B.K., 2000. Methods for increasing the biogas potential from the recalcitrant organic matter contained in manure. *Water Science and Technology*, 41, 189-194.

Angelidaki, I., Ellegaard, L., 2003. Co-digestion of manure and organic wastes in centralised biogas plants - Status and future trends. *Applied Biochemistry and Biotechnology*, 109, 95-105.

Anozie, A.N., Layokun, S.K., Okeke, C.U., 2005. An evaluation of a batch pilot-scale digester for gas production from agricultural wastes. *Energy Sources*, 27, 1301-1311.

APHA, 1976. Standard methods for the examination of water and wastewater. 14 ed. APHA, Washington D.C.

Ardic, I., Taner, F., 2005. Effects of thermal, chemical and thermochemical pre-treatments to increase biogas production yield of chicken manure. *Fresenius Environmental Bulletin*, 14, 373-380.

Arnaiz, C., Buffiere, P., Elmaleh, S., Lebrato, J., Moletta, R., 2003. Anaerobic digestion of dairy wastewater by inverse fluidisation: The inverse fluidised bed and the inverse turbulent bed reactors. *Environmental Technology*, 24, 1431-1443.

Astrom, K.J., Albertos, P., Quevedo, J., 2001. PID control. *Control Engineering Practice*, 9, 1159-1161.

Aye, T.T., Loh, K.C., 2003. Biodegradation of high strength phenolic wastewater in a modified external loop inversed fluidised bed airlift bioreactor (EIFBAB). *Canadian Journal of Chemical Engineering*, 81, 1246-1250.

Babuska, R., Damen, M.R., Hellinga, C., Maarleveld, H., 2003. Intelligent adaptive control of bioreactors. *Journal of Intelligent Manufacturing*, 14, 255-265.

Baloch, M.I., Akunna, J.C., Collier, P.J., 2006. Assessment of morphology for anaerobic-granular particles. *Water Environment Research*, 78, 643-646.

Bendixen, H.J., 1994. Safeguards against pathogens in Danish biogas plants. *Water Science and Technology*, 30, 171-180.

Bernard, O., Hadj-Sadok, Z., Dochain, D., 2000. Software sensors to monitor the dynamics of microbial communities: Application to anaerobic digestion. *Acta Biotheoretica*, 48, 197-205.

Bernard, O., Pollt, M., Hadj-Sadok, Z., Pengov, M., Dochain, D., Estaben, M., Labat, P., 2001. Advanced monitoring and control of anaerobic wastewater treatment plants: software sensors and controllers for an anaerobic digester. *Water Science and Technology*, 43, 175-182.

Bertin, L., Berselli, S., Fava, F., Petrangeli-Papini, M., Marchetti, L., 2004. Anaerobic digestion of olive mill wastewaters in biofilm reactors packed with granular activated carbon and "Manville" silica beads. *Water Research*, 38, 3167-3178.

Beteau, J.F., Otton, V., Hihn, J.Y., Delpech, F., Cheruy, A., 2005. Modelling of anaerobic digestion in a fluidised bed with a view to control. *Biochemical Engineering Journal*, 24, 255-267.

Bjornsson, L., Murto, M., Jantsch, T.G., Mattiasson, B., 2001. Evaluation of new methods for the monitoring of alkalinity dissolved hydrogen and the microbial community in anaerobic digestion. *Water Research*, 35, 2833-2840.

Blanco, M., Coello, J., Iturriaga, H., Maspoch, S., Pagès, J., 1999. Calibration in non-linear near infrared reflectance spectroscopy: a comparison of several methods. *Analytica Chimica Acta*, 384, 2, 207-214.

Boe, K., Batstone, D.J., Angelidaki, I., 2005. Online headspace chromatographic method for measuring VFA in biogas reactor. *Water Science and Technology*, 52, 473-478.

Bolzonella, D., Battistoni, P., Susini, C., Cecchi, F., 2006. Anaerobic codigestion of waste activated sludge and OFMSW: the experiences of Viareggio and Treviso plants (Italy). *Water Science and Technology*, 53, 203-211.

Bonmati, A., Flotats, X., Mateu, L., Campos, E., 2001. Study of thermal hydrolysis as a pre-treatment to mesophilic anaerobic digestion of pig slurry. *Water Science and Technology*, 44, 109-116.

Boone, D.R., Xun, L.Y., 1987. Effects of pH, temperature, and nutrients on propionate degradation by a methanogenic enrichment culture. *Applied and Environmental Microbiology*, 53, 1589-1592.

Borja, R., Rincon, B., Raposo, F., Dominguez, J.R., Millan, F., Martin, A., 2004. Mesophilic anaerobic digestion in a fluidised-bed reactor of wastewater from the production of protein isolates from chickpea flour. *Process Biochemistry,* 39, 1913-1921.

Bos, R., van der Mei, H.C., Busscher, H.J., 1995. A quantitative method to study coadhesion of microorganisms in a parallel flow chamber. II: Analysis of the kinetics of coadhesion. *Journal of Microbiological Methods*, 23, 169-182.

Bossier, P., Poels, J., Vanassche, P., Verstraete, W., 1986. Influence of the dimensional characteristics of polyurethane foam on high-rate anaerobic-digestion of piggery manure. *Biotechnology Letters*, 8, 901-906.

Bouallagui, H., Ben Cheikh, R., Marouani, L., Hamdi, M., 2003. Mesophilic biogas production from fruit and vegetable waste in a tubular digester. *Bioresource Technology*, 86, 85-89.

Bouallagui, H., Torrijos, A., Godon, J.J., Moletta, R., Ben Cheikh, R., Touhami, Y., Delgenes, J.P., Di, A.H., 2004. Two-phase anaerobic digestion of fruit and vegetable wastes: bioreactor performance. *Biochemical Engineering Journal*, 21, 193-197.

Bouallagui, H., Touhami, Y., Cheikh, R.B., Hamdi, M., 2005. Bioreactor performance in anaerobic digestion of fruit and vegetable wastes. *Process Biochemistry*, 40, 989-995.

Bradshaw, D.J., Homer, K.A., Marsh, P.D., Beighton, D., 1994. Metabolic cooperation in oral microbial communities during growth on mucin. *Microbiology*, 140, 3407-3412.

Breitenbucher, K., Siegl, M., Knupfer, A., Radke, M., 1990. Open-pore sintered glass as a high-efficiency support medium in bioreactors - New results and long-term experiences achieved in high-rate anaerobic-digestion. *Water Science and Technology*, 22, 25-32.

Britz, T.J., Van Der Merwe, M., 1993. Anaerobic treatment of baker's yeast effluent using a hybrid digester with polyurethane as support material. *Biotechnology Letters,* 15, 755-760.

Bruker Spectroscopic Software OPUS Quant, 2004. Bruker Optics Limited, Banner Lane, Coventry CV4 9GH, England.

Buchholz, K., Diekmann, H., Jordening, H.J., Pellegrini, A., Zellner, G., 1992. Anaerobic purification of waste-water from sugar production in fluidized-bed reactors. *Chemie Ingenieur Technik*, 64, 556-558.

Buckland, B.C., 1984. The translation of scale in fermentation processes: The impact of computer process control. *Nature Biotechnology*, 2, 875-883.

Bull, M.A., Sterritt, R.M., Lester, J.N., 1983. Response of the anaerobic fluidized bed reactor to transient changes in process parameters. *Water Research*, 17, 1563-1568.

Burton, C.H., Turner, C., 2003. Manure management, treatment strategies for sustainable agriculture. 2nd ed. Silsoe Research Institute.

Busscher, H.J., Cowan, M.M., Van der Mei, H.C., 1992. On the relative importance of specific and non-specific approaches to oral microbial adhesion. *Fems Microbiology Reviews*, 88, 199-200.

Busscher, H.J., Van der Mei, H.C., 2000. Initial microbial adhesion events: mechanisms and implications. in: D.G. Allison, P. Gilbert, H.M. Lappin-Scott, M. Wilson (Eds.), Community structure and co-operation in biofilms. Cambridge University Press, Cambridge, pp. 25-52.

Callaghan, F.J., Wase, D.A.J., Thayanithy, K., Forster, C.F., 1999. Co-digestion of waste organic solids: batch studies. *Bioresource Technology*, 67, 117-122.

Calzada, J.F., Arriola, M.C., Castaneda, H.O., Godoy, J.E., Rolz, C., 1984. Methane from coffee pulp juice: Experiments using polyurethane foam reactors. *Biotechnology Letters*, 6, 385-388.

Cecchi, F., Traverso, P.G., Cescon, P., 1986. Anaerobic-Digestion of Organic Fraction of Municipal Solid-Wastes - Digester Performance. *Science of the Total Environment*, 56, 183-197.

Chae, K.J., Jang, A., Yim, S.K., Kim, I.S., 2008. The effects of digestion temperature and temperature shock on the biogas yields from the mesophilic anaerobic digestion of swine manure. *Bioresource Technology*, 99, 1-6.

Chambers, B.J., Smith, K.A., Pain, B.F., 2000. Strategies to encourage better use of nitrogen in animal manures. *Soil Use and Management*, 16, 157-161.

Chanakya, H.N., Borgaonkar, S., Rajan, M.G.C., Wahi, M., 1993. Two phase fermentation of whole leaf biomass to biogas. *Biomass and Bioenergy*, 5, 5, 359-367.

Chanakya, H.N., Srivastav, G.P., Abraham, A.A., 1998. High rate biomethanation using spent biomass as bacterial support. *Current Science*, 74, 1054-1059.

Chen, S.F., Yakunin, A.F., Kuznetsova, E., Busso, D., Pufan, R., Proudfoot, M., Kim, R., Kim, S.H., 2004. Structural and functional characterization of a novel phosphodiesterase from Methanococcus jannaschii. *Journal of Biological Chemistry*, 279, 31854-31862.

Cho, J.K., Park, S.C., Chang, H.N., 1995. Biochemical methane potential and solid-state anaerobic-digestion of Korean food wastes. *Bioresource Technology*, 52, 245-253.

Chynoweth, D.P., Turick, C.E., Owens, J.M., Jerger, D.E., Peck, M.W., 1993. Biochemical Methane Potential of Biomass and Waste Feedstocks. *Biomass & Bioenergy*, 5, 95-111.

Clarkson, W.W., Xiao, W., 2000. Bench-scale anaerobic bioconversion of newsprint and office paper. *Water Science and Technology*, 41, 93-100.

Coates, J.D., Coughlan, M.F., Colleran, E., 1996. Simple method for the measurement of the hydrogenotrophic methanogenic activity of anaerobic sludges. *Journal of Microbiological Methods*, 26, 237-246.

Cohen, A., Breure, A.M., Vanandel, J.G., Vandeursen, A., 1982. Influence of phase-separation on the anaerobic-digestion of glucose. Part II. Stability and kinetic responses to shock loadings. *Water Research*, 16, 449-455.

Cord-Ruwisch, R., Mercz, T.I., Hoh, C.Y., Strong, G.E., 1997. Dissolved hydrogen concentration as an on-line control parameter for the automated operation and optimization of anaerobic digesters. *Biotechnology and Bioengineering*, 56, 626-634.

Dauhoo, M.Z., Soobhug, M., 2003. An adaptive weighted bisection method for finding roots of non-linear equations. *International Journal of Computer Mathematics*, 80, 7, 897-906.

Damasceno, L.H.S., Rodrigues, J.A.D., Ratusznei, S.M., Zaiat, M., Foresti, E., 2007. Effects of feeding time and organic loading in an anaerobic sequencing batch biofilm reactor (ASBBR) treating diluted whey. *Journal of Environmental Management*, 85, 927-935.

De Baere, L., Boelens, J., 1999. The treatment of grey and mixed solid waste by means of anaerobic digestion: future developments. in: J. MataAlvarez, A. Tilche, F. Cecchi (Eds.), 2nd International Symposium on anaerobic digestion of solid waste, Barcelona, pp. 302-305.

De Baere, L., 2000. Anaerobic digestion of solid waste: state-of-the-art. *Water Science and Technology*, 41, 283-290.

de Bok, F.A.M., Plugge, C.M., Stams, A.J.M., 2004. Interspecies electron transfer in methanogenic propionate degrading consortia. *Water Research*, 38, 1368-1375.

de la Rubia, M.A., Perez, M., Romero, L.I., Sales, D., 2006. Effect of solids retention time (SRT) on pilot scale anaerobic thermophilic sludge digestion. *Process Biochemistry*, 41, 79-86.

De Man, A.W.A., Grin, P.C., Roersma, R.E., Grolle, K.C.F., Lettinga, G., 1986. Anaerobic treatment of municipal waste water at low temperatures. Anaerobic treatment. A grown-up technology. Aquatech '86, Amsterdam.

Demirer, G.N., Chen, S., 2005. Two-phase anaerobic digestion of unscreened dairy manure. *Process Biochemistry*, 40, 3542-3549.

Demirer, G.N., Chen, S.L., 2005. Anaerobic digestion of dairy manure in a hybrid reactor with biogas recirculation. *World Journal of Microbiology & Biotechnology*, 21, 1509-1514.

Denac, M., Griffin, K., Lee, P.L., Greenfield, P.F., 1988. Selection of controlled variables for a high-rate anaerobic reactor. *Environmental Technology Letters*, 9, 1029-1040.

De Visser, H., Huisert, A., Klop, A., Ketelaar, R.S., (1993). Autumn-cut grass silage as roughage component in dairy cow rations. 2. Rumen degradation, fermentation and kinetics. *Netherlands Journal of Agricultural Science*, 41, 221-234.

Di Berardino, S., Costa, S., Converti, A., 2000. Semi-continuous anaerobic digestion of a food industry wastewater in an anaerobic filter. *Bioresource Technology*, 71, 261-266.

Di Pinto, A.C., Limoni, N., Passino, R., Rozzi, A., Tomei, M.C., 1990. Anaerobic process control by automated bicarbonate monitoring. in: R. Briggs (Ed.) Instrumentation, control and automation of water and waste water treatment and transport systems. Advances in water pollution control. Pergamon Press, London, pp. 51-58.

Dohanyos, M., Zabranska, J., Jenicek, P., 1997. Enhancement of sludge anaerobic digestion by using of a special thickening centrifuge. *Water Science and Technology*, 36, 145-153.

Dugba, P.N., Zhang, R. 1999. Treatment of dairy wastewater with two-stage anaerobic sequencing batch reactor systems — thermophilic versus mesophilic operations. *Bioresource Technology*, 38, 225-233.

Dunn, M.J., 1992. Protein determination of total protein concentration. in: E.L.V. Harris, S. Angal (Eds.), Protein Purification Methods. IRL Press, Oxford.

Elmitwalli, T.A., Oahn, K.L.T., Zeeman, G., Lettinga, G., 2002. Treatment of domestic sewage in a two-step anaerobic filter / anaerobic hybrid system at low temperature. *Water Research*, 36, 2225-2232.

Esbensen, K.H., Friis-Petersen, H.H., Petersen, L., Holm-Nielsen, J.B., Mortensen, P.P., 2007. Representative process sampling – in practice: Variographic analysis and estimation of total sampling errors (TSE). *Chemometrics and Intelligent Laboratory Systems*, 88, 41-59.

Fang, H.H.P., Chung, D.W.C., 1999. Anaerobic treatment of proteinaceous wastewater under mesophilic and thermophilic conditions. *Water Science and Technology*, 40, 77-84.

Farhan, M.H., ChinHong, P.H., Keenan, J.D., Shieh, W.K., 1997. Performance of anaerobic reactors during pseudo-steady-state operation. *Journal of Chemical Technology and Biotechnology*, 69, 45-57.

Fazolo, A., Foresti, E., Zaiat, M., 2007. Removal of nitrogen and organic matter in a radial-flow aerobic-anoxic immobilized Biomass reactor used in the post-treatment of anaerobically treated effluent. *Applied Biochemistry and Biotechnology*, 142, 44-51.

Feitkenhauer, H., von Sachs, E., Meyer, U., 2002. On-line titration of volatile fatty acids for the process control of anaerobic digestion plants. *Water Research*, 36, 212-218.

Feitkenhauer, H., Meyer, U., 2003. A new method for the fast determination of kinetic parameters in anaerobic digestion processes and application to textile wet processing wastewater. *Water Science and Technology*, 48, 203-210.

Feitkenhauer, H., Meyer, U., 2004. Software sensors based on titrimetric techniques for the monitoring and control of aerobic and anaerobic bioreactors. *Biochemical Engineering Journal*, 17, 147-151.

Femat, R., Mendez-Acosta, H.O., Steyer, J.P., Gonzalez-Alvarez, V., 2004. Temperature oscillations in a biological reactor with recycle. *Chaos Solitons & Fractals*, 19, 875-889.

Ferrec, Y., Taboury, J., Sauer, H., Chavel, P., 2006. Optimal geometry for Sagnac and Michelson interferometers used as spectral imagers. *Optical Engineering*, 45, 11,

Fezzani, B., Ben Cheikh, R., 2007. Thermophilic anaerobic co-digestion of olive mill wastewater with olive mill solid wastes in a tubular digester. *Chemical Engineering Journal*, 132, 195-203.

Ficara, E., Rozzi, A., Cortelezzi, P., 2003. Theory of pH-stat titration. *Biotechnology and Bioengineering*, 82, 28-37.

Forster-Carneiro, T., Perez, M., Romero, L.I., Sales, D., 2007. Dry-thermophilic anaerobic digestion of organic fraction of the municipal solid waste: Focusing on the inoculum sources. *Bioresource Technology*, 98, 3195-3203.

Frigon, J.C., Guiot, S.R., 1995. Impact of liquid-to-gas hydrogen mass transfer on substrate conversion efficiency of an upflow anaerobic sludge bed and filter reactor. *Enzyme and Microbial Technology*, 17, 1080-1086.

Frolund, B., Griebe, T., Nielsen, P.H., 1995. Enzymatic-Activity in the Activated-Sludge Floc Matrix. *Applied Microbiology and Biotechnology*, 43, 755-761.

Fukuzaki, S., Nishio, N., Nagai, S., 1990. The use of polyurethane foam for microbial retention in methanogenic fermentation of propionate. *Applied Microbiology and Biotechnology*, 34, 408-413.

Funk, T., Gu, W.W., Friedrich, S., Wang, H.X., Gencic, S., Grahame, D.A., Cramer, S.P., 2004. Chemically distinct Ni sites in the A-cluster in subunit beta of the Acetyl-CoA decarbonylase/synthase complex from Methanosarcina thermophila: Ni L-edge absorption and x-ray magnetic circular dichroism analyses. *Journal of the American Chemical Society*, 126, 88-95.

Fynn, G.H., Whitmore, T.N., 1982. Colonization of polyurethane reticulated foam biomass support particle by methanogen species. *Biotechnology Letters*, 4, 577-582.

Fynn, G.H., Whitmore, T.N., 1984. Retention of methanogens in colonized reticulated polyurethane foam biomass support particle. *Biotechnology Letters*, 6, 81-86.

Gannoun, H., Ben Othman, N., Bouallagui, H., Moktar, H., 2007. Mesophilic and thermophilic anaerobic co-digestion of olive mill wastewaters and abattoir

wastewaters in an upflow anaerobic filter. *Industrial & Engineering Chemistry Research*, 46, 6737-6743.

Gaudy, A.F., 1962. Colorimetric determination of protein and carbohydrate. *Industrial Water Wastes*, 7, 17-22.

Genovesi, A., Harmand, J., Steyer, J.P., 1999. A fuzzy logic based diagnosis system for the on-line supervision of an anaerobic digester pilot-plant. *Biochemical Engineering Journal*, 3, 171-183.

Gerardi, M.H., 2003. The Microbiology of Anaerobic Digesters. 1 ed. Wiley - Interscience.

Gershenfeld, A., 1999. The nature of mathematical modelling. Cambridge University Press, Cambridge, pp147-148.

Ghosh, S., Conrad, J. R., Klass, D.L., 1975. Anaerobic acidogenesis of sewage sludge. *Journal of Water Pollution Control Fed.* 47, 30.

Ghosh, S., Henry, M. P., 1981. Stabilization and gasification of soft-drink manufacturing waste by conventional and two-phase anaerobic digestion. *Proceedings of the 36th Industrial Waste Conference*, Purdue University.

Ghosh, S., Ombregt, J. P., Pipyn, P., 1985. Methane production from industrial wastes by two-phase anaerobic digestion. *Water Research*, 19, 9, 1083-1088.

Ghosh, S., 1997. Anaerobic digestion for renewable energy and environmental restoration. 8th International Conference on Anaerobic Digestion., Sendai International Center, Sendai, Japan., pp. 9-16.

Gijzen, H.J., Schoenmakers, T.J.M., Caerteling, C.G.M., Vogels, G.D., 1988. Anaerobic degradation of papermill sludge in a two-phase digester containing rumen microorganisms and colonized polyurethane foam. *Biotechnology Letters*, 10, 61-66.

Gijzen, H.J., Kansiime, F., 1996. Comparison of start-up of an upflow anaerobic sludge blanket reactor and a polyurethane carrier reactor. *Water Science and Technology*, 34, 509-515.

Givens, D.I., DeBoever, J.L., Deaville, E.R., 1997. The principles, practices and some future applications of near infrared spectroscopy for predicting the nutritive value of foods for animals and humans. *Nutrition Research Reviews*, 10, 83-114.

Givens, D.I., Deaville, E.R., 1999. The current and future role of near infrared reflectance spectroscopy in animal nutrition: a review. *Australian Journal of Agricultural Research*, 50, 1131-1145.

Gizachew, L., Smit, G.N., 2005. Crude protein and mineral composition of major crop residues and supplemental feeds produced on Vertisols of the Ethiopian highland. *Animal Feed Science and Technology*, 119, 143-153.

Gomec, C.Y., 2006. Behaviour of the anaerobic CSTR in the presence of scum during primary sludge digestion and the role of pH. *Journal of Environmental Science and Health Part a-Toxic/Hazardous Substances & Environmental Engineering*, 41, 1117-1127.

Gomez, X., Cuetos, M.J., Cara, J., Moran, A., Garcia, A.I., 2006. Anaerobic co-digestion of primary sludge and the fruit and vegetable fraction of the municipal solid wastes - Conditions for mixing and evaluation of the organic loading rate. *Renewable Energy*, 31, 2017-2024.

Gomez-Lahoz, C., Fernandez-Gimenez, B., Garcia-Herruzo, F., Rodriguez-Maroto, J.M., Vereda-Alonso, C., 2007. Biomethanization of mixtures of fruits and vegetables solid wastes and sludge from a municipal wastewater treatment plant. *Journal of Environmental Science and Health Part a-Toxic/Hazardous Substances & Environmental Engineering*, 42, 481-487.

Gujer, W., Zehnder, A.J.B. 1983. Conversion processes in anaerobic digestion. *Water Science and Technology*, 15, 127-167.

Gunaseelan, V.N., 1994. Methane production from parthenium-hysterophorus L, a terrestrial weed, in semicontinuous fermenters. Biomass & Bioenergy, 6, 391-398.

Gunaseelan, V.N., 1995. Effect of inoculum substrate ratio and pre-treatments on methane yield from Parthenium. *Biomass & Bioenergy*, 8, 39-44.

Guwy, A.J., Hawkes, F.R., Wilcox, S.J., Hawkes, D.L., 1997. Neural network and on-off control of bicarbonate alkalinity in a fluidised-bed anaerobic digester. *Water Research*, 31, 2019-2025.

Guwy, A.J., Hawkes, F.R., Hawkes, D.L., Rozzi, A.G., Hydrogen production in a high rate fluidised bed anaerobic digester. *Water Research*, 31, 1921-1928.

Hansen, K.H., Angelidaki, I., Ahring, B.K., 1998. Anaerobic digestion of swine manure: Inhibition by ammonia. *Water Research*, 32, 5-12.

Hansson, M., Nordberg, A., Mathisen, B., 2003. On-line NIR monitoring during anaerobic treatment of municipal solid waste. *Water Science and Technology*, 48, 9-13.

Harper, S.R. & Pohland, F.G., 1986. Recent development in hydrogen management during anaerobic biological waste water treatment. *Biotechnology and Bioengineering*, 28, 585-602.

Hartmann, H., Ahring, B.K., 2005. Anaerobic digestion of the organic fraction of municipal solid waste: Influence of co-digestion with manure. *Water Research*, 39, 1543-1552.

Hashimoto, A.G., Varel, V.H., Chen, Y.R., 1981. Ultimate Methane Yield from Beef-Cattle Manure - Effect of Temperature, Ration Constituents, Antibiotics and Manure Age. *Agricultural Wastes*, 3, 241-256.

Hawkes, F.R., Guwy, A.J., Rozzi, A.G., Hawkes, D.L., 1993. A new instrument for online measurement of bicarbonate alkalinity. *Water Research*, 27, 167-170.

Heertjes, P.M., Vandermeer, R.R., 1978. Dynamics of liquid flow in an up-flow reactor used for anaerobic treatment of wastewater. *Biotechnology and Bioengineering*, 20, 1577-1594.

Hegde, G., Pullammanappallil, P., 2007. Comparison of thermophilic and mesophilic one-stage, batch, high-solids anaerobic digestion. *Environmental Technology*, 28, 361-369.

Hill, D.T., Bolte, J.P., 1992. Bioretentive properties of synthetic media for anaerobic-digestion of animal waste. *Transactions of the Asae*, 35, 711-715.

Hills, D.J., Roberts, D.W., 1982. Conversion of tomato, peach and honeydew solid-waste into methane gas. *Transactions of the Asae*, 25, 820-826.

HMSO, 1978. The measurement of electrical conductivity and the laboratory determination of the pH value of natural, treated and waste waters. Her Majesty's Stationery Office, London.

Holm-Nielsen, J. B., Dahl, C. K., Esbensen, K. H., 2006. Representative sampling for process analytical characterization of heterogeneous bioslurry systems - a reference study of sampling issues in PAT. *Chemometrics and Intelligent Laboratory Systems*, 83, 114-126.

Holm-Nielsen, J.B., Andree, H., Lindorfer, H., Esbensen, K.H., 2007. Transflexive embedded near infrared monitoring for key process intermediates in anaerobic digestion/biogas production. *Journal of near Infrared Spectroscopy*, 15, 123-135.

Holm-Nielsen, J.B., Lomberg, C.J., Oleskowicz-Popiel, P., Esbensen, K.H. 2008. On-line near infrared monitoring of glycerol-boosted anaerobic digestion processes:

Evaluation of process analytical technologies. *Biotechnology and Bioengineering*, 99, 302-313.

Holubar, P., Zani, L., Hager, M., Froschl, W., Radak, Z., Braun, R., 2000. Modelling of anaerobic digestion using self-organizing maps and artificial neural networks. *Water Science and Technology*, 41, 149-156.

Holubar, P., Zani, L., Hager, M., Froschl, W., Radak, Z., Braun, R., 2002. Advanced controlling of anaerobic digestion by means of hierarchical neural networks. *Water Research*, 36, 2582-2588.

Holubar, P., Zani, L., Hager, M., Frochl, W., Radak, Z., Braun, R., 2003. Start-up and recovery of a biogas-reactor using a hierarchical neural network-based control tool. *Journal of Chemical Technology and Biotechnology*, 78, 847-854.

Hu, Z.H., Yu, H.Q., 2005. Application of rumen micro organisms for enhanced anaerobic fermentation of corn stover. *Process Biochemistry*, 40, 2371-2377.

Hu, Z.H., Yu, H.Q., 2006. Anaerobic digestion of cattail by rumen cultures. *Waste Management*, 26, 1222-1228.

Huang, J.S., Chou, H.H., Ohara, R., Wu, C., 2006. Consecutive reaction kinetics involving a layered structure of the granule in UASB reactors. *Water Research*, 40, 2947-2957.

Husted, S., 1994. Seasonal-variation in methane emission from stored slurry and solid manures. *Journal of Environmental Quality*, 23, 585-592.

Inanc, B., Matsui, S., Ide, S., 1996. Propionic acid accumulation and controlling factors in anaerobic treatment of carbohydrate: effects of H_2 and pH. *Water Science and Technology*, 34, (5-6), 317-325.

Jantsch, T.G., Mattiasson, B., 2003. A simple spectrophotometric method based on pH-indications for monitoring partial and total alkalinity in anaerobic processes. *Environmental Technology*, 24, 1061-1067.

Jantsch, T.G., Mattiasson, B., 2004. An automated spectrophotometric system for monitoring buffer capacity in anaerobic digestion processes. *Water Research*, 38, 3645-3650.

Jenkins, S.R., Morgan, J.M., Zhang, X., 1991. Measuring the usable carbonate alkalinity of operating anaerobic digesters. *Research Journal of the Water Pollution Control Federation*, 63, 28-34.

Kalyuzhnyi, S.V., 1997. Batch anaerobic digestion of glucose and its mathematical modelling .2. Description, verification and application of model. *Bioresource Technology*, 59, 249-258.

Karim, K., Hoffmann, R., Klasson, K.T., Al-Dahhan, M.H., 2005. Anaerobic digestion of animal waste: Effect of mode of mixing. *Water Research*, 39, 3597-3606.

Kim, J., Park, C., Kim, T.H., Lee, M., Kim, S., Kim, S.W., Lee, J., 2003. Effects of various pre-treatments for enhanced anaerobic digestion with waste activated sludge. *Journal of Bioscience and Bioengineering*, 95, 271-275.

Kim, M., Ahn, Y.H., Speece, R.E., 2002. Comparative process stability and efficiency of anaerobic digestion; mesophilic vs. thermophilic. *Water Research*, 36, 4369-4385.

Kim, M., Gomec, C.Y., Ahn, Y., Speece, R.E., 2003. Hydrolysis and acidogenesis of particulate organic material in mesophilic and thermophilic anaerobic digestion. *Environmental Technology*, 24, 1183-1190.

Kivaisi, A.K., Elipenda, S., 1995. Application of rumen microorganisms for enhanced anaerobic degradation of bagasse and maize bran. *Biomass and Bioenergy,* 8, 1, 45-50.

Kivaisi, A.K., Gijzen, H.J., Dencamp, H.J.M.O., Vogels, G.D., 1992. Conversion of cereal residues into biogas in a rumen-derived process. *World Journal of Microbiology & Biotechnology*, 8, 428-433.

Kivaisi, A.K., Mtila, M., 1998. Production of biogas from water hyacinth (Eichhornia crassipes) (Mart) (Solms) in a two-stage bioreactor. *World Journal of Microbiology & Biotechnology*, 14, 125-131.

Kizilkaya, R., Bayrakli, B., 2005. Effects of N-enriched sewage sludge on soil enzyme activities. *Applied Soil Ecology*, 30, 192-202.

Knezevic, Z., Mavinic, D.S., Anderson, B.C., 1995. Pilot-scale evaluation of anaerobic co-digestion of primary and pre-treated waste activated-sludge. *Water Environment Research*, 67, 835-841.

Knol, W., Vandermost, M.M., Waart, J.D., 1978. Biogas production by anaerobic digestion of fruit and vegetable waste - Preliminary-study. *Journal of the Science of Food and Agriculture*, 29, 822-830.

Korenaga, T., Takahashi, T., Moriwake, T., Sanuki, S., 1990. Water quality monitoring system using flow-through sensing device. in: R. Briggs (Ed.) Instrumentation,

control and automation of water and waste water treatment and transport systems. Advances in water pollution control. Pergamon press., London.

Kumar, A., Miglani, P., Gupta, R.K., Bhattacharya, T.K., 2006. Impact of Ni(II), Zn(II) and Cd(II) on biogassification of potato waste. *Journal of Environmental Biology*, 27, 61-66.

Kunte, D.P., Yeole, T.Y., Ranade, D.R., 2004. Two-stage anaerobic digestion process for complete inactivation of enteric bacterial pathogens in human night soil. *Water Science and Technology*, 50, 103-108.

Lahav, O., Morgan, B.E., 2004. Titration methodologies for monitoring of anaerobic digestion in developing countries - a review. *Journal of Chemical Technology and Biotechnology*, 79, 1331-1341.

Lardon, L., Punal, A., Steyer, J.P., 2004. On-line diagnosis and uncertainty management using evidence theory - Experimental illustration to anaerobic digestion processes. *Journal of Process Control*, 14, 747-763.

Lettinga, G., Vanvelsen, A.F.M., Hobma, S.W., Dezeeuw, W., Klapwijk, A., 1980. Use of the upflow sludge blanket (USB) reactor concept for biological wastewater-treatment, especially for anaerobic treatment. *Biotechnology and Bioengineering*, 22, 699-734.

Lettinga, G., Hobma, S.W., Pol, L.W.H., Dezeeuw, W., Dejong, P., Grin, P., Roersma, R., 1983. Design Operation and Economy of Anaerobic Treatment. *Water Science and Technology*, 15, 177-195.

Lettinga, G., 1995. Anaerobic-Digestion and Waste-Water Treatment Systems. Antonie Van Leeuwenhoek International *Journal of General and Molecular Microbiology*, 67, 3-28.

Levenspiel, O., 1999. Chemical reaction engineering. 3rd ed. Wiley., New York.

Lima, C.A.A., Ribeiro, R., Foresti, E., Zaiat, M., 2005. Morphological study of biomass during the start-up period of a fixed-bed anaerobic reactor treating domestic sewage. *Brazilian Archives of Biology and Technology*, 48, 841-849.

Lissens, G., Thomsen, A.B., De Baere, L., Verstraete, W., Ahring, B.K., 2004. Thermal wet oxidation improves anaerobic biodegradability of raw and digested biowaste. *Environmental Science & Technology*, 38, 3418-3424.

Lissens, G., Verstraete, W., Albrecht, T., Brunner, G., Creuly, C., Seon, J., Dussap, G., Lasseur, C., 2004. Advanced anaerobic bioconversion of lignocellulosic waste for

bioregenerative life support following thermal water treatment and biodegradation by Fibrobacter succinogenes. *Biodegradation*, 15, 173-183.

Liu, D.W., Liu, D.P., Zeng, R.J., Angelidaki, I., 2006. Hydrogen and methane production from household solid waste in the two-stage fermentation process. *Water Research*, 40, 2230-2236.

Liu, G.T., Peng, X.Y., Long, T.R., 2006. Advance in high-solid anaerobic digestion of organic fraction of municipal solid waste. *Journal of Central South University of Technology*, 13, 151-157.

Liu, H., Fang, H.H.P., 2002. Extraction of extracellular polymeric substances (EPS) of sludges. *Journal of Biotechnology*, 95, 249-256.

Liu, J., Olsson, G., Mattiasson, B., 2004. Control of an anaerobic reactor towards maximum biogas production. *Water Science and Technology*, 50, 189-198.

Liu, J., Olsson, G., Mattiasson, B., 2004. Monitoring and control of an anaerobic upflow fixed-bed reactor for high-loading-rate operation and rejection of disturbances. *Biotechnology and Bioengineering*, 87, 43-53.

Liu, J., Olsson, G., Mattiasson, B., 2004. On-line monitoring of a two-stage anaerobic digestion process using a BOD analyzer. *Journal of Biotechnology*, 109, 263-275.

Liu, Y., Tay, J.H., 2002. The essential role of hydrodynamic shear force in the formation of biofilm and granular sludge. *Water Research*, 36, 1653-1665.

Liu, Y., Xu, H.L., Yang, S.F., Tay, J.H., 2003. Mechanisms and models for anaerobic granulation in upflow anaerobic sludge blanket reactor. *Water Research*, 37, 661-673.

Liu, Y.Q., Liu, Y., Tay, J.H., 2004. The effects of extracellular polymeric substances on the formation and stability of biogranules. *Applied Microbiology and Biotechnology*, 65, 143-148.

Lowry, O.H., Rosebrough, N.J., Farr, A.L., Randall, R.J., 1951. Protein measurement with the Folin phenol reagent. *Journal of Biological Chemistry*, 193, 265-275.

Lund, B., Jensen, V.F., Have, P., Ahring, B., 1996. Inactivation of virus during anaerobic digestion of manure in laboratory scale biogas reactors. *Antonie Van Leeuwenhoek International Journal of General and Molecular Microbiology*, 69, 25-31.

Luyben, W.L., 1990. Process modelling. Simulation and control for chemical engineering. 2 ed. McGraw-Hill, New York.

Macarie, H., 2000. Overview of the application of anaerobic treatment to chemical and petrochemical wastewaters. *Water Science and Technology*, 42, 201-213.

Malley, D. F., Yesmin, L., Eilers, R. G., 2002. Rapid analysis of hog manure and manure-amended soils using near-infrared spectroscopy. *Journal of the American Soil Science Society*, 66, 1677-1686.

Malley, D.F., McClure, C., Martin, P.D., Buckley, K., McCaughey, W.P., 2005. Compositional analysis of cattle manure during composting using a field-portable near-infrared spectrometer. *Communications in Soil Science and Plant Analysis*, 36, 455-475.

Mao, T., Hong, S.Y., Show, K.Y., Tay, J.H., Lee, D.J., 2004. A comparison of ultrasound treatment on primary and secondary sludges. *Water Science and Technology*, 50, 91-97.

Maqueda, C., Perez-Rodriguez, J.L., Lebrato, J., 1998. An evaluation of clay minerals as support materials in anaerobic digesters. *Environmental Technology*, 19, 811-819.

MarsiliLibelli, S., Beni, S., 1996. Shock load modelling in the anaerobic digestion process. *Ecological Modelling*, 84, 215-232.

Martin, D.J., 2001. Accelerated biogas production without leachate recycle. *Renewable Energy*, 24, 535-538.

Martin, D.J., Potts, L.G.A., Heslop, V.A., 2003. Reaction mechanisms in solid-state anaerobic digestion - I. The reaction front hypothesis. *Process Safety and Environmental Protection*, 81, 171-179.

Martin, D.J., Potts, L.G.A., Heslop, V.A., 2003. Reaction mechanisms in solid-state anaerobic digestion - II. The significance of seeding. *Process Safety and Environmental Protection*, 81, 180-188.

Mata-Alvarez, J., 2002. Biomethanization of the organic fraction of municipal solid wastes. IWA Publishing.

Mathiot, S., Escoffier, Y., Ehlinger, F., Couderc, J.P., Leyris, J.P., Moletta, R., 1992. Control parameter variations in an anaerobic fluidized-bed reactor subjected to organic shock loads. *Water Science and Technology*, 25, 93-101.

McCarty, G.W., Reeves, J.B., Reeves, V.B., Follett, R.F., Kimble, J.M., 2002. Mid-infrared and near-infrared diffuse reflectance spectroscopy for soil carbon measurement. *Soil Science Society of America Journal*, 66, 640–646.

McInerney, M.J., Mackie, R.I., Bryant, M.P., 1981. Syntrophic association of a butyrate-degrading bacterium and methanosarcina enriched from bovine rumen fluid. *Applied Environmental Microbiology*, 41, (3) 826-828.

McMahon, K.D., Stroot, P.G., Mackie, R.I., Raskin, L., 2001. Anaerobic co-digestion of municipal solid waste and biosolids under various mixing conditions - II: Microbial population dynamics. *Water Research*, 35, 1817-1827.

Melidis, P., Georgiou, D., Aivasidis, A., 2003. Scale-up and design optimization of anaerobic immobilized cell reactors for wastewater treatment. *Chemical Engineering and Processing*, 42, 897-908.

Mendez, R., Omil, F., Soto, M., Lema, J.M., 1992. Pilot-plant studies on the anaerobic treatment of different wastewaters from a fish-canning factory. *Water Science and Technology*, 25, 37-44.

Meredith, W.D., 1990. Recent innovations in instrumentation for sewage treatment plant monitoring and control. in: R. Briggs (Ed.) Instrumentation, control, and automation of water and waste water treatment and transport Systems. Advances in water pollution control. Pergamon press., London.

Mijaylova-Nacheva, P., Pena-Loera, B., Cuevas-Velasco, S., 2006. Anaerobic treatment of organic chemical wastewater using packed bed reactors. *Water Science and Technology*, 54, 67-77.

Mishima, D., Tateda, M., Ike, M., Fujita, M., 2006. Comparative study on chemical pre-treatments to accelerate enzymatic hydrolysis of aquatic macrophyte biomass used in water purification processes. *Bioresource Technology*, 97, 2166-2172.

Mladenovska, Z., Hartmann, H., Kvist, T., Sales-Cruz, M., Gani, R., Ahring, B.K., 2006. Thermal pre-treatment of the solid fraction of manure: impact on the biogas reactor performance and microbial community. *Water Science and Technology*, 53, 59-67.

Moletta, R., 2005. Winery and distillery wastewater treatment by anaerobic digestion *Water Science and Technology*, 51, 1, 137-144.

Moller, H.B., Sommer, S.G., Ahring, B.K., 2004. Biological degradation and greenhouse gas emissions during pre-storage of liquid animal manure. *Journal of Environmental Quality*, 33, 27-36.

Moller, H.B., Sommer, S.G., Ahring, B.K., 2004. Methane productivity of manure, straw and solid fractions of manure. *Biomass & Bioenergy*, 26, 485-495.

Moosbrugger, R.E., Wentzel, M.C., Ekama, G.A., Marais, G.V., 1993. A 5 pH point titration method for determining the carbonate and SCFA weak acid bases in anaerobic systems. *Water Science and Technology*, 28, 237-245.

Morel, E., Tartakovsky, B., Guiot, S.R., Perrier, M., 2006. Design of a multi-model observer-based estimator for anaerobic reactor monitoring. *Computers & Chemical Engineering*, 31, 78-85.

Mosey, F.E., Fernandes, X.A., 1989. Patterns of hydrogen in biogas from the anaerobic-digestion of milk-sugars. *Water Science and Technology*, 21, 187-196.

Mouneimne, A.H., Carrere, H., Bernet, N., Delgenes, J.P., 2003. Effect of saponification on the anaerobic digestion of solid fatty residues. *Bioresource Technology*, 90, 89-94.

Mshandete, A., Bjornsson, L., Kivaisi, A.K., Rubindamayugi, M.S.T., Mattiasson, B., 2006. Effect of particle size on biogas yield from sisal fibre waste. *Renewable Energy*, 31, 2385-2392.

Nachaiyasit, S., Stuckey, D.C., 1997. The effect of shock loads on the performance of an anaerobic baffled reactor (ABR). 2. Step and transient hydraulic shocks at constant feed strength. *Water Research*, 31, 2747-2754.

Nallathambi Gunaseelan, V., 2004. Biochemical methane potential of fruits and vegetable solid waste feedstocks *Biomass & Bioenergy*, 26, 389-399.

Nebot, E., Romero, L.I., Quiroga, J.M., Sales, D., 1995. Effect of the feed frequency on the performance of anaerobic filters. *Anaerobe*, 1, 113-120.

Nielsen, H.B., Mladenovska, Z., Westermann, P., Ahring, B.K., 2004. Comparison of two-stage thermophilic (68 degrees C / 55 degrees C) anaerobic digestion with one-stage thermophilic (55 degrees C) digestion of cattle manure. *Biotechnology and Bioengineering*, 86, 291-300.

Nielsen, H.B., Uellendahl, H., Ahring, B.K., 2007. Regulation and opimization of the biogas process: Propionate as a key parameter. *Biomass and Bioenergy*, 31, 820-830.

Nielsen, V.C., 1985. Installation and operation of digesters on farms. in: B.F. Pain, R.Q. Hepherd (Eds.), Anaerobic digestion of farm waste. NIRD Technical Bulletins, Reading, pp. 87-95.

Nordberg, A., Hansson, M., Sundh, I., Nordkvist, E., Carlsson, H., Mathisen, B., 2000. Monitoring of a biogas process using electronic gas sensors and near-infrared spectroscopy (NIR). *Water Science and Technology*, 41, 1-8.

OKeefe, D.M., Owens, J.M., Chynoweth, D.P., 1996. Anaerobic composting of crab-picking wastes for by-product recovery. *Bioresource Technology*, 58, 265-272.

Oldshue, 1966. Fermentation mixing scale-up techniques. *Biotechnology and Bioengineering*, 8, 3-24.

Olivet, D., Valls, J., Gordillo, M.A., Freixo, A., Sanchez, A., 2005. Application of residence time distribution technique to the study of the hydrodynamic behaviour of a full-scale wastewater treatment plant plug-flow bioreactor. *Journal of Chemical Technology and Biotechnology*, 80, 425-432.

Olsson, G., Nielsen, M.K., Yuan, Z., Lynggaard-Jensen, A., Steyer, J.P., 2005. Instrumentation, control and automation in wastewater systems. IWA Publishing.

Ong, H.K., Greenfield, P.F., Pullammanappallil, P.C., 2002. Effect of mixing on biomethanation of cattle-manure slurry. *Environmental Technology*, 23, 1081-1090.

Owen, W.F., Stuckey, D.C., Healy, J.B., Young, L.Y., McCarty, P.L., 1979. Bioassay for monitoring biochemical methane potential and anaerobic toxicity. *Water Research*, 13, 485-492.

Owens, J.M., Chynoweth, D.P., 1993. Biochemical methane potential of municipal solid-waste (MSW) components. *Water Science and Technology*, 27, 1-14.

Paavola, T., Syvasalo, E., Rintala, J., 2006. Co-digestion of manure and biowaste according to the EC animal by-products regulation and Finnish national regulations. *Water Science and Technology*, 53, 223-231.

Pain, B.F., Hepherd, R.Q., 1985. Anaerobic digestion of livestock wastes. in: B.F. Pain, R.Q. Hepherd (Eds.), Anaerobic digestion of farm waste. NIRD Technical Bulletins, Reading, pp. 9-14.

Parawira, W., Murto, M., Read, J.S., Mattiasson, B., 2007. A study of two-stage anaerobic digestion of solid potato waste using reactors under mesophilic and thermophilic conditions. *Environmental Technology*, 28, 1205-1216.

Parr, J.F., Hornick, S.B., 1993. Utilization of municipal wastes. in: F.B. Metting (Ed.) Soil microbial ecology. Marcel Dekker, Inc., New York, pp. 545-559.

Pauss, R., Guiot, S., 1993. Hydrogen Monitoring in Anaerobic Sludge Bed Reactors at Various Hydraulic Regimes and Loading Rates. *Water Environment Research*, 65, 276-280.

Pauss, R., Samson, R., Guiot, S., 1990. Continuous measurement of dissolved H_2 in an anaerobic reactor using a new hydrogen fuel cell detector. *Biotechnology and Bioengineering,* 35, 492-501.

Pavlostathis, S.G., Giraldo-Gomez, E., 1991. Kinetics of anaerobic treatment: A critical review. *Critical Reviews in Environmental Control,* 21, 411–490.

Perez, M., Romero, L.I., Nebot, E., Sales, D., 1997. Colonisation of a porous sintered-glass support in anaerobic thermophilic bioreactors. *Bioresource Technology*, 59, 177-183.

Perez, M., Romero, L.I., Rodriguez-Cano, R., Sales, D., 2006. Anaerobic thermophilic colonization of porous support. *Chemical and Biochemical Engineering Quarterly*, 20, 203-208.

Perez, M., Romero, L.I., Sales, D., 2001. Organic matter degradation kinetics in an anaerobic thermophilic fluidised bed bioreactor. *Anaerobe,* 7, 1, 25-35.

Perez-Garcia, M., Romero-Garcia, L.I., Rodriguez-Cano, R., Sales-Marquez, D., 2005. High rate anaerobic thermophilic technologies for distillery wastewater treatment. *Water Science and Technology*, 51, 191-198.

Petersson, A., Thomsen, M.H., Hauggaard-Nielsen, H., Thomsen, A.B., 2007. Potential bioethanol and biogas production using lignocellulosic biomass from winter rye, oilseed rape and faba bean. *Biomass & Bioenergy*, 31, 812-819.

Pind, P. F., Angelidaki, I., Ahring, B. K., 2003. Dynamics of the anaerobic process: Effects of volatile fatty acids. *Biotechnology and Bioengineering* 82, 7, 791-801.

Pinho, S.C., Foresti, E., Zaiat, M., 2006. Degradation of partially soluble wastewater in an anaerobic sequencing batch biofilm reactor: role of impeller type. *Environmental Engineering Science*, 23, 803-813.

Pinho, S.C., Ratusznei, S.M., Rodrigues, J.A.D., Foresti, E., Zaiat, M., 2004. Influence of the agitation rate on the treatment of partially soluble wastewater in anaerobic sequencing batch biofilm reactor. *Water Research*, 38, 4117-4124.

Poels, J., Vanassche, P., Verstraete, W., 1984. High-rate anaerobic-digestion of piggery manure with polyurethane sponges as support material. *Biotechnology Letters*, 6, 747-752.

Pohland, F.G., 1992. Anaerobic treatment: fundamental concepts, applications and new horizons. In: Design of anaerobic processes for the treatment of industrial and municipal wastes. Ed. Malina, J.F., Pohland, F.G. Technomic Pub. Co.

Pohland, F.G., Bloodgood, D.E., 1963. Laboratory studies on mesophilic and thermophilic anaerobic sludge digestion. *Journal of Water Pollution Control Federation*, 35, 1, 11-42.

Pohland, F. G., Ghosh, S., 1971. Developments in anaerobic treatment processes. in: R. P. Canale (Ed.) Biological Waste Treatment. Interscience New York pp. 85-106

Pol, L.W.H., Dezeeuw, W.J., Velzeboer, C.T.M., Lettinga, G., 1983. Granulation in UASB-reactors. *Water Science and Technology*, 15, 291-304.

Polit, M., Genovesi, A., Claudet, B., 2001. Fuzzy logic observers for a biological wastewater treatment process. *Applied Numerical Mathematics*, 39, 173-180.

Pons, M.N., Le Bonte, S., Potier, O., 2004. Spectral analysis and fingerprinting for biomedia characterisation. *Journal of Biotechnology*, 113, 211-230.

Puhakka, J.A., Alavakeri, M., Shieh, W.K., 1992. Anaerobic treatment of kraft pulp-mill waste activated-sludge – Gas production and solids reduction. *Bioresource Technology*, 39, 61-68.

Pullammanappallil, P.C., Chynoweth, D.P., Lyberatos, G., Svoronos, S.A., 2001. Stable performance of anaerobic digestion in the presence of a high concentration of propionic acid. *Bioresource Technology*, 78, 165-169.

Pullammanappallil, P.C., Svoronos, S.A., Chynoweth, D.P., Lyberatos, G., 1998. Expert system for control of anaerobic digesters. *Biotechnology and Bioengineering*, 58, 13-22.

Rasi, S., Veijanen, A., Rintala, J., 2007. Trace compounds of biogas from different biogas production plants. *Energy*, 32, 1375-1380.

Reich, G., 2005. Near-infrared spectroscopy and imaging: Basic principles and pharmaceutical applications. *Advanced Drug Delivery Reviews*, 57, 1109-1143.

Reeve, J.N., Morgan, R.M., Nölling, J., 1997. Environmental and molecular regulation of methanogenesis. *Water Science and Technology*, 36, (6-7) 1-6.

Rivard, C.J., Adney, W.S., Himmel, M.E., 1991. Enzymes for anaerobic municipal solid waste disposal. In: Enzymes in biomass conversion. (ed. Leatham, G.F., Himmel, M.E.) ACS Syposium Series 460. American Chemical Society, Washington D.C.

Rivard, C.J., Vinzant, T.B., Adney, W.S., Grohmann, K., Himmel, M.E., 1990. Anaerobic digestibility of two processed municipal-solid-waste materials. *Biomass*, 23, 201-214.

Robbins, J.E., Gerhardt, S.A., Kappel, T.J., 1989. Effects of total ammonia on anaerobic-digestion and an example of digester performance from cattle manure protein mixtures. *Biological Wastes*, 27, 1-14.

Rodrigues, J.C., Nascimento, A.C., Alves, A., Osorio, N.M., Pires, A.S., Gusmao, J.H., da Fonseca, M.M.R., Ferreira-Dias, S., 2005. Calibration of near-infrared spectroscopy for solid fat content of fat blends analysis using nuclear magnetic resonance data. *Analytica Chimica Acta*, 544, 213-218.

Rodrigues, L.S., Silva, I.J., Oliveira, P.R., Campos, C.M.M., Silva, F.L., 2004. Efficiency of seeding material in anaerobic treatment a swine liquid waste: an in vitro trial. *Arquivo Brasileiro De Medicina Veterinaria E Zootecnia*, 56, 647-652.

Rodríguez, A.G., Mandaluniz, N., Flores, G., Oregui, L.M., 2005. A gas production technique as a tool to predict organic matter digestibility of grass and maize silage. *Animal Feed Science and Technology,* 123-124, 267-276.

Romano, R.T., Zhang, R.H., 2008. Co-digestion of onion juice and wastewater sludge using an anaerobic mixed biofilm reactor. *Bioresource Technology*, 99, 631-637.

Rozzi, A., Massone, A., Antonelli, M., 1997. A VFA measuring biosensor based on nitrate reduction. *Water Science and Technology*, 36, 183-189.

Rozzi, A., Passino, R., 1985. State of the art anaerobic digesters in Europe. in: B.F. Pain, R.Q. Hepherd (Eds.), Anaerobic digestion of farm waste. NIRD Technical Bulletins, Reading, pp. 115-124.

Rozzi, A., Remigi, E., Buckley, C., 2001. Methanogenic activity measurements by the MAIA biosensor: instructions guide. *Water Science and Technology*, 44, 287-294.

Rutter, P.R., Vincent, B., 1980. The adhesion of microorganisms to surfaces: physico-chemical aspects. in: R.C.W. Berkeley, J.M. Lynch, J. Melling, P.R. Rutter, B. Vincent (Eds.), Microbial adhesion to surfaces. Ellis Horwood, London, pp. 79-91.

Saeys, W., Mouazen, A.M., Ramon, H., 2005a. Potential for on-site and on-line analysis of pig manure using visible and near infrared reflectance spectroscopy. *Biosystems Engineering*, 91, 393-402.

Saeys, W., Xing, J., De Baerdemaeker, J., Ramon, H. 2005b. Comparison of transflectance and reflectance ot analyse hog manures. *Journal of Near Infrared Spectroscopy*, 13, 99-107.

Sahlstrom, L., 2003. A review of survival of pathogenic bacteria in organic waste used in biogas plants. *Bioresource Technology*, 87, 161-166.

Salkinoja-Salonen, M.S., Nyns, E.J., Sutton, P.M., vandenberg, L., Wheatley, A.D., 1983. Starting-up of anaerobic fixed-film reactor. *Water Science and Technology*, 15, 305-308.

Sandberg, M., Ahring, B.K., 1992. Anaerobic treatment of fish-meal process waste-water in a UASB reactor at high pH. *Applied Microbiology and Biotechnology*, 36, 800-804.

Schink, B., 1992. Syntrophism among Prokaryotes. in: A. Balows, H.G. Truper, M. Dworkin, W. Harder, K.H. Scheifer (Eds.), The Prokaryotes: A Handbook on the Biology of Bacteria: Ecophysiology, Isolation, Identification, Applications. Springer-Verlag., New York, pp. 276-299.

Schmidt, J.E., Ahring, B.K., 1993. Effects of hydrogen and formate on the degradation of propionate and butyrate in thermophilic granules from an upflow anaerobic sludge blanket reactor. *Applied and Environmental Microbiology*, 59, 2546-2551.

Shin, H.S., Youn, J.H., Kim, S.H., 2004. Hydrogen production from food waste in anaerobic mesophilic and thermophilic acidogenesis. *International Journal of Hydrogen Energy*, 29, (13), 1355-1363.

Show, K.Y., Tay, J.H., 1999. Influence of support media on biomass growth and retention in anaerobic filters. *Water Research*, 33, 1471-1481.

Siegert, I., Banks, C., 2005. The effect of volatile fatty acid additions on the anaerobic digestion of cellulose and glucose in batch reactors. *Process Biochemistry*, 40, 3412-3418.

Silverstein, R.M., Webster, F.X., Kiemle, D.J., 2005. Spectrometric Identification of Organic Compounds. 7 ed. Wiley, New York.

Smet, E., Van Langenhove, H., De Bo, I., 1999. The emission of volatile compounds during the aerobic and the combined anaerobic/aerobic composting of biowaste. *Atmospheric Environment*, 33, 1295-1303.

Smith, B.C., 1998. The basics of infrared interpretation. in: Infrared Spectral Interpretation: A systematic approach. CRC Press, pp. 7-15.

Smith, L.C., Elliot, D.J., James, A., 1996. Mixing in upflow anaerobic filters and its influence on performance and scale-up. *Water Research*, 30, 3061-3073.

Smith, P.H., Wah, R.A. 1966. Kinetics of acetate metabolism during sludge digestion. *Applied Microbiology,* 14, 368-371.

Spanjers, H., Bouvier, J.C., Steenweg, P., Bisschops, I., van Gils, W., Versprille, B., 2006. Implementation of an in-line infrared monitor in full-scale anaerobic digestion process. *Water Science and Technology*, 53, 55-61.

Stadlbauer, E.A., Oey, L.N., Weber, B., Jansen, K., Weidle, R., Lohr, H., Ohme, W., Doll, G., 1994. Anaerobic purification of brewery waste water in biofilm reactors with and without a methanation cascade. *Water Science and Technology*, 30, 395-404.

Stephenson, R.J., Patoine, A., Guiot, S.R., 1999. Effects of oxygenation and upflow liquid velocity on a coupled anaerobic/aerobic reactor system. *Water Research*, 33, 2855-2863.

Steyer, J.P., Bouvier, J.C., Conte, T., Gras, P., Harmand, J., Delgenes, J.P., 2002. On-line measurements of COD, TOC, VFA, total and partial alkalinity in anaerobic digestion processes using infra-red spectrometry. *Water Science and Technology*, 45, 133-138.

Steyer, J.P., Bouvier, J.C., Conte, T., Gras, P., Sousbie, P., 2002. Evaluation of a four year experience with a fully instrumented anaerobic digestion process. *Water Science and Technology*, 45, 495-502.

Strik, D.P.B.T.B., Domnanovich, A.M., Zani, L., Braun, R., Holubar, P., 2005. Prediction of trace compounds in biogas from anaerobic digestion using the MATLAB neural network toolbox. *Environmental Modelling & Software*, 20, 803-810.

Strong, G.E., Cord-Ruwisch, R., 1995. In-situ dissolved hydrogen probe for monitoring anaerobic digesters under overload conditions. *Biotechnology and Bioengineering*, 45, 63-68.

Stroot, P.G., McMahon, K.D., Mackie, R.I., Raskin, L., 2001. Anaerobic co-digestion of municipal solid waste and biosolids under various mixing conditions - I. Digester performance. *Water Research*, 35, 1804-1816.

Stuart, B., 1997. Biological applications of infrared spectroscopy. John Wiley & Sons Ltd, Chichester.

Sung, S.W., Liu, T., 2003. Ammonia inhibition on thermophilic anaerobic digestion. *Chemosphere*, 53, 43-52.

Suzuki, T., McCrabb, G.J., Nishida, T., Indramanee, S., Kurihara, M., 2007. Construction and operation of ventilated-hood type respiration calorimeters for in-vivo measurement of methane production and energy partition in ruminants. in:

H.P.S, Makkar, P.E. Vercoe. (Eds) Measuring methane production from ruminants. Springer Publishing.

Tafdrup, S., 1995. Viable energy production and waste recycling from anaerobic digestion of manure and other biomass materials. *Biomass & Bioenergy*, 9, 303-314.

Tanaka, S., Kobayashi, T., Kamiyama, K., Bildan, M., 1997. Effects of thermochemical pre-treatment on the anaerobic digestion of waste activated sludge. *Water Science and Technology*, 35, 209-215.

Thermo Electron Corporation, 2005. PLSplus IQ user's guide. Thermo Galactic, 18 Commerce Way, Suite 5000. Woburn, MA, USA.

Thompson, M., Ellison, S.L.R., Wood, R. 2002. Harmonized guidelines for single-laboratory validation of methods of analysis (IUPAC technical report). *Pure and Applied Chemistry*, 74, 835-855.

Tiehm, A., Nickel, K., Zellhorn, M., Neis, U., 2001. Ultrasonic waste activated sludge disintegration for improving anaerobic stabilization. *Water Research*, 35, 2003-2009.

Tilche, A., Bortone, G., Forner, G., Indulti, M., Stante, L., Tesini, O., 1994. Combination of anaerobic-digestion and denitrification in a hybrid upflow anaerobic filter integrated in a nutrient removal treatment-plant. *Water Science and Technology*, 30, 405-414.

Urgun-Demirtas, M., Singh, D., Pagilla, K., 2007. Laboratory investigation of biodegradability of a polyurethane foam under anaerobic conditions. *Polymer Degradation and Stability*, 92, 1599-1610.

Van Bodegom, P.M., Scholten, J. C. M., Stams, A. J. M., 2004. Direct inhibition of methanogenesis by ferric iron. *FEMS Microbiology Ecology* 49, (2), 261-268

Van der Mei, H.C., Meinders, J.M., Busscher, H.J., 1994. The influence of ionic strength and pH on diffusion of microorganisms with different structural surface structures. *Microbiology,* 140, 3413-3419.

Van Soest, P. J., Robertson, J.B., Lewis, B.A., 1991. Methods for dietary fiber, neutral detergent fiber, and nonstarch polysaccharides in relation to animal production. *Journal of Dairy Science*, 74, 3583–3597.

Varesche, M.B.A., Zaiat, M., Vieira, L.G.T., Vazoller, R.F., Foresti, E., 1997. Microbial colonization of polyurethane foam matrices in horizontal-flow anaerobic

immobilized-sludge reactor. *Applied Microbiology and Biotechnology*, 48, 534-538.

Vavilin, V.A., Angelidaki, I., 2005. Anaerobic degradation of solid material: Importance of initiation centres for methanogenesis, mixing intensity, and 2D distributed model. *Biotechnology and Bioengineering*, 89, 113-122.

Viscarra Rossel, R.A., Walvoort, D.J.J., McBratney, A.B., Janik, L.J., Skjemstad, J.O., 2006. Visible, near infrared, mid infrared or combined diffuse reflectance spectroscopy for simultaneous assessment of various soil properties. *Geoderma*, 131, 59–75.

von Sachs, J., Meyer, U., Rys, P., Feitkenhauer, H., 2003. New approach to control the methanogenic reactor of a two-phase anaerobic digestion system. *Water Research*, 37, 973-982.

Wang, Q.H., Kuninobu, M., Ogawa, H.I., Kato, Y., 1999. Degradation of volatile fatty acids in highly efficient anaerobic digestion. *Biomass & Bioenergy*, 16, 407-416.

West, R., 1985. Matching energy supply and demand. in: B.F. Pain, R.Q. Hepherd (Eds.), Anaerobic digestion of farm waste. NIRD Technical Bulletins, Reading, pp. 55-71.

Williams, P.C., 2001. Implementation of near-infrared technology. In: P.C. Williams, K. Norris, (Eds.), Near-Infrared Technology in the Agricultural and Food Industries, 2nd ed. American Association of Cereal Chemists Inc., St. Paul, Minnesota, USA, pp. 145–169.

Williams, P.C., 2003. Near-infrared technology - Getting the best out of light. *PDK Grain*, Nanaimo, Canada.

Wimpenny, J., 2000. An overview of biofilm. in: D.G. Allison, P. Gilbert, H.M. Lappin-Scott, M. Wilson (Eds.), Community structure and co-operation in biofilms. Cambridge University Press, Cambridge, pp. 1-24.

Wong, M.H., Cheung, Y.H., 1995. Gas production and digestion efficiency of sewage sludge containing elevated toxic metals. *Bioresource Technology*, 54, 261-268.

Yang, J., Bos, R., Belder, G.F., Engel, J., Busscher, H.J., 1999. Deposition of oral bacteria and polystyrene particles to quartz and dental enamel in a parallel plate and stagnation point flow chamber. *Journal of Colloid and Interface Science*, 220, 410-418.

Yang, P.F., Zhang, R.H., MeGarvey, J.A., Benernann, J.R., 2007. Biohydrogen production from cheese processing wastewater by anaerobic fermentation using

mixed microbial communities. *International Journal of Hydrogen Energy*, 32, 4761-4771.

Yang, Y., Tada, C., Tsukahara, K., Sawayama, S., 2004. Methanogenic community and performance of fixed- and fluidized-bed reactors with reticular polyurethane foam with different pore sizes. *Materials Science & Engineering C-Biomimetic and Supramolecular Systems*, 24, 803-813.

Yang, Y., Tsukahara, K., Sawayama, S., 2007. Performance and methanogenic community of rotating disk reactor packed with polyurethane during thermophilic anaerobic digestion. *Materials Science & Engineering C-Biomimetic and Supramolecular Systems*, 27, 767-772.

Yang, Y.N., Tada, C., Miah, M.S., Tsukahara, K., Yagishita, T., Sawayama, S., 2004. Influence of bed materials on methanogenic characteristics and immobilized microbes in anaerobic digester. *Materials Science & Engineering C-Biomimetic and Supramolecular Systems,* 24, 413-419.

Yang, Z.L., Han, L.J., Fan, X., 2006. Rapidly estimating nutrient contents of fattening pig manure from floor scrapings by near infrared reflectance spectroscopy. *Journal of near Infrared Spectroscopy*, 14, 261-268.

Yeole, T.Y., Gokhale, S., Hajarnis, S.R., Ranade, D.R.,1997. Effect of brackish water on biogas production from cattle dung and methanogens. *Bioresource Technology,* 58, 3, 323-325.

Yu, H.Q., Fang, H.H.P., 2002. Acidogenesis of dairy wastewater at various pH levels. *Water Science and Technology*, 45, 201-206.

Yu, H.Q., Fang, H.H.P., Gu, G.W., 2002. Comparative performance of mesophilic and thermophilic acidogenic upflow reactors. *Process Biochemistry*, 38, 447-454.

Zahller, J.D., Bucher, R.H., Ferguson, J.F., Stensel, H.D., 2007. Performance and stability of two-stage anaerobic digestion. *Water Environment Research*, 79, 488-497.

Zellner, G., Alberto J.L., Conway de Macario, M., Conway de Macario, E., 1997. A study of three anaerobic methanogenic bioreactors reveals that syntrophs are diverse and different from reference organisms. *FEMS Microbiology Ecology*, 22, (4), 295-301.

Zellner, G., Geveke, M., Diekmann, H., 1991. Start-up and operation of a fluidized-bed reactor oxidizing butyrate by a defined syntrophic population. *Biotechnology Letters*, 13, 687-691.

Zhang, Y.S., Zhang, Z.Y., Sugiura, N., Maekawa, T., 2002. Monitoring of methanogen density using near-infrared spectroscopy. *Biomass & Bioenergy*, 22, 489-495.

Zhang, Y.S., Zhang, Z.Y., Suzuki, K., Maekawa, T., 2003. Uptake and mass balance of trace metals for methane producing bacteria. *Biomass & Bioenergy*, 25, 427-433.

Zoetemeyer, R.J., Vandenheuvel, J.C., Cohen, A., 1982. pH influence on acidogenic dissimilation of glucose in an anaerobic digester. *Water Research*, 16, 303-311.

Abbreviations

ADF	Acid detergent fibre
ADL	Acid detergent lignin
AF	Anaerobic filter
AHR	Anaerobic hybrid reactor
ASTM	American Society of Testing and Materials
BMP	Biochemical methane potential
BOD_5	Biochemical oxygen demand (five day assay)
BOD_{st}	Biochemical oxygen demand (short term)
C:N ratio	Carbon to nitrogen ratio
COD	Chemical oxygen demand
CSTR	Completely stirred tank reactor
EPS	Extracellular polymeric substances
EU	European Union
FFBP	Feed forward back propagation
FT-NIRS	Fourier transform near infrared spectroscopy
HDPE	High density polyethylene
HRT	Hydraulic retention time
ID	Internal diameter
IRS	Infrared spectroscopy
LEL	Lower explosive limit
MAIA	Methanogenic activity and inhibition analyser
MIR	Mid infrared
MSW	Municipal solid waste
NIRS	Near infrared spectroscopy
NDF	Neutral detergent fibre
OD	Outer diameter
PCA	Principal component analysis
PE	Polyethylene
PFR	Plug flow reactor
PI	Proportional integral controller
PID	Proportional integral derivative controller
PLFA	Phospholipid fatty acid

PLS	Partial least squares
PTFE	Polytetrafluoroethene
PVC	Polyvinyl chloride
RMSECV	Root mean square error of cross validation
RMSEE	Root mean square error of estimation
RMSEP	Root mean square error of prediction
RTD	Residence time distribution
SSE	Sum of squared errors
STP	Standard temperature and pressure
TOC	Total organic carbon
TS	Total solids
UASB	Upflow anaerobic sludge blanket
VS	Volatile solids